DDX11 Helicase in Warsaw Breakage Syndrome, DNA Damage Response and Sister Chromatid Cohesion

Faramarz, A.

2020

document version
Publisher's PDF, also known as Version of record

DDX11 Helicase in Warsaw Breakage Syndrome, DNA Damage Response and Sister Chromatid Cohesion

Atiq Faramarz

Reading committee:

Prof.dr. R.H. Brakenhoff
Prof.dr. H. van Attikum
Prof. dr. J.W.M. Martens
dr. K.S. Wendt
dr. M.B. Bierings

VRIJE UNIVERSITEIT

DDX11 HELICASE IN WARSAW BREAKAGE SYNDROME, DNA DAMAGE RESPONSE AND SISTER CHROMATID COHESION

ACADEMISCH PROEFSCHRIFT

ter verkrijging van de graad Doctor aan

de Vrije Universiteit Amsterdam,

op gezag van de rector magnificus

prof.dr. V. Subramaniam,

in het openbaar te verdedigen

ten overstaan van de promotiecommissie

van de Faculteit der Geneeskunde

op dinsdag 31 maart 2020 om 9.45 uur

in de aula van de universiteit,

De Boelelaan 1105

door

Atiqullah Faramarz

geboren te Bazarak Panjshir, Afghanistan

Promotor: Prof. dr. H. te Riele

Copromotors: dr. R. M. F. Wolthuis and dr. J. de Lange

Table of content

Chapter 1

Molecular Regulation of Sister Chromatid Cohesion and Biological Functions of the Cohesin Complex

Atiq Faramarz, Rob Wolthuis and Job de Lange

1. The cohesin complex

Successful cell division requires the tightly controlled duplication and subsequent equal distribution of the DNA. In the synthesis phase (S-phase) of the cell cycle, every chromosome is copied, which creates two identical sister chromatids. In order to provide each daughter cell with the right set of chromosomes, these sister chromatids remain connected until metaphase, when they are bipolarly attached to the mitotic spindle. Next, in anaphase, the sister chromatids are separated and pulled towards opposite poles of the cell. Prior to anaphase, 'cohesion' between the two sister chromatids is ensured by a circular protein complex called 'cohesin', most likely via co-entrapment of two DNA strands inside one huge ring, although other models have also been proposed (paragraph 2).

Most cohesin components and regulators are conserved in different species (***Box 1***). The complex consists of three core subunits: SMC1A and SMC3, two members of the structural maintenance of chromosomes family, and a non-SMC subunit, sister chromatid cohesion 1 (Scc1/RAD21). The long SMC proteins possess similar structures, folding back on themselves by antiparallel coiled coils. SMC1A and SMC3 bind each other directly at their hinge domains. Their amino and carboxyl termini form ATPase heads[1,2], which are bridged by RAD21 (***Figure 1***)[3]. The C-terminus of RAD21 binds the SMC1A head domain, whereas the N-terminus interacts with SMC3 coiled coil domain[4,5]. In addition, the cohesin complex harbourstwo differentclasses of Huntingtin/EF3/PP2A/Tor1 (HEAT) structural repeat containing subunits, the stromal antigens proteins SA1/SA2, as well as PDS5A/PDS5B. The first non-core cohesin subunit is either SA1 or SA2, which binds the complex through two SA-binding motifs in RAD21[3,6,7]. The second HEAT-repeat containing cohesion protein is either PDS5A or PDS5B.

SA1 and SA2 share 70% homology and are at least in part functionally redundant [6]but there are some functional differences. SA2 appears to be more ubiquitously expressed [8]. Cohesin-SA1 is particularly involved in gene regulation and replication of the telomeres whereas cohesin-SA2 is associated predominantly with sister chromatid cohesion [9,10]. Furthermore, SA1-depleted Hela cells fail to repair double-strand breaks while the depletion of SA2 has no effect on successful repair [11]. Particularly STAG2, the gene that encodes SA2, is frequently mutated in human cancer (see ***Section 4***). However, a detailed understanding of its biological functions and the way its inactivation contributes to cancer is still missing [12]. As mentioned above, the PDS5 proteins contain a highly conserved HEAT-repeat domain, comprising a binding site for RAD21 [13]. The two vertebrate PDS5 proteins, PDS5A and PDS5B, with 70% sequence homology [14,15,16], can interact with both Cohesin-SA1 and Cohesin-SA2 complexes [15]. Interestingly, PDS5 proteins are dynamically involved in cohesion maintenance as well as cohesin release, through regulatory interactions with Sororin and WAPL, respectively. Knockout of PDS5A or PDS5B in mice causes embryonic lethality in the perinatal stage as a result of organ malformation and developmental disorder similar to a rare genetic disorder,

Cornelia de Lange Syndrome (**CdLS**), but no obvious sister chromatid cohesion defects were observed in these cells [17].

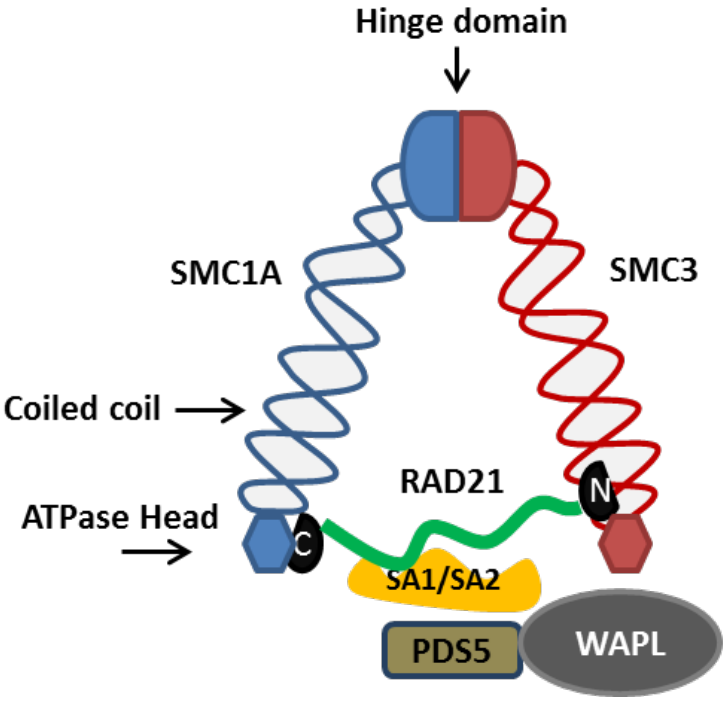

Figure 1: Structural composition of the cohesin complex.*The SMC1A protein (blue) is connected via its hinge domain to SMC3 (red). Both proteins are folded back onto themselves to form their parts of the DNA entrapping proteinaceous ring structure, which also includes RAD21 (in green). RAD21 binds the HEAT repeat containing proteins SA1/SA2 and PDS5A/B, as well as the cohesin removal catalyzing enzyme WAPL (which also contains HEAT repeats).*

However, another mouse study revealed that both PDS5A and PDS5B are involved in sister chromatid cohesion by undermining ESCO2 and Sororin activities. Cells from PDS5B null mice displayed aneuploidy and an impaired spindle assembly checkpoint [18]. This study proposed that

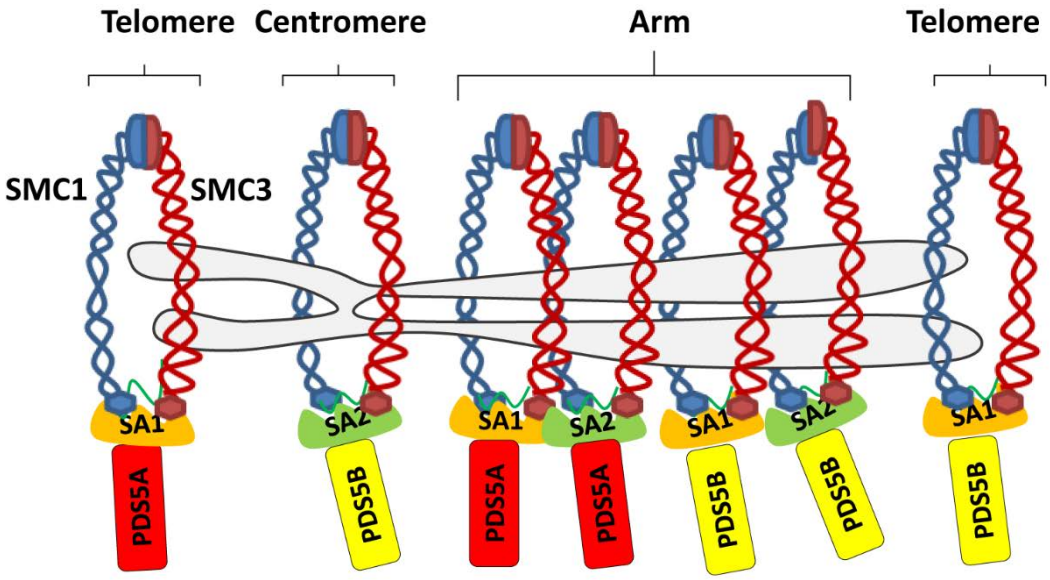

Figure 2: Different compositions of the cohesin complex. *Cohesin-SA1-PDS5A and cohesin-SA1-PDS5B are predominantly responsible for telomere cohesion. The Cohesin-SA2-PDS5B complex is specially associated with centromere cohesion. Arm cohesion requires both SA and PDS5 proteins to interact with the cohesin complex* [18].

both cohesin-SA1-PDS5A and cohesin-SA1-PDS5B are associated with telomere cohesion, whereas cohesin-SA2-PDS5B is particularly involved in centromere cohesion. Establishment of arm cohesion requires the simultaneous cooperation of each of the SA and PDS5 proteins [18] (*Figure 2*). PDS5B also interacts with Haspin, a protein kinase phosphorylating Histone H3 during mitosis which is required to protect centromere cohesion [19,20].

2. Models of DNA Entrapment by Cohesin

The cohesin complex topologically holds two DNA segments together [4,21]. Several models have been proposed for how this is achieved, including the "embrace model", "bracelet model" and "snap model". The embrace model (*Figure 3A*), in which cohesin embraces the two sister chromatids within a single ring, is the most accepted and arguably the simplest model [3]. The other models are based on the concept of cohesin oligomerization [22,23]. The bracelet model (*Figure 3B*) proposes that a set of SMC1A/SMC3 heterodimers of different cohesins are connected by RAD21, establishing oligomeric filaments in a bracelet-like fashion that wrap around the two sister chromatids and entrap them without getting closed [22]. In the snap model (*Figure 3C*), two cohesin complexes, each binding one sister chromatid, are interconnected via their coiled-coil domains [23].

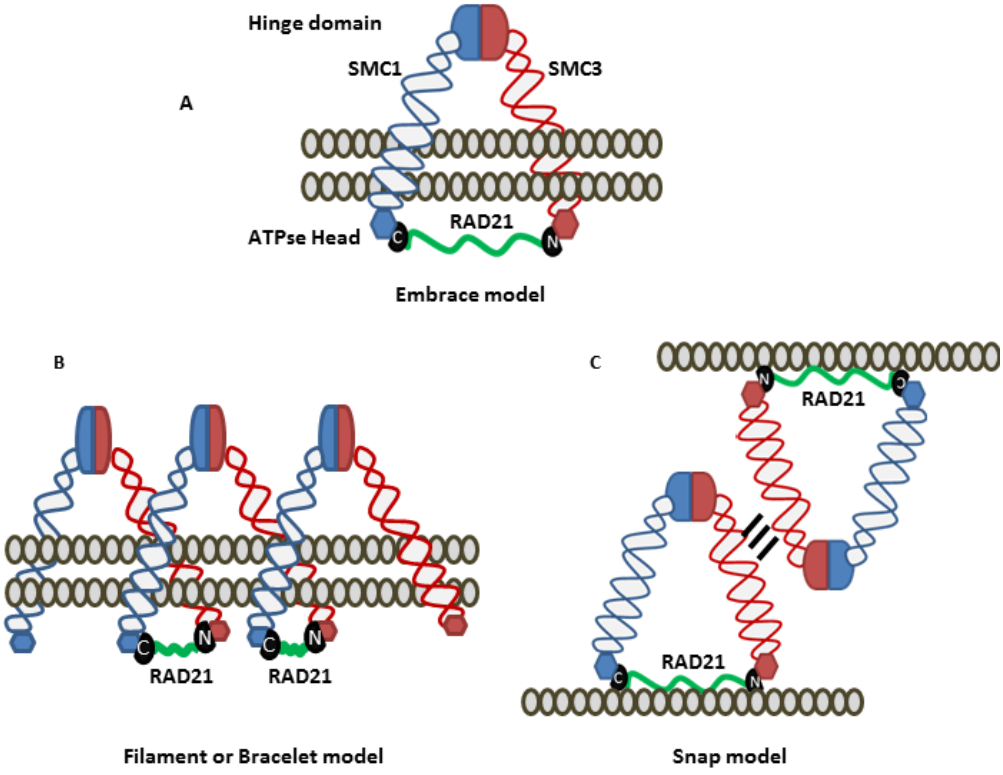

Figure 3: Models of DNA entrapment. *(A) in the embrace model, one cohesin ring embraces two sister chromatids. (B) in the bracelet model, cohesin rings form multimeric filaments that are wrapped around DNA. (C) in the snap model, each sister chromatid is bound by one cohesin complex, which bind each other through the coiled coil domains of SMC3.*

BOX 1. Overview of proteins involved in Sister Chromatid Cohesion

Cohesion complex proteins are evolutionary conserved. Some of their encoding genes have been found to be mutated in human developmental syndromes such as Cornelia de Lange Syndrome (CdLS), Roberts Syndrome (RBS), CAID (Chronic Atrial and Intestinal Dysrhythmia) and WABS (Warsaw Breakage Syndrome). Also see Chapter 2 of this thesis.

Function	H.sapiens	S.cerevisiae	S.pombe	X.Laevis	D.rerio	Associated diseases
Cohesin core subunits	SMC1A	Smc1	Psm1	smc1	Smc1a	**CdLS**
	SMC3/CSPG6	Smc3	Psm3	smc3/cspg6	Smc3	
	RAD21	Mcd1/Scc1	Rad21	rad21/mc/nxp1/scc1	Rad21a, Rad21b	
Cohesin HEAT- proteins	STAG1/SA1/SCC3A	Scc3 (Irr1)	Psc3	stag1/sa1	Stag2	
	STAG2/SA2/SCC3B			stag2/sa2	Stag2	
	PDS5A	Pds5	Pds5	Pds5a	Pds5a	
	PDS5B/AS3/APRIN			pds5b/as3/aprin	Pds5b	
Cohesion Establishment	Sororin/CDCA5			sororin/cdca5	Cdca5	
	ESCO1	Eco1/Ctf7	Eso1	esco1	Esco1	
	ESCO2			esco2/rbs/efo2	Esco2	**RBS**
Cohesin Recycling	HDAC8	Hos1		hdac8	Hdac8	**CdLS**
Cohesin Loading	NIPBL/SCC2/DELANGIN	Scc2	Mis4	nipbl/scc2/delangin	Nipbla/Scc2a/Nipblb/Scc2b	
	MAU2/SCC4	Scc4	Ss13	mau2/scc4	Mau2	
Cohesion Dissociation	WAPAL/WAPL	Rad61/Wpl1	Wapl	Wapal	Wapl/KIAA0261	
	Securin	Pds1	Cut2		Pttg1	
	Separase	Esp1	Cut1	espl1	espl1/cds	
	PLK1	Cdc5	Plo1	Plk1/plk	Plk1/plk	
	Shugoshin (SGOL1)	Sgo1	Sgo1/Sgo2	Sgol1/Sgo1	Sgol1	**CAID**
Replication Fork Stability	DDX11	Chl1	SPAC3G6.11	Chl1		**WABS**
	WDHD1/AND-1	Ctf4	Mcl1	and1/ctf4		
	CHTF18	Ctf18	Chl12	Chtf18/ctf18	Chtf18/ctf18	
	Tipin	Csm3	Swi3	tipin/xtipin	Tipin	
	Timeless	Tof1	Swi1		timeless/tim	
	Claspin	Mrc1	Mrc1	Clspn		
	CHTF8	Ctf8	Ctf8	Chtf8/ctf8	Chtf8	

3. The regulation of sister chromatid cohesion

3.1 Cohesin loading The cohesin complex is found to be enriched in pericentromeric regions as well as in cohesin-associated regions (CARs) that are 1-4 kb long and spread with 2-35 kb gap intervals along chromosome arms [24–28]. Studies in yeast have revealed that cohesin loading onto DNA already occurs in telophase and is mediated by the dedicated and highly conserved 'loader complex' SCC2/SCC4, called NIPBL/MAU2 in humans [29–33]. Heterozygous mutations in NIPBL are the main cause of CLdS (see Chapter 2 of this thesis) [34,35]. Although SCC2-SCC4 is shown to load cohesin in a DNA sequence non-specific way *in vitro* [36], evidence *in vivo* suggests that preferred loading sites may exist. For example, human NIPBL was shown to interact with the Mediator complex, a transcriptional co-activator, to facilitate cohesin loading at promoter regions [37]. Furthermore, budding yeast SCC2-SCC4 collaborates with the chromatin remodeling complex, which leads to cohesin loading at nucleosome-free regions [38], and Xenopus SCC2-SCC4 can bind the MCM2-7 pre-replication origin complex and Cdc7-Dbf4 kinase [39]. These factors may support the loading of cohesion at specific locations on chromosomes. Apart from site-specific loading preferences, cohesin positioning may also be affected by regulation of its 'sliding' over the chromatin. Analysis of the mouse genome indicates that cohesin rings can either be 'pushed' forward by RNA polymerases or may passively diffuse along DNA, until they either encounter CTCF boundaries or are unloaded by WAPL [40].

SCC2 and SCC4 contain HEAT-repeats and tetricopeptide-repeats respectively, which are motifs important for chromosome association and chromosome dynamics [16,41]. Protein crystallography studies revealed that the flexible N-terminus of SCC2 is enclosed by SCC4's tetricopeptide-repeats that form a cylindrical-shape [41,42]. How DNA enters the cohesin ring is under debate. At the moment three possible entry gates have been proposed, either the hinge domain [43,44] or the sites where RAD21 interacts with SMC1A or SMC3 [45,46]. ***Figure 4A*** displays one of these models, in which the hinge domain forms the entry gate. The SCC2-SCC4 loader complex stimulates cohesin's ATPase activity, resulting in the separation of SMC1A and SMC3 hinge and subsequent DNA entrapment [36,47–49]. Both cohesin loading *in vivo* and DNA entrapment in biochemical reconstitution systems are shown to be ATP-dependent [36,37], suggesting that the opening gate is associated with the actions of the SMC ATPase head [46]. Indeed, experiments in budding yeast showed that ATP hydrolysis is essential for cohesin-DNA association [2,43]. Using *in vitro* cysteine-cross-linking experiments, Chapard *et al.* recently provided evidence for dynamic compartmentalization of the cohesin ring, involving engagement of SMC1/3 head, ATP hydrolysis and SMC3 acetylation [50]. They propose that sister DNAs are entrapped in a so-called K compartment, a sub-compartment between the SMC1/3 heads and the kleisin subunit (SCC1 in yeast) [50].

3.2 Cohesion establishment and maintenance In G1 phase of the cell cycle, cohesin continuously cycles to entrap and release DNA, the latter being dependent on cohesin's antagonist WAPL. To ensure long-term stability of sister chromatid cohesion, the cohesin rings that hold the sister

chromatids together must be stably closed. This so-called 'cohesion establishment' occurs in concert with the passing DNA replication fork and requires local inhibition of WAPL activity [18,51]. Cohesion establishment is dependent on the acetylation of SMC3 on two highly conserved Lysines near its ATPase domain (K112/K113 in yeast and K105/K106 in humans), a process which is mediated by Eco1 in yeast and both ESCO1 and ESCO2 in humans. These acetylations inhibit the ATP binding and hydrolysis cycle of cohesin after it has entrapped DNA, thereby strengthening the association of cohesin with the other sister chromatid or trigger cohesin oligomerization [52]. In animal cells, both acetylated cohesin and DNA replication also result in the recruitment of Sororin via the FGF (phenylalanine-glycine-phenylalanine) motif of PDS5. This interaction causes conformational changes in the cohesin complex, which then dislocates and removes WAPL from the cohesin complex (***Figure 4B***) [51,53]. Studies in yeast showed that, beside Eco1, several other replication fork stability factors, such as AND-1/Ctf4, Timeless/Tof1, Tipin/Csm3 and Claspin/Mrc1 contribute to the timely establishment of sister chromatid cohesion [54–56]. Pair-wise depletion of these factors lead to sister chromatid cohesion defects [57]. At the molecular level, these proteins may contribute to cohesin acetylation, suggesting they influence the activity or positioning of Eco1 or the ESCO1/2 enzymes [58]. These experiments point to the existence of critical connections between the regulation of DNA replication and the establishment of sister chromatid cohesion.

3.3 The prophase pathway At the beginning of mitosis, most of the cohesion complexes are removed from chromosome arms, in a process that may facilitate proper anaphase and support recycling of cohesion subunits. The dissociation of cohesin from DNA is regulated in a stepwise fashion via two pathways (***Figure 4C,D).*** Arm cohesin is removed in prophase and prometaphase, whereas centromeric cohesin is removed at the metaphase-to-anaphase transition. During prophase and prometaphase, several mitotic kinases, including PLK1, CDK1 and Aurora B are promoting the removal of arm cohesin through phosphorylation of SA2, Sororin, PDS5 and WAPL[59–67]. Subsequently, WAPL binds PDS5 and opens the RAD21-SMC3 interface in an ATPase dependent manner (***Figure 4C***) [15,68]. The exact molecular mechanism by which these phosphorylations make cohesin vulnerable to WAPL activity is not clearly understood.

Recently, studies in yeast suggested that a sub-population of cohesin loses its ability to connect sister chromatids ('cohesiveness'), while it remains bound to DNA, involving de-phosphorylation of RAD21 [69]. This requires a cooperation between WAPL and phosphatase PP4. PP4 dephosphorylates Rad21 phospho-Serine 164 and/or 165, exposing these amino acids to WAPL unloading activity [69]. However, the kinase responsible for RAD21 phosphorylation still needs to be identified. Future studies will further unravel the detailed molecular mechanism of cohesin unloading in prophase, such as identification of the regulatory enzymes involved and their targets and how specific protein modifications might affect stable interactions between cohesin and sister chromatids.

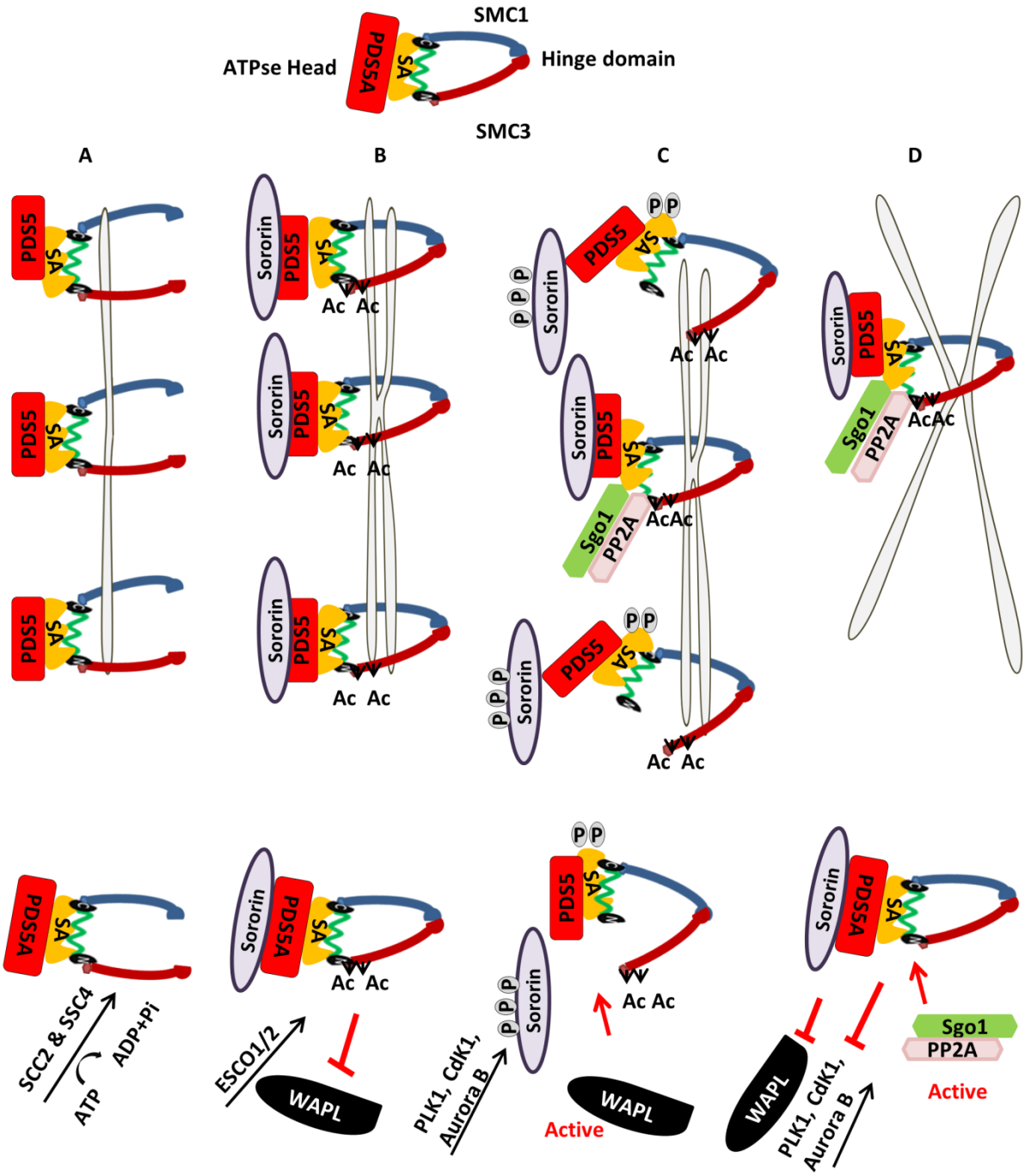

Figure 4: Cohesin's regulation during different phases of cell cycle. *(A) SCC2 and SCC4 proteins are responsible for the loading of cohesins on DNA, either via the opening of the hinge domain or the or opening of the RAD21-SMC3 interaction (not shown) in an ATP-dependent manner. (B) Acetylation of the cohesin subunit SMC3 by ESCO1 and ESCO2 is important for establishment of sister chromatid cohesion. This leads to the recruitment of sororin, which removes WAPL from cohesin and thereby neutralizes its antiestablishment activity. (C) In prophase, cohesin rings are removed in a phosphorylation-dependent manner from chromosome arms, whereas centromere cohesins are protected from this pathway by phosphorylated SGOL1 and PP2A [63]. (D) The presence of only centromere cohesins but not arm cohesins results in the typical X-shape chromosomes. At the metaphase-to-anaphase-transition, the protease Separase is responsible*

for cleavage of RAD21, to remove the remaining cohesins from the centromere and allow separation of the sister chromatids. In order to reset cohesion process, HDAC8 needs to deacetylate cohesins, preparing them for the next cell cycle.

3.4 Sister chromatid separation Centromere cohesins are required to resist the pulling forces that are generated by the mitotic spindle in prometaphase, when all chromosomes are being attached to microtubules from opposite poles, in a process called chromosome bi-orientation (***Figure 5***). Simultaneously, the spindle assembly checkpoint (SAC) inhibits the metaphase-to-anaphase transition. The SAC is kept active by kinetochores that are not bioriented, stimulating production of the mitotic checkpoint complex (MCC), composed of BubR1, Bub3, Mad2 and Cdc20[70,71]. Mad2, together with its binding partner Mad1 and checkpoint kinase Mps1, supports SAC activation and localization at unattached kinetochores [72]. Both the appropriate attachments of sister chromatid kinetochores to the mitotic spindle and the generated pulling tensions help to silence the SAC, resulting in the disassembly of the MCC and release of Cdc20. Cdc20, in a way supported by its phosphorylation by Cyclin B1-Cdk1, interacts with the Anaphase-Promoting Complex/Cyclosome (APC/C) [70,71,73–75], a multisubunit E3 ubiquitin ligase that targets numerous substrates to the proteasome, through a D-box (RxxLxxxxN) or a KEN-box (KENxxxN) degron [7677,78]. Two important APC/C substrates at the metaphase to anaphase transition are Securin and Cyclin B1. Securin degradation allows the release of the protease Separase, leading to RAD21 cleavage and separation of sister chromatids, whereas Cyclin B1 degradation inactivates Cdk1, leading to cytokinesis and mitotic exit [79–82]. In order to reset cohesin, HDAC8 (Hos1 in yeast), a zinc-dependent deacetylase, needs to deacetylate SMC3[83,84] and prepare cohesin complexes for the next cell cycle. Once SMC3 is de-acetylated, new assembly of remaining cohesin complexes and their DNA replication-associated acetylation is required for passage through the next cell cycle.

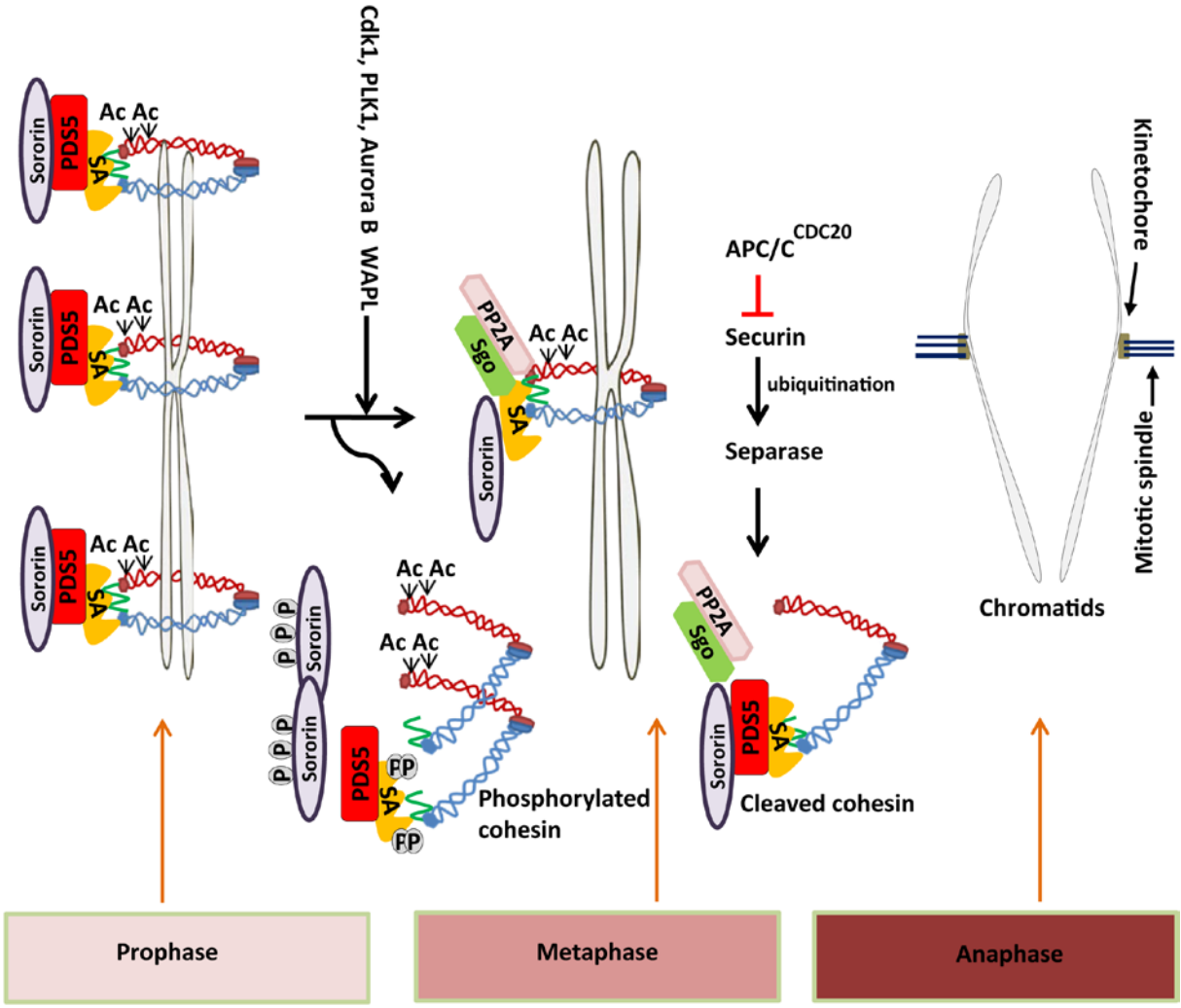

Figure 5: Stepwise cohesin dissociation and sister chromatid segregation. *The bulk of arm cohesins are removed in a phosphorylation-dependent manner in prophase. However, centromere cohesins are protected from this pathway by Cdk1, phosphorylating SGOL1 and PP2A* [63]*. At the metaphase-to-anaphase-transition, the APC/C degrades Securin, which releases the protease Separase. Separase cleaves RAD21 to remove the remaining centromere cohesins.*

4. Cohesion Regulatory Proteins

4.1. WAPL (Wings-Apart Like) stimulates the release of cohesin from DNA by binding to the SMC3 ATPase domain and promoting the opening of the SMC3-RAD21 interface in an ATPase-dependent manner [51,85–87]. The C-terminal domain of WAPL contains HEAT repeats that are very important for its specific binding to cohesin, whereas its N-terminal domain seems to be less specific, interacting with both PDS5 and cohesin [88]. WAPL knockout mice are not viable [89,90] and its depletion in human cells results in hyper-cohesion, segregation errors and a p53-dependent G2-arrest in the next cell cycle or aneuploidy if p53 is absent [89,91,92]. Moreover, single molecule dynamics experiments show that WAPL (but also PDS5) negatively regulates cohesin translocation [93], and WAPL depletion causes the differential expression of more than thousand different genes [90]. In addition to WAPL, cohesin core subunits and other regulatory factors are

also involved in gene regulation. For a more extensive review of this research field see Zhu et al., 2019 [94]. WAPL overexpression is reported in cancer, e.g. cervical cancer and invasive squamous cell carcinoma [89,95] and WAPL-overexpressing cells develop tumors when injected into nude mice [89]. These observations suggest that WAPL may somehow act as an oncogene. Recently, depletion of WAPL (similar to depletion of PDS5A/B) was demonstrated to affect normal replication fork progression. This suggests that removing cohesins, which are located ahead of DNA replication forks, is necessary to guarantee smooth and unperturbed DNA replication [95], or facilitate rapid replication-associated repair in case of DNA replication stress. Indeed, depletion of WAPL leads to MRE11-dependent DNA-double strand breaks (DSB) accumulation. This study pinpoints a new and exciting role for WAPL in replication fork progression and maintaining genomic stability [95].

4.2 Sororin Whereas no Sororin ortholog is present in yeast, it is essential for establishment and maintenance of sister chromatid cohesion during DNA replication in metazoans [96,97]. Key to this function is its ability to counteract the cohesin unloading activity of WAPL. Studies in *Xenopus* egg extracts, Hela cells and plants showed that sororin becomes dispensable upon depletion of WAPL [51,98,99]. Sororin interacts with SA2 through twelve C-terminal amino acids of Sororin [100], and with both PDS5A and PDS5B via their FGF motif [51]. This latter interaction is facilitated by both DNA replication and by acetylation of SMC3 [51,98], causes conformational changes in the cohesin complex and dislocates WAPL from PDS5, thereby stabilizing cohesion [43,51,85,101]. Remarkably, Ladurner et al showed that the interaction of Sororin with cohesin, rather than cohesin acetylation, is limiting for how many cohesin complexes remain stably associated with chromatin during G2-phase [102]. This interaction is shown to be transient, allowing only a limited portion of cohesin complexes to bind chromatin, suggesting that unbound cohesins might be required for other functions [102]. Altered RNA splicing contributes to the regulation of Sororin protein levels and mutations in splicing factors are shown to cause decreased Sororin pre-mRNAs and subsequent chromatid cohesion defects [103,104]. Interestingly, Sororin is also reported to play a role in DNA damage repair, where siRNA mediated depletion of Sororin in oocytes induced high level of γH2AX foci formation [105].
Sororin depletion is shown to cause both cohesion defects and decreased cohesin-chromatin binding [51,88,97]. Furthermore, WAPL depletion reduces Sororin and SGOL1-PP2A requirement for the establishment of sister chromatid cohesion and protection of centromeric cohesins, respectively [51,88,97].

4.3 The acetylating ESCO1/ESCO2 enzymes All members of the Eco (Establishment of Cohesion) family proteins possess a PCNA-interacting protein (PIP) motif. PCNA (Proliferating Cell Nuclear Antigen) is a DNA sliding clamp that tethers replicative polymerases to the DNA. The PIP-box in yeast Eco1 is essential for both sister chromatid cohesion and Eco1-chromatin interaction [106]. Eco1 also interacts with many other components of the replication fork, including the replication factor C complex (RFC), which loads PCNA onto DNA, the DNA helicase Chl1 (ChlR1/DDX11 in humans) and the Okazaki fragment maturation flap endonuclease 1 (FEN1)

[55,58,106,107]. Eco1 moves with the replisome during replication[106] and in humans, ESCO1 and ESCO2-deficient cells exhibit DNA replication defects as a consequence of impeded cohesin acetylation [108]. Recently, ESCO2 (but not ESCO1) was shown to interact with the main replicative helicase, MCM2-7, enabling ESCO2 to travel with replicating replisomes and acetylating cohesive cohesin in the vicinity of the replication fork [109,110]. In addition, ESCO2-MCM interaction saves ESCO2 from proteasomal degradation, which is promoted post-replicatively by an E3 ubiquitin ligase complex (CUL4A-DDB1-VPRBP) and the APC/C [110]. These observations all fit with a role of Eco1 orthologues in establishing sister chromatid cohesion during DNA replication.

ESCO1 and ESCO2 are both zinc-finger-containing proteins with a highly conserved acetyltransferase domain but differ in their N-termini [111]. Although they are both to some degree required for SMC3 acetylation, they appear to have partially non-overlapping functions [112]. ESCO1 and ESCO2 are regulated differently during the cell cycle: whereas ESCO1 is continuously expressed, ESCO2 expression peaks at S- and G2-phase. Depletion of ESCO1 results in milder cohesion defects as compared to ESCO2 depletion. In line, ESCO1 is found to acetylate cohesin in a replication-independent manner and co-localizes with cohesin at CTCF sites, associated with genome wide transcription silencing [113]. Moreover, only ESCO1 appears to be dependent on PDS5 to acetylate SMC3 [114], suggesting that ESCO1 may have developed an alternative mechanism to specifically contribute to cohesin's role in gene transcription. Interestingly, while ESCO2 knockout is embryonic lethal in mice [112], bi-allelic inactivation of human ESCO2 is observed in patients with the cohesinopathy Roberts Syndrome (Chapter 2 of this thesis).

4.4 The DNA Helicases Chl1 and DDX11 DDX11/ChlR1, called Chl1 in yeast, are members of the iron-sulfur containing helicase family, which includes Xeroderma pigmentosum group D (XPD), FANCJ and RTEL1 (***Figure 6***). These proteins are intimately involved in maintaining genomic stability and their mutant forms cause rare genetic syndromes[126].

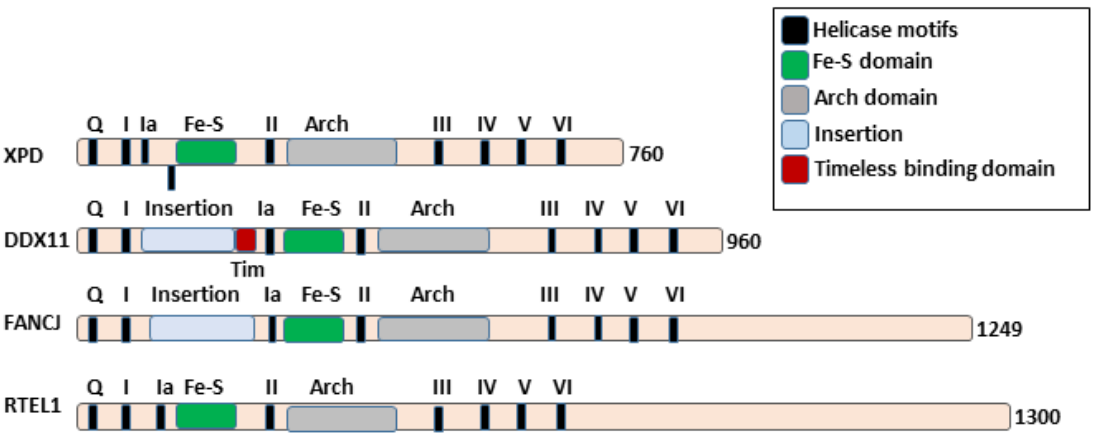

Figure 6: *Schematic representation of different human iron-sulfur containing helicases. Black refers to conserved helicase domains. Green: Fe-S domain; blue: insertions which are only present in DDX11 and FANCJ; red: Timeless binding domain; gray: Arch domain).*

Bi-allelic mutations in DDX11 cause a rare developmental disorder, the cohesinopathy Warsaw Breakage Syndrome (WABS) (discussed in Chapter 2). WABS mitotic chromosomes display defective sister chromatid cohesion but the molecular basis of this observation is not understood. Several studies in both human and yeast cells showed genetic and physical interactions of DDX11 with replication-associated proteins [55,107,115]. These include the DNA sliding clamp PCNA, Ctf18-RFC, implicated in both replication fork stabilization and sister chromatid cohesion, Ctf4 (a replication factor), FEN-1 (a structure specific endonuclease-1) [107,116,117] and the Fork Protection Complex (FPC), which is composed of Timeless and Tipin and is associated with the stabilization of the replication forks 118. Biochemical studies elucidated a role of PCNA and its loader Ctf18-RFC in enhancing DDX11 helicase activity, extending its unwinding capacity from 100bp to 500bp [106,108,117]. Studies in budding yeast reported that Chl1 is associated with Ctf4 through a CIP-box (Ctf4-interacting protein), which is also present in two other Ctf4-interacting proteins (DNA polymerase α p180 polypeptide and Sld5 GINGS subunit) involved in DNA replication54. Furthermore, FPC deficiency results in cohesion defects which are rescued by DDX11 overexpression [55,116,119–122], and similar to FPC also DDX11 contributes to stabilizing stalled replication forks [123,124].

Consistent with this, DDX11 is able to unwind "difficult to replicate" DNA structures like hairpins, found in 5' flap structured DNA [125], and antiparallel G-quadruplex (G4) DNA, thereby contributing to genomic stability [126]. Chapter 5 and 6 of this thesis describe that DDX11 contributes to both replication fork progression and sister chromatid cohesion.

Apparently, DDX11 performs its sister chromatin cohesion role in concert with DNA replication. While the exact mechanism of DDX11 involvement in sister chromatid cohesion, coupled to DNA replication, needs to be further explored, two main models have been proposed [107,54]. Since replication fork progression is continuously confronted with DNA lesions and replication obstacles, the first model proposed an important role for DDX11 helicase activity. It suggests that DDX11 helicase activity is involved in resolving DNA secondary structures, such as G4 DNA and hairpins structures, formed on the lagging strand [125,107]. The secondary DNA structures would hamper normal replication fork progression and Okazaki fragments maturation, thereby affecting both normal sister chromatid cohesion and chromosomal stability. The second model proposes a distinguishable DDX11 role in sister chromatid cohesion by physical interaction with cohesin via Ctf4 54. In this model, physical interaction between DDX11 during S phase positions cohesin in a way which enables cohesin to embrace sister chromatids as well as facilitates cohesin acetylation.

5. Non-canonical functions of cohesin

5.1 The role of cohesin in chromosome compaction Chromosome compaction is predominantly mediated by the condensin protein complex, another member of the SMC protein family. Condensin is a ring-like protein complex like cohesin, composed of two core subunits, SMC2 and SMC4 and three non-SMC subunits; a kleisin CAP-H, heat-repeat containing CAP-D2 and CAP-G [127]. However, different studies showed that also cohesin plays a role in chromosome compaction[128–130]. For example, studies in yeast, using single-molecule experiments, demonstrated that cohesin was able to compact DNA [129], and a recent study revealed a cooperation between cohesin and condensin maintaining chromosome organization and chromosome compaction [130]. Cohesin is believed to regulate compaction of the entire mitotic chromosomes, through intra-arm loops. Studies using Hi-C also show a genome-wide involvement of condensin in regulating chromosome compaction[131] (Gibcus et al Science 2018). Moreover, the cohesin unloading protein WAPL contributes to chromosome compaction activity of cohesin in meiosis [132].

5.2 The role of cohesin in DNA damage repair Cohesin complexes are recruited to double strand break (DSB) sites in S and G2 phase to establish *de novo* cohesion in yeast [133,134] and human cells [135,136]in order to facilitate homologous recombination and activation of the S-phase checkpoint [137–139]. Heterozygous deletion of RAD21 in mice leads to defective homologous recombination and increased sensitivity to ionizing radiation [140]. In budding yeast, Scc1 is shown to be phosphorylated by Chk1 upon DNA damage which subsequently promotes its acetylation by Eco1 to re-establish sister chromatid cohesion[141]. Experiments in both human and mouse cells demonstrated that in response to DNA damage, SMC1A and SMC3 are phosphorylated by ATM/NBS1 and ATR, two key kinases that regulate S-phase checkpoint activation and DNA repair [142,143]. ATM phosphorylates SMC1A at Ser957 and Ser966 in an NBS1-dependent fashion [137] and SMC3 at Ser1067 and Ser1083 [143]. SMC3-pSer1067 is reduced upon depletion of the checkpoint kinase Chk2, contributing to the idea that Chk2 regulates the intra S-phase checkpoint through SMC3 phosphorylation [143]. *Vice versa*, mammalian cohesin facilitates activating Chk2 phosphorylation on Thr68 [144], indicating a positive feedback loop.

Cohesin depletion results in both deregulation of gene expression, dysregulation of genes involved in DNA-damage response as well as aberrant spreading of phosphorylated Histone H2AX, which is involved in the DSB response [145]. Additionally, cohesin contributes to the stabilizing and restart of stalled replication forks [146], and cohesin was recently reported to regulate histone modification and transcription in response to DSBs [145].

Additional post-translational modifications of cohesin may be important. For example, in response to the DNA damage response, SUMOylation of different components of cohesin complex are believed to play a role in stabilization of a DNA template at the damage sites [147]. SCC1 is shown to be SUMOylated by SUMO E3 ligase Mms21/Nse2 at many lysine residues in

its C-terminus, e.g. after treating cells with the DNA damaging agent methyl methanesulfonate (MMS) or in the presence of double stranded breaks [148]. In conclusion, cohesin plays a prominent role in regulating the responses to DNA damage, which represents an important aspect of its involvement in genetic diseases and tumorigenesis. Future studies are required to shed light on the exact molecular mechanisms and how these different post-replicative modifications are coordinated.

5.3 The role of cohesin in the regulation of gene transcription NIPBL-mutated cells of both mouse and human have normal sister chromatid cohesion but show aberrant gene expression [149–151]. In mammalian cells, cohesin is reported to have 25.000 to 120.000 binding-sites in intergenic regions, from which 50 to 70% co-localize with the CCCTC-motif binding factor CTCF [152–155]. CTCF has 11 zinc finger domains which are important for DNA binding and functions as a chromatin insulator. Its interaction with cohesin appears to be crucial to counteract transcriptional activation [152]. Conversely, cohesin/CTCF-binding sites are also important for the long-range interaction of chromatins, facilitating contacts between promoters and distal enhancers to promote transcription [156]. Also, cohesin is reported to play a main role in forming chromatin loops through extrusion, contributing to genome organization by creating spatial domains [157,158]. This loop-extrusion model proposes that cohesin (or cohesins) produce these loops, a process which stops upon encountering CTCF binding sites on both sides of the loop [158]. Furthermore, cohesin also mediates contacts between transcription factors and enhancers [37,159] (*Figure 7*). Cohesin co-localizes with estrogen receptor alpha (ER) in cancer cells and two transcription factors, HNF4A and CEBPA, in liver cells, suggesting its involvement in tissue-specific oncogenic gene transcription [160].

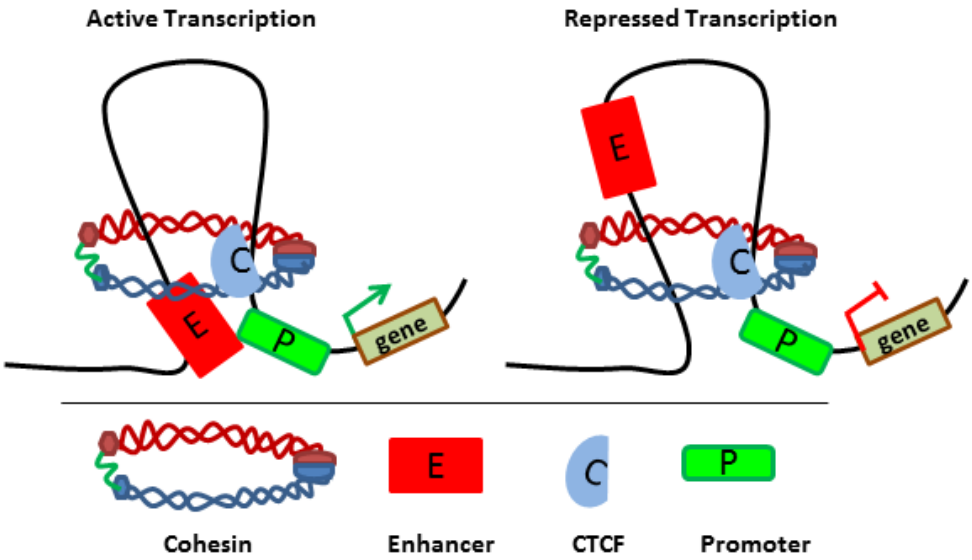

Figure 7: Cohesin involvement in transcriptional regulation and loop-formation. *Cohesin binding enables CTCF to execute either transcriptional activation or repression by forming chromatin loops. A: If a chromatin loop brings the enhancer and promoter in proper vicinity, it triggers*

transcriptional activation. B: If the loop keeps the enhancer and promoter distant, transcriptional repression takes place.

6. Cohesion and Cancer

6.1 Summary Accumulating evidence suggests that cohesin mutations play an important role in the development of several types of cancer. However, cohesion deregulation could have many different effects, such as genomic instability, aneuploidy, changes in gene expression, enhanced susceptibility to DNA damage or deregulated stem cell differentiation [161–164]. Which of these are most relevant for tumorigenesis remains unknown [162,164] . Barber *et al.* were the first to report somatic mutations in SMC1A, SMC3 and NIPBL in colorectal cancer [165]. Later, mutations of SMC1A, SMC3, RAD21 and SA2 were found in different forms of leukemia [166–168], as well as many other types of cancers [169–177]. In particular, *STAG2* (the gene encoding SA2) is a pivotal tumor suppressor gene [178,179] found to be mutated in acute myeloid leukemia, glioblastoma multiforme, Ewing sarcoma, melanoma, cervical carcinoma, urothelial carcinomas, colorectal cancer, endometrial carcinoma and renal-cell carcinoma [166,180–186].

6.2 STAG2 mutations in development and tumorigenesis Since the *STAG2* gene is located on the X-chromosome, one of which undergoes X-inactivation in females [187], one mutational hit may be sufficient to disturb its function. Initial studies in human glioblastoma cells showed that STAG2 mutations were linked to genomic instability and aneuploidy, including monosomies, trisomies and *de novo* translocations. Transcriptional profile analysis in these cell lines suggested that STAG2 did not affect gene transcription [185]. STAG2 inactivation was also shown to cause aneuploidy in bladder cancer and colorectal cancers [182,185,186,188]. By contrast, other studies reported nearly diploid karyotypes in STAG2 mutated cancers, including acute myeloid leukemia, bladder cancer and breast cancer, suggesting no correlations between SA2 mutations and aneuploidy [161,168,182,189–192].

Interestingly, experiments in different cell lines showed that tumor-derived STAG2 mutations, including truncating and missense mutants, do not have a detectable effect on sister chromatid cohesion and ploidy. The mutant SA2 proteins were able to interact with cohesin complexes as efficiently as WT SA2 protein [161,193], suggesting that the tumorigenic effect of STAG2 inactivation is unrelated to the cohesion complex. Of note, STAG2 mutated glioblastoma multiforme cells exhibited decreased protein levels of other cohesin subunits, as well as reduced interactions of WAPL, PDS5A and PDS5B with the cohesin ring [193]. Recently, experiments in STAG2-deficient cell pairs (glioblastoma, Ewing sarcoma and hTERT) were shown to display increased sensitivity to a panel of chemotherapeutic agents and small molecule inhibitors [194]. STAG2 deficiency correlated with a significant decrease in cell survival, accompanied with accumulating DNA double-strand breaks and replication fork collapse.

STAG2 is also associated with a new syndrome in three female patients with loss-of-function heterozygous mutations in *STAG2*, identifying STAG2 as a dosage sensitive gene [195]. The

patients suffer from developmental and nervous system abnormalities, microcephaly, deafness, craniofacial abnormalities and congenital heart defects. Surprisingly and unlike previous findings [185], the absence of functional SA2 in the patient cells does not result in obviously defective sister chromatid cohesion. Consistent with a model in which STAG2 contributes to other cellular effects than replicative sister chromatid cohesion, STAG2 duplications have also been reported to affect individuals clinically [196,197]. Recently, also a male patient with an inactivating STAG2 mutation has been reported, who suffers from dysmorphic features such as developmental delay, microcephaly and polydactyly [198].

Taken together, these studies suggest a complicated involvement of SA2 in different biological processes like transcription, sister chromatid cohesion and tumorigenesis. The fact that only one individual is diagnosed with an inactivating STAG2 mutation thus far and SA2 is proposed to affect the patient's development in a dosage sensitive manner suggests that entire loss of STAG2 might be lethal. Creating mouse models with various STAG2 mutations would enable us to answer these important questions. How STAG2 mutations cause tumorigenesis remains unclear. However, as 85% of STAG2 mutations in cancer are reported to be truncating, disrupting the coding sequence, it is proposed to be a tumor suppressor gene. Also aneuploidy, in case this is a true result of SA2 depletion, could be the main driver of cancer. Yet, not all STAG2 mutated cancer cells exhibit aneuploidy and genomic instability. Importantly, SA2 is the only cohesin subunit that interacts directly with a transcription insulator, CTCF [199] and this role of SA2 in transcription regulation could underlie its involvement in tumorigenesis and human development, probably through counteracting transcription activation of tumor suppressor genes and important developmental genes respectively. Taken together, further studies are required to substantiate these preliminary findings about SA2 involvement in the new cohesinopathy syndrome and tumorigenesis.

6.3 Clinical exploitation of cancer cells with mutations in the Cohesin components The existence of impaired cohesion in tumor cells may provide a unique treatment opportunity. Indeed, combined impairment of sister chromatid cohesion and DNA replication synergistically affects viability in yeast, C*. elegans* and human cells [200–203]. In addition, PARP inhibitor sensitivity was found in cells with mutations in *SMC1A*[148], *STAG2* [204] and *DDX11 (*Chapter 3 of this thesis). In Chapter 4 of this thesis, we unravel a particular sensitivity to partial APC/C inhibition in cancer-derived cells showing cohesion weakness in metaphase spreads. Our results point to a model in which cancers displaying reduced sister chromatid cohesion are prone to enter a fatal arrest upon a mild mitotic delay, presumably caused by a trigger of premature sister chromatid cohesion, keeping the SAC active. This may have implications for future treatment options of tumor cells with impaired sister chromatid cohesion (also see chapter 7 of this thesis, box 1).
Together, these findings suggest that cohesin-mutated tumors may possess specific sensitivities, which can specifically be targeted and create clinical benefits, for example for half a million patients worldwide with cohesin/STAG2-mutated tumors [12].

7. Aims and outline of this thesis

This thesis is centered on the DNA helicase DDX11. In 2010, bi-allelic mutations in the DDX11 gene were identified to underlie Warsaw Breakage Syndrome (WABS) and WABS cells displayed increased sensitivity to a number of DNA damaging drugs as well as spontaneous sister chromatid cohesion. Sequence analysis classified DDX11 as a FeS cluster DNA helicase, but its exact functions were incompletely understood. This thesis aimed to further elucidate the molecular activities and genetic interactions of DDX11, as well as the cellular and clinical consequences of DDX11 deficiency. Moreover, as defective sister chromatid cohesion is an emerging feature of tumor cells, DDX11 deficient cells served as a suitable model system to identify putative weak spots of cohesion defective cells as a lead for the development of novel cancer therapeutics.

Chapter 1 provides a general introduction of the regulation of sister chromatid cohesion and an overview of the molecular regulation of the cohesin complex. In chapter 2, we discuss the current understanding of the different syndromes related to cohesion dysfunction ('cohesinopathies') and their clinical features, genetic causes as well as their possible links with cancer predisposition. In chapter 3, we show that DDX11, as well as the Fanconi gene FANCM, are determinants of PARP inhibitor sensitivity. Genetic interactions of DDX11 are explored in Chapter 4 and 5. Chapter 4 reveals that DDX11 deficiency is synthetically lethal with impaired APC/C activity, due to cohesion fatigue resulting from prolonged metaphase duration in the presence of pulling forces of the mitotic spindle. We also demonstrate that tumor cells with cohesion defects can selectively be killed with the APC/C inhibitor apcin. In chapter 5, we show synthetic lethality of DDX11 and the acetyltransferase ESCO2, which is causally related to severely enhanced loss of sister chromatid cohesion. We also demonstrate that DDX11 is required for normal replication fork progression, hinting to a role for DDX11 at DNA replication forks. In chapter 6, we identify multiple new WABS patients and provide evidence that residual DDX11 activity is probably present in all WABS patients. We show that the helicase activity of DDX11 is essential for sister chromatid cohesion, which is in contrast with other reports. This chapter also reveals G-quadruplexes to be *in vivo* substrates for DDX11, possibly in the context of DNA replication forks. Finally, chapter 7 provides a summary and discussion of the findings presented in this thesis, as well as future perspectives.

.

References:

1. Hirano, T. The ABCs of SMC proteins: two-armed ATPases for chromosome condensation, cohesion, and repair. *Genes Dev.*16, 399–414 (2002).
2. Arumugam, P. *et al.* ATP Hydrolysis Is Required for Cohesin's Association with Chromosomes. *Curr. Biol.*13, 1941–1953 (2003).
3. Haering, C. H., Löwe, J., Hochwagen, A. & Nasmyth, K. Molecular Architecture of SMC Proteins and the Yeast Cohesin Complex. *Mol. Cell*9, 773–788 (2002).
4. Gligoris, T. G. *et al.* Closing the cohesin ring: structure and function of its Smc3-kleisin interface. *Science*346, 963–7 (2014).
5. Huis in 't Veld, P. J. *et al.* Characterization of a DNA exit gate in the human cohesin ring. *Science (80-.).*346, 968–972 (2014).
6. Zhang, N. *et al.* Characterization of the interaction between the cohesin subunits Rad21 and SA1/2. *PLoS One*8, e69458 (2013).
7. Zhang, J. *et al.* Acetylation of Smc3 by Eco1 is required for S phase sister chromatid cohesion in both human and yeast. *Mol. Cell*31, 143–51 (2008).
8. Losada, A., Yokochi, T., Kobayashi, R. & Hirano, T. Identification and characterization of SA/Scc3p subunits in the Xenopus and human cohesin complexes. *J. Cell Biol.*150, 405–16 (2000).
9. Remeseiro, S., Cuadrado, A., Gómez-López, G., Pisano, D. G. & Losada, A. A unique role of cohesin-SA1 in gene regulation and development. *EMBO J.*31, 2090–102 (2012).
10. Remeseiro, S. *et al.* Cohesin-SA1 deficiency drives aneuploidy and tumourigenesis in mice due to impaired replication of telomeres. *EMBO J.*31, 2076–89 (2012).
11. Canudas, S. & Smith, S. Differential regulation of telomere and centromere cohesion by the Scc3 homologues SA1 and SA2, respectively, in human cells. *J. Cell Biol.*187, 165–73 (2009).
12. van der Lelij, P. *et al.* Synthetic lethality between the cohesin subunits STAG1 and STAG2 in diverse cancer contexts. *Elife*6, (2017).
13. Muir, K. W. *et al.* Structure of the Pds5-Scc1 Complex and Implications for Cohesin Function. *Cell Rep.*14, 2116–2126 (2016).
14. Sumara, I., Vorlaufer, E., Gieffers, C., Peters, B. H. & Peters, J. M. Characterization of vertebrate cohesin complexes and their regulation in prophase. *J. Cell Biol.*151, 749–62 (2000).
15. Losada, A., Yokochi, T. & Hirano, T. Functional contribution of Pds5 to cohesin-mediated cohesion in human cells and Xenopus egg extracts. *J. Cell Sci.*118, 2133–41 (2005).
16. Neuwald, A. F. & Hirano, T. HEAT repeats associated with condensins, cohesins, and other complexes involved in chromosome-related functions. *Genome Res.*10, 1445–52 (2000).
17. Zhang, B. *et al.* Dosage effects of cohesin regulatory factor PDS5 on mammalian development: implications for cohesinopathies. *PLoS One*4, e5232 (2009).
18. Carretero, M., Ruiz-Torres, M., Rodríguez-Corsino, M., Barthelemy, I. & Losada, A. Pds5B is required for cohesion establishment and Aurora B accumulation at centromeres.

*EMBO J.*32, 2938–49 (2013).

19. Zhou, L. *et al.* The N-Terminal Non-Kinase-Domain-Mediated Binding of Haspin to Pds5B Protects Centromeric Cohesion in Mitosis. *Curr. Biol.*27, 992–1004 (2017).
20. Goto, Y. *et al.* Pds5 Regulates Sister-Chromatid Cohesion and Chromosome Bi-orientation through a Conserved Protein Interaction Module. *Curr. Biol.*27, 1005–1012 (2017).
21. Haering, C. H., Farcas, A.-M., Arumugam, P., Metson, J. & Nasmyth, K. The cohesin ring concatenates sister DNA molecules. *Nature*454, 297–301 (2008).
22. Huang, C. E., Milutinovich, M. & Koshland, D. Rings, bracelet or snaps: fashionable alternatives for Smc complexes. *Philos. Trans. R. Soc. Lond. B. Biol. Sci.*360, 537–42 (2005).
23. Milutinovich, M. & Koshland, D. E. Molecular biology. SMC complexes--wrapped up in controversy. *Science*300, 1101–2 (2003).
24. Blat, Y. & Kleckner, N. Cohesins bind to preferential sites along yeast chromosome III, with differential regulation along arms versus the centric region. *Cell*98, 249–59 (1999).
25. Hartman, T., Stead, K., Koshland, D. & Guacci, V. Pds5p is an essential chromosomal protein required for both sister chromatid cohesion and condensation in Saccharomyces cerevisiae. *J. Cell Biol.*151, 613–26 (2000).
26. Laloraya, S., Guacci, V. & Koshland, D. Chromosomal addresses of the cohesin component Mcd1p. *J. Cell Biol.*151, 1047–56 (2000).
27. Glynn, E. F. *et al.* Genome-wide mapping of the cohesin complex in the yeast Saccharomyces cerevisiae. *PLoS Biol.*2, E259 (2004).
28. Lengronne, A. *et al.* Cohesin relocation from sites of chromosomal loading to places of convergent transcription. *Nature*430, 573–8 (2004).
29. Ciosk, R. *et al.* Cohesin's binding to chromosomes depends on a separate complex consisting of Scc2 and Scc4 proteins. *Mol. Cell*5, 243–54 (2000).
30. Fernius, J. *et al.* Cohesin-dependent association of scc2/4 with the centromere initiates pericentromeric cohesion establishment. *Curr. Biol.*23, 599–606 (2013).
31. Watrin, E. *et al.* Human Scc4 is required for cohesin binding to chromatin, sister-chromatid cohesion, and mitotic progression. *Curr. Biol.*16, 863–74 (2006).
32. Takahashi, T. S., Yiu, P., Chou, M. F., Gygi, S. & Walter, J. C. Recruitment of Xenopus Scc2 and cohesin to chromatin requires the pre-replication complex. *Nat. Cell Biol.*6, 991–6 (2004).
33. Gillespie, P. J. & Hirano, T. Scc2 couples replication licensing to sister chromatid cohesion in Xenopus egg extracts. *Curr. Biol.*14, 1598–603 (2004).
34. Krantz, I. D. *et al.* Cornelia de Lange syndrome is caused by mutations in NIPBL, the human homolog of Drosophila melanogaster Nipped-B. *Nat. Genet.*36, 631–5 (2004).
35. Tonkin, E. T., Wang, T.-J., Lisgo, S., Bamshad, M. J. & Strachan, T. NIPBL, encoding a homolog of fungal Scc2-type sister chromatid cohesion proteins and fly Nipped-B, is mutated in Cornelia de Lange syndrome. *Nat. Genet.*36, 636–41 (2004).
36. Murayama, Y. & Uhlmann, F. Biochemical reconstitution of topological DNA binding by

the cohesin ring. *Nature*505, 367–71 (2014).

37. Kagey, M. H. *et al.* Mediator and cohesin connect gene expression and chromatin architecture. *Nature*467, 430–5 (2010).

38. Lopez-Serra, L., Kelly, G., Patel, H., Stewart, A. & Uhlmann, F. The Scc2-Scc4 complex acts in sister chromatid cohesion and transcriptional regulation by maintaining nucleosome-free regions. *Nat. Genet.*46, 1147–51 (2014).

39. Takahashi, T. S., Basu, A., Bermudez, V., Hurwitz, J. & Walter, J. C. Cdc7-Drf1 kinase links chromosome cohesion to the initiation of DNA replication in Xenopus egg extracts. *Genes Dev.*22, 1894–905 (2008).

40. Busslinger, G. A. *et al.* Cohesin is positioned in mammalian genomes by transcription, CTCF and Wapl. *Nature*544, 503–507 (2017).

41. Chao, W. C. H. *et al.* Structural Studies Reveal the Functional Modularity of the Scc2-Scc4 Cohesin Loader. *Cell Rep.*12, 719–25 (2015).

42. Hinshaw, S. M., Makrantoni, V., Kerr, A., Marston, A. L. & Harrison, S. C. Structural evidence for Scc4-dependent localization of cohesin loading. *Elife*4, e06057 (2015).

43. Buheitel, J. & Stemmann, O. Prophase pathway-dependent removal of cohesin from human chromosomes requires opening of the Smc3-Scc1 gate. *EMBO J.*32, 666–76 (2013).

44. Srinivasan, M. *et al.* The Cohesin Ring Uses Its Hinge to Organize DNA Using Non-topological as well as Topological Mechanisms. *Cell*173, 1508 (2018).

45. Murayama, Y. & Uhlmann, F. DNA Entry into and Exit out of the Cohesin Ring by an Interlocking Gate Mechanism. *Cell*163, 1628–1640 (2015).

46. Murayama, Y. DNA entry, exit and second DNA capture by cohesin: insights from biochemical experiments. *Nucleus*9, 492 (2018).

47. Hu, B. *et al.* ATP hydrolysis is required for relocating cohesin from sites occupied by its Scc2/4 loading complex. *Curr. Biol.*21, 12–24 (2011).

48. Arumugam, P., Nishino, T., Haering, C. H., Gruber, S. & Nasmyth, K. Cohesin's ATPase activity is stimulated by the C-terminal Winged-Helix domain of its kleisin subunit. *Curr. Biol.*16, 1998–2008 (2006).

49. Weitzer, S., Lehane, C. & Uhlmann, F. A model for ATP hydrolysis-dependent binding of cohesin to DNA. *Curr. Biol.*13, 1930–40 (2003).

50. Chapard C. *et al*. Sister DNA Entrapment between Juxtaposed Smc Heads and Kleisin of the Cohesin Complex. Mol Cell. 224-237 (2019).

51. Nishiyama, T. *et al.* Sororin mediates sister chromatid cohesion by antagonizing Wapl. *Cell*143, 737–49 (2010).

52. Heidinger-Pauli, J. M., Onn, I. & Koshland, D. Genetic evidence that the acetylation of the Smc3p subunit of cohesin modulates its ATP-bound state to promote cohesion establishment in Saccharomyces cerevisiae. *Genetics*185, 1249–56 (2010).

53. Rowland, B. D. *et al.* Building sister chromatid cohesion: smc3 acetylation counteracts an antiestablishment activity. *Mol. Cell*33, 763–74 (2009).

54. Samora, C. P. *et al.* Ctf4 Links DNA Replication with Sister Chromatid Cohesion

Establishment by Recruiting the Chl1 Helicase to the Replisome. *Mol. Cell*63, 371–84 (2016).

55. Mayer, M. L. Identification of Protein Complexes Required for Efficient Sister Chromatid Cohesion. *Mol. Biol. Cell*15, 1736–1745 (2004).

56. Xu, H., Boone, C. & Klein, H. L. Mrc1 is required for sister chromatid cohesion to aid in recombination repair of spontaneous damage. *Mol. Cell. Biol.*24, 7082–90 (2004).

57. Xu, H., Boone, C. & Brown, G. W. Genetic dissection of parallel sister-chromatid cohesion pathways. *Genetics*176, 1417–29 (2007).

58. Borges, V., Smith, D. J., Whitehouse, I. & Uhlmann, F. An Eco1-independent sister chromatid cohesion establishment pathway in S. cerevisiae. *Chromosoma*122, 121–34 (2013).

59. Waizenegger, I. C., Hauf, S., Meinke, A. & Peters, J. M. Two distinct pathways remove mammalian cohesin from chromosome arms in prophase and from centromeres in anaphase. *Cell*103, 399–410 (2000).

60. Dreier, M. R., Bekier, M. E. & Taylor, W. R. Regulation of sororin by Cdk1-mediated phosphorylation. *J. Cell Sci.*124, 2976–87 (2011).

61. Giménez-Abián, J. F. *et al.* Regulation of sister chromatid cohesion between chromosome arms. *Curr. Biol.*14, 1187–93 (2004).

62. Hauf, S. *et al.* Dissociation of cohesin from chromosome arms and loss of arm cohesion during early mitosis depends on phosphorylation of SA2. *PLoS Biol.*3, e69 (2005).

63. Liu, H., Rankin, S. & Yu, H. Phosphorylation-enabled binding of SGO1-PP2A to cohesin protects sororin and centromeric cohesion during mitosis. *Nat. Cell Biol.*15, 40–9 (2013).

64. Losada, A., Hirano, M. & Hirano, T. Cohesin release is required for sister chromatid resolution, but not for condensin-mediated compaction, at the onset of mitosis. *Genes Dev.*16, 3004–16 (2002).

65. Nishiyama, T., Sykora, M. M., Huis in 't Veld, P. J., Mechtler, K. & Peters, J.-M. Aurora B and Cdk1 mediate Wapl activation and release of acetylated cohesin from chromosomes by phosphorylating Sororin. *Proc. Natl. Acad. Sci. U. S. A.*110, 13404–9 (2013).

66. Sumara, I. *et al.*The dissociation of cohesin from chromosomes in prophase is regulated by Polo-like kinase. *Mol. Cell*9, 515–25 (2002).

67. Zhang, N., Panigrahi, A. K., Mao, Q. & Pati, D. Interaction of Sororin protein with polo-like kinase 1 mediates resolution of chromosomal arm cohesion. *J. Biol. Chem.*286, 41826–37 (2011).

68. Shintomi, K. & Hirano, T. Releasing cohesin from chromosome arms in early mitosis: opposing actions of Wapl-Pds5 and Sgo1. *Genes Dev.*23, 2224–36 (2009).

69. Birot, A. *et al.* A second Wpl1 anti-cohesion pathway requires dephosphorylation of fission yeast kleisin Rad21 by PP4. *EMBO J.*36, 1364–1378 (2017).

70. Sudakin, V., Chan, G. K. & Yen, T. J. Checkpoint inhibition of the APC/C in HeLa cells is mediated by a complex of BUBR1, BUB3, CDC20, and MAD2. *J. Cell Biol.*154, 925–36 (2001).

71. London, N. & Biggins, S. Signalling dynamics in the spindle checkpoint response. *Nat. Rev. Mol. Cell Biol.*15, 736–47 (2014).

72. Sharp-Baker, H. & Chen, R. H. Spindle checkpoint protein Bub1 is required for kinetochore localization of Mad1, Mad2, Bub3, and CENP-E, independently of its kinase activity. *J. Cell Biol.*153, 1239–50 (2001).

73. Brady, D. M. *et al.* Complex formation between Mad1p, Bub1p and Bub3p is crucial for spindle checkpoint function. *Curr. Biol.*10, 675–8 (2000).

74. Kraft, C. *et al.* Mitotic regulation of the human anaphase-promoting complex by phosphorylation. *EMBO J.*22, 6598–609 (2003).

75. Jia, L., Kim, S. & Yu, H. Tracking spindle checkpoint signals from kinetochores to APC/C. *Trends Biochem. Sci.*38, 302–11 (2013).

76. Sudakin, V. *et al.* The cyclosome, a large complex containing cyclin-selective ubiquitin ligase activity, targets cyclins for destruction at the end of mitosis. *Mol. Biol. Cell*6, 185–97 (1995).

77. Glotzer, M., Murray, A. W. & Kirschner, M. W. Cyclin is degraded by the ubiquitin pathway. *Nature*349, 132–138 (1991).

78. Pfleger, C. M. & Kirschner, M. W. The KEN box: an APC recognition signal distinct from the D box targeted by Cdh1. *Genes Dev.*14, 655–65 (2000).

79. Uhlmann, F., Wernic, D., Poupart, M. A., Koonin, E. V & Nasmyth, K. Cleavage of cohesin by the CD clan protease separin triggers anaphase in yeast. *Cell*103, 375–86 (2000).

80. Zou, H., McGarry, T. J., Bernal, T. & Kirschner, M. W. Identification of a vertebrate sister-chromatid separation inhibitor involved in transformation and tumorigenesis. *Science*285, 418–22 (1999).

81. Stemmann, O., Zou, H., Gerber, S. A., Gygi, S. P. & Kirschner, M. W. Dual inhibition of sister chromatid separation at metaphase. *Cell*107, 715–26 (2001).

82. Peters, N. T. & Kropf, D. L. Kinesin-5 motors are required for organization of spindle microtubules in Silvetia compressa zygotes. *BMC Plant Biol.*6, 19 (2006).

83. Deardorff, M. A. *et al.* HDAC8 mutations in Cornelia de Lange syndrome affect the cohesin acetylation cycle. *Nature*489, 313–7 (2012).

84. Deardorff, M. A., Porter, N. J. & Christianson, D. W. Structural aspects of HDAC8 mechanism and dysfunction in Cornelia de Lange syndrome spectrum disorders. *Protein Sci.*25, 1965–1976 (2016).

85. Chan, K.-L. *et al.* Cohesin's DNA exit gate is distinct from its entrance gate and is regulated by acetylation. *Cell*150, 961–74 (2012).

86. Yu, H. Magic Acts with the Cohesin Ring. *Mol. Cell*61, 489–491 (2016).

87. Chatterjee, A., Zakian, S., Hu, X.-W. & Singleton, M. R. Structural insights into the regulation of cohesion establishment by Wpl1. *EMBO J.*32, 677–87 (2013).

88. Ouyang, Z. *et al.* Structure of the human cohesin inhibitor Wapl. *Proc. Natl. Acad. Sci. U. S. A.*110, 11355–60 (2013).

89. Oikawa, K. *et al.*Expression of a novel human gene, human wings apart-like (hWAPL), is associated with cervical carcinogenesis and tumor progression. *Cancer Res.*64, 3545–9 (2004).

90. Tedeschi, A. *et al.* Wapl is an essential regulator of chromatin structure and chromosome

segregation. *Nature***501**, 564–568 (2013).

91. Ciosk, R. *et al.* An ESP1/PDS1 complex regulates loss of sister chromatid cohesion at the metaphase to anaphase transition in yeast. *Cell***93**, 1067–76 (1998).

92. Haarhuis, J. H. I. *et al.* WAPL-Mediated Removal of Cohesin Protects against Segregation Errors and Aneuploidy. *Curr. Biol.***23**, 2071–2077 (2013).

93. Kanke, M., Tahara, E., Huis In't Veld, P. J. & Nishiyama, T. Cohesin acetylation and Wapl-Pds5 oppositely regulate translocation of cohesin along DNA. *EMBO J.***35**, 2686–2698 (2016).

94. Zhu Z, Wang X. Roles of cohesin in chromosome architecture and gene expression. Semin Cell Dev Biol. 90:187-193 (2019).

95. Lu, X., Cui, J., Fu, M. & Wang, W. Human wings apart-like gene is specifically overexpressed in cervical cancer. *Oncol. Lett.***12**, 171–176 (2016).

96. Carvajal-Maldonado, D. *et al.* Perturbing cohesin dynamics drives MRE11 nuclease-dependent replication fork slowing. *Nucleic Acids Res.***47**, 1294 (2018).

97. Rankin, S. Sororin, the cell cycle and sister chromatid cohesion. *Cell Cycle***4**, 1039–42 (2005).

97. Schmitz, J. *et al.* Sororin is required for stable binding of cohesin to chromatin and for sister chromatid cohesion in interphase. *Curr. Biol.***17**, 630–6 (2007).

98. Lafont, A. L., Song, J. & Rankin, S. Sororin cooperates with the acetyltransferase Eco2 to ensure DNA replication-dependent sister chromatid cohesion. *Proc. Natl. Acad. Sci. U. S. A.***107**, 20364–9 (2010).

99. De, K., Sterle, L., Krueger, L., Yang, X. & Makaroff, C. A. Arabidopsis thaliana WAPL is essential for the prophase removal of cohesin during meiosis. *PLoS Genet.***10**, e1004497 (2014).

100. Zhang, N. & Pati, D. C-terminus of Sororin interacts with SA2 and regulates sister chromatid cohesion. *Cell Cycle***14**, 820–6 (2015).

101. Eichinger, C. S., Kurze, A., Oliveira, R. A. & Nasmyth, K. Disengaging the Smc3/kleisin interface releases cohesin from Drosophila chromosomes during interphase and mitosis. *EMBO J.***32**, 656–65 (2013).

102. Ladurner, R. *et al.* Sororin actively maintains sister chromatid cohesion. *EMBO J.***35**, 635–53 (2016).

103. Watrin, E., Demidova, M., Watrin, T., Hu, Z. & Prigent, C. Sororin pre-mRNA splicing is required for proper sister chromatid cohesion in human cells. *EMBO Rep.***15**, 948–55 (2014).

104. van der Lelij, P. *et al.* SNW1 enables sister chromatid cohesion by mediating the splicing of sororin and APC2 pre-mRNAs. *EMBO J.***33**, 2643–58 (2014).

105. Huang, C.-J. *et al.* The cohesion stabilizer sororin favors DNA repair and chromosome segregation during mouse oocyte meiosis. *Vitr. Cell. Dev. Biol. - Anim.***53**, 258–264 (2017).

106. Moldovan, G.-L., Pfander, B. & Jentsch, S. PCNA Controls Establishment of Sister

Chromatid Cohesion during S Phase. *Mol. Cell*23, 723–732 (2006).

107. Rudra, S. & Skibbens, R. V. Sister chromatid cohesion establishment occurs in concert with lagging strand synthesis. *Cell Cycle*11, 2114–21 (2012).

108. Terret, M.-E., Sherwood, R., Rahman, S., Qin, J. & Jallepalli, P. V. Cohesin acetylation speeds the replication fork. *Nature*462, 231–234 (2009).

109. Ivanov, M. P. *et al.* The replicative helicase MCM recruits cohesin acetyltransferase ESCO2 to mediate centromeric sister chromatid cohesion. *EMBO J.*37, e97150 (2018).

110. Minamino, M., Higashi, T. L., Bouchoux, C. & Uhlmann, F. Topological in vitro loading of the budding yeast cohesin ring onto DNA. *Life Sci. alliance*1, (2018).

111. Hou, F. & Zou, H. Two human orthologues of Eco1/Ctf7 acetyltransferases are both required for proper sister-chromatid cohesion. *Mol. Biol. Cell*16, 3908–18 (2005).

112. Whelan, G. *et al.* Cohesin acetyltransferase Esco2 is a cell viability factor and is required for cohesion in pericentric heterochromatin. *EMBO J.*31, 71–82 (2012).

113. Rahman, S., Jones, M. J. K. & Jallepalli, P. V. Cohesin recruits the Esco1 acetyltransferase genome wide to repress transcription and promote cohesion in somatic cells. *Proc. Natl. Acad. Sci. U. S. A.*112, 11270–5 (2015).

114. Minamino, M. *et al.*Esco1 Acetylates Cohesin via a Mechanism Different from That of Esco2. *Curr. Biol.*25, 1694–706 (2015).

115. Petronczki, M. *et al.* Sister-chromatid cohesion mediated by the alternative RF-CCtf18/Dcc1/Ctf8, the helicase Chl1 and the polymerase-alpha-associated protein Ctf4 is essential for chromatid disjunction during meiosis II. *J. Cell Sci.*117, 3547–59 (2004).

116. Ansbach, A. B. *et al.*RFCCtf18 and the Swi1-Swi3 complex function in separate and redundant pathways required for the stabilization of replication forks to facilitate sister chromatid cohesion in Schizosaccharomyces pombe. *Mol. Biol. Cell*19, 595–607 (2008).

117. Farina, A. *et al.* Studies with the human cohesin establishment factor, ChlR1. Association of ChlR1 with Ctf18-RFC and Fen1. *J. Biol. Chem.*283, 20925–36 (2008).

118. Leman, A. R. & Noguchi, E. Local and global functions of Timeless and Tipin in replication fork protection. *Cell Cycle*11, 3945–55 (2012).

119. Warren, C. D. *et al.* S-phase checkpoint genes safeguard high-fidelity sister chromatid cohesion. *Mol. Biol. Cell*15, 1724–35 (2004).

120. Errico, A. & Costanzo, V. Differences in the DNA replication of unicellular eukaryotes and metazoans: known unknowns. *EMBO Rep.*11, 270–278 (2010).

121. Leman, A. R., Noguchi, C., Lee, C. Y. & Noguchi, E. Human Timeless and Tipin stabilize replication forks and facilitate sister-chromatid cohesion. *J. Cell Sci.*123, 660–70 (2010).

122. Smith-Roe, S. L. *et al.* Timeless functions independently of the Tim-Tipin complex to promote sister chromatid cohesion in normal human fibroblasts. *Cell Cycle*10, 1618–24 (2011).

123. Sherwood, R., Takahashi, T. S. & Jallepalli, P. V. Sister acts: coordinating DNA replication and cohesion establishment. *Genes Dev.*24, 2723–31 (2010).

124. Onn, I., Heidinger-Pauli, J. M., Guacci, V., Unal, E. & Koshland, D. E. Sister chromatid cohesion: a simple concept with a complex reality. *Annu. Rev. Cell Dev. Biol.*24, 105–29

(2008).

125. Bharti, S. K. *et al.*Molecular functions and cellular roles of the ChlR1 (DDX11) helicase defective in the rare cohesinopathy Warsaw breakage syndrome. *Cell. Mol. Life Sci.*71, 2625–2639 (2014).

126. Wu, Y. *et al.* Biochemical characterization of Warsaw breakage syndrome helicase. *J. Biol. Chem.*287, 1007–21 (2012).

127. Hirano, T. Chromosome territories meet a condensin. *PLoS Genet.*8, e1002939 (2012).

128. Ding, D.-Q. *et al.*Meiotic cohesins modulate chromosome compaction during meiotic prophase in fission yeast. *J. Cell Biol.*174, 499–508 (2006).

129. Sun, M., Nishino, T. & Marko, J. F. The SMC1-SMC3 cohesin heterodimer structures DNA through supercoiling-dependent loop formation. *Nucleic Acids Res.*41, 6149–60 (2013).

130. Schalbetter, S. A. *et al.* SMC complexes differentially compact mitotic chromosomes according to genomic context. *Nat. Cell Biol.*19, 1071–1080 (2017).

131. Gibcus JH. *et al.* A pathway for mitotic chromosome formation. Science. 9;359(6376), (2018).

132. Challa, K., Lee, M.-S., Shinohara, M., Kim, K. P. & Shinohara, A. Rad61/Wpl1 (Wapl), a cohesin regulator, controls chromosome compaction during meiosis. *Nucleic Acids Res.*44, 3190–203 (2016).

133. Sjögren, C. & Nasmyth, K. Sister chromatid cohesion is required for postreplicative double-strand break repair in Saccharomyces cerevisiae. *Curr. Biol.*11, 991–5 (2001).

134. Ström, L. *et al.* Postreplicative recruitment of cohesin to double-strand breaks is required for DNA repair. *Mol. Cell*16, 1003–15 (2004).

135. Kim, K. P. *et al.* Sister cohesion and structural axis components mediate homolog bias of meiotic recombination. *Cell*143, 924–37 (2010).

136. Bauerschmidt, C. *et al.* Cohesin promotes the repair of ionizing radiation-induced DNA double-strand breaks in replicated chromatin. *Nucleic Acids Res.*38, 477–87 (2010).

137. Yazdi, P. T. *et al.* SMC1 is a downstream effector in the ATM/NBS1 branch of the human S-phase checkpoint. *Genes Dev.*16, 571–82 (2002).

138. Nasmyth, K. & Haering, C. H. Cohesin: its roles and mechanisms. *Annu. Rev. Genet.*43, 525–58 (2009).

139. Feeney, K. M., Wasson, C. W. & Parish, J. L. Cohesin: a regulator of genome integrity and gene expression. *Biochem. J.*428, 147–61 (2010).

140. Xu, H. *et al.* Rad21-cohesin haploinsufficiency impedes DNA repair and enhances gastrointestinal radiosensitivity in mice. *PLoS One*5, e12112 (2010).

141. Heidinger-Pauli, J. M., Unal, E., Guacci, V. & Koshland, D. The kleisin subunit of cohesin dictates damage-induced cohesion. *Mol. Cell*31, 47–56 (2008).

142. Kim, S.-T., Xu, B. & Kastan, M. B. Involvement of the cohesin protein, Smc1, in Atm-dependent and independent responses to DNA damage. *Genes Dev.*16, 560–70 (2002).

143. Luo, H. *et al.* Regulation of intra-S phase checkpoint by ionizing radiation (IR)-dependent and IR-independent phosphorylation of SMC3. *J. Biol. Chem.*283, 19176–83 (2008).

144. Watrin, E. & Peters, J.-M. The cohesin complex is required for the DNA damage-induced

G2/M checkpoint in mammalian cells. *EMBO J.*28, 2625–35 (2009).

145. Caron, P. *et al.* Cohesin protects genes against γH2AX Induced by DNA double-strand breaks. *PLoS Genet.*8, e1002460 (2012).

146. Tittel-Elmer, M. *et al.* Cohesin association to replication sites depends on rad50 and promotes fork restart. *Mol. Cell*48, 98–108 (2012).

147. Rudra, S. & Skibbens, R. V. Cohesin codes - interpreting chromatin architecture and the many facets of cohesin function. *J. Cell Sci.*126, 31–41 (2013).

148. McAleenan, A. *et al.* Post-replicative repair involves separase-dependent removal of the kleisin subunit of cohesin. *Nature*493, 250–4 (2013).

149. Castronovo, P. *et al.* Premature chromatid separation is not a useful diagnostic marker for Cornelia de Lange syndrome. *Chromosome Res.*17, 763–71 (2009).

150. Revenkova, E. *et al.* Cornelia de Lange syndrome mutations in SMC1A or SMC3 affect binding to DNA. *Hum. Mol. Genet.*18, 418–27 (2009).

151. Liu, J. *et al.* Transcriptional dysregulation in NIPBL and cohesin mutant human cells. *PLoS Biol.*7, e1000119 (2009).

152. Parelho, V. *et al.* Cohesins functionally associate with CTCF on mammalian chromosome arms. *Cell*132, 422–33 (2008).

153. Rubio, E. D. *et al.* CTCF physically links cohesin to chromatin. *Proc. Natl. Acad. Sci. U. S. A.*105, 8309–14 (2008).

154. Stedman, W. *et al.*Cohesins localize with CTCF at the KSHV latency control region and at cellular c-myc and H19/Igf2 insulators. *EMBO J.*27, 654–66 (2008).

155. Wendt, K. S. *et al.* Cohesin mediates transcriptional insulation by CCCTC-binding factor. *Nature*451, 796–801 (2008).

156. Mishiro, T. *et al.* Architectural roles of multiple chromatin insulators at the human apolipoprotein gene cluster. *EMBO J.*28, 1234–45 (2009).

157. Nasmyth, K. Disseminating the Genome: Joining, Resolving, and Separating Sister Chromatids During Mitosis and Meiosis. *Annu. Rev. Genet.*35, 673–745 (2001).

158. Dekker, J. & Mirny, L. The 3D Genome as Moderator of Chromosomal Communication. *Cell*164, 1110–1121 (2016).

159. Faure, A. J. *et al.* Cohesin regulates tissue-specific expression by stabilizing highly occupied cis-regulatory modules. *Genome Res.*22, 2163–75 (2012).

160. Schmidt, D. *et al.* A CTCF-independent role for cohesin in tissue-specific transcription. *Genome Res.*20, 578–88 (2010).

161. Mullenders, J. *et al.* Cohesin loss alters adult hematopoietic stem cell homeostasis, leading to myeloproliferative neoplasms. *J. Exp. Med.*212, 1833–50 (2015).

162. Losada, A. Cohesin in cancer: chromosome segregation and beyond. *Nat. Rev. Cancer*14, 389–393 (2014).

163. Mazumdar, C. *et al.* Leukemia-Associated Cohesin Mutants Dominantly Enforce Stem Cell Programs and Impair Human Hematopoietic Progenitor Differentiation. *Cell Stem Cell*17, 675–88 (2015).

164. Hill, V. K., Kim, J.-S. & Waldman, T. Cohesin mutations in human cancer. *Biochim. Biophys.*

*Acta*1866, 1–11 (2016).

165. Barber, T. D. *et al.* Chromatid cohesion defects may underlie chromosome instability in human colorectal cancers. *Proc. Natl. Acad. Sci. U. S. A.*105, 3443–8 (2008).

166. Rocquain, J. *et al.* Alteration of cohesin genes in myeloid diseases. *Am. J. Hematol.*85, 717–9 (2010).

167. Dolnik, A. *et al.* Commonly altered genomic regions in acute myeloid leukemia are enriched for somatic mutations involved in chromatin remodeling and splicing. *Blood*120, e83-92 (2012).

168. Kon, A. *et al.* Recurrent mutations in multiple components of the cohesin complex in myeloid neoplasms. *Nat. Genet.*45, 1232–7 (2013).

169. Brennan, C. W. *et al.* The somatic genomic landscape of glioblastoma. *Cell*155, 462–77 (2013).

170. Evers, L. *et al.* STAG2 is a clinically relevant tumor suppressor in pancreatic ductal adenocarcinoma. *Genome Med.*6, 9 (2014).

171. Jones, D. T. W. *et al.* Dissecting the genomic complexity underlying medulloblastoma. *Nature*488, 100–5 (2012).

172. Kim, M. S., An, C. H., Yoo, N. J. & Lee, S. H. Frameshift mutations of chromosome cohesion–related genes SGOL1 and PDS5B in gastric and colorectal cancers with high microsatellite instability. *Hum. Pathol.*44, 2234–2240 (2013).

173. Lu, L.-Y. *et al.* Polo-like kinase 1 is essential for early embryonic development and tumor suppression. *Mol. Cell. Biol.*28, 6870–6 (2008).

174. Mei, J., Huang, X. & Zhang, P. Securin is not required for cellular viability, but is required for normal growth of mouse embryonic fibroblasts. *Curr. Biol.*11, 1197–201 (2001).

175. Stephens, P. J. *et al.* The landscape of cancer genes and mutational processes in breast cancer. *Nature*486, 400–4 (2012).

176. Yamada, H. Y. *et al.* Haploinsufficiency of SGO1 results in deregulated centrosome dynamics, enhanced chromosomal instability and colon tumorigenesis. *Cell Cycle*11, 479–88 (2012).

177. Singh, V. P. & Gerton, J. L. Cohesin and human disease: lessons from mouse models. *Curr. Opin. Cell Biol.*37, 9–17 (2015).

178. Leiserson, M. D. M. *et al.*Pan-cancer network analysis identifies combinations of rare somatic mutations across pathways and protein complexes. *Nat. Genet.*47, 106–14 (2015).

179. Lawrence, M. S. *et al.* Discovery and saturation analysis of cancer genes across 21 tumour types. *Nature*505, 495–501 (2014).

180. Cancer Genome Atlas Research Network *et al.* Comprehensive Molecular Characterization of Papillary Renal-Cell Carcinoma. *N. Engl. J. Med.*374, 135–145 (2016).

181. Gelot, C. *et al.* The Cohesin Complex Prevents the End Joining of Distant DNA Double-Strand Ends. *Mol. Cell*61, 15–26 (2016).

182. Balbás-Martínez, C. *et al.* Recurrent inactivation of STAG2 in bladder cancer is not associated with aneuploidy. *Nat. Genet.*45, 1464–9 (2013).

183. Tirode, F. *et al.* Genomic landscape of Ewing sarcoma defines an aggressive subtype with co-association of STAG2 and TP53 mutations. *Cancer Discov.***4**, 1342–53 (2014).

184. Esiashvili, N., Goodman, M. & Marcus, R. B. Changes in incidence and survival of Ewing sarcoma patients over the past 3 decades: Surveillance Epidemiology and End Results data. *J. Pediatr. Hematol. Oncol.***30**, 425–30 (2008).

185. Solomon, D. A. *et al.* Mutational inactivation of STAG2 causes aneuploidy in human cancer. *Science***333**, 1039–43 (2011).

186. Solomon, D. A. *et al.* Frequent truncating mutations of STAG2 in bladder cancer. *Nat. Genet.***45**, 1428–1430 (2013).

187. Cotton, A. M. *et al.* Landscape of DNA methylation on the X chromosome reflects CpG density, functional chromatin state and X-chromosome inactivation. *Hum. Mol. Genet.***24**, 1528–39 (2015).

188. Cucco, F. *et al.* Mutant cohesin drives chromosomal instability in early colorectal adenomas. *Hum. Mol. Genet.***23**, 6773–8 (2014).

189. Welch, J. S. *et al.* The origin and evolution of mutations in acute myeloid leukemia. *Cell***150**, 264–78 (2012).

190. Walter, M. J. *et al.* Clonal architecture of secondary acute myeloid leukemia. *N. Engl. J. Med.***366**, 1090–8 (2012).

191. Taylor, C. F., Platt, F. M., Hurst, C. D., Thygesen, H. H. & Knowles, M. A. Frequent inactivating mutations of STAG2 in bladder cancer are associated with low tumour grade and stage and inversely related to chromosomal copy number changes. *Hum. Mol. Genet.***23**, 1964–74 (2014).

192. Repo, H. *et al.* The Expression of Cohesin Subunit SA2 Predicts Breast Cancer Survival. *Appl. Immunohistochem. Mol. Morphol. AIMM***24**, 615–621 (2016).

193. Kim, J.-S. *et al.* Intact Cohesion, Anaphase, and Chromosome Segregation in Human Cells Harboring Tumor-Derived Mutations in STAG2. *PLoS Genet.***12**, e1005865 (2016).

194. Mondal, G., Stevers, M., Goode, B., Ashworth, A. & Solomon, D. A. A requirement for STAG2 in replication fork progression creates a targetable synthetic lethality in cohesin-mutant cancers. *Nat. Commun.***10**, 1686 (2019).

195. Mullegama, S. V. *et al.* De novo loss-of-function variants in *STAG2* are associated with developmental delay, microcephaly, and congenital anomalies. *Am. J. Med. Genet. Part A* (2017). doi:10.1002/ajmg.a.38207

196. Di Benedetto, D. *et al.* Definition of minimal duplicated region encompassing the XIAP and STAG2 genes in the Xq25 microduplication syndrome. *Am. J. Med. Genet. A***164A**, 1923–30 (2014).

197. Kumar, R. *et al.* Increased STAG2 dosage defines a novel cohesinopathy with intellectual disability and behavioral problems. *Hum. Mol. Genet.***24**, 7171–81 (2015).

198. Mullegama, S. V. *et al.* Mutations in *STAG2* cause an X-linked cohesinopathy associated with undergrowth, developmental delay, and dysmorphia: Expanding the phenotype in males. *Mol. Genet. Genomic Med.***7**, e00501 (2019).

199. Xiao, T., Wallace, J. & Felsenfeld, G. Specific sites in the C terminus of CTCF interact with the SA2 subunit of the cohesin complex and are required for cohesin-dependent

insulation activity. *Mol. Cell. Biol.*31, 2174–83 (2011).

200. van der Lelij, P. *et al.* Warsaw breakage syndrome, a cohesinopathy associated with mutations in the XPD helicase family member DDX11/ChlR1. *Am. J. Hum. Genet.*86, 262–6 (2010).

201. de Lange, J. *et al.* Defective sister chromatid cohesion is synthetically lethal with impaired APC/C function. *Nat. Commun.*6, 8399 (2015).

202. McLellan, J. *et al.* Synthetic lethal genetic interactions that decrease somatic cell proliferation in Caenorhabditis elegans identify the alternative RFC CTF18 as a candidate cancer drug target. *Mol. Biol. Cell*20, 5306–13 (2009).

203. van der Lelij, P. *et al.* The cellular phenotype of Roberts syndrome fibroblasts as revealed by ectopic expression of ESCO2. *PLoS One*4, e6936 (2009).

204. Bailey, M. L. *et al.* Glioblastoma cells containing mutations in the cohesin component STAG2 are sensitive to PARP inhibition. *Mol. Cancer Ther.*13, 724–32 (2014).

205. Farmer, H. *et al.* Targeting the DNA repair defect in BRCA mutant cells as a therapeutic strategy. *Nature*434, 917–921 (2005).

206. Bryant, H. E. *et al.* Specific killing of BRCA2-deficient tumours with inhibitors of poly(ADP-ribose) polymerase. *Nature*434, 913–917 (2005).

207. Liu, Y. *et al.* Somatic mutation of the cohesin complex subunit confers therapeutic vulnerabilities in cancer. *J. Clin. Invest.*128, 2951–2965 (2018).

Chapter 2

Cohesinopathies: Clinical Features, Genetics and Cellular Characteristics

Atiq Faramarz, Rob Wolthuis and Job de Lange
to be submitted

Abstract

Cohesin is a multi-subunit protein complex associated with various aspects of multiplication and organization of the genome, including timely chromosome segregation, DNA replication, DNA damage repair, and control of gene expression. Mutations in regulators and structural components of the cohesin complex may impair or disrupt sister chromatid cohesion, such as observed in a class of genetic instability syndromes called cohesinopathies. Clinically, cohesinopathies are associated with a spectrum of developmental aberrations such as growth and mental retardation, microcephaly and congenital abnormalities. Thus far, four cohesinopathy syndromes have been identified. The most severe, Roberts/SC phocomelia syndrome (RBS), is caused by bi-allelic mutations in ESCO2[2].Cornelia de Lange syndrome (CdLS) is a result of mutations in SMC1A, SMC3, RAD21, HDAC8 or NIPBL [3-8]. Warsaw Breakage Syndrome (WABS) is associated with mutations in ChlR1/DDX11 [9-14,15]. Chronic Atrial and Intestinal Dysrhythmia (CAID), a recently characterized cohesinopathy syndrome, is caused by mutations in SGOL1 [16]. Finally, disorders related to altered SA2 dosage have been described[17-19]. How mutations in cohesin subunits or its interacting partners lead to a range of clinical symptoms observed in these cohesinopathies is not well understood. In this review, we discuss the current understanding of the different cohesinopathy syndromes including clinical features, genetic causes, underlying biology and their possible links with cancer predisposition.

Cohesin functions and molecular architecture

Cohesinopathy syndromes are related to impaired function of the cohesin protein complex. The large, circular structure of cohesin enables it to entrap chromosomes and thereby regulate multiple aspects of their organization.The canonical function of cohesin is to facilitate sister chromatid cohesion upon DNA duplication: keeping newly synthesized sister chromatids together from S phase until the spindle checkpointhas ensured their proper bi-orientation on the mitotic spindle prior to their controlled segregation in anaphase. The inter-molecular activity of cohesin that is needed to connect sister chromatids may also underlie its contribution to homologous recombination in post-replicative cells, possibly by keeping the repair template in close proximity of the broken strand [20]. In addition, cohesin possesses an intra-molecular activitythat promotes the formation of loops, which contributes to DNA condensation [21] and also mediates transcriptional insulation by CTCF binding [22,23]. Finally, cohesin may have distinctive roles in rDNA looping, rRNA synthesis and regulated protein translation [24-26].

The core of the cohesin ring is composed of SMC1A, SMC3 and RAD21. RAD21 also interacts with SA1 or SA2 and with PDS5A or PDS5B. The PDS5 subunits control cohesin's association with chromatin. DNA loading into pre-assembled cohesin rings is promoted by the loader complex, composed of NIPBL and MAU2 [27,28], whereas its release from DNA can be catalyzed by WAPL and PDS5[29,30]. The acetyltransferases ESCO1 and ESCO2 acetylate SMC3, which leads to stable closure of cohesin rings around duplicated chromosomes right after the DNA replication fork by counteracting the effects of WAPL [31,32]. Multiple phosphorylation events stimulate WAPL-dependent cohesin removal from chromosome arms during prophase. Cohesion around centromeric rings is specifically resistant to WAPL activity, as it is protected by the PP2A

phosphatase, which is specifically recruited to centromeres by SGOL1 [33,34]. When cells have properly aligned their chromosomes at the metaphase plate, these centromeric cohesin rings are subsequently removed through proteolytic cleavage by Separase, a protease that is liberated from its inhibitor Securin by Securin protein degradation at the metaphase to anaphase transition [35]. Deacetylation of SMC3 is subsequently mediated by HDAC8, which presumably enables efficient recycling of WAPL released cohesin complexes to be used in subsequent G1 phases. Mutations in a number of these cohesin components and regulators underlie several related developmental syndromes(*Figure 1*). Here we discuss the clinical features, genetic causes and cellular characteristics of these cohesinopathies, as well as their possible association with genomic instability and cancer predisposition.

Figure 1: Overview of sister chromatid cohesion proteins, associated with different cohesinopathy syndromes.

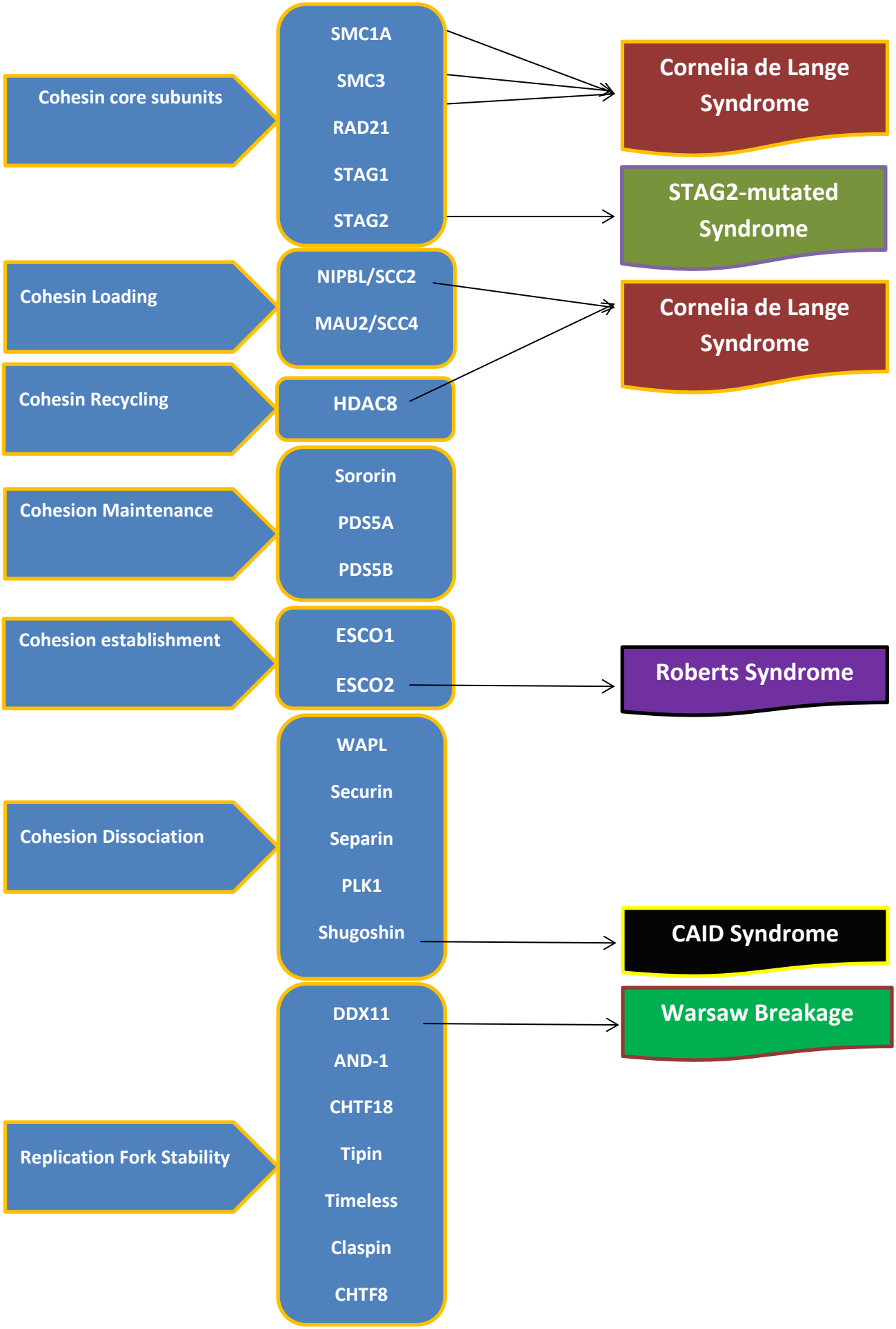

1. Cornelia de Lange Syndrome

1.1 Clinical features and genetics

Cornelia de Lange Syndrome (CdLS), also known as Brachmann de Lange Syndrome, is caused by autosomal dominant or X-linked mutations in NIPBL, SMC1A, SMC3, RAD21 or HDAC8 [3,4,6-8,36,37] and occurs in an estimated 1:10,000 live births [38]. CdLS patients display diverse clinical symptoms, involving various degrees of growth defects, intellectual disability, specific facial features, hearing loss and malformations in the upper extremities, heart and gastrointestinal systems [39,40].

The diagnosis of CdLS is mainly based on clinical abnormalities.Despite the known clinical features, mild cases of CdLS are not easy to recognize [40,41]. In order to certify the diagnosis, mutational analysis of the known CdLS genes is required. Since CdLS patients commonly carry NIPBL mutations, the sequence analysis of this gene is usually the initial step in DNA diagnostics [3,8,36], followed by sequencing of other candidate genes. Nevertheless, 20-30% of CdLS patients cannot be diagnosed due to the presence of somatic mosaicism or mutations in as yet unidentified genes [42,43].

The majority (around 65%) of CdLS cases is caused by mutations in NIPBL [26]. Deletions or mutations resulting in truncated NIPBL are correlated with more severe clinical abnormalities. On the other hand, patients with less damaging mutations, e.g. missense mutations and a common 3bp (in-frame) deletion in the SMC3 gene, display milder forms of CdLS [44,45]. It is worth to note that the position of the mutations within the gene may also correlate with disease severity. For example, deletion of exon 32 of NIPBL, which encodes a portion of the HEAT domain, gives rise to more severe clinical symptoms than the deletion of some other exons (e.g. exons 35-47) [45]. Recently, the X-linked gene HDAC8 was found to be mutated in 5% of CdLS. These HDAC8 CdLS patients display moderate clinical abnormalities [36]. The type of mutations identified thus far are missense mutations, nonsense mutations, frameshift mutations and chromosomal micro-deletions [46-48]. In addition, the hitherto reported mutations in the RAD21 gene are missense mutations, frameshift mutations and whole exon deletions [36,49]. Similar to SMC1A and SMC3 mutations these correlated with mild clinical phenotypes, although this conclusion is based on fewer CdLS cases diagnosed. Noteworthy, three CdLS patients with somatic mosaicism of mutated NIPBL and SMC3 genes were reported. While this small number precludes conclusions about genotype-phenotype correlation in these mosaic patients [43,50,51], nevertheless, taken together, the clinical severity of CdLS generally seems to correlate with the severity of the underlying mutations.

1.2 Affected cohesin functions in Cornelia de Lange Syndrome

How mutations of either cohesin core subunits (SMC1A, SMC3 and RAD21) or its regulatory genes (NIPBL, HDAC8) cause CdLS, is not yet clear. Possibly, cohesin's role in the regulation of gene expression, particularly those in developmental programs, might underliethe symptoms of CdLS [52,53]. Indeed, studies from vertebrate animal models, mice and zebrafish, have

demonstrated that NIPBL deficiency caused global gene expression changes, which are strongly correlated with CdLS-like developmental abnormalities [54]. Also, cells from CdLS display no obvious signs of defects in mitotic sister chromatid cohesion (*Figure 2*), which suggests that mainly non-replicative functions of cohesin are affected in these patients [55]. Cohesin has multiple functions that contribute to transcription regulation, such as acting as a facilitatorbetween promoters and distal enhancers, as well as stabilizing chromatin loops [56,57]. Consistent with this, NIPBL-mutated cells from mouse, human and other organisms are shown to have dysregulated gene expression but normal sister chromatid cohesion [52,53]. 1501 genes were demonstrated to be differentially expressed in CdLS cells, compared to control [52], and expression of certain genes was tightly associated with clinical severity of CdLS.

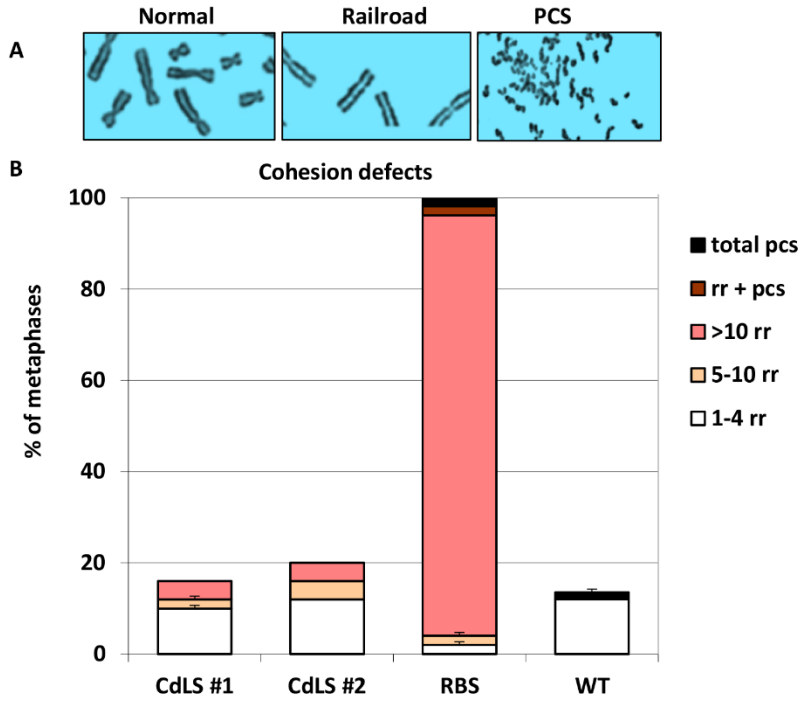

Figure 2.Examples of sister chromatid cohesion defects in lymphoblast cell lines of CdLS, RBS and WT.*(A)Examples of metaphase chromosomes with normal and railroad appearance, as well as premature chromatid separation (PCS) (B) Both CdLS cell lines show normal sister chromatid cohesion, comparable to WT. By contrast, the positive control, an RBS-derived cell line, shows defective sister chromatid cohesion. Analysis of is sister chromatid cohesion has been described previously [58].*

1.3 Cornelia de Lange syndrome and cancer predisposition

Single tumors were reported to co-occur with CdLS [59-62], including superasellar germinoma, papilloma of the choroid, adenocarcinoma of the esophagus, Wilms tumor and infantile haemangioendothelioma of the liver [59-61,63]. Nevertheless, the cancer incidence in CdLS patients does not appear to be increased significantly [62,64], suggesting that mutations in cohesion pathways associated with CdLS do not predispose to aneuploidy, genomic instability and cancer[65].

2. Roberts/SC phocomelia syndrome

2.1 Clinical features and genetics

Roberts/SC Phocomelia Syndrome (RBS) was first reported in 1919 by Johan B Roberts, who described three siblings born to consanguineous Italian parents [66]. Later, a very similar disease was described with ESCO2 mutations, called Pseudothalidomide or SC Phocomelia Syndrome [67]. At first, researchers regarded Roberts and SC Phocomelia Syndromes as two separate disorders but Zergollern and Hitrec concluded they overlapped as Roberts-SC Phocomelia syndrome [68]. Approximately 150 cases of RBS are reported worldwide. Life expectancy for RBS covers a fairly large range,varying from death at birth to approximately 30 years old.

Clinically, RBS is characterized by very diverse abnormalities that differ between affected individuals, even among the members of the same family. The majority of patients with RBS have shortened arm- and leg-bones (hypomelia), microcephaly, craniofacial defects, mental retardation and growth retardation [69,70]. The diagnosis of RBS is based on the clinical abnormalities, mutational analysis of the ESCO2 gene and cytogenetic testing, where metaphase spreads are analyzed for sister chromatid cohesion. RBS metaphase cells are mainly characterized by specific loss of cohesion at their centromeres, leading to so-called railroad (RR) chromosomes (***Figure 2, Figure 4***). RBS diagnosis, based only on clinical manifestations may be challenging because the RBS clinical phenotypes overlap with the clinical abnormalities of multiple other diseases, including Fanconi anemia and Cornelia de Lange syndrome [71].

The different types of ESCO2 mutations that have been reported so far lead either to total loss of protein expression or to impairment of its acetyltransferase activity. Interestingly, from the approximately thirty different types of ESCO2 mutations that have been confirmed, the majority were homozygous inactivating mutations (***Figure 3A***). In addition, several compound heterozygous mutations have been identified, of which 66% creates frameshift variants [72] (***Figure 3B***). Both the types and the locations of the ESCO2 mutations do not predict the diseases severity, suggesting that there might be no correlations between genotype and phenotype [70].

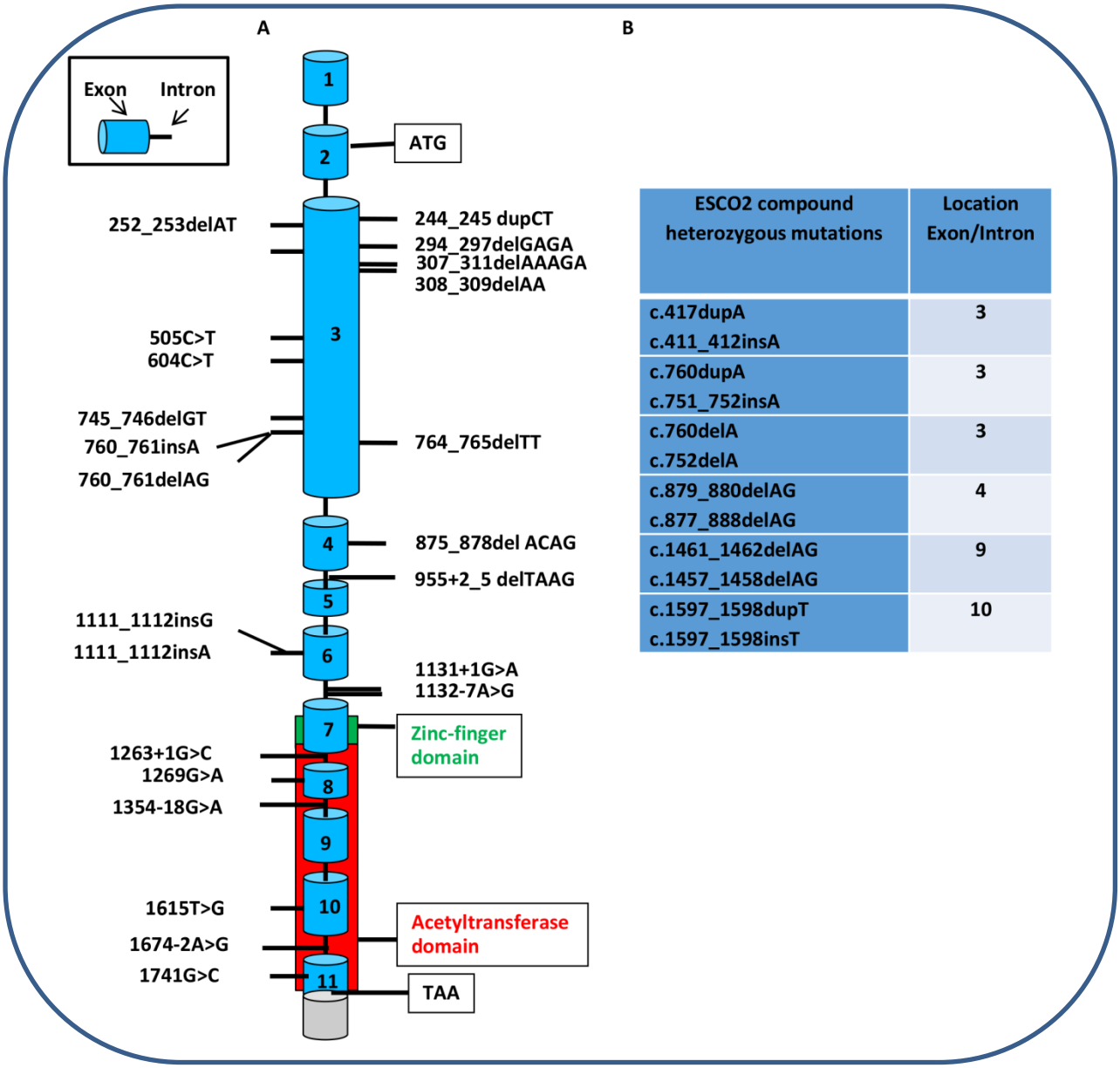

ESCO2 compound heterozygous mutations	Location Exon/Intron
c.417dupA c.411_412insA	3
c.760dupA c.751_752insA	3
c.760delA c.752delA	3
c.879_880delAG c.877_888delAG	4
c.1461_1462delAG c.1457_1458delAG	9
c.1597_1598dupT c.1597_1598insT	10

Figure 3.*(A) Illustration of the ESCO2 gene and the positions of homozygous mutations so far documented* [73]*. (B) List of compound heterozygous mutations identified in different RBS patients* [27].

2.2 Affected cohesin functions in Roberts syndrome

ESCO1 and ESCO2 (the two vertebrate homologs of yeast Eco1) are both zinc-finger-containing proteins with a highly conserved acetyltransferase domain and only differ in their N-termini[74]. Studies in various model organisms shed light on the involvement of ESCO2 in different biological processes. For example, mouse models revealed that loss of ESCO2 results in termination of development at pre-implantation and post-implantation stages of embryos [75]. Importantly, gene expression profiling in yeast and human suggested that the absence of Eco1 or ESCO2, respectively, inhibited protein translation and altered expression pattern of 1600

genes[76]. Experiments in yeast,zebrafish, and human cells showed that Eco1/ESCO2 mutations induce aberrant nucleolar arrangement, thereby reducing the production of ribosomal RNA (rRNA) [24,77]. At the cellular level, RBS metaphase cells are characterized by defects in sister chromatid cohesion (*Figure 4*). An early study showed that RBS cells havereduced proliferation rates, which may be an explanationfor the growth retardation of RBS patients [78]. In addition, ESCO2 has also been reported to interact with proteins involved in neurogenesis [79]. Of note, ESCO2 knockdown in zebrafish was recently reported to affect tissue and bone development by downregulating the expression of the cx43/gja1 gene[80], which encodes a member of connexin protein family. Cx43/gja1 is reported to be involved in intercellular communication and physiological processes such as normal embryonic development and coordinated contraction of hearth muscles [81]. Thus, reduced proliferation resulting from mitotic defects and elevated levels of apoptosis [82], reduced rRNA levels, impaired protein production and neural differentiation may all contribute to the clinical phenotypes in RBS.

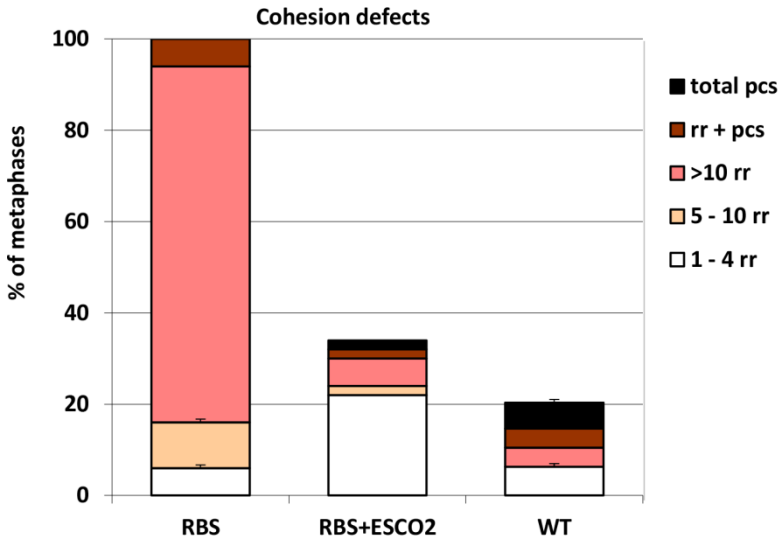

Figure 4.*Examples of sister chromatid cohesion analysis in RBS cells. Sister chromatid cohesion defects in RBS cells, RBS+ESCO2 cDNA and wild type cells. All RBS cells show defective sister chromatid cohesion, mostly railroads (RR) and some premature chromatid separation (PCS). Cohesion defects in RBS cells are rescued by the transfection of ESCO2 cDNA [71] (for sister chromatid analysis see legends of figure 2).*

2.3 Roberts syndrome and cancer predisposition

Cohesin and cohesin-interacting proteins are intimately involved in maintaining genome stability by preventing aneuploidy and gross chromosome alterations, which are considered to be hallmarks of cancer [83-85]. Some early studies reported a little higher frequency of aneuploidy and abnormal nuclear morphology in a number of RBS cases [78]. However, comparing multiple studies with RBS cells, there appear to be remarkably few connections between ESCO2

mutations and increased aneuploidy[86,87]. Notably, RBS cells show hypersensitivity to DNA damaging drugs like Mitomycin C, Camptothecin, Etoposide, and gamma radiation, suggesting that ESCO2 may play a role in different DNA repair pathways to preserve genome integrity [88,89]. So far, only three RBS individuals have been reported to develop cancer [69,90,91]. Recently, low expression of ESCO2 was reported in colorectal cancer to be associated with lymphatic and distant metastasis, accompanied with shorter overall/disease-free survival [92]. In zebrafish, ESCO2 mutations may result in genomic instability, aneuploidy, activation of DNA damage response and apoptosis [82]. Taken together,evidence linking ESCO2 mutations and RBS to aneuploidy and cancer development is limited. Attempts by our group (in collaboration with the group of Hein te Riele, NKI-AVL, Amsterdam) and others to generate RBS mouse models failed [93]. Heterozygous mice appeared to develop normally, but bi-allelic ESCO2 inactivation was lethal at pre-implantation stage [93]. Developing animal models with inducible and/or tissue-specific possibilities to knock-out ESCO2 might shed light on the question whether ESCO2 mutations contribute to aneuploidy and cancer. However, Hein te Riele's group showed that induced inactivation of ESCO2 was incompatible with proliferation of murine intestinal stem cells in vivo or mouse embryonic fibroblasts *in vitro* (data not shown).

3. Warsaw Breakage Syndrome

3.1 Clinical features and genetics

Warsaw breakage syndrome (WABS) was first diagnosed by our group in 2010 in a 14 years old male patient from Poland [14]. Afterwards, 22 more individuals were diagnosed to suffer from WABS [10-14, 15][*table 1*]. WABS is caused by bi-allelic mutations in the iron-sulfur containing helicase homologuous to yeast Chl1, named ChlR1 or DDX11.

Table1. Overview of DDX11 mutations found in WABS patients thus far.

	DDX11 Mutations	Protein	Predicted effect	Location	Reference
WABS01	IVS22+2T>C c.2689_2691del	p.Cys754Profs*9 p.Lys897del	frameshift in frame deletion	Intron 22 Exon 26	van der Lelij, P. et al (2010)
Case 2 (3 patients)	c.788G>A	p.Arg263Gln	missense	Exon 7	Capo-Chichi, J-M. et al (2013)
Case 3	IVS5+ 1G >A c.1888delC	splice site p.Arg630Glyfs*23	- frameshift	Intron 5 Exon 19	Bailey, C. et al (2015)
Case 4	IVS19-1G>A c.1523T>G	splice site p.Leu508Arg	- missense	Intron 19 Exon 16	Eppley, S et al (2017)
Case 5 Patient 1 Patient 2 Patient 3/4 Patient 5	c.606delC c.2372G>A c.1133G>C c.2576T>G c.2576T>G	p.Tyr202* p.Arg791Gln p.Arg378Pro p.Val859Gly p.Ala880Glyfs*94	frameshift missense missense missense frameshift	Exon 5 Exon 23 Exon 10 Exon 26	Alkhunaizi E, et al (2018)
Case 6 (2 patients)	c.907_920del c.2507T > C	p.Lys303Glufs*22 p.Leu836Pro	frameshift missense	Exon 9 Exon 25	Bottega R, et al (2019)
Case 7 (2 patients)	IVS1763-1G>C	splice site	-	Intron 17	Rabin R, et al (2019)
WABS02	c.169G>C IVS26-1G>A	p.Gly57Arg splice site	missense -	Exon 3 Intron 25	Chapter 3
WABS03	c.419G>A c.1403dup	p.Arg140Gln p.Gly472Valfs*	missense frameshift	Exon 4 Exon 13	Chapter 3
WABS04	c.1930G>A c2114G>A	p.Val644Met p.Cys705Tyr	missense missense	Exon 19 Exon 21	Chapter 3
WABS05 WABS06	c.1672C>T c.2571C>A	Arg558* p.Ser857Arg	frameshift missense	Exon 17 Exon 26	Chapter 3
WABS07* WABS08*	IVS17-1G>C c.1946-1948delGTC	splice site p.Gly650del	- in frame deletion	Intron 17 Exon 19	Chapter 3

**Fetus: (from WABS07 no material for DDX11 mutation analysis)*

WABS patients are clinically characterized by growth and mental retardation, microcephaly, abnormal skin pigmentations and, distinctively, deafness [14]. Because of the rarity of this syndrome, a standard protocol for the diagnosis of WABS is not available thus far. However, one can exploit the known clinical anomalies, WABS cellular sensitivity to camptothecin-induced chromosomal breakage, defects in sister chromatids cohesion and mutational analysis of DDX11.

The presence of the pseudogene DDX12p, which has 98% sequence similarity to DDX11, hampers the identification of DDX11 mutations [94]. In addition, multiple sub-telomeric DDX11L family members, derived from a portion of the primate DDX11 gene (with 98.5% sequence similarity with the exons 18, 22-25 and 3' UTR of DDX11)[95] further complicate the reliable sequencing of DDX11. Since only a limited number of WABS patients have been reported, a correlation between genotype and phenotype cannot be established yet.

Complete loss of DDX11 is lethal in mouse embryogenesis [96,97], and the known WABS patients have at least one missense/ not-truncating mutation. These observationssuggest that WABS cells retain at least some DDX11 functionality (Chapter 6 of this thesis). The exact mechanism whereby mutations in DDX11 give rise to WABS clinical phenotypes has yet to be established.

3.2 Affected cohesin functions in Warsaw Breakage Syndrome

DDX11 is an iron-sulfur domain containing helicase. Purified DDX11 enzyme from insect or human cells is able to unwind duplex DNA substrates with 5' or 3' single stranded overhangs in a 5' to 3' direction [94,98]. DDX11 is intimately involved in DNA replication by interacting both physically and genetically with replication-associated proteins and components of the DNA replication fork [99-101]. DDX11 is reported to interact with Ctf18-RFC, a PCNA loader complex, implicated in both replication fork stabilization and establishment of sister chromatid cohesion. Biochemical studies indicate that that PCNA and Ctf18-RFC enhance DDX11 helicase activity from 100bp to 500bp, and its absence leads to declined SMC3 acetylation [98]. Chl1 also interacts with Ctf4 (And1), a component of the replisome progression complex involved in lagging strand DNA synthesis. In yeast, Ctf4 contributes to establishment of sister chromatid cohesion [102]. The interaction of Ctf4-Chl1 was recently reported to depend on a Ctf4-Interacting Protein-(CIP) box which is essential for the establishment of sister chromatid cohesion and regulation of replication fork progression during S-phase [103]. In addition, DDX11 binds the lagging strand processing protein FEN1 and increases its flap endonuclease activity [98].

Since WABS cells show severe sister chromatid cohesion defects, including railroad track appearances (RR) and premature chromatid separation (PCS) (***Figure 5***) and DDX11/Chl1 is implicated at the replication fork, it is believed that DDX11 (or Chl1) functions to connect DNA replication to proper establishment of sister chromatid cohesion [103,104]. In addition, DDX11 is reported to be involved in Scc2 recruitment [105]. Experiments in yeast suggest that during S-phase, Chl1 plays a role in the recruitment of cohesin and its loader protein, Scc2 and this

recruitment affects cohesin acetylation and establishment of sister chromatid cohesion. In agreement with this, Chl1 mutant cells are shown to have diminished Smc3 acetylation[105].

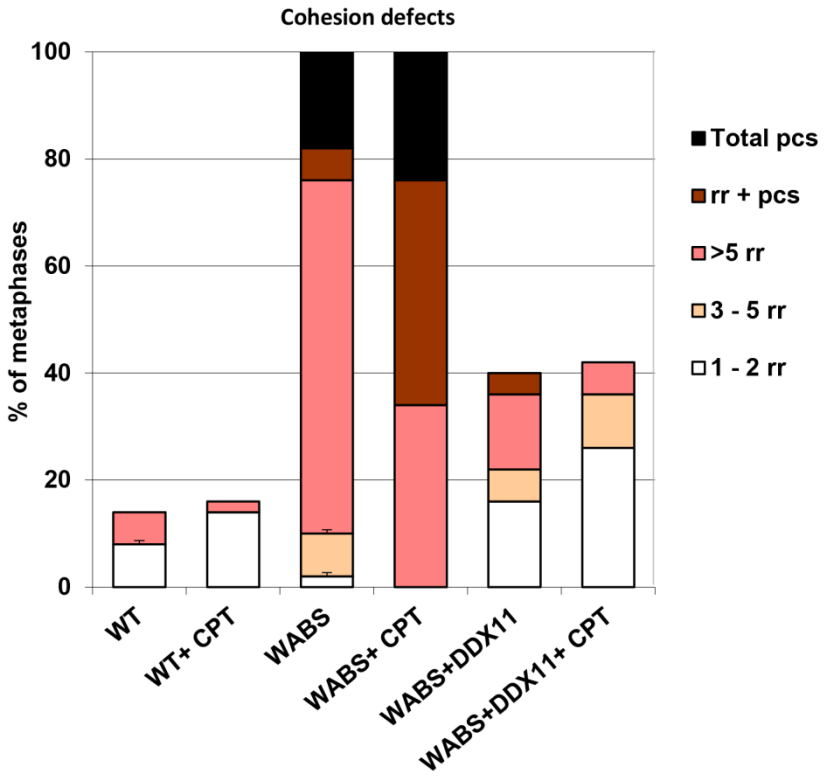

Figure 5:*Overview of sister chromatid cohesion defects in WABS lymphoblasts. Metaphases of WABS lymphoblast display almost 100% cohesion-defective chromatids. Upon treatment with the topoisomerase I inhibitor camptothecin, WABS cohesion defects shift from railroads to PCS. Overexpression of DDX11 in the WABS cells rescues the cytogenetic defects (for methods see legend figure 2).*

Furthermore, various studies in yeast and human point to the involvement of DDX11 in maintaining genome integrity through establishment of sister chromatid cohesion. Also, WABS cells are sensitive to different DNA-damaging agents, such as topoisomerase-I inhibitor Camptothecin, cross-linking agent Mitomycin C and PARP inhibitor [106] (Chapter 3 of this thesis), suggesting that DDX11 is also implemented in DNA damage repair pathways to preserve genomic stability [14]. Studies in mouse models showed that depletion of DDX11 causes embryonic lethality due to high frequency of aneuploidy and genomic instability [96,97]. Consistent with this, loss of DDX11 in mouse and Hela cells showed G2/M cell cycle arrest and apoptosis [96,97]. Furthermore, experiments in *C.elegans* demonstrated that DDX11 (Chl-1 in *C.elegans*) plays a role in chromosome stability and DNA repair [107].

We propose a model (***Figure 6***) and speculate how DDX11 contributes to establishment of sister chromatid cohesion. Since we and other groups reported that DDX11 is involved in resolving secondary DNA structures during replication of the lagging strand [108,109] (Chapter 5 and 6 of this thesis), smoothening DNA at replication fork by DDX11 might facilitate cohesion establishment

by ESCO1 and ESCO2 and support normal DNA replication fork progression. Alternatively, the inability to resolve such structures in the absence of DDX11 may lead to DNA double stranded breaks, repair of which requires WAPL/PDS5-dependent cohesin removal to provide access of repair factors to the break site (Benedict et al, submitted manuscript). Either way, this would inevitably lead to cohesion loss.

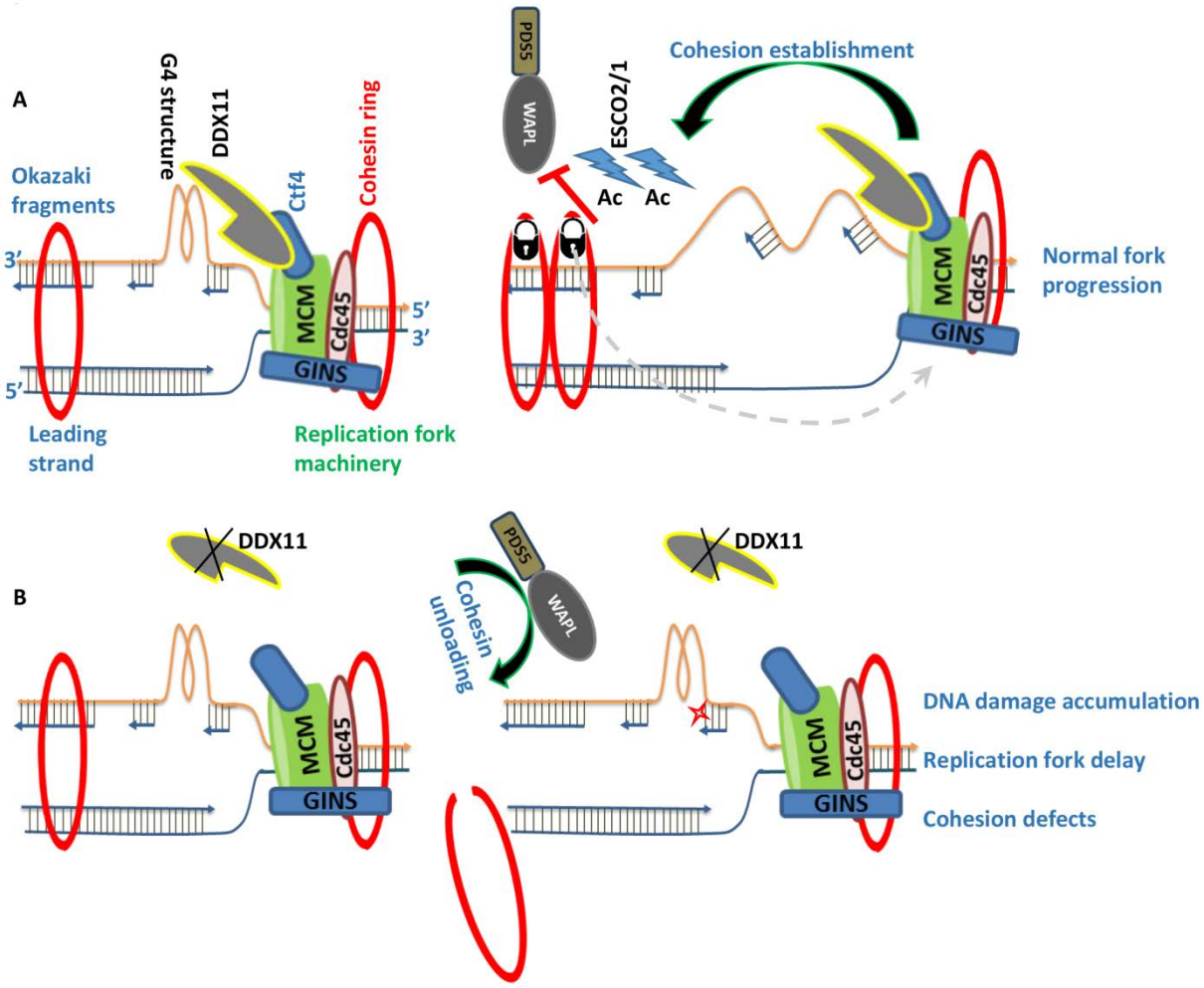

Figure 6:Proposed model showing the contribution of DDX11 in replication fork progression and sister chromatid cohesion. *(A) DDX11 is associated with dissolving secondary DNA structures such as G4, during DNA replication on the lagging strand. (B) In the absence of DDX11, unsolved G4-structure may lead to DNA double stranded breaks. The repair of these breaks requires removal of cohesins by WAPL/PDS5, to provide access of DNA repair machinery to the break site. This may eventually lead to cohesion loss at multiple sites throughout the genome.*

Future studies in model organisms with heterozygous deletion of DDX11 or mutations leading to haploinsufficiency might provide clues about DDX11 functions in development. Further, WABS patient cells and their complemented counterparts are powerful tools to be used for gene expression profiling, studying the role of DDX11 in controlling gene expression, especially genes controlling growth and development.

3.3 Warsaw Breakage Syndrome and cancer predisposition

Based on the small number of WABS cases, it is difficult to find a connection between DDX11 mutations in WABS patients and cancer predisposition. However, the DDX11 gene has been reported to play a role in survival of advanced melanomas [110], whereby, RNA expression analysis has shown 8 fold increase of DDX11 in first stage invasive melanoma cells, compared to noninvasive melanomas. In line with this and according whole cancer genome analyses, DDX11 was found to be highly upregulated in tumor tissues, suggesting that it may function as an oncogene[111]. Oppositely, DDX11 down-regulation has also been described in number of cancer cells, such as colorectal cancer, non-Hodgkin lymphoma, leading to sister chromatid cohesion defects and genomic instability [112,113]. In summary, despite the role of DDX11 in DNA replication and maintaining genome stability, its association with cancer predisposition remains unclear.

4. Chronic Atrial and Intestinal Dysrhythmia Syndrome

4.1 Clinical features and genetics

Chronic Atrial and Intestinal Dysrhythmia (CAID) was first reported in 2014 and is caused by mutation of the *SGOL1* (Shugoshin) gene [16]. The founder mutation, identified in a group of 16 French Canadians and 1 Swedish person, is a substitution of a highly conserved residue (c.67A>G; p.Lys23Glu in SGOL1), and predicted to be deleterious for protein function.

CAID is clinically characterized by a combination of abnormal heart rhythms (cardiac arrhythmias) and pseudo-obstruction of the intestine [16]. These clinical abnormalities are different compared to the common clinical abnormalities e.g. growth and mental retardation, of other cohesinopathies. However, at cellular level, CAID metaphase cells are shown to have defects in sister chromatid cohesion like in RBS and WABS, which characterizes CAID as a new member of the cohesinopathy family.

4.2 Shugoshin functions

The role of Shugoshin (SGOL1) in maintaining sister chromatid cohesion is well characterized [101]. Shugoshin, which means guardian spirit in Japanese, is a protein that safeguards centromeric cohesins against WAPL activity. WAPL activity increases during prophase and is responsible for unloading of arm cohesins [114], which also requires action of mitotic kinases Aurora B, PLK1 and Cyclin-dependent kinase 1 (CDK1), that phosphorylate two components of cohesin, SA2 and Sororin [115-118]. Centromeric cohesins are however protected by SGOL1 and its interacting partner, Protein Phosphatase 2 (PP2A), which counteract WAPL unloading activity [33,34]. As a result, SGOL1 depletion in cells of different organisms have severe consequences such as sister chromatid cohesion defects, mis-segregation and mitotic arrest [16,33]. How missense mutations in SGOL1 cause CAID clinical abnormalities remains unclear. It is remarkable that heart and intestinal tissues are particularly affected.

5. STAG2 cohesinopathy syndrome

5.1 Clinical phenotypes of STAG2-mutated Syndrome

An eight years old girl was recently diagnosed with a heterozygous nonsense mutation in the cohesin subunit STAG2, affecting normal protein expression. Based on the known role of SA2 as a cohesion subunit and the clinical phenotype of the patient, this disease is classified as a new cohesinopathy syndrome [19].

The patient suffers from developmental abnormalities, nervous system anomalies, microcephaly, deafness, craniofacial abnormalities and congenital heart defects, which are mainly similar to the other cohesinopathy syndromes. Analysis of patient's metaphase spreads showed normal sister chromatid cohesion, which is also in line with our findings where the inactivation of STAG2 does not lead to detectable sister chromatid cohesion defects (data not shown). Nevertheless, some studies have reported that depletion of SA2 may result in sister chromatid cohesion defects [119].

5.2 STAG2 functions

SA2, a HEAT repeat containing protein, binds to the cohesin complex via two SA-binding motifs in the RAD21 protein [120]. In vertebrates, two homologues exist: STAG1 (SA1) and STAG2. Cohesin interacts either with SA1 or SA2, but not both [121]. SA2-cohesin is believed to be involved in sister chromatid cohesion, whereas SA1-cohesin is predominantly associated with gene regulation [122]. SA2 also interacts with cohesion accessory proteins, such as PDS5 and Sororin, to maintain sister chromatid cohesion [31]. SA2 phosphorylation is demonstrated to play an important role in removing Sororin from cohesin complex and contributing to unloading of arm cohesins [Chapter 1 of this thesis]. Furthermore, SA2 is reported to be an important interacting partner of CCCTC-binding factor (CTCF) and this interaction is required for cohesin enrichment at specific loci through the genome, but not for cohesin loading onto DNA [22,123].

How STAG2 deficiency impacts normal development remains complex, due to its involvement in multiple processes of chromosome biology such as sister chromatid cohesion, transcription and tumorigenesis [23,119]. SA2-mutated syndrome cells provide a unique tool for studying the role of STAG2 in transcription and understand its involvement in human development. Also, identification of SA2 genetic and/or physical interactions would be important to understand more about its molecular functions.

5.3 Role of STAG2 mutations in cancer

STAG2 is strongly associated with tumorigenesis and is the most frequently mutated subunit of cohesin in various cancer types [Chapter 1 of this thesis]. How STAG2 mutation may lead to cancer remains under debate. Recently, a role of SA2 in DNA replication fork progression has been reported [124]. STAG2 knockout in RPE1 cells led to disruption of the interaction between

cohesin and replication forks, accompanied with stalled/collapsed replication forks and impaired SMC3 acetylation. In line with this, some evidence indicated that STAG2 mutations caused aneuploidy [119]. Thus, the absence of STAG2 may cause genomic instability and aneuploidy, facilitating the creation of oncogenic structural variants, such as gene amplification, deletion and rearrangement. Further, SA2 mutation in brain cancer cells, glioblastoma multiforme, was reported to affect the expression of other cohesin subunits, as well as the abundance of cohesin regulatory subunits to interact with cohesin core complex [125]. These findings suggest that decreased level of cohesin and its regulatory partners could be responsible for tumorigenesis by affecting many different cellular processes like sister chromatid cohesion, transcription, DNA damage repair and genomic stability.

6. Summary and conclusions

Cohesinopathies comprise a group of syndromes caused by defects in the regulators and structural components of the cohesin complex. The clinical and cellular consequences of these defects can be very diverse. Whereas the majority of the cohesinopathies share the same clinical abnormalities such as growth and mental retardation, symptoms from CAID syndrome do not conform to the characteristic pattern. At cellular level, CdLS and SA2-mutated syndrome, unlike other cohesinopathies, do not display sister chromatid cohesion defects. To date, five cohesinopathies are registered, CdLS, RBS, WABS, CAID and SA2-mutated syndrome, caused by a mutation in either one of nice genes. Furthermore, uncharacterized and sporadic cases of cohesinopathies were also reported in the literature. Recently, thanks to deep-sequencing techniques, seventeen patients from sixteen families were identified with STAG1 (encoding the cohesin subunit SA1) mutations [126]. These patients suffer from milder clinical phenotypes compared to the other cohesinopathies. Thus far, no functional studies, e.g. sister chromatid cohesion analysis, have been performed. Additionally, SA2 duplication in Xq25 duplication syndrome was reported to cause clinical abnormalities [17,18,126,127]. Xq25 duplication syndrome is an X-linked neurodevelopmental disorder characterized by developmental and intellectual abnormalities [127]. Initially, the size of duplication was believed to be very large, affecting multiple genes in these patients [128], but recent comparative genome hybridization assay on six new patients refined the critical duplicated region to only encompass the SA2 gene [127]. Increased copy number of the SA2 gene is believed to affect downstream target genes and high SA2 expression might be responsible for the patients' clinical phenotypes. Xq25 duplication syndrome was therefore considered as a new cohesinopathy. Further functional studies are required to understand how SA2 duplication can affect development.

7. Methods

Cohesion defect analysis For cohesion defect analysis, cells were incubated with 200 ng/mL Demecolcin (Sigma-Aldrich) in medium for 20 min, harvested, resuspended in 75 mM KCl for 20 min and fixed in methanol/acetic acid (3:1). Cells were dropped onto glass slides, stained with 5% Giemsa (Merck) and cohesion defects were microscopically analyzed. Per condition, 25 metaphases per slide were counted on two coded slides as technical replicate. For coding, we covered the text, randomly distributed the slides on the bench and numbered the slides in random order.

Reference

1. Vega, H. *et al.* Roberts syndrome is caused by mutations in ESCO2, a human homolog of yeast ECO1 that is essential for the establishment of sister chromatid cohesion. *Nat. Genet***37**, 468-470 (2005).
2. Deardorff, M.A. *et al.* Mutations in cohesin complex members SMC3 and SMC1A cause a mild variant of cornelia de Lange syndrome with predominant mental retardation. *Am J Hum Genet***80**, 485-494 (2007).
3. Deardorff, M.A. *et al.* RAD21 mutations cause a human cohesinopathy. *Am J Hum Genet***90**, 1014-1027 (2012).
4. Decroos, C. *et al.* Biochemical and structural characterization of HDAC8 mutants associated with Cornelia de Lange syndrome spectrum disorders. *Biochemistry***54**, 6501-6513 (2015).
5. Krantz, I.D. *et al.* Cornelia de Lange syndrome is caused by mutations in NIPBL, the human homolog of Drosophila melanogaster Nipped-B. *Nat. Genet***36**, 631-635 (2004).
6. Musio, A. *et al.* X-linked Cornelia de Lange syndrome owing to SMC1L1 mutations. *Nat Genet***38**, 528-530 (2006).
7. Tonkin, E.T., Wang, T.J., Lisgo, S., Bamshad, M.J. & Strachan, T. NIPBL, encoding a homolog of fungal Scc2-type sister chromatid cohesion proteins and fly Nipped-B, is mutated in Cornelia de Lange syndrome. *Nat. Genet***36**, 636-641 (2004).
8. Alkhunaizi, E. *et al.* Warsaw breakage syndrome: Further clinical and genetic delineation. *Am J Med Genet A***176**, 2404-2418 (2018).
9. Bailey, C., Fryer, A.E. & Greenslade, M. Warsaw Breakage Syndrome--A further report, emphasising cutaneous findings. *Eur J Med Genet***58**, 235-237 (2015).
10. Bottega, R. *et al.* Two further patients with Warsaw breakage syndrome. Is a mild phenotype possible? *Mol Genet Genomic Med*, e639 (2019).
11. Capo-Chichi, J.M. *et al.* Identification and biochemical characterization of a novel mutation in DDX11 causing Warsaw breakage syndrome. *Hum. Mutat***34**, 103-107 (2013).
12. Eppley, S., Hopkin, R.J., Mendelsohn, B. & Slavotinek, A.M. Clinical Report: Warsaw Breakage Syndrome with small radii and fibulae. *Am J Med Genet A***173**, 3075-3081 (2017).
13. van der Lelij, P. *et al.* Warsaw breakage syndrome, a cohesinopathy associated with mutations in the XPD helicase family member DDX11/ChlR1. *Am. J. Hum. Genet***86**, 262-266 (2010).
14. Rabin, R. *et al.* Study of carrier frequency of Warsaw breakage syndrome in the Ashkenazi Jewish population and presentation of two cases. *Am J Med Genet A***179**, 2144-2151 (2019).
15. Chetaille, P. *et al.* Mutations in SGOL1 cause a novel cohesinopathy affecting heart and gut rhythm. *Nat Genet***46**, 1245-1249 (2014).
16. Di Benedetto, D. *et al.* Definition of minimal duplicated region encompassing the XIAP and STAG2 genes in the Xq25 microduplication syndrome. *Am J Med Genet A***164A**, 1923-1930 (2014).
17. Kumar, R. *et al.* Increased STAG2 dosage defines a novel cohesinopathy with intellectual disability and behavioral problems. *Hum Mol Genet***24**, 7171-7181 (2015).
18. Mullegama, S.V. *et al.* De novo loss-of-function variants in STAG2 are associated with developmental delay, microcephaly, and congenital anomalies. *Am J Med Genet A***173**, 1319-1327 (2017).
19. Kim, B.J. *et al.* Genome-wide reinforcement of cohesin binding at pre-existing cohesin sites in response to ionizing radiation in human cells. *J. Biol. Chem***285**, 22784-22792 (2010).
20. Kagey, M.H. *et al.* Mediator and cohesin connect gene expression and chromatin architecture. *Nature***467**, 430-435 (2010).
21. Parelho, V. *et al.* Cohesins functionally associate with CTCF on mammalian chromosome arms. *Cell***132**, 422-433 (2008).
22. Wendt, K.S. *et al.* Cohesin mediates transcriptional insulation by CCCTC-binding factor. *Nature***451**, 796-801 (2008).

23. Bose, T. *et al.* Cohesin proteins promote ribosomal RNA production and protein translation in yeast and human cells. *PLoS. Genet***8**, e1002749 (2012).
24. Xu, B., Sowa, N., Cardenas, M.E. & Gerton, J.L. L-leucine partially rescues translational and developmental defects associated with zebrafish models of Cornelia de Lange syndrome. *Hum Mol Genet***24**, 1540-1555 (2015).
25. Zakari, M., Yuen, K. & Gerton, J.L. Etiology and pathogenesis of the cohesinopathies. *Wiley Interdiscip Rev Dev Biol***4**, 489-504 (2015).
26. Ciosk, R. *et al.* Cohesin's binding to chromosomes depends on a separate complex consisting of Scc2 and Scc4 proteins. *Mol Cell***5**, 243-254 (2000).
27. Watrin, E. & Peters, J.M. Cohesin and DNA damage repair. *Exp. Cell Res***312**, 2687-2693 (2006).
28. Kueng, S. *et al.*Wapl controls the dynamic association of cohesin with chromatin. *Cell***127**, 955-967 (2006).
29. Losada, A., Yokochi, T. & Hirano, T. Functional contribution of Pds5 to cohesin-mediated cohesion in human cells and Xenopus egg extracts. *J Cell Sci***118**, 2133-2141 (2005).
30. Carretero, M., Ruiz-Torres, M., Rodriguez-Corsino, M., Barthelemy, I. & Losada, A. Pds5B is required for cohesion establishment and Aurora B accumulation at centromeres. *EMBO J***32**, 2938-2949 (2013).
31. Nishiyama, T. *et al.* Sororin mediates sister chromatid cohesion by antagonizing Wapl. *Cell***143**, 737-749 (2010).
32. Katis, V.L., Galova, M., Rabitsch, K.P., Gregan, J. & Nasmyth, K. Maintenance of cohesin at centromeres after meiosis I in budding yeast requires a kinetochore-associated protein related to MEI-S332. *Curr Biol***14**, 560-572 (2004).
33. McGuinness, B.E., Hirota, T., Kudo, N.R., Peters, J.M. & Nasmyth, K. Shugoshin prevents dissociation of cohesin from centromeres during mitosis in vertebrate cells. *PLoS. Biol***3**, e86 (2005).
34. Uhlmann, F., Wernic, D., Poupart, M.A., Koonin, E.V. & Nasmyth, K. Cleavage of cohesin by the CD clan protease separin triggers anaphase in yeast. *Cell***103**, 375-386 (2000).
35. Deardorff, M.A. *et al.* HDAC8 mutations in Cornelia de Lange syndrome affect the cohesin acetylation cycle. *Nature***489**, 313-317 (2012).
36. Gillis, L.A. *et al.* NIPBL mutational analysis in 120 individuals with Cornelia de Lange syndrome and evaluation of genotype-phenotype correlations. *Am J Hum Genet***75**, 610-623 (2004).
37. Opitz, J.M. The Brachmann-de Lange syndrome. *Am J Med Genet***22**, 89-102 (1985).
38. Dorsett, D. & Krantz, I.D. On the molecular etiology of Cornelia de Lange syndrome. *Ann N Y Acad Sci***1151**, 22-37 (2009).
39. Kline AD1, K.I., Sommer A, Kliewer M, Jackson LG, FitzPatrick DR, Levin AV, Selicorni A Cornelia de Lange syndrome: clinical review, diagnostic and scoring systems, and anticipatory guidance. *Am J Med Genet A. 2007 Jun 15;143A(12):1287-96.* **2007 Jun 15;143A(12)**

1287-1296. (2007).
40. Barisic, I. *et al.* Descriptive epidemiology of Cornelia de Lange syndrome in Europe. *Am J Med Genet A***146A**, 51-59 (2008).
41. Banait, N., Fenton, A. & Splitt, M. Cornelia de Lange syndrome due to mosaic NIPBL mutation: antenatal presentation with sacrococcygeal teratoma. *BMJ Case Rep***2015** (2015).
42. Huisman, S.A., Redeker, E.J., Maas, S.M., Mannens, M.M. & Hennekam, R.C. High rate of mosaicism in individuals with Cornelia de Lange syndrome. *J Med Genet***50**, 339-344 (2013).
43. Cucco, F. & Musio, A. Genome stability: What we have learned from cohesinopathies. *Am J Med Genet C Semin Med Genet***172**, 171-178 (2016).
44. Mannini, L., Cucco, F., Quarantotti, V., Krantz, I.D. & Musio, A. Mutation spectrum and genotype-phenotype correlation in Cornelia de Lange syndrome. *Hum Mutat***34**, 1589-1596 (2013).

45. Feng, L., Zhou, D., Zhang, Z., Liu, Y. & Yang, Y. Exome sequencing identifies a de novo mutation in HDAC8 associated with Cornelia de Lange syndrome. *J Hum Genet***59**, 536-539 (2014).
46. Kaiser, F.J. *et al.* Loss-of-function HDAC8 mutations cause a phenotypic spectrum of Cornelia de Lange syndrome-like features, ocular hypertelorism, large fontanelle and X-linked inheritance. *Hum Mol Genet***23**, 2888-2900 (2014).
47. Parenti, I. *et al.* Expanding the clinical spectrum of the 'HDAC8-phenotype' - implications for molecular diagnostics, counseling and risk prediction. *Clin Genet***89**, 564-573 (2016).
48. Minor, A. *et al.* Two novel RAD21 mutations in patients with mild Cornelia de Lange syndrome-like presentation and report of the first familial case. *Gene***537**, 279-284 (2014).
49. Ansari, M. *et al.* Genetic heterogeneity in Cornelia de Lange syndrome (CdLS) and CdLS-like phenotypes with observed and predicted levels of mosaicism. *J Med Genet***51**, 659-668 (2014).
50. Pie, J. *et al.* Special cases in Cornelia de Lange syndrome: The Spanish experience. *Am J Med Genet C Semin Med Genet***172**, 198-205 (2016).
51. Liu, J. *et al.* Transcriptional dysregulation in NIPBL and cohesin mutant human cells. *PLoS Biol***7**, e1000119 (2009).
52. Revenkova, E. *et al.* Cornelia de Lange syndrome mutations in SMC1A or SMC3 affect binding to DNA. *Hum Mol Genet***18**, 418-427 (2009).
53. Kawauchi, S. *et al.* Using mouse and zebrafish models to understand the etiology of developmental defects in Cornelia de Lange Syndrome. *Am J Med Genet C Semin Med Genet***172**, 138-145 (2016).
54. Castronovo, P. *et al.*Premature chromatid separation is not a useful diagnostic marker for Cornelia de Lange syndrome. *Chromosome Res***17**, 763-771 (2009).
55. Faure, A.J. *et al.* Cohesin regulates tissue-specific expression by stabilizing highly occupied cis-regulatory modules. *Genome Res***22**, 2163-2175 (2012).
56. Mishiro, T. *et al.* Architectural roles of multiple chromatin insulators at the human apolipoprotein gene cluster. *EMBO J***28**, 1234-1245 (2009).
57. de Lange, J. *et al.* Defective sister chromatid cohesion is synthetically lethal with impaired APC/C function. *Nat. Commun***6**, 8399 (2015).
58. de Leon, F.C. *et al.* Brachmann-Cornelia de Lange syndrome with a papilloma of the choroid plexus: analyses of molecular genetic characteristics of the patient and the tumor. A single-case study. *Childs Nerv Syst***31**, 141-146 (2015).
59. DuVall, G.A. & Walden, D.T. Adenocarcinoma of the esophagus complicating Cornelia de Lange syndrome. *J Clin Gastroenterol***22**, 131-133 (1996).
60. Maruiwa, M. *et al.* Cornelia de Lange syndrome associated with Wilms' tumour and infantile haemangioendothelioma of the liver: report of two autopsy cases. *Virchows Arch A Pathol Anat Histopathol***413**, 463-468 (1988).
61. Santoro, C. *et al.* Unusual association of non-anaplastic Wilms tumor and Cornelia de Lange syndrome: case report. *BMC Cancer***16**, 365 (2016).
62. Sugita, K. *et al.* Cornelia de Lange syndrome associated with a suprasellar germinoma. *Brain Dev***8**, 541-546 (1986).
63. Liu, J. & Krantz, I.D. Cornelia de Lange syndrome, cohesin, and beyond. *Clin. Genet***76**, 303-314 (2009).
64. Kon, A. *et al.* Recurrent mutations in multiple components of the cohesin complex in myeloid neoplasms. *Nat Genet***45**, 1232-1237 (2013).
65. Roberts, J.B. Salvage of the Hand by Timely Reparative Surgery. *Ann Surg***70**, 627-632 (1919).
66. Herrmann, J. & Opitz, J.M. The SC phocomelia and the Roberts syndrome: nosologic aspects. *Eur J Pediatr***125**, 117-134 (1977).
67. Zergollern, L. & Hitrec, V. Four siblings with Robert's syndrome. *Clin Genet***21**, 1-6 (1982).

68. Schule, B., Oviedo, A., Johnston, K., Pai, S. & Francke, U. Inactivating mutations in ESCO2 cause SC phocomelia and Roberts syndrome: no phenotype-genotype correlation. *Am. J. Hum. Genet***77**, 1117-1128 (2005).
69. Vega, H. *et al.* Phenotypic variability in 49 cases of ESCO2 mutations, including novel missense and codon deletion in the acetyltransferase domain, correlates with ESCO2 expression and establishes the clinical criteria for Roberts syndrome. *J. Med. Genet***47**, 30-37 (2010).
70. van der Lelij, P., Oostra, A.B., Rooimans, M.A., Joenje, H. & de Winter, J.P. Diagnostic Overlap between Fanconi Anemia and the Cohesinopathies: Roberts Syndrome and Warsaw Breakage Syndrome. *Anemia***2010**, 565268 (2010).
71. Afifi, H.H. *et al.* Expanding the mutation and clinical spectrum of Roberts syndrome. *Congenit Anom (Kyoto)***56**, 154-162 (2016).
72. Gordillo, M. *et al.* The molecular mechanism underlying Roberts syndrome involves loss of ESCO2 acetyltransferase activity. *Hum. Mol. Genet***17**, 2172-2180 (2008).
73. Hou, F. & Zou, H. Two human orthologues of Eco1/Ctf7 acetyltransferases are both required for proper sister-chromatid cohesion. *Mol. Biol. Cell***16**, 3908-3918 (2005).
74. Whelan, G., Kreidl, E., Peters, J.M. & Eichele, G. The non-redundant function of cohesin acetyltransferase Esco2: some answers and new questions. *Nucleus***3**, 330-334 (2012).
75. Harris, B. *et al.* Cohesion promotes nucleolar structure and function. *Mol Biol Cell***25**, 337-346 (2014).
76. Xu, B., Lee, K.K., Zhang, L. & Gerton, J.L. Stimulation of mTORC1 with L-leucine rescues defects associated with Roberts syndrome. *PLoS Genet***9**, e1003857 (2013).
77. Tomkins, D.J. & Sisken, J.E. Abnormalities in the cell-division cycle in Roberts syndrome fibroblasts: a cellular basis for the phenotypic characteristics? *Am. J. Hum. Genet***36**, 1332-1340 (1984).
78. Leem, Y.E. *et al.* Esco2 promotes neuronal differentiation by repressing Notch signaling. *Cell Signal***23**, 1876-1884 (2011).
79. Banerji, R., Eble, D.M., Iovine, M.K. & Skibbens, R.V. Esco2 regulates cx43 expression during skeletal regeneration in the zebrafish fin. *Dev Dyn***245**, 7-21 (2016).
80. Pogoda, K., Kameritsch, P., Retamal, M.A. & Vega, J.L. Regulation of gap junction channels and hemichannels by phosphorylation and redox changes: a revision. *BMC Cell Biol***17 Suppl 1**, 11 (2016).
81. Percival, S.M. *et al.* Variations in dysfunction of sister chromatid cohesion in esco2 mutant zebrafish reflect the phenotypic diversity of Roberts syndrome. *Dis Model Mech***8**, 941-955 (2015).
82. Caron, P. *et al.* Cohesin protects genes against gammaH2AX Induced by DNA double-strand breaks. *PLoS Genet***8**, e1002460 (2012).
83. Cipressa, F. *et al.* A role for Separase in telomere protection. *Nat Commun***7**, 10405 (2016).
84. Gelot, C., Guirouilh-Barbat, J. & Lopez, B.S. The cohesin complex prevents the end-joining of distant DNA double-strand ends in S phase: Consequences on genome stability maintenance. *Nucleus***7**, 339-345 (2016).
85. German, J. Roberts' syndrome. I. Cytological evidence for a disturbance in chromatid pairing. *Clin Genet***16**, 441-447 (1979).
86. Tomkins, D., Hunter, A. & Roberts, M. Cytogenetic findings in Roberts-SC phocomelia syndrome(s). *Am J Med Genet***4**, 17-26 (1979).
87. Van den Berg, D.J. & Francke, U. Sensitivity of Roberts syndrome cells to gamma radiation, mitomycin C, and protein synthesis inhibitors. *Somat Cell Mol Genet***19**, 377-392 (1993).
88. van der Lelij, P. *et al.*The cellular phenotype of Roberts syndrome fibroblasts as revealed by ectopic expression of ESCO2. *PLoS. One***4**, e6936 (2009).
89. Ogilvy, C.S., Pakzaban, P. & Lee, J.M. Oculomotor nerve cavernous angioma in a patient with Roberts syndrome. *Surg Neurol***40**, 39-42 (1993).

90. Wenger, S.L. *et al.* Rhabdomyosarcoma in Roberts syndrome. *Cancer Genet Cytogenet***31**, 285-289 (1988).
91. Guo, X.B., Huang, B., Pan, Y.H., Su, S.G. & Li, Y. ESCO2 inhibits tumor metastasis via transcriptionally repressing MMP2 in colorectal cancer. *Cancer Manag Res***10**, 6157-6166 (2018).
92. Whelan, G. *et al.* Cohesin acetyltransferase Esco2 is a cell viability factor and is required for cohesion in pericentric heterochromatin. *EMBO J* (2011).
93. Hirota, Y. & Lahti, J.M. Characterization of the enzymatic activity of hChlR1, a novel human DNA helicase. *Nucleic Acids Res***28**, 917-924 (2000).
94. Costa, V. *et al.* DDX11L: a novel transcript family emerging from human subtelomeric regions. *BMC. Genomics***10**, 250 (2009).
95. Cota, C.D. & Garcia-Garcia, M.J. The ENU-induced cetus mutation reveals an essential role of the DNA helicase DDX11 for mesoderm development during early mouse embryogenesis. *Dev Dyn***241**, 1249-1259 (2012).
96. Inoue, A. *et al.* Loss of ChlR1 helicase in mouse causes lethality due to the accumulation of aneuploid cells generated by cohesion defects and placental malformation. *Cell Cycle***6**, 1646-1654 (2007).
97. Farina, A. *et al.* Studies with the human cohesin establishment factor, ChlR1. Association of ChlR1 with Ctf18-RFC and Fen1. *J. Biol. Chem***283**, 20925-20936 (2008).
98. Mayer, M.L. *et al.* Identification of protein complexes required for efficient sister chromatid cohesion. *Mol Biol Cell***15**, 1736-1745 (2004).
99. Petronczki, M. *et al.* Sister-chromatid cohesion mediated by the alternative RF-CCtf18/Dcc1/Ctf8, the helicase Chl1 and the polymerase-alpha-associated protein Ctf4 is essential for chromatid disjunction during meiosis II. *J. Cell Sci***117**, 3547-3559 (2004).
100. Rudra, S. & Skibbens, R.V. Sister chromatid cohesion establishment occurs in concert with lagging strand synthesis. *Cell Cycle***11**, 2114-2121 (2012).
101. Hanna, J.S., Kroll, E.S., Lundblad, V. & Spencer, F.A. Saccharomyces cerevisiae CTF18 and CTF4 are required for sister chromatid cohesion. *Mol Cell Biol***21**, 3144-3158 (2001).
102. Samora, C.P. *et al.* Ctf4 Links DNA Replication with Sister Chromatid Cohesion Establishment by Recruiting the Chl1 Helicase to the Replisome. *Mol Cell***63**, 371-384 (2016).
103. Borges, V., Smith, D.J., Whitehouse, I. & Uhlmann, F. An Eco1-independent sister chromatid cohesion establishment pathway in S. cerevisiae. *Chromosoma* (2013).
104. Rudra, S. & Skibbens, R.V. Chl1 DNA Helicase Regulates Scc2 Deposition Specifically during DNA-Replication in Saccharomyces cerevisiae. *PLoS. One***8**, e75435 (2013).
105. Stoepker, C. *et al.* DNA helicases FANCM and DDX11 are determinants of PARP inhibitor sensitivity. *DNA Repair (Amst)***26**, 54-64 (2015).
106. Chung, G., O'Neil, N.J. & Rose, A.M. CHL-1 provides an essential function affecting cell proliferation and chromosome stability in Caenorhabditis elegans. *DNA Repair (Amst)***10**, 1174-1182 (2011).
107. Bharti, S.K. *et al.* Molecular functions and cellular roles of the ChlR1 (DDX11) helicase defective in the rare cohesinopathy Warsaw breakage syndrome. *Cell Mol. Life Sci***71**, 2625-2639 (2014).
108. Wu, Y., Sommers, J., Khan, I., de, W.J. & Brosh, R. Biochemical characterization of Warsaw Breakage Syndrome helicase. *J. Biol. Chem* (2011).
109. Bhattacharya, C., Wang, X. & Becker, D. The DEAD/DEAH box helicase, DDX11, is essential for the survival of advanced melanomas. *Mol Cancer***11**, 82 (2012).
110. Pisani, F.M., Napolitano, E., Napolitano, L.M.R. & Onesti, S. Molecular and Cellular Functions of the Warsaw Breakage Syndrome DNA Helicase DDX11. *Genes (Basel)***9** (2018).
111. Barber, T.D. *et al.* Chromatid cohesion defects may underlie chromosome instability in human colorectal cancers. *Proc. Natl. Acad. Sci. U. S. A***105**, 3443-3448 (2008).
112. Perez-Benavente, B. *et al.* GSK3-SCF(FBXW7) targets JunB for degradation in G2 to preserve chromatid cohesion before anaphase. *Oncogene* (2012).

113. Yu, H. Magic Acts with the Cohesin Ring. *Mol Cell***61**, 489-491 (2016).
114. Dreier, M.R., Bekier, M.E., 2nd & Taylor, W.R. Regulation of sororin by Cdk1-mediated phosphorylation. *J Cell Sci***124**, 2976-2987 (2011).
115. Gimenez-Abian, J.F. *et al.* Regulation of sister chromatid cohesion between chromosome arms. *Curr. Biol***14**, 1187-1193 (2004).
116. Hauf, S. *et al.* Dissociation of cohesin from chromosome arms and loss of arm cohesion during early mitosis depends on phosphorylation of SA2. *PLoS. Biol***3**, e69 (2005).
117. Liu, H., Rankin, S. & Yu, H. Phosphorylation-enabled binding of SGO1-PP2A to cohesin protects sororin and centromeric cohesion during mitosis. *Nat. Cell Biol***15**, 40-49 (2013).
118. Solomon, D.A. *et al.* Mutational inactivation of STAG2 causes aneuploidy in human cancer. *Science***333**, 1039-1043 (2011).
119. Zhang, N. *et al.* Characterization of the interaction between the cohesin subunits Rad21 and SA1/2. *PLoS One***8**, e69458 (2013).
120. Sumara, I., Vorlaufer, E., Gieffers, C., Peters, B.H. & Peters, J.M. Characterization of vertebrate cohesin complexes and their regulation in prophase. *J Cell Biol***151**, 749-762 (2000).
121. Remeseiro, S., Cuadrado, A., Gomez-Lopez, G., Pisano, D.G. & Losada, A. A unique role of cohesin-SA1 in gene regulation and development. *EMBO J***31**, 2090-2102 (2012).
122. Busslinger, G.A. *et al.* Cohesin is positioned in mammalian genomes by transcription, CTCF and Wapl. *Nature***544**, 503-507 (2017).
123. Mondal, G., Stevers, M., Goode, B., Ashworth, A. & Solomon, D.A. A requirement for STAG2 in replication fork progression creates a targetable synthetic lethality in cohesin-mutant cancers. *Nat Commun***10**, 1686 (2019).
124. Kim, J.S. *et al.* Intact Cohesion, Anaphase, and Chromosome Segregation in Human Cells Harboring Tumor-Derived Mutations in STAG2. *PLoS Genet***12**, e1005865 (2016).
125. Lehalle, D. *et al.* STAG1 mutations cause a novel cohesinopathy characterised by unspecific syndromic intellectual disability. *J Med Genet***54**, 479-488 (2017).
126. Leroy, C. *et al.* Xq25 duplication: the crucial role of the STAG2 gene in this novel human cohesinopathy. *Clin Genet***89**, 68-73 (2016).
127. Philippe, A. *et al.* Xq25 duplications encompassing GRIA3 and STAG2 genes in two families convey recognizable X-linked intellectual disability with distinctive facial appearance. *Am J Med Genet A***161A**, 1370-1375 (2013).

Chapter 3

DNA Helicases FANCM and DDX11 Are Determinants of PARP Inhibitor Sensitivity

Stoepker C, Faramarz A, Rooimans MA, van Mil SE, Balk JA, Velleuer E, Ameziane N, Te Riele H, de Winter JP

Published in DNA Repair, 2015 Feb;26:54-64

Abstract

The encouraging response rates of BRCA1- and BRCA2-mutated cancers toward PARP inhibitors make it worthwhile to identify other potential determinants of PARP inhibitor responsiveness. Since the Fanconi anemia (FA) pathway coordinates several DNA repair pathways, including homologous recombination in which BRCA1 and BRCA2 play important roles, we investigated whether this pathway harbors other predictors of PARP inhibitor sensitivity. Lymphoblastoid cell lines derived from individuals with FA or clinically related syndromes, such as Warsaw breakage syndrome, were tested for PARP inhibitor sensitivity. Remarkably, we found a strong variability in PARP inhibitor sensitivity among different FANCD1/BRCA2-deficient lymphoblasts, suggesting that PARP inhibitor response depends on the type of FANCD1/BRCA2 mutation. We identified the DNA helicases FANCM and DDX11 as determinants of PARP inhibitor response. These results may extend the utility of PARP inhibition as effective anticancer treatment.

1. Introduction

Traditional cancer chemotherapy can cause severe side effects due to its aspecific action on normal cells [1]. One strategy to specifically kill cancer cells exploits the concept of synthetic lethality, in which simultaneous inactivation of two or more genes causes cell death, whereas inactivation of only one of these genes is tolerated [2–4]. Since tumor cells harbor genetic changes that are absent in normal cells, synthetic lethal targeting could be therapeutically advantageous. E.g., inhibition of the abundant and extensively studied enzyme poly (ADP-ribose) polymerase 1 (PARP-1) that plays an important role in the repair of DNA single strand breaks (SSBs) [5,6], was found to be lethal in tumors with mutations in BRCA1 or BRCA2 [7,8]. These tumors are deficient in repairing DNA double strand breaks (DSBs) by homologous recombination (HR) [9,10].

Therefore, the initial model for the synthetic lethal interaction between BRCA deficiency and PARP inhibition hypothesized that continuous inhibition of PARP leads to unrepaired SSBs, which are converted to DSBs during S phase. These breaks are irreparable in BRCA-deficient cells, and consequently lead to apoptosis [7,8]. An alternative model proposed that PARP inhibitors trap PARP-1 onto DNA repair intermediates, causing replication fork blocking lesions, which require homologous recombination to be repaired [11–13]. PARP as well as HR proteins have an important role in reactivating stalled replication forks, which might also explain the observed PARP-BRCA synthetic lethality [12,14,15].

Given the promising response of BRCA-mutated breast and ovarian cancers to PARP inhibitors [4,16], it is of interest to identify additional determinants of PARP inhibitor sensitivity, thereby extending their utility in cancer therapy. Recently, PALB2-, RAD51C- and SLX4-deficiency have been coupled to PARP inhibitor sensitivity [17–19]. Bi-allelic germ-line mutations in BRCA2, PALB2 or SLX4 cause Fanconi anemia (FA), a genomic instability syndrome characterized by congenital abnormalities, bone marrow failure and a high risk to develop cancer, whereas mutations in RAD51C lead to an FA-like syndrome [20–25]. To date, 16 FA proteins have been identified that act together in the FA pathway to repair DNA replication fork blocking lesions, such as DNA interstrand crosslinks [26,27]. FA proteins can be divided into two groups: the FA core complex consisting of FANCA, -B, -C, -E, -F, -G, -L and -M, which is required for the monoubiquitination of FANCD2-FANCI, and a group of proteins that function downstream or independently of this posttranslational modification (FANCD1/BRCA2, FANCJ/BRIP1, FANCN/PALB2, FANCO/RAD51C, FANCP/SLX4 and FANCQ/XPF).

Although FANCM is part of the FA core complex, it may also function outside the FA pathway to stabilize or re-initiate stalled replication forks [28]. In the present study, we used lymphoblasts and head and neck tumor cell lines from FA patients to investigate whether and to which extent deficiency in FA proteins confers PARP inhibitor sensitivity. In addition, lymphoblasts of individuals with cohesinopathies (e.g., Roberts syndrome and Warsaw break-age syndrome, which have some diagnostic overlap with FA) were tested for sensitivity to PARP inhibition.

2. Materials and methods

Cell culture

For an overview of all cell lines used in this study see Table 1. Epstein–Barr virus (EBV)-transformed lymphoblasts were cultured in RPMI1640 medium supplemented with 10% fetal bovine serum (FBS) and sodium pyruvate (1 mM). Fibroblasts immortalized with SV40 large T antigen and head and neck squamous carcinoma cell lines were grown in DMEM supplemented with 10% FBS and 1 mM sodium pyruvate. Stable cell lines: EUFA867- L + FANCA, EUFA867 HSC72OT fusion 1–3 and VU1202-L + DDX11, clones 1–3 were previously generated [29,30]. VU-SCC-1131 cells were functionally corrected by transduction with a phoenix retro- viral construct containing FANCC-GFP and selected on puromycin dihydrochloride (P8833, 1 μg/ml, Sigma). VU-SCC-1365 and VU- SCC-1604 cell lines stably expressing FANCA or FANCL, respectively, were generated by transfection with a pIRESneo construct containing cDNAs encoding FANCA-flag or flag-FANCL and selected on 400 μg/ml G418 sulfate (Calbiochem).

Cell growth inhibition assays

PARP inhibitor (KU0058948), cisplatin (CDDP), camptothecin and mitomycin C (MMC)-induced growth inhibition assays were performed as previously described [31]. In brief, cells were seeded in multiple flasks with increasing concentrations of the indicated drug. After untreated cells made 3 population doublings, the relative cell number compared to untreated cells for each drug concentration was determined using a Coulter counter.

Western blot analysis

For preparation of whole-cell extracts, cells were lysed for 10 min in lysis buffer (50 mM Tris–HCl (pH 7.4), 150 mM NaCl and 1% Triton X-100 supplemented with protease (complete EDTA free tablets, Roche) and phosphatase inhibitors (PhosSTOP, Roche)). Proteins were separated on a 3–8% Tris–Acetate NuPAGE gradient gel (Invitrogen) and transferred to Immobilon-P membrane overnight. The membrane was blocked with 5% dry milk in TBST (10 mM Tris–HCl (pH 7.4), 150 mM NaCl, 0.05% Tween-20) and incubated with the indicated primary antibodies. After washing with TBST, the membrane was incubated with horseradish peroxidase-conjugated secondary antibody and proteins were visualized with ECL (GE Healthcare). The following primary antibodies were used: rabbit polyclonal anti-BRCA2 (1:1000, A303- 434A, Bethyl Laboratories) and mouse monoclonal anti-FANCD2 (1:500, FI17, sc-20022, Santa Cruz Biotechnologies).

Immunofluorescence

Wild type, BRCA2-, DDX11- or FANCM-deficient lymphoblasts were treated with 100 nM MMC for 16 h and dropped onto Squarix Immunoselect® adhesion slides (Squarix biotechnology) in PBS. Immortalized fibroblasts and head and neck tumor cell lines were grown on sterile chamber slides (Nunc) and treated with 200 nM MMC for 16 h. Cells were pre-permeabilized

with 0.25% Triton X- 100 in PBS (1 min on ice) prior to fixation with 4% paraformaldehyde for 15 min at room temperature. Cells were permeabilized with 0.5% Triton X-100 in PBS (20 min at room temperature). Unspecific binding sites were blocked by incubating with 10% FBS in PBS for 1 h at room temperature. Slides were then incubated with rabbit anti-RAD51 (1:1000, a gift from Dr. R. Kanaar) overnight at 4 ◦C or with rabbit polyclonal anti-FANCD2 (1:200, NB100-182, Novus Bio- logicals) for 2 h at room temperature and washed with 0.2% Triton X-100. Subsequently, slides were incubated with goat anti-rabbit ALEXA488 (1:500, A-11008, Invitrogen) for 2 h at room temperature. After excess antibody was removed by washing with 0.2% Triton X-100, cells were counterstained with TO-PRO®-3 iodide (1:500, T3605, Invitrogen, for 15 min at room temperature), washed with PBS and embedded. Slides were analyzed with a confocal microscope (Carl Zeiss).

BRCA2 sequencing

The presence of BRCA2 mutations was examined by direct Sanger sequencing of the entire coding region and intron–exon boundaries on genomic DNA isolated from EBV-immortalized lymphoblasts. Primer pairs that were used are available on request.

Cell cycle analysis

Lymphoblasts were untreated or exposed for 7 days to PARP inhibitor (400 nM) and permeabilized in buffer containing 100 mM Tris–HCl (pH 7.5), 150 mM NaCl, 0.5 mM MgCl2, 1 mM CaCl2, 0.2% BSA and 0.1% IGEPAL (CA-630, Sigma). DNA was stained with PI/RNase staining buffer (BD Pharmingen) for 15 min and analyzed by flow cytometry.

Chromosomal breakage assay

Lymphoblasts were cultured for 48 h in the absence or presence of 2000 nM PARP inhibitor. After treatment with 200 ng/ml demecolcin (Sigma) for 30 min, cells were harvested, treated with 0.075 M KCl for 20 min at room temperature and fixed with 75% methanol, 25% acetic acid. Subsequently, cells were dropped onto glass slides and stained with 5% Giemsa (Merck). For each cell culture, 50 metaphases were analyzed for chromosomal break- age events. All scoring was performed on coded slides to prevent counting bias.

siRNA knockdown of BRCA2, DDX11 and FANCM in wild type fibroblasts

SV40-immortalized fibroblasts (Fen5280 SV) plated in 96-well plates were reverse transfected with siRNAs (final concentration 25 nM) targeting BRCA2, DDX11 and/or FANCM using Lipofectamine RNAiMAX (Invitrogen) according to the manufacturer's proto- col. Non-targeting siCONTROL#2 (siCON) (Dharmacon) was used as a negative control. Twenty-four hours following transfection, increasing concentrations of PARP inhibitor were added. After 5 days, cell viability was determined by the CellTiter-Blue assay (Promega).

Table 1

Cell line	Gender	Mutated Gene	Mutation 1 *Predicted protein change*	Mutation 2 *Predicted protein change*	Ref.
HSC93	?	Wild type	na	na	-
MAN-EBV	M	Wild type	na	na	-
RUFA-EBV	M	Wild type	na	na	-
VU012-L	M	Wild type	na	na	-
EUFA689-L	F	*FANCA*	c.3788_3790del	c.3788_3790del	[29]
			p.Phe1263del	*p.Phe1263del*	
HSC72OT	?	*FANCA*	Deletion exon 18-28	Deletion exon 18-28	[30]
			p.?	*p.?*	
HSC230	M	*FANCB*[a]	c.1856_1857insT	-	[31]
			*p.Arg619Serfs*39*		
		FANCD1	c.2808_2811del	c.9976A>T	[20]
		(/BRCA2)	*p.Ala938Profs*21*	*p.Lys3326**	
EUFA178-L	M	*FANCB*[a]	Deletion promoter_exon 1	-	[31]
			No protein		
EUFA1386-L	M	*FANCB*[a]	c.829dup	-	[31]
			*p.Cys277Leufs*31*		
EUFA158-L	F	*FANCC*	c.67del (also known as 322delG)	c.67del (also known as 322delG)	[32]
			*p.Asp23Ilefs*23*	*p.Asp23Ilefs*23*	
EUFA1289-L	M	*FANCD2*	c.206-2A>T	c.1414-71_1545+256del459	[33]
			*p.Ala69Aspfs*7*	*p.Glu472_Lys515del*	
EUFA816-L	M	*FANCI*	c.3853C>T	c.3350-88A>G	[34]
			*p.Arg1285**	*p.Glu1117fs*	
EUFA868-L	F	*FANCL*	c.837-15_837-9delins177	c.837-15_837-9delins177	[35]
			p.?	*p.?*	
EUFA867-L	F	*FANCM*	c.2171C>A	c.4222+1978_4300del	[36]
			*p.Ser724**	*p.?*	
		FANCA	c.2557C>T	c.709+5G>A	[37]
			*p.Arg853**	*p.?*	
HSC62	M	*FANCD1*	c.8488-1G>A	c.8488-1G>A	[20]
		(/BRCA2)	*p.Trp2830_Lys2833del*	*p.Trp2830_Lys2833del*	
EUFA208-L	F	*FANCD1*	c.7878G>C	c.756_757del	Current study
		(/BRCA2)	*p.Trp2626Cys*	*p.Asp252Glufs*2*	
EUFA423-L	F	*FANCD1*	c.7463_7464insAT	c.9672dup	[20]
		(/BRCA2)	*p.Asp2489**	*p.Tyr3225Ilefs*30*	
EUFA579-L	F	*FANCD1*	c.7007G>A	5609_5610delinsAG	[20]
		(/BRCA2)	*p.?*	*p.Phe1870**	
EUFA932-L	M	*FANCD1*	c.2957dup	c.7684T>C	Current study
		(/BRCA2)	*p.Asn986Lysfs*2*	*p.Phe2562Leu*	

Table 1 continued

EUFA943-L	M	*FANCD1*	c.480_489del	c.480_489del	Current study
		(/BRCA2)	*p.Gly162Phefs*7*	*p.Gly162Phefs*7*	
EUFA1389-L	F	*FANCD1*	c.1597del	Deletion exon 15-16	Current study
		(BRCA2)	*p.Thr533Leufs*25*	*p.?*	
EUFA696-L	F	*FANCJ*	c.2392C>T	c.2492+2dup	[38]
		(/BRIP1)	*p.Arg798**	*p.?*	
EUFA1341-L	F	*FANCN*	c.1653T>A	Deletion exon 1-10	[21]
		(/PALB2)	*p.Tyr551**	*p.?*	
EUFA1354-L	M	*FANCP*	c.286del	c.286del	[24]
		(/SLX4)	*p.Thr96Leufs*30*	*p.Thr96Leufs*30*	
FA104	F	*FANCQ*	c.1484_1488del	c.2065C>A	[27]
		(/XPF)	*p.Thr495Asnfs*6*	*p.Arg689Ser*	
VU1177-L	F	*ESCO2*	c.1111dup	c.1111dup	[39]
			*p.Thr371Asnfs*32*	*p.Thr371Asnfs*32*	
VU1199-L	M	*ESCO2*	c.879_880del	c.879_880del	[39]
			*p.Arg293Serfs*7*	*p.Arg293Serfs*7*	
VU1202-L	M	*DDX11*	c.2689_2691del	c.2271+2T>C	[40]
			p. Lys897del	*p.?*	
CdLS11165	M	*NIPBL*[b]	c.3813_3815del	-	[41]
			p.Lys1271del		
CdLS11167	F	*NIPBL*[b]	c.3940dup	-	[41]
			*p.Thr1314Asnfs*9*		
EUFA1341F SV40	F	*FANCN*	c.1653T>A	Deletion exon 1-10	[21]
		(/PALB2)	*p.Tyr551**	*p.?*	
VU1199F SV40	M	*ESCO2*	c.879_880del	c.879_880del	[39]
			*p.Arg293Serfs*7*	*p.Arg293Serfs*7*	
VU-SCC-1131	F	*FANCC*	c.67del (also known as 322delG)	c.67del (also known as 322delG)	[42]
			*p.Asp23Ilefs*23*	*p.Asp23Ilefs*23*	
VU-SCC-1365	M	*FANCA*	c.3788-3790del	c.3788-3790del	[42]
			p. Phe1263del	*p.Phe1263del*	
VU-SCC-1604	F	*FANCL*	c.483_487del	c.906C>G	Current study
			*p.Glu161Aspfs*31*	*p.Ile302Met*	

[a] *X-linked inheritance,* [b] *autosomal dominant inheritance. Na = not applicable, F = female, M = male. All lymphoblastoid cell lines and fibroblasts were EBV- or SV40-immortalized, respectively. The following transcript reference sequences were used: FANCA NM_000135.2; FANCB NM_001018113.1; FANCC NM_000136.2; FANCD1/BRCA2 NM_000059.3; FANCD2 NM_001018115.1; FANCI NM_001113378.1; FANCL NM_001114636.1; FANCM NM_020937.2; BRIP1/FANCJ NM_032043.2; PALB2/FANCN NM_024675.3; SLX4/FANCP NM_032444.2; XPF/FANCQ NM_005236.2; ESCO2 NM_001017420.2; DDX11 NM_030653.3 and NIPBL NM_015384.4.*

3. Results

3.1. PARP inhibitor sensitivity depends on the type of BRCA2 mutation

Complementation group D1 of the genomic instability syndrome Fanconi anemia (FA) was found to be caused by bi-allelic mutations in the well-known breast cancer susceptibility gene BRCA2 [20]. Since BRCA2-deficient breast cancer cells are hypersensitive to PARP inhibitors [7,8], we examined whether BRCA2-deficient EBV-immortalized lymphoblastoid cell lines derived from FA-D1 patients are also sensitive to PARP inhibition. None of the wild type lymphoblasts was sensitive to the PARP inhibitor Olaparib (KU0058948), as compared to BRCA2- deficient EUFA423 lymphoblasts (***Fig. 1a***). Remarkably, there was a large difference in IC50 values between different BRCA2-defective lymphoblastoid cell lines: EUFA943 lymphoblasts were the most sensitive with an IC50 value of 4.0 ± 0.8 nM, whereas HSC62 cells were only marginally sensitive (IC50 356.6 30.0 nM) (***Fig. 1b***). These cell lines were also the most and least sensitive, respectively, to other DNA damaging agents, such as mitomycin C (MMC) (***Fig. 1c***) or camptothecin (***Fig. 1d***). Hence, in these cell lines, PARP inhibitor sensitivity was correlated with MMC and camptothecin sensitivity. To elucidate why some BRCA2-deficient lymphoblasts were more sensitive to PARP inhibitor than others, BRCA2 expression and RAD51 focus formation were investigated (for an overview of all data see ***Fig. 1g***). Previously, Howlett et al. [20] demonstrated that EUFA423 and HSC62 cells express a truncated BRCA2 protein, which we clearly confirmed for EUFA423 cells (***Fig. 1e***). The distinction between normal size or truncated BRCA2 protein is difficult to visualize with Western blotting for HSC62 cells, because this cell line expresses BRCA2 protein with an in-frame deletion of only 4 amino acids. BRCA2 expression was not or hardly observed in three highly sensitive cell lines (EUFA943- L, EUFA579-L and EUFA1389-L), however, in another sensitive cell line, EUFA208-L, BRCA2 protein of approximately normal size was detected. The absence of BRCA2 protein expression can be explained by a frameshift mutation (c.1597del) and a large deletion of exon 15–16 in EUFA1389 cells, a homozygous frameshift mutation (c.480-489del) in EUFA943 cells and a splice site (c.7007G > A) and nonsense mutation (c.5609 5610delinsAG) in EUFA579 cells (see ***Table 1*** and ***Fig. 1g*** for an overview of mutations present in our panel of cell lines). In EUFA208 and in EUFA932 cells, one frameshift and one missense mutation in BRCA2 were found. The missense mutations were both present in the BRCA2 helical domain, which interacts with SHFM1/DSS1 [44,45]. This interaction is important for homologous recombination and hence contributes to genomic stability [46,47]. Despite the fact that both cell lines expressed BRCA2, EUFA208 cells (IC50 7.2 ± 2.1 nM) were more sensitive to PARP inhibitor than EUFA932 cells (IC50 121.8 71.8 nM). BRCA2 recruits RAD51 to double strand breaks to mediate homologous recombination [48,49]. To assess if HR repair activity was affected in FA-D1 lymphoblasts expressing mutant BRCA2 pro- tein, MMC-induced RAD51 nuclear focus formation was analyzed by immunofluorescence as an indirect marker of HR. Upon treatment with MMC, RAD51 focus formation was only unambiguously observed in wild type HSC93 lymphoblasts and in the least sensitive HSC62 cells (***Fig. 1g***), suggesting that the mutant BRCA2

protein in HSC62 has partial activity. The mild phenotype of HSC62 cells was also reflected in the clinical characteristics of the FA patient of whom this cell line was derived.

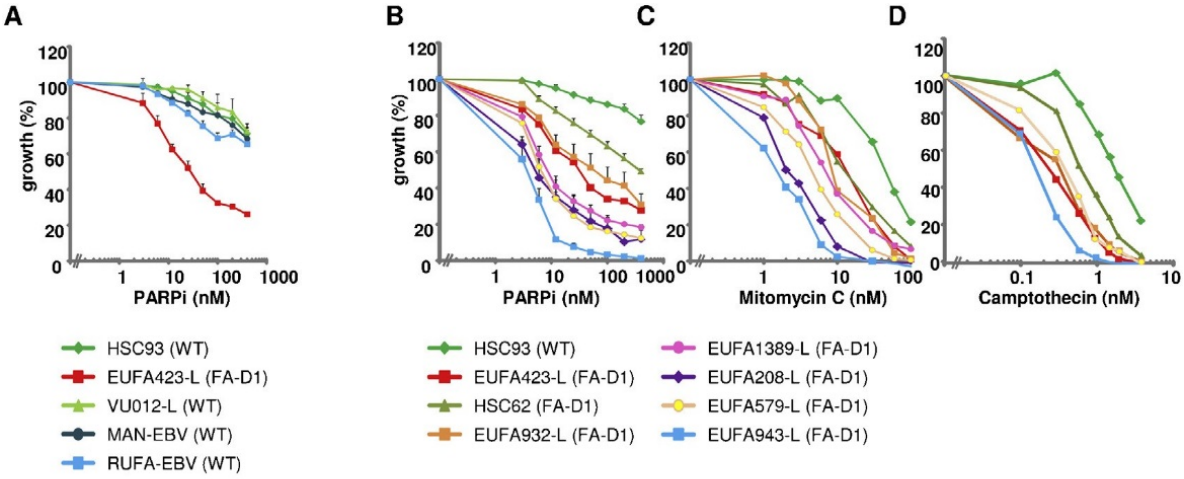

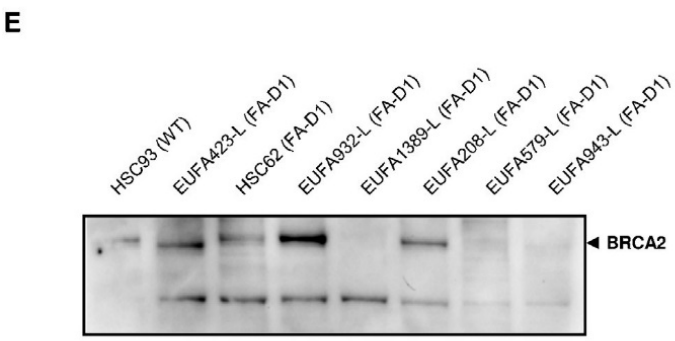

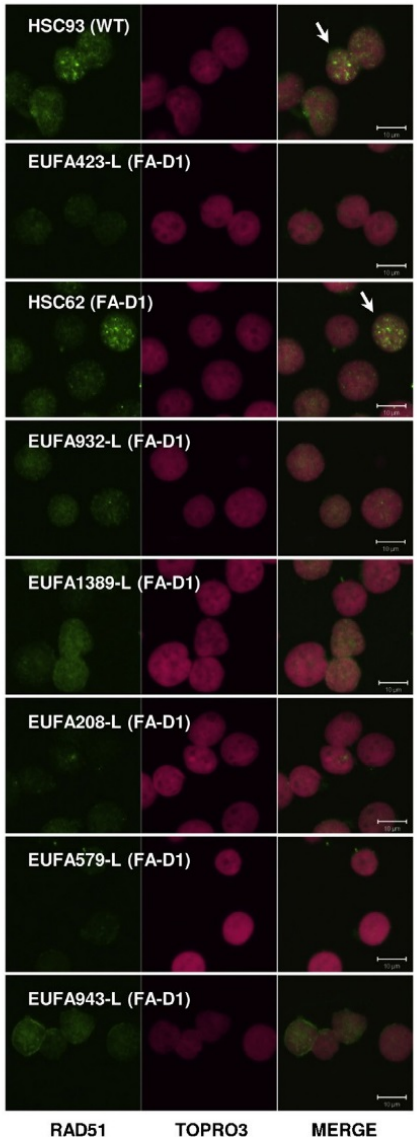

G

Cell line	IC_{50} value (nM)	BRCA2 protein expression *Mutation*	RAD51 foci
HSC93 (WT)	> 400	Normal	Normal
HSC62 (FA-D1)	356.6 ± 30.0	Truncated *Homozygous in-frame deletion 4 amino acids*	Normal
EUFA932-L (FA-D1)	121.8 ± 71.8	Normal *Frameshift insertion and missense mutation*	Absent/ low
EUFA423-L (FA-D1)	31.6 ± 3.7	Truncated *Two heterozygous frameshift insertions*	Absent/ low
EUFA1389-L (FA-D1)	8.7 ± 1.5	Absent *Frameshift deletion and large deletion exon 15-16*	Absent/ low
EUFA208-L (FA-D1)	7.2 ± 2.1	Normal *Frameshift deletion and missense mutation*	Absent/ low
EUFA579-L (FA-D1)	6.9 ± 1.1	Absent/ low *Splice site and nonsense mutation*	Absent/ low
EUFA943-L (FA-D1)	4.0 ± 0.8	Absent/ low *Homozygous frameshift deletion*	Absent/ low

Fig. 1. Variety in PARP inhibitor sensitivity due to different mutations in BRCA2. *(A) Different EBV-immortalized wild type lymphoblasts are resistant to PARP inhibitor (PARPi), whereas the*

indicated BRCA2-mutant lymphoblasts (FA-D1) derived from FA patients are sensitive (B). PARP inhibitor sensitivity of BRCA2-mutant lymphoblasts is correlated with mitomycin C (C) and camptothecin (D) sensitivity. Lymphoblasts were continuously exposed to different concentrations PARP inhibitor (0–400 nM), mitomycin C (0–100 nM) or camptothecin (0–4 nM). After three population doublings of untreated cells, cell number for each drug concentration was determined using a Coulter counter. The data represent the percentage growth compared to untreated cells. The error bars show standard error of the mean of at least 3 independent experiments.(E) Western blot analysis showing BRCA2 protein expression in BRCA2-mutant lymphoblasts. (F) RAD51 foci (green and indicated by arrows) are evidently present in the control cell line HSC93 and the BRCA2-deficient cell line HSC62 upon mitomycin C treatment, but absent in the other BRCA2-defective lymphoblasts. Cell lines were treated with 100 nM MMC for 24 h. TOPRO3 was used as a nuclear counterstaining. (G) An overview of IC50 values (nM), BRCA2 protein expression and RAD51 focus formation of BRCA2-mutant lymphoblasts, showing a wide variety in PARP inhibitor sensitivity.

Although this patient scored positive in the chromosomal breakage assay and had the classical thumb abnormalities, he had not developed bone marrow failure or cancer at the age of 30, while the majority of FA patients with bi- allelic mutations in BRCA2 has a severe phenotype with early onset bone marrow failure and high incidence of childhood solid cancers [20,50,51]. These results indicate that although all BRCA2 mutations conferred the FA phenotype, PARP inhibitor sensitivity depends on the type of BRCA2 mutation and the level of BRCA2 inactivation.

3.2. FA lymphoblasts with mutations in FANCM are hypersensitive to PARP inhibitor

A panel of FA lymphoblastoid cell lines with mutations in FA genes other than BRCA2 (Table 1) was also tested for PARP inhibitor sensitivity. FA proteins can be divided into two groups: a sub-set that is essential for FANCD2-FANCI monoubiquitination and a group of proteins that function downstream of this posttranslational modification [26]. Lymphoblasts with mutations in the genes FANCA, FANCB, FANCC and FANCL, which encode proteins required for FANCD2-FANCI monoubiquitination, as well as those deficient in FANCD2 and FANCI, had IC50 values above 400 nM and were therefore classified as PARP inhibitor resistant (***Fig. 2a***). Among these resistant cell lines, there was one cell line (HSC230) derived from a FA patient who was classified to complementation group FA-B by cell fusion and the presence of a FANCB mutation [34]. How- ever, HSC230 cells also contained two BRCA2 variants: a deleterious frameshift mutation (c.2808 2811del) and a nonsense mutation (p.Lys3326*) [20]. This latter variant is known as a polymorphic stop and was found in >1% of normal individuals [52]. HSC230 cells were not sensitive to PARP inhibition, indicating that neither FANCB- deficiency nor the polymorphic stop in BRCA2 conferred sensitivity to PARP inhibitor and that the resulting truncated BRCA2 protein was able to repair PARP inhibitor induced DNA damage.Lymphoblasts with mutations in the genes FANCJ, FANCQ/XPF or FANCP/SLX4, which function downstream of FANCD2-FANCI monoubiquitination, were also not particularly sensitive. In contrast, lymphoblastoid cell lines with a defect in FANCM (EUFA867-L) or FANCN/PALB2 (EUFA1341-L) were hypersensitive to

PARP inhibition with IC50 values of 41.0 1.9 and 2.5 0.3 nM PARP inhibitor, respectively (*Fig. 2b*). In addition to bi-allelic FANCM mutations, EUFA867-L cells also have bi-allelic mutations in FANCA [29]. To investigate whether PARP inhibitor sensitivity was solely due to FANCM-deficiency, EUFA867 lymphoblasts stably expressing FANCA were tested for PARP inhibitor responsive- ness. As shown in *Fig. 2c*, overexpression of FANCA in EUFA867 cells did not restore PARP inhibitor resistance, indicating that FANCA did not affect sensitivity to PARP inhibitor. This was further strengthened by the PARP inhibitor resistant phenotype in the FANCA-deficient lymphoblastoid cell lines EUFA689-L and HSC72OT (*Fig. 2a and c*). Moreover, cell fusion of FANCM- and FANCA-deficient EUFA867 lymphoblasts with FANCA-deficient HSC72OT lymphoblasts (EUFA867-L HSC72OT fusion 1–3), in which FANCM- but not FANCA-deficiency was corrected, resulted in PARP inhibitor resistance, whereas MMC sensitivity remained (*Fig. 2d*). These results demonstrate that FANCM deficiency was responsible for the observed sensitivity to PARP inhibitor and that FANCM has a role in the cellular defense against PARP inhibitor.

Fig.2.FANCN- and FANCM-deficient lymphoblasts are PARP inhibitor sensitive. Lymphoblasts with mutations in genes encoding upstream FA proteins necessary for FANCD2 monoubiquitination are not sensitive to PARP inhibitor (PARPi) *(A), whereas mutations in FANCN (EUFA1341-L) and FANCM (EUFA867-L) cause PARP inhibitor sensitivity (B). Lymphoblasts were continuously exposed to PARP inhibitor and cell growth was determined by counting after untreated cells had reached at least three population doublings. The data represent mean ± S.E.M. (standard error of the mean) of 2 or 3 independent experiments. Different cell growth inhibition assays were combined into one graph. For each assay, HSC93 and BRCA2-deficient EUFA423 cells were used as controls. (C) EUFA867 lymphoblasts stably express- ing wild type FANCA are still sensitive to PARP inhibitor, whereas correction of FANCM- but not FANCA-deficiency by cell fusion of EUFA867-L with HSC72OT cells (EUFA867-L × HSC72OT fusion 1–3) restores PARP inhibitor resistance. HSC93 and BRCA2-deficient EUFA423 cells were used as controls. (D) Overexpression of FANCA in EUFA867 or correction of FANCM by cell fusions did not rescue MMC sensitivity.*

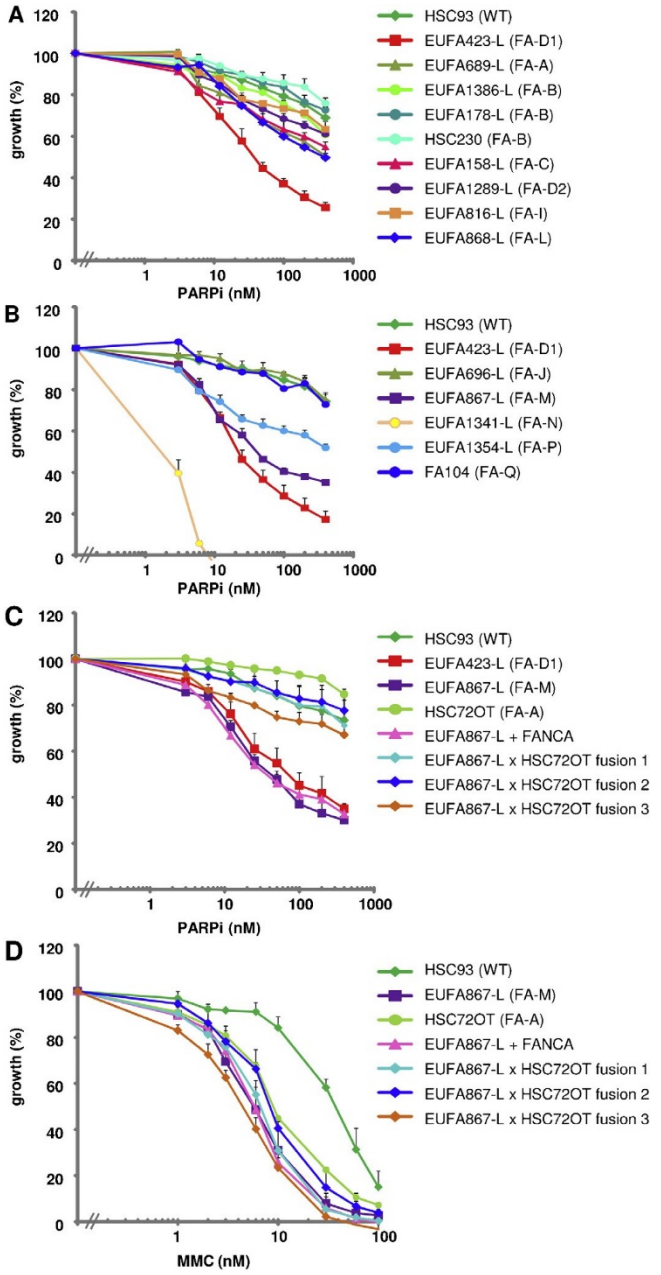

3.3. DDX11 is a determinant of PARP inhibitor responsiveness

FA patients are diagnosed by performing the widely used chromosomal breakage test: upon treatment with MMC, FA deficient cells exhibit a significant increase in chromosomal breaks. However, MMC-induced chromosomal breakage has also been observed in other syndromes, such as Roberts syndrome and Warsaw breakage syndrome, and misdiagnosis may occur [53]. Since a subset of FA cells was sensitive to PARP inhibitors, we also tested lymphoblastoid cell lines derived from Roberts and Warsaw breakage syndrome patients for PARP inhibitor sensitivity. These syndromes together with Cornelia de Lange syndrome are characterized by defects in sister chromatid cohesion andtherefore termed cohesinopathies [30,54]. As shown

in ***Fig. 3a***, lymphoblasts from individuals with Roberts (VU1177-L and VU1199-L) or Cornelia de Lange syndrome (CdLS11165 and CdLS11167) were resistant to PARP inhibitors. Interestingly, lymphoblasts from a Warsaw breakage syndrome patient (VU1202-L) with bi-allelicmutations in DDX11 were almost as sensitive to PARP inhibitors as the BRCA2-deficient cell line EUFA423-L (***Fig. 3b***). This PARP inhibitor sensitivity phenotype was rescued by introducing DDX11 cDNA into VU1202 lymphoblasts, showing that DDX11 is important for cellular protection against PARP inhibitors.

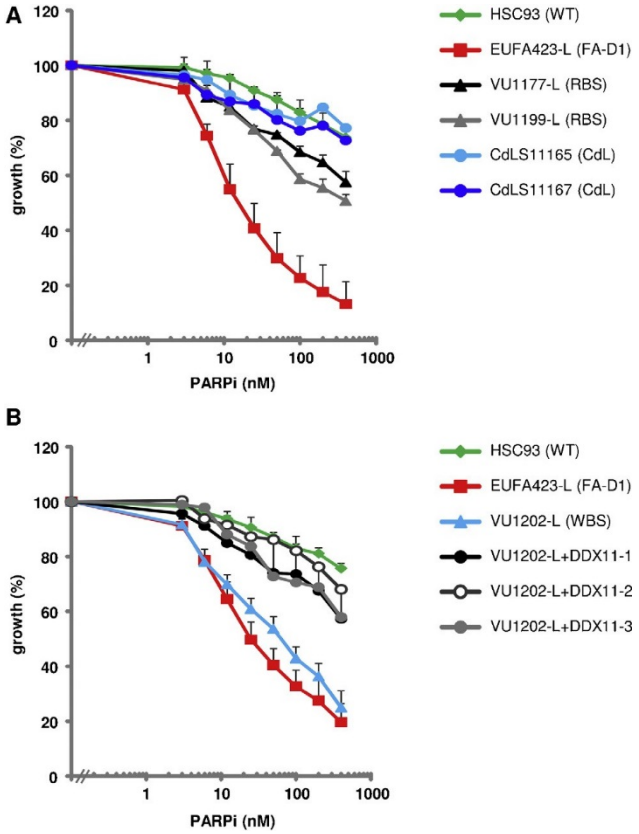

Fig. 3. DDX11-deficient lymphoblasts are sensitive to PARP inhibitor. *(A) Lymphoblasts derived from individuals with Roberts syndrome (RBS) or Cornelia de Lange (CdL) syndrome with mutations in ESCO2 or NIPBL, respectively, are resistant to PARP inhibitor (PARPi). (B) Warsaw Breakage syndrome (WBS) patient-derived lymphoblasts (VU1202-L) with bi-allelic mutations in DDX11 are PARP inhibitor sensitive. The sensitive phenotype of VU1202 cells was restored by introducing DDX11 cDNA. Wild type (HSC93) and BRCA2-deficient (EUFA423-L) lymphoblasts were used as controls. Multiple experiments were combined to one graph. The data represent the mean and standard error of the mean of at least 2 experiments, except for VU1202-L + DDX11-2 and 3.*

3.4. Increased G2/M accumulation and chromosomal breakage in PARP inhibitor sensitive cells

We have used patient-derived lymphoblastoid cell lines to show that besides BRCA2 and PALB2, FANCM and DDX11 are determinants of PARP inhibitor responsiveness. Since FA-deficient cells treated with ICL-inducing agents arrest in the G2/M phase of the cell cycle and exhibit increased chromosomal breakage, we per- formed cell cycle analysis and the chromosomal breakage test to investigate whether a similar cellular phenotype ensues from treatment with PARP inhibitor (***Fig. 4a and b***). BRCA2-, FANCM- and DDX11-deficient cells showed a PARP inhibitor induced increase in sub-G1 (<2N) and G2 (4N) content, indicating increased apoptosis and arrest in the G2/M phase of the cell cycle, respectively (***Fig. 4a***). This increase was lower in wild type cells

(HSC93) and PARP inhibitor resistant FANCA-deficient cells (HSC72OT). How- ever, a clearly increased number of chromosomal breaks was only observed in the BRCA2-deficient lymphoblastoid cell line EUFA423- L (***Fig. 4b***). After treatment with PARP inhibitor, 49% of EUFA423 cells contained one or more breaks, whereas this percentage was6 and 20% in wild type and PARP inhibitor resistant FANCA- defective cells, respectively. In the PARP inhibitor sensitive cell lines EUFA867 and VU1202, breaks occurred in 28% and 26% of cells, respectively, which is more than in wild-type cells (6%) but similar to PARP inhibitor resistant FANCA-defective cells (20%). One model of the synthetic lethal interaction between PARP inhibition and HR deficiency hypothesized that PARP inhibition eventually leads to irreparable DNA double strand breaks [7,8]. Our data indicate that this model may explain PARP inhibitor sensitivityof BRCA2-deficient cells but not of FANCM- or DDX11-defective cells.

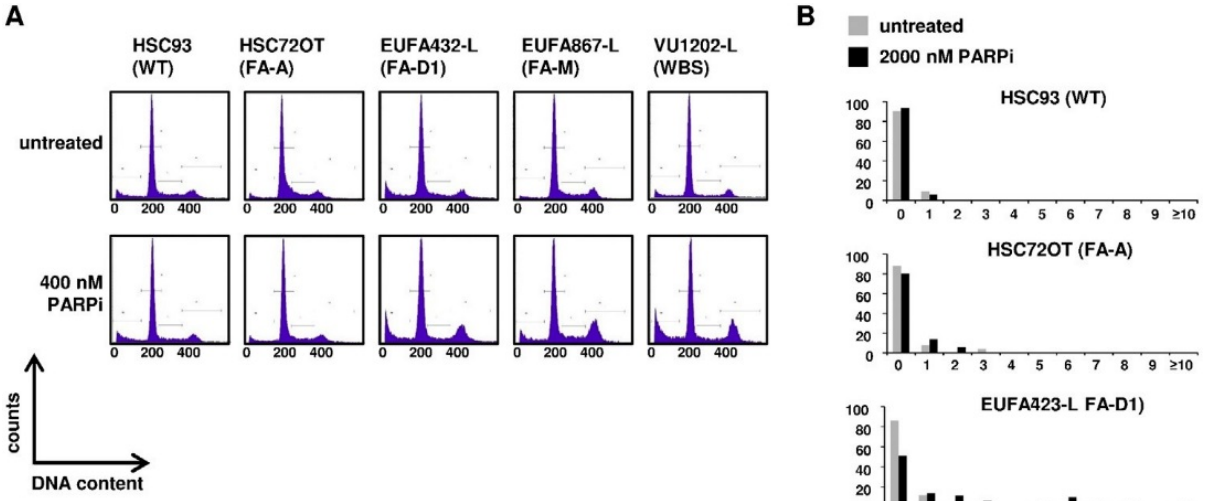

Cell line	PARPi	<2N (%)	2N (%)	2N-4N (%)	4N (%)	>4N (%)
HSC93 (WT)	-	11.97	63.72	12.71	12.74	0.49
	+	14.91	63.66	10.73	11.69	0.40
HSC72OT (FA-A)	-	6.43	67.33	16.71	11.42	1.00
	+	7.58	66.63	13.16	13.58	1.23
EUFA423-L (FA-D1)	-	14.89	60.87	11.13	12.95	1.65
	+	16.89	51.79	8.53	19.67	4.04
EUFA867-L (FA-M)	-	6.32	64.66	13.81	15.98	0.96
	+	11.42	51.05	14.29	22.96	1.87
VU1202-L (WBS)	-	10.79	69.73	7.89	11.95	0.56
	+	23.43	48.02	7.96	20.38	1.10

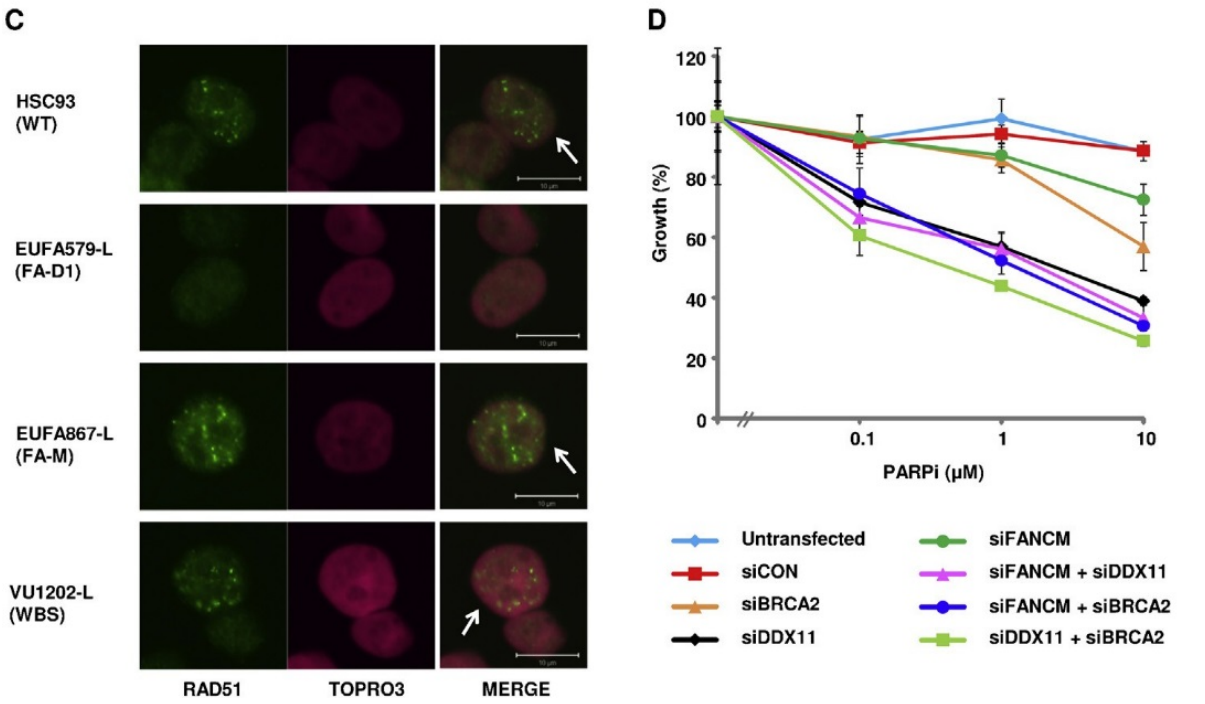

Fig. 4. Cell cycle analysis, chromosomal breakage and RAD51 focus formation in PARP inhibitor sensitive cell lines. *(A) BRCA2-, FANCM- and DDX11-deficient lymphoblasts have increased sub-G1 (<2N) and G2/M (4N) population of cells upon PARP inhibitor treatment. (B) Chromosomal breakage in untreated and PARP inhibited EUFA423 (FA-D1), EUFA867 (FA-M) and VU1202*

(WBS) lymphoblasts. (C) RAD51 focus formation upon mitomycin C treatment in FANCM- and DDX11-deficient lymphoblasts. Representative images of RAD51 foci (green and indicated by arrows) are shown in FANCM-(EUFA857-L) and DDX11-(VU1202-L) deficient cells. HSC93 (wild type) and BRCA2-deficient EUFA579 cells were used as controls. Cells were treated with 100 nM MMC, fixed after 24 h and stained with anti-RAD51. Nuclei were visualized with TOPRO3. (D) SV40- immortalized fibroblasts (Fen5280SV) were transfected with the indicated siRNAs and treated with increasing concentrations of PARP inhibitor. Untransfected and siCON (non-targeting)-transfected cells were used as negative controls.

3.5. RAD51 focus formation and epistatic relationships in FANCM- and DDX11-deficient lymphoblasts

BRCA2 and PALB2 are directly involved in homologous recombination and cells that lack these proteins do not show RAD51 foci [21,49,55]. Therefore, RAD51 focus formation may be a biomarkerfor PARP inhibitor response. To investigate this possibility, RAD51 focus formation was analyzed in FANCM- and DDX11-deficient lymphoblasts. As shown in ***Fig. 4c***, both lymphoblastoid cell lines as well as the control cell line HSC93 were able to form RAD51 foci upon treatment with mitomycin C. In contrast, the BRCA2- deficient cell line EUFA579 lacked RAD51 foci. These results indicate that RAD51 focus formation cannot be used as a general biomarker for PARP inhibitor response. This data might suggest that BRCA2, FANCM and DDX11 function in different pathways in the defense against PARP inhibitor induced damage. To investigate this further, we transfected SV40-immortalized wild type fibroblasts with siRNAs against BRCA2, FANCM and/or DDX11 (***Fig. 4d***). Knockdown of BRCA2, DDX11 or FANCM in wild type fibroblasts resulted in PARP inhibitor sensitization, thereby further confirming that these proteins are determinants of PARP inhibitor response. Knockdown of BRCA2 further increased PARP inhibitor sensitivity of FANCM knockdown cells and also, albeit to a lesser extent, of DDX11 knock- down cells. However, fibroblasts transfected with siRNAs targeting both FANCM and DDX11 were as sensitive to PARP inhibition as siDDX11-transfected cells alone, indicating that DDX11-deficiency is epistatic with FANCM-deficiency. Taken together, these data suggest that FANCM and DDX11 function in the same pathway, whereas BRCA2 acts in another pathway to prevent PARP inhibitor induced DNA damage.

3.6. FA head and neck tumor cell lines are not particularly sensitive to PARP inhibitor

FA patients have an extremely high risk to develop tumors of the head and neck region. Treatment of these patients is complicated because of the hypersensitivity of FA cells to chemotherapeutic drugs and novel treatment options are urgently awaited. Since defects in upstream FA genes did not confer PARP inhibitor sensitivity in normal lymphoblastoid cell lines (see Section 3.2), we tested PARP inhibitor responsiveness in three FA head and neck cancer cell lines (VU-SCC-1131 (FA-C), VU-SCC-1365 (FA-A) and VU-SCC-1604 (FA-L)). These tumor cell lines were sensitive to MMC (***Fig. 5a***) and cisplatin (CDDP) (***Fig. 5b***), a hallmark of FA cells. As

expected, FANCD2 monoubiquitination (*Fig. 5c*) and focus formation (*Fig. 5d*) were absent, because these cell lines have mutations in upstream FA genes. Functional correction of these cell lines made them 10- fold more resistant to MMC and CDDP and restored the ability to monoubiquitinate FANCD2 and to form FANCD2 foci (*Fig. 5a–d*). In contrast, FA-A and FA-C cell lines were not PARP inhibitor sensitive and functional correction did not affect PARP inhibitor responsiveness. Although, FANCL-deficient VU-SCC-1604 cells appeared slightly more sensitive to PARP inhibitor than the corrected VU- SCC-1604 cells and the FA-A and FA-C cell lines, the sensitivity was not as profound as in PALB2-deficient fibroblasts (*Fig. 5e*). Our data demonstrate that defects in upstream FA genes in normal lymphoblasts as well as in HNSCC cells do not confer hypersensitivity to PARP inhibitor. Since most FA patients belong to upstream FA-complementation groups, PARP inhibition is likely to be unsuccessful in the treatment of FA head and neck cancer. However, this therapy might be successful in non-FA patients with tumors containing mutations in genes that determine PARP inhibitor sensitivity, such as BRCA2, DDX11 or FANCM.

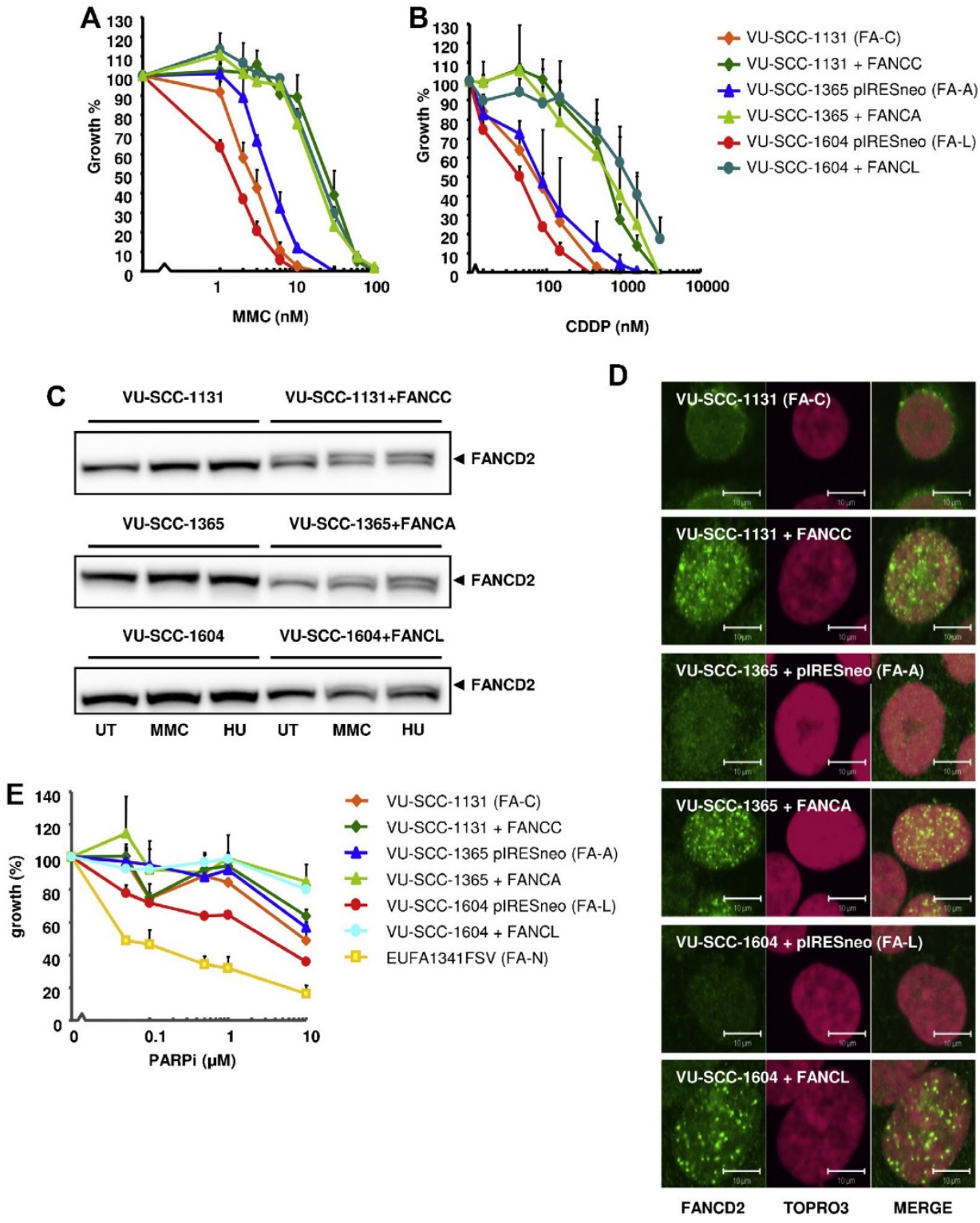

Fig. 5. Upstream FA pathway defects do not affect sensitivity to PARP inhibitors in HNSCC cell lines. Head and neck tumor cell lines (VU-SCC-1131 (FANCC-deficient), VU- SCC-1365 (FANCA-deficient) and VU-SCC-1604 (FANCL-deficient)) derived from FA patients are hypersensitive to mitomycin C (MMC) *(A) and cisplatin (CDDP) (B). Functional correction of these cell lines makes them 10-fold more resistant to these agents. VU-SCC-1365 and VU-SCC-1604 were transfected with an empty pIRESneo construct. The data represent mean ± S.E.M. (standard error of the mean) of three independent experiments. FA-deficient head and neck tumor cell lines lack*

FANCD2 monoubiquitination(C)and focus formation (D), which is restored after functional complementation. Western blot analysis was used to determine FANCD2 monoubiquitination of untreated(UT), MMC-(200 nM) or hydroxyurea (HU) treated cells. Representative images of MMC-induced FANCD2 foci (green) are shown. Nuclei were visualized by TOPRO3. (E) PARP inhibitor (PARPi) response in FA tumor cell lines. The data represent mean ± S.E.M. of three independent experiments. For the cell growth inhibition assays, cells were continuously exposed to different concentrations PARP inhibitor, MMC or CDDP. Cell growth was compared to untreated cells and determined by counting cell number or colonies.

4. Discussion

In an effort to find determinants of PARP inhibitor sensitivity, we investigated whether defects in FA proteins other than BRCA2 are synthetic lethal with PARP inhibition. Using lymphoblastoid cell lines from individuals with FA or clinically related syndromes, we identified FANCM and DDX11 as determinants of PARP inhibitorresponsiveness. Furthermore, we show that the response to PARP inhibitors of BRCA2-mutant cells depends on the type of mutation. In our study we primarily used EBV-immortalized lymphoblastoid cell lines with different genetic defects. This allowed a detailed analysis of the role of different proteins in the response to PARP inhibitors within one specific cell type. In these lymphoblasts, the major determinants of PARP inhibitor sensitivity were the homologous recombination proteins BRCA2 and PALB2, but also the DNA helicases FANCM and DDX11. FA core complex proteins as well as FANCI and FANCD2 appeared to be dispensable for PARP inhibitor tolerance. Consistent with our results, HPV E6 and E7 immortalized fibroblasts established from FA patients with mutations in the FA genes FANCA, FANCD2, FANCI or FANCL were not sensitive to PARP inhibitor KU0058948 [19]. However, DT40 cells deficient in FANCC, FANCD2 or FANCG and mouse embryonic fibroblasts lacking Fanca, Fancc or Fancd2 were sensitive to the same PARP inhibitor, suggesting a species- and/or cell-culture-specific requirement for theFA core complex in conferring PARP inhibitor resistance [13,56]. Several of our observations indicate that increased double-strand break formation combined with defective homology- directed break repair may explain PARP inhibitor sensitivity in BRCA2-defective cells but not in FANCM- or DDX11-defective cells.

(1) Although RAD51 focus formation has been suggested as a biomarker to identify tumors that will respond to PARP inhibition, we have demonstrated here that PARP inhibitor sensitive FANCM- and DDX11-deficient lymphoblasts were still able to form RAD51 foci. Therefore, RAD51 focus formation may be a relevant marker for BRCA2-deficient tumors, but not for PARP inhibitor sensitivity in general. (2) Double-strand break formation following PARP inhibition was strongly increased in BRCA2-deficient cells, but not in FANCM or DDX11-defective cells. Together with normal RAD51 focus formation, this suggests that double-strand breaks induced by PARP inhibition were effectively repaired in FANCM- or DDX11- defective cells. (3) Knockdown of BRCA2 reduced cell survival in FANCM or DDX11 knockdown cells whereas FANCM knockdown did not reduce survival of DDX11 knockdown cells. Taken together, these

results indicate that different mechanisms exist for PARP inhibitor sensitivity in BRCA2-defective cells on the one side and FANCM- or DDX11-defective cells on the other.

The PARP inhibitor sensitivity of FANCM and DDX11-defective cells may be related to DNA replication, since recent studies demonstrated that PARP inhibitors not only caused DNA breaks but also formed replication fork blocking lesions [11–13]. In this respect, PARP inhibitors resemble topoisomerase inhibitors like camptothecin [57,58]. Interestingly, the cell lines that were PARP inhibitor sensitive were also sensitive to camptothecin, indicating that failure of repairing replication fork blocking lesions contributes to cytotoxicity. PARP and HR proteins as well as FANCM play important roles in restarting stalled replication forks [14,15,59]. FANCM is a multifunctional protein that not only recruits the FA core complex to stalled replication forks but also the Bloom's syndrome complex [60]. Besides an important role in ensuring replisome stability in S phase, FANCM is also involved in checkpoint activation upon dam- age [28,61,62]. Errors in DNA damage cell cycle checkpoints and in bypass of replication-blocking lesions might lead to PARP inhibitor sensitivity [63]. Therefore, it is possible that replisome instability and checkpoint defects due to FANCM deficiency both contribute to PARP inhibitor sensitivity.

Problems with replication fork maintenance may also underlie the observed PARP inhibitor sensitivity in DDX11-deficient cells. DDX11 is involved in the establishment of sister chromatid cohesion, which occurs in a replication dependent manner during S phase [64]. The replication fork protection (RFP) complex, consist- ing of Timeless and Tipin, can interact and stabilize DDX11, leading to stable association of the cohesion complex with chromatin [65]. Moreover, DDX11 interacts with and enhances the activity of FEN1,a flap endonuclease involved in lagging-strand DNA synthesis [66]. Depletion of FEN1 also leads to cohesion defects and FEN1-deficient DT40 cells are sensitive to PARP inhibitor [13,66]. These results suggests that lagging-strand synthesis might be important for sister chromatid cohesion. Defective sister chromatid cohesion due to DDX11-deficiency might interfere with bypass of replication- blocking lesions caused by PARP inhibitor.

By investigating PARP inhibitor sensitivity in the setting of patient derived lymphoblastoid cell lines, we could demonstrate the importance of examining PARP inhibitor sensitivity in the con-text of truncating mutations instead of reduced protein levels byusing RNA interference. Depending on the mutation in BRCA2, mutant cells were more or less sensitive to PARP inhibition or to other DNA damaging agents, such as mitomycin C or camptothecin. Consistent with this observation, a previous report [19] showed variations in PARP inhibitor sensitivity depending on the type of SLX4 mutation. SLX4 seems to play an important role in repairing PARP inhibitor induced damage via the interactions with MUS81 and to a lesser extent with SLX1 [19]. EUFA1354 lymphoblasts with bi-allelic mutations in SLX4 were not particularly sensitive to PARP inhibition. This cell line expresses a truncated SLX4 protein that is able to interact with MUS81 and SLX1 [24] and therefore, might beless sensitive to PARP inhibitor. Thus, PARP inhibitor response may vary due to different underlying mutations in BRCA2 or SLX4.

In summary, FANCM and DDX11 were newly identified as determinants of PARP inhibitor sensitivity. Since FANCM and DDX11 mutations occur in tumors (COSMIC database), these results suggest that PARP inhibition might be a valuable anti-cancer approach not only for BRCA-associated cancers but also for other tumors. However, caution is necessary because PARP inhibitor sensitivity might dependent on the kind of mutation.

Conflicts of interest statement

The authors declare that there are no conflicts of interest.

Acknowledgements

We thank Roland Kanaar for providing the RAD51 antibody; Roelie van der Willik for help in BRCA2 Western blotting and RobM. Wolthuis and Ruud H. Brakenhoff for helpful discussions and comments. We acknowledge financial support from Cancer Center Amsterdam (CCA) and Fanconi Anemia Research Fund (FARF), Portland, OR, U.S.A.

References

[1]S. Hellman, E.E. Vokes, Advancing current treatments for cancer, Sci. Am. 275 (1996) 118–123.
[2]L.H. Hartwell, P. Szankasi, C.J. Roberts, A.W. Murray, S.H. Friend, Integrating genetic approaches into the discovery of anticancer drugs, Science 278 (1997) 1064–1068.
[3]W.G. Kaelin Jr., The concept of synthetic lethality in the context of anticancer therapy, Nat. Rev. Cancer 5 (2005) 689–698.
[4]D.A. Chan, A.J. Giaccia, Harnessing synthetic lethal interactions in anticancer drug discovery, Nat. Rev. Drug Discov. 10 (2011) 351–364.
[5]M.J. Menissier-de, M. Molinete, G. Gradwohl, F. Simonin, G. de Murcia, Zinc- binding domain of poly(ADP-ribose)polymerase participates in the recognition of single strand breaks on DNA, J. Mol. Biol. 210 (1989) 229–233.
[6]V. Schreiber, F. Dantzer, J.C. Ame, G. de Murcia, Poly(ADP-ribose): novel functions for an old molecule, Nat. Rev. Mol. Cell Biol. 7 (2006) 517–528.
[7]H.E. Bryant, N. Schultz, H.D. Thomas, K.M. Parker, D. Flower, E. Lopez, S. Kyle,M. Meuth, N.J. Curtin, T. Helleday, Specific killing of BRCA2-deficient tumours with inhibitors of poly(ADP-ribose) polymerase, Nature 434 (2005) 913–917.
[8]H. Farmer, N. McCabe, C.J. Lord, A.N. Tutt, D.A. Johnson, T.B. Richardson, M. San- tarosa, K.J. Dillon, I. Hickson, C. Knights, N.M. Martin, S.P. Jackson, G.C. Smith,A. Ashworth, Targeting the DNA repair defect in BRCA mutant cells as a therapeutic strategy, Nature 434 (2005) 917–921.
[9]M.E. Moynahan, J.W. Chiu, B.H. Koller, M. Jasin, Brca1 controls homology- directed DNA repair, Mol. Cell 4 (1999) 511–518.
[10]M.E. Moynahan, A.J. Pierce, M. Jasin, BRCA2 is required for homology-directed repair of chromosomal breaks, Mol. Cell 7 (2001) 263–272.
[11]C.E. Strom, F. Johansson, M. Uhlen, C.A. Szigyarto, K. Erixon, T. Helleday, Poly (ADP-ribose) polymerase (PARP) is not involved in base excision repair but PARP inhibition traps a single-strand intermediate, Nucleic Acids Res. 39 (2011) 3166–3175.
[12]T. Helleday, The underlying mechanism for the PARP and BRCA synthetic lethality: clearing up the misunderstandings, Mol. Oncol. 5 (2011) 387–393.
[13]J. Murai, S.Y. Huang, B.B. Das, A. Renaud, Y. Zhang, J.H. Doroshow, J. Ji, S. Takeda,Y. Pommier, Trapping of PARP1 and PARP2 by clinical PARP inhibitors, Cancer Res. 72 (2012) 5588–5599.
[14]H.E. Bryant, E. Petermann, N. Schultz, A.S. Jemth, O. Loseva, N. Issaeva, F. Johans- son, S. Fernandez, P. McGlynn, T. Helleday, PARP is activated at stalled forks to mediate Mre11-dependent replication restart and recombination, EMBO J. 28 (2009) 2601–2615.
[15]Y.G. Yang, U. Cortes, S. Patnaik, M. Jasin, Z.Q. Wang, Ablation of PARP-1 does not interfere with the repair of DNA double-strand breaks, but compromises the reactivation of stalled replication forks, Oncogene 23 (2004) 3872–3882.
[16]P.C. Fong, D.S. Boss, T.A. Yap, A. Tutt, P. Wu, M. Mergui-Roelvink, P. Mortimer,H. Swaisland, A. Lau, M.J. O'Connor, A. Ashworth, J. Carmichael, S.B. Kaye, J.H. Schellens, J.S.de Bono,

Inhibition of poly(ADP-ribose) polymerase in tumors from BRCA mutation carriers, N. Engl. J. Med. 361 (2009) 123–134.
[17]R. Buisson, A.M. Dion-Cote, Y. Coulombe, H. Launay, H. Cai, A.Z. Stasiak, A. Stasiak, B. Xia, J.Y. Masson, Cooperation of breast cancer proteins PALB2 and piccolo BRCA2 in stimulating homologous recombination, Nat. Struct. Mol. Biol. 17 (2010) 1247–1254.
[18]A. Min, S.A. Im, Y.K. Yoon, S.H. Song, H.J. Nam, H.S. Hur, H.P. Kim, K.H. Lee, S.W. Han, D.Y. Oh, T.Y. Kim, M.J. O'Connor, W.H. Kim, Y.J. Bang, RAD51C-deficient cancer cells are highly sensitive to the PARP inhibitor olaparib, Mol. Cancer Ther. 12 (2013) 865–877.
[19]Y. Kim, G.S. Spitz, U. Veturi, F.P. Lach, A.D. Auerbach, A. Smogorzewska, Regulation of multiple DNA repair pathways by the Fanconi anemia protein SLX4, Blood 121 (2013) 54–63.
[20]N.G. Howlett, T. Taniguchi, S. Olson, B. Cox, Q. Waisfisz, C. De Die-Smulders, N. Persky, M. Grompe, H. Joenje, G. Pals, H. Ikeda, E.A. Fox, A.D. D'Andrea, Biallelic inactivation of BRCA2 in Fanconi anemia, Science 297 (2002) 606–609.
[21]B. Xia, J.C. Dorsman, N. Ameziane, V.Y. de, M.A. Rooimans, Q. Sheng, G. Pals, A. Errami, E. Gluckman, J. Llera, W. Wang, D.M. Livingston, H. Joenje, J.P. de Winter, Fanconi anemia is associated with a defect in the BRCA2 partner PALB2, Nat. Genet. 39 (2007) 159–161.
[22]S. Reid, D. Schindler, H. Hanenberg, K. Barker, S. Hanks, R. Kalb, K. Neveling, P. Kelly, S. Seal, M. Freund, M. Wurm, S.D. Batish, F.P. Lach, S. Yetgin, H. Neitzel,H. Ariffin, M. Tischkowitz, C.G. Mathew, A.D. Auerbach, N. Rahman, Biallelic mutations in PALB2 cause Fanconi anemia subtype FA-N and predispose to childhood cancer, Nat. Genet. 39 (2007) 162–164.
[23] Y. Kim, F.P. Lach, R. Desetty, H. Hanenberg, A.D. Auerbach, A. Smogorzewska, Mutations of the SLX4 gene in Fanconi anemia, Nat. Genet. 43 (2011) 142–146.
[24]C. Stoepker, K. Hain, B. Schuster, Y. Hilhorst-Hofstee, M.A. Rooimans, J. Steltenpool, A.B. Oostra, K. Eirich, E.T. Korthof, A.W. Nieuwint, N.G. Jaspers, T. Bettecken, H. Joenje, D. Schindler, J. Rouse, J.P. de Winter, SLX4, a coordinator of structure-specific endonucleases, is mutated in a new Fanconi anemia subtype, Nat. Genet. 43 (2011) 138–141.
[25]F. Vaz, H. Hanenberg, B. Schuster, K. Barker, C. Wiek, V. Erven, K. Neveling, D. Endt, I. Kesterton, F. Autore, F. Fraternali, M. Freund, L. Hartmann, D. Grimwade,R.G. Roberts, H. Schaal, S. Mohammed, N. Rahman, D. Schindler, C.G. Mathew, Mutation of the RAD51C gene in a Fanconi anemia-like disorder, Nat. Genet. 42 (2010) 406–409.
[26] M.C. Kottemann, A. Smogorzewska, Fanconi anaemia and the repair of Watson and Crick DNA crosslinks, Nature 493 (2013) 356–363.
[27]M. Bogliolo, B. Schuster, C. Stoepker, B. Derkunt, Y. Su, A. Raams, J.P. Trujillo, J. Minguillon, M.J. Ramirez, R. Pujol, J.A. Casado, R. Banos, P. Rio, K. Knies, S. Zuniga,J. Benitez, J.A. Bueren, N.G. Jaspers, O.D. Scharer, J.P. de Winter, D. Schindler,J. Surralles, Mutations in ERCC4, encoding the DNA-repair endonuclease XPF, cause Fanconi anemia, Am. J. Hum. Genet. 92 (2013) 800–806.
[28]R.A. Schwab, A.N. Blackford, W. Niedzwiedz, ATR activation and replication fork restart are defective in FANCM-deficient cells, EMBO J. 29 (2010) 806–818.
[29]T.R. Singh, S.T. Bakker, S. Agarwal, M. Jansen, E. Grassman, B.C. Godthelp,A.M. Ali, C.H. Du, M.A. Rooimans, Q. Fan, K. Wahengbam, J. Steltenpool, P.R. Andreassen, D.A. Williams,

H. Joenje, J.P. de Winter, A.R. Meetei, Impaired FANCD2 monoubiquitination and hypersensitivity to camptothecin uniquely characterize Fanconi anemia complementation group M, Blood 114 (2009) 174–180.
[30]P. van der Lelij, K.H. Chrzanowska, B.C. Godthelp, M.A. Rooimans, A.B. Oostra, M. Stumm, M.Z. Zdzienicka, H. Joenje, J.P. de Winter, Warsaw breakage syndrome, a cohesinopathy associated with mutations in the XPD helicase family member DDX11/ChlR1, Am. J. Hum. Genet. 86 (2010) 262–266.
[31]H. Joenje, J.R. Lo ten Foe, A.B. Oostra, C.G. van Berkel, M.A. Rooimans, T. Schroeder-Kurth, R.D. Wegner, J.J. Gille, M. Buchwald, F. Arwert, Classification of Fanconi anemia patients by complementation analysis: evidence for a fifth genetic subtype, Blood 86 (1995) 2156–2160.
[32]M. Wijker, N.V. Morgan, S. Herterich, C.G. van Berkel, A.J. Tipping, H.J. Gross,J.J. Gille, G. Pals, M. Savino, C. Altay, S. Mohan, I. Dokal, J. Cavenagh, J. Marsh,W.M. van, J.J. Ortega, D. Schuler, E. Samochatova, M. Karwacki, A.N. Bekassy, M. Abecasis, W. Ebell, M.L. Kwee, R.T. de, C.G. Mathew, Heterogeneous spectrum of mutations in the Fanconi anaemia group A gene, Eur. J. Hum. Genet. 7 (1999) 52–59.
[33] H. Joenje, M. Levitus, Q. Waisfisz, A. D'Andrea, I. Garcia-Higuera, T. Pearson, C.G. van Berkel, M.A. Rooimans, N. Morgan, C.G. Mathew, F. Arwert, Complementation analysis in Fanconi anemia: assignment of the reference FA-H patient to group A, Am. J. Hum. Genet. 67 (2000) 759–762.
[34]A.R. Meetei, M. Levitus, Y. Xue, A.L. Medhurst, M. Zwaan, C. Ling, M.A. Rooimans,P. Bier, M. Hoatlin, G. Pals, J.P. de Winter, W. Wang, H. Joenje, X-linked inheritance of Fanconi anemia complementation group B, Nat. Genet. 36 (2004) 1219–1224.
[35]J.P. de Winter, L. van der Weel, G.J. de, S. Stone, Q. Waisfisz, F. Arwert, R.J. Scheper, F.A. Kruyt, M.E. Hoatlin, H. Joenje, The Fanconi anemia protein FANCF forms a nuclear complex with FANCA, FANCC and FANCG, Hum. Mol. Genet. 9 (2000) 2665–2674.
[36]R. Kalb, K. Neveling, H. Hoehn, H. Schneider, Y. Linka, S.D. Batish, C. Hunt, M. Berwick, E. Callen, J. Surralles, J.A. Casado, J. Bueren, A. Dasi, J. Soulier, E. Gluck- man, C.M. Zwaan, S.R. van, G. Pals, J.P. de Winter, H. Joenje, M. Grompe, A.D. Auerbach, H. Hanenberg, D. Schindler, Hypomorphic mutations in the gene encoding a key Fanconi anemia protein, FANCD2, sustain a significant group of FA-D2 patients with severe phenotype, Am. J. Hum. Genet. 80 (2007) 895–910.
[37]J.C. Dorsman, M. Levitus, D. Rockx, M.A. Rooimans, A.B. Oostra, A. Haitjema,S.T. Bakker, J. Steltenpool, D. Schuler, S. Mohan, D. Schindler, F. Arwert, G. Pals,C.G. Mathew, Q. Waisfisz, J.P. de Winter, H. Joenje, Identification of the Fanconi anemia complementation group I gene, FANCI, Cell. Oncol. 29 (2007) 211–218.
[38]A.R. Meetei, J.P. de Winter, A.L. Medhurst, M. Wallisch, Q. Waisfisz, H.J. van de Vrugt, A.B. Oostra, Z. Yan, C. Ling, C.E. Bishop, M.E. Hoatlin, H. Joenje, W. Wang, A novel ubiquitin ligase is deficient in Fanconi anemia, Nat. Genet. 35 (2003) 165–170.
[39]A.R. Meetei, A.L. Medhurst, C. Ling, Y. Xue, T.R. Singh, P. Bier, J. Steltenpool, S. Stone, I. Dokal, C.G. Mathew, M. Hoatlin, H. Joenje, J.P. de Winter, W. Wang, A human ortholog of

archaeal DNA repair protein Hef is defective in Fanconi anemia complementation group M, Nat. Genet. 37 (2005) 958–963.
[40]Elghalbzouri-Maghrani, J. Steltenpool, M.A. Rooimans, G. Pals, F. Arwert, C.G. Mathew, M.Z. Zdzienicka, K. Hiom, J.P. de Winter, H. Joenje, The DNA helicase BRIP1 is defective in Fanconi anemia complementation group J, Nat. Genet. 37 (2005) 934–935.
[41] H. Vega, Q. Waisfisz, M. Gordillo, N. Sakai, I. Yanagihara, M. Yamada, G.D. van,H. Kayserili, C. Xu, K. Ozono, E.W. Jabs, K. Inui, H. Joenje, Roberts syndrome is caused by mutations in ESCO2, a human homolog of yeast ECO1 that is essential for the establishment of sister chromatid cohesion, Nat. Genet. 37 (2005) 468–470.
[42] M.G. Vrouwe, E. Elghalbzouri-Maghrani, M. Meijers, P. Schouten, B.C. Godthelp,Z.A. Bhuiyan, E.J. Redeker, M.M. Mannens, L.H. Mullenders, A. Pastink, F. Darroudi, Increased DNA damage sensitivity of Cornelia de Lange syndrome cells: evidence for impaired recombinational repair, Hum. Mol. Genet. 16 (2007) 1478–1487.
[43] H.J. van Zeeburg, P.J. Snijders, G. Pals, M.A. Hermsen, M.A. Rooimans, G. Bagby,J. Soulier, E. Gluckman, J. Wennerberg, C.R. Leemans, H. Joenje, R.H. Brakenhoff, Generation and molecular characterization of head and neck squamous cell lines of fanconi anemia patients, Cancer Res. 65 (2005) 1271–1276.
[44] N.J. Marston, W.J. Richards, D. Hughes, D. Bertwistle, C.J. Marshall, A. Ashworth, Interaction between the product of the breast cancer susceptibility gene BRCA2 and DSS1, a protein functionally conserved from yeast to mammals, Mol. Cell. Biol. 19 (1999) 4633–4642.
[45]H. Yang, P.D. Jeffrey, J. Miller, E. Kinnucan, Y. Sun, N.H. Thoma, N. Zheng, P.L. Chen, W.H. Lee, N.P. Pavletich, BRCA2 function in DNA binding and recombination from a BRCA2-DSS1-ssDNA structure, Science 297 (2002) 1837–1848.
[46] K. Gudmundsdottir, C.J. Lord, E. Witt, A.N. Tutt, A. Ashworth, DSS1 is required for RAD51 focus formation and genomic stability in mammalian cells, EMBO Rep. 5 (2004) 989–993.
[47]N. Siaud, M.A. Barbera, A. Egashira, I. Lam, N. Christ, K. Schlacher, B. Xia, M. Jasin, Plasticity of BRCA2 function in homologous recombination: genetic interac- tions of the PALB2 and DNA binding domains, PLoS Genet. 7 (2011) e1002409.
[48]A.K. Wong, R. Pero, P.A. Ormonde, S.V. Tavtigian, P.L. Bartel, RAD51 interacts with the evolutionarily conserved BRC motifs in the human breast cancer susceptibility gene brca2, J. Biol. Chem. 272 (1997) 31941–31944.
[49]S.S. Yuan, S.Y. Lee, G. Chen, M. Song, G.E. Tomlinson, E.Y. Lee, BRCA2 is required for ionizing radiation-induced assembly of Rad51 complex in vivo, Cancer Res. 59 (1999) 3547–3551.
[50]B. Hirsch, A. Shimamura, L. Moreau, S. Baldinger, M. Hag-alshiekh, B. Bostrom, S. Sencer, A.D. D'Andrea, Association of biallelic BRCA2/FANCD1 mutations with spontaneous chromosomal instability and solid tumors of childhood, Blood 103 (2004) 2554–2559.
[51]J.E. Wagner, J. Tolar, O. Levran, T. Scholl, A. Deffenbaugh, J. Satagopan, L. Ben-Porat, K. Mah, S.D. Batish, D.I. Kutler, M.L. MacMillan, H. Hanenberg,A.D. Auerbach, Germline mutations in BRCA2: shared genetic susceptibility to breast cancer, early onset leukemia, and Fanconi anemia, Blood 103 (2004) 3226–3229.

[52]S. Mazoyer, A.M. Dunning, O. Serova, J. Dearden, N. Puget, C.S. Healey, S.A. Gayther, J. Mangion, M.R. Stratton, H.T. Lynch, D.E. Goldgar, B.A. Ponder,G.M. Lenoir, A polymorphic stop codon in BRCA2, Nat. Genet. 14 (1996) 253–254.
[53] P. van der Lelij, A.B. Oostra, M.A. Rooimans, H. Joenje, J.P. de Winter, Diagnostic overlap between Fanconi anemia and the cohesinopathies: Roberts syndrome and Warsaw breakage syndrome, Anemia 2010 (2010) 565268.
[54] J. Liu, I.D. Krantz, Cohesin and human disease, Annu. Rev. Genomics Hum. Genet. 9 (2008) 303–320.
[55] B. Xia, Q. Sheng, K. Nakanishi, A. Ohashi, J. Wu, N. Christ, X. Liu, M. Jasin, F.J. Couch, D.M. Livingston, Control of BRCA2 cellular and clinical functions by a nuclear partner, PALB2, Mol. Cell 22 (2006) 719–729.
[56]N. McCabe, N.C. Turner, C.J. Lord, K. Kluzek, A. Bialkowska, S. Swift, S. Giavara,M.J. O'Connor, A.N. Tutt, M.Z. Zdzienicka, G.C. Smith, A. Ashworth, Deficiency in the repair of DNA damage by homologous recombination and sensitivity to poly(ADP-ribose) polymerase inhibition, Cancer Res. 66 (2006) 8109–8115.
[57]Y.H. Hsiang, M.G. Lihou, L.F. Liu, Arrest of replication forks by drug-stabilized topoisomerase I-DNA cleavable complexes as a mechanism of cell killing by camptothecin, Cancer Res. 49 (1989) 5077–5082.
[58]Y. Pommier, Topoisomerase I inhibitors: camptothecins and beyond, Nat. Rev. Cancer 6 (2006) 789–802.
[59]A.N. Blackford, R.A. Schwab, J. Nieminuszczy, A.J. Deans, S.C. West, W. Niedzwiedz, The DNA translocase activity of FANCM protects stalled replication forks, Hum. Mol. Genet. 21 (2012) 2005–2016.
[60]A.J. Deans, S.C. West, FANCM connects the genome instability disorders Bloom's syndrome and Fanconi anemia, Mol. Cell 36 (2009) 943–953.
[61]S.J. Collis, A. Ciccia, A.J. Deans, Z. Horejsi, J.S. Martin, S.L. Maslen, J.M. Skehel, S.J. Elledge, S.C. West, S.J. Boulton, FANCM and FAAP24 function in ATR-mediated checkpoint signaling independently of the Fanconi anemia core complex, Mol. Cell 32 (2008) 313–324.
[62]S. Luke-Glaser, B. Luke, S. Grossi, A. Constantinou, FANCM regulates DNA chain elongation and is stabilized by S-phase checkpoint signalling, EMBO J. 29 (2010) 795–805.
[63]N.C. Turner, C.J. Lord, E. Iorns, R. Brough, S. Swift, R. Elliott, S. Rayter, A.N. Tutt, A. Ashworth, A synthetic lethal siRNA screen identifying genes mediating sensitivity to a PARP inhibitor, EMBO J. 27 (2008) 1368–1377.
[64]A. Lengronne, J. McIntyre, Y. Katou, Y. Kanoh, K.P. Hopfner, K. Shirahige, F. Uhlmann, Establishment of sister chromatid cohesion at the S. cerevisiae replication fork, Mol. Cell 23 (2006) 787–799.
[65] A.R. Leman, C. Noguchi, C.Y. Lee, E. Noguchi, Human timeless and tipin stabilize replication forks and facilitate sister-chromatid cohesion, J. Cell Sci. 123 (2010) 660–670.
[66] A. Farina, J.H. Shin, D.H. Kim, V.P. Bermudez, Z. Kelman, Y.S. Seo, J. Hurwitz, Studies with the human cohesin establishment factor, ChlR1. Association of ChlR1 with Ctf18-RFC and Fen1, J. Biol. Chem. 283 (2008) 20925–20936.

Chapter 4

Defective Sister Chromatid Cohesion Is Synthetically Lethal with Impaired APC/C Function

Job de Lange, Atiq Faramarz, Anneke B. Oostra, Renee X. de Menezes, Ida H. van der Meulen, Martin A. Rooimans, Davy A. Rockx, Ruud H. Brakenhoff, Victor W. van Beusechem, Randall W. King, Johan P. de Winter, and Rob M. F. Wolthuis

Published in Nature Communications,2015 Oct 1;6:8399

Summary:

Warsaw breakage syndrome (WABS) is caused by defective DDX11, a DNA helicase that is essential for chromatid cohesion. Here, a paired genome-wide siRNA screen in patient-derived cell lines reveals that WABS cells do not tolerate partial depletion of individual APC/C subunits or the spindle checkpoint inhibitor $p31^{comet}$. A combination of reduced cohesion and impaired APC/C function also leads to fatal mitotic arrest in diploid RPE1 cells. Moreover, WABS cell lines, and several cancer cell lines with cohesion defects, display a highly increased response to a new cell-permeable APC/C inhibitor, apcin, but not to the spindle poison paclitaxel. Synthetic lethality of APC/C inhibition and cohesion defects strictly depends on a functional mitotic spindle checkpoint as well as on intact microtubule pulling forces. This indicates that the underlying mechanism involves cohesion fatigue in response to mitotic delay, leading to spindle checkpoint re-activation and lethal mitotic arrest. Our results point to APC/C inhibitors as promising therapeutic agents targeting cohesion-defective cancers.

INTRODUCTION

Cell division requires the duplication of all chromosomes, followed by their segregation as two identical sister chromatids into two new daughter cells. Sister chromatid cohesion holds sister chromatids together until their proper separation is initiated at the metaphase-to-anaphase transition. Pairing of sister chromatids is achieved by a huge ring-shaped protein complex named cohesin, which consists of Smc1, Smc3, Rad21 (Scc1 in yeast) and either SA1 or SA2 (Scc3 in yeast). Besides keeping sister chromatids paired during early stages of mitosis, cohesin's DNA tethering capacity facilitates multiple additional processes in the cell, such as DNA repair, ribosome biogenesis, regulation of gene transcription and initiation of DNA replication[1]. Defects in the cohesion network are the cause of several rare genetic diseases named cohesinopathies. These include Cornelia de Lange Syndrome (CdLS, caused by mutations in NIPBL, Smc1A, Smc3, Rad21 or HDAC8[2-5]), Roberts Syndrome (RBS, caused by ESCO2 mutations[6, 7]) and Warsaw Breakage Syndrome (WABS, caused by DDX11 mutations[8]). Whereas it is not clear whether these predispositions are linked to an increased cancer risk, mutations in genes encoding cohesin subunits and regulators have been reported in a substantial number of human tumors[9-15]. Cohesion defects may thus form a new hall mark of cancer that could be exploited in therapy.

When cells enter mitosis, the bulk of cohesin is removed from chromosome arms during prophase, in a manner dependent on phosphorylation of cohesin subunits by mitotic kinases and the cohesion antagonist Wapl (reviewed in [16]). However, centromeres are protected against loss of cohesion by Sgo1, which attracts a phosphatase to prevent phosphorylation of the Wapl antagonist Sororin, and SA2 [17-21]. During prometaphase, the kinetochores of paired sister chromatids attach to the mitotic spindle and subsequently come under tension of spindle pulling forces. Resisting spindle pulling forces is an important function of sister chromatid cohesion, preventing premature sister chromatid separation until the last pair of sister chromatids becomes bi-oriented on the mitotic spindle. The occurrence of prematurely separated sister chromatids which lose microtubule-kinetochore attachments activates the spindle assembly checkpoint (SAC)[22]. Continuous arrest of cells in the SAC may lead to cell death or highly aneuploid daughter cells [23].

The SAC is an evolutionary conserved signaling cascade that acts in prometaphase and keeps cyclin B1-Cdk1 active during the process of chromosome bi-orientation[24, 25]. Proper attachment of all the paired sister chromatids to the spindle and their alignment to the cell equator is a stochastic process that can take roughly up to one hour in normal cells. Maintenance of cyclin B1-Cdk1 activity during this phase is essential to keep the mitotic state until bi-orientation is complete. Simultaneously, Separase, a Rad21 protease, must be kept inactivated to protect centromere cohesion. The SAC is kept activate by kinetochores that are not properly attached to spindle microtubules, stimulating production of the mitotic checkpoint complex (MCC), composed of BubR1, Bub3, Mad2 and Cdc20[26]. The MCC blocks the anaphase promoting complex or cyclosome (APC/C), a multi-subunit E3 ubiquitin ligase, so that three of its substrates

remain stable for multiple hours: Securin, which blocks Separase[27], cyclin B1, which keeps Cdk1 active to keep cells in mitosis[28], and geminin, which blocks premature DNA replication licensing [29]. Achievement of proper attachment and centromere tension silences the SAC, activating APC/C-Cdc20. This leads to degradation of Securin to release Separase, cleaving the cohesin subunit Rad21 and allowing chromatid separation to opposite spindle poles. Cyclin B1 degradation occurs at the same time and causes inactivation of Cdk1, initiation of cytokinesis and mitotic exit[30]. Geminin is also degraded, preparing cells for DNA replication[29].

SAC silencing may involve multiple mechanisms, such as tension-sensitive kinetochore phosphorylations[31], activation of phosphatases that antagonize certain mitotic kinases[32] and dynein-microtubule-mediated stripping of SAC proteins from kinetochores upon microtubule attachment[33]. Furthermore, p31^{comet} promotes the release of Mad2 from the MCC, thereby initiating Cdc20 release downstream of kinetochores[34-37].

Cancer arises by an accumulation of genetic and epigenetic alteration in cancer genes, disturbing the normal signaling routes in the cell. This can make tumor cells highly dependent on a specific pathway that remains intact, while in healthy cells the back-up pathway still exists. The phenomenon that two genes or two signaling pathways can compensate each other, but inactivation of both diminishes cell viability, is called 'synthetic lethality'. Such interactions between pathways can be exploited to eradicate tumor cells without many side effects on normal tissues[38]. Here, we aim to identify pathways that are specifically lethal in combination with defects in sister chromatid cohesion, to start to develop of a new targeted cancer therapy. We use a patient fibroblast cell line in which DDX11 mutations cause cohesion defects[8] in parallel with its functionally corrected counterpart as model system and subject these cell lines to siRNA screens in order to find lethal interactors. We find that the DDX11 mutant cells are hyper-sensitive to inhibition of the APC/C. APC/C inhibition to a level that is tolerated by normal cells, causes a detrimental further loss of chromatid cohesion during mitosis in cohesion defective cells, and subsequently induces mitotic death. This lethality is observed in a range of different cohesion defective cells and requires a functional SAC. In line with this observation, treatment with the recently published cell permeable APC/C inhibiting drug apcin is particularly toxic in cell lines with defective sister chromatid cohesion, including tumor cell lines.

RESULTS

A genome-wide siRNA screen in DDX11 mutant cells

We generated SV40-immortalized fibroblasts derived from a Warsaw Breakage Syndrome patient and functionally corrected the cohesion defects in this cell line (railroad chromosomes, RR, and premature sister chromatid separations, PCS, ***Fig. 1a***,[39]) by stable transfection of DDX11 cDNA (***Fig. 1a***,[39]). We used these two cell lines, hereafter named DDX11^{-} and DDX11^{+} cells, to screen for genes whose inactivation is specifically lethal in cohesion-defective cells by performing whole-genome siRNA screens. An overview of the procedure is provided in ***Fig. 1b***. Briefly, cells were reverse transfected in 384-well plates with single-target pools of four distinct siRNAs using an automated platform and viability was measured after 4 days using the CellTiter-Blue assay. We computed p-values and false discovery rates (FDR) for the difference in cell viability with each siRNA between the two cell lines (Supplementary ***Fig. 1***). This revealed 113 siRNAs with FDR<0.1. We excluded 32 genes based on updated library annotation according to NCBI RefSeq58 or because they exhibited the highest lethality in DDX11^{+} cells and cherry-picked 17 additional genes with FDR slightly above the threshold, so in total 98 hits were selected (Supplementary Data 1).

We rescreened these 98 hits in DDX11^{-} and DDX11^{+} cells with deconvoluted sets of 4 siRNAs. Subsequently, we calculated the differential effect (ratio DDX11+ / DDX11-) and toxicity (lethality in DDX11+ cells) for every individual siRNA (Supplementary Data 2). Interestingly, of 19 genes showing ratio >2 and toxicity <50%, we identified *APC2*, *APC3/Cdc27* and *APC4*, whichencode three different components of the Anaphase Promoting Complex or Cyclosome (APC/C).

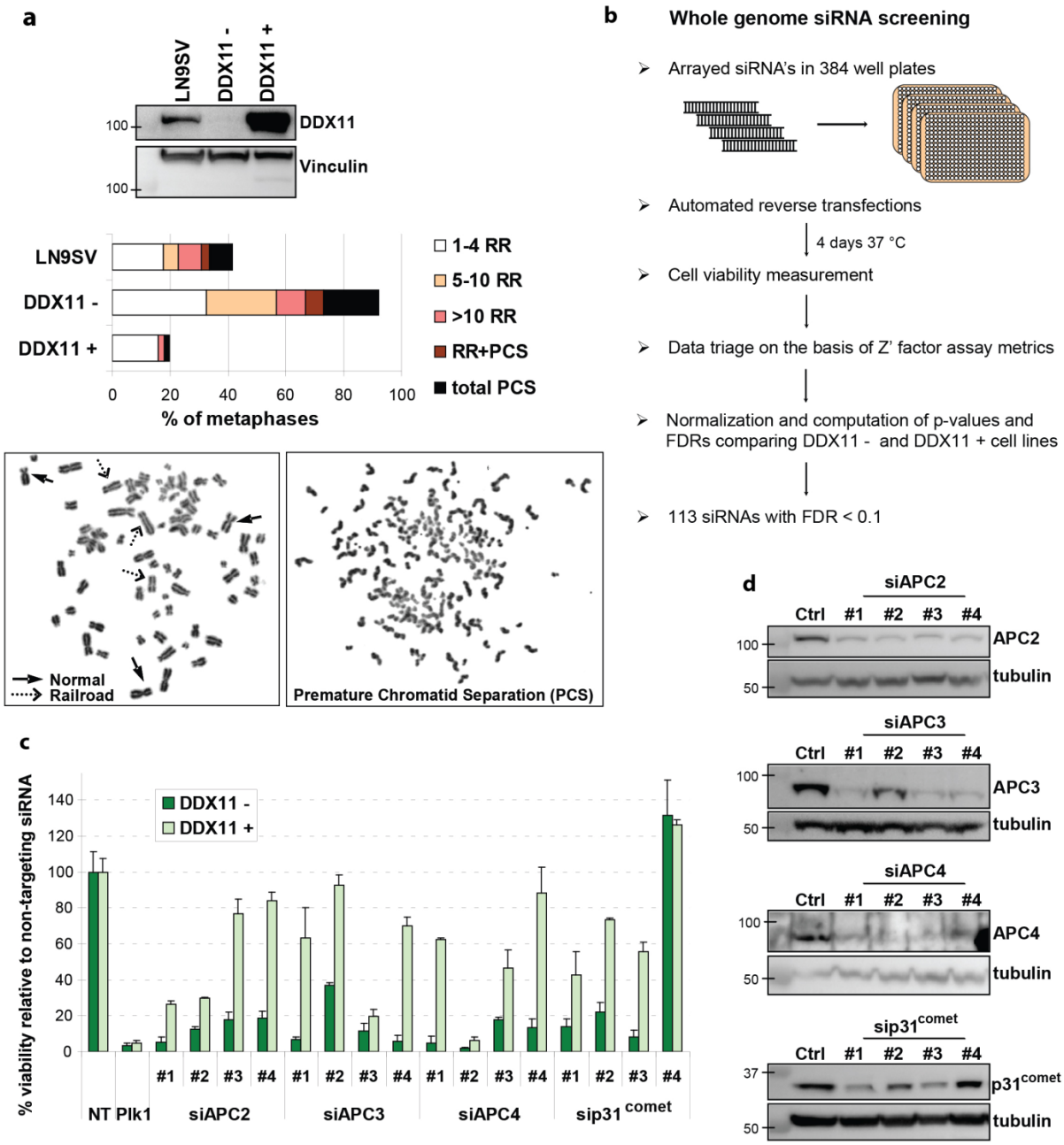

Figure 1:Genome-wide siRNA screen in DDX11 mutant cells. *(a) Western blot and cohesion defect analysis of DDX11⁻ and DDX11⁺ cells next to SV40-immortalized wild-type LN9SV fibroblasts. Combined data of two independent metaphase preparations are shown. Two examples of two metaphases illustrate normal and railroad (RR) chromosomes as well as premature chromatid separation (PCS). (b) Schematic representation of the genome-wide siRNA screening procedure using Dharmacon's siARRAY whole human genome siRNA library. Three independent siRNA screens for both cell lines were performed. (c) The same platform was used to perform two independent deconvolution experiments with a selection of 98 hits in both cell lines, of which the results of four genes are shown. Error bars denote standard deviations of two independent experiments. (d) Cells were transfected with the indicated siRNAs and protein levels were analyzed after three days by western blot.*

Moreover, we also identified *Mad2L1BP/p31^{comet}*, which encodes a negative regulator of the APC/C inhibitor Mad2. Accompanying western blots (***Fig. 1c, d***) suggested that the weaker effects of siAPC3#2 and sip31^{comet}#4 in DDX11^{-} cells result from lower knockdown efficiency. The toxicity of siAPC2#1, siAPC2#2, siAPC3#3 and siAPC4#2 in DDX11^{+} cells might relate to an induction of off-target effects by these RNAi oligos. The increased sensitivity of DDX11^{-} cells to APC2 inhibition was confirmed with an additional pool of four unrelated APC2 targeting siRNAs (Supplementary ***Fig. 2***). Together, these results indicate that DDX11 mutant cells are highly sensitive to knockdown of APC/C subunits.

Cohesion defects sensitize to APC/C inhibition

We investigated the response to APC/C inhibition in a number of cell lines from our laboratory with known cohesion status. Two head and neck squamous cell carcinoma (HNSCC) cell lines, isolated from a single patient, represent a highly related panel of cells. Importantly however, they differ in their sister chromatid cohesion status. Sister chromatid cohesion is normal in UM-SCC-14C but disturbed in UM-SCC-14B[40] (***Fig. 2a***). Of three luminal-type breast cancer cell lines, OCUB-M cells exhibit severe cohesion defects, whereas most metaphases of MCF7 and CAMA-1 cells appear normal (***Fig. 2a***). Depletion of APC3 or p31^{comet} induced the strongest growth inhibition in UM-SCC-14B and OCUB-M cells (***Fig. 2b,c***). Similarly, APC/C knockdown showed a stronger effect in ESCO2^{-} cells, derived from a Roberts Syndrome patient[41], as compared to its functionally corrected counterpart ESCO2^{+} (Supplementary ***Fig. 3***). We conclude that increased sensitivity to APC/C inhibition is not restricted to DDX11 mutant cells, but could be a more general feature of cells in which the cohesion of sister chromatids during metaphase is weak.

Interestingly, a new APC/C-inhibiting compound named apcin has recently been developed[42], which partially inhibits APC/C activity. Apcin acts by competitively binding to the mitosis-specific APC/C cofactor Cdc20 and hampering the ubiquitination of D-Box containing substrates[42]. As expected, apcin phenocopied the effects of the APC/C-Cdc20 impairing siRNAs in the DDX11^{-} and DDX11^{+} cell panel (Supplementary ***Fig. 4***). We then analyzed a larger panel of HNSCC and luminal breast cancer cell lines of which metaphase spreads had been analyzed in our laboratory. Sensitivity to apcin was corrected for the number of cell divisions during three days treatment. This revealed a remarkable and significant correlation between thepresence of cohesion defects in tumor cells and sensitivity to apcin (***Fig. 2d***). Interestingly, the cohesion status did not correlate well with sensitivity to paclitaxel (***Fig. 2e***), which activates the SAC by interfering with microtubule dynamics and spindle forces.

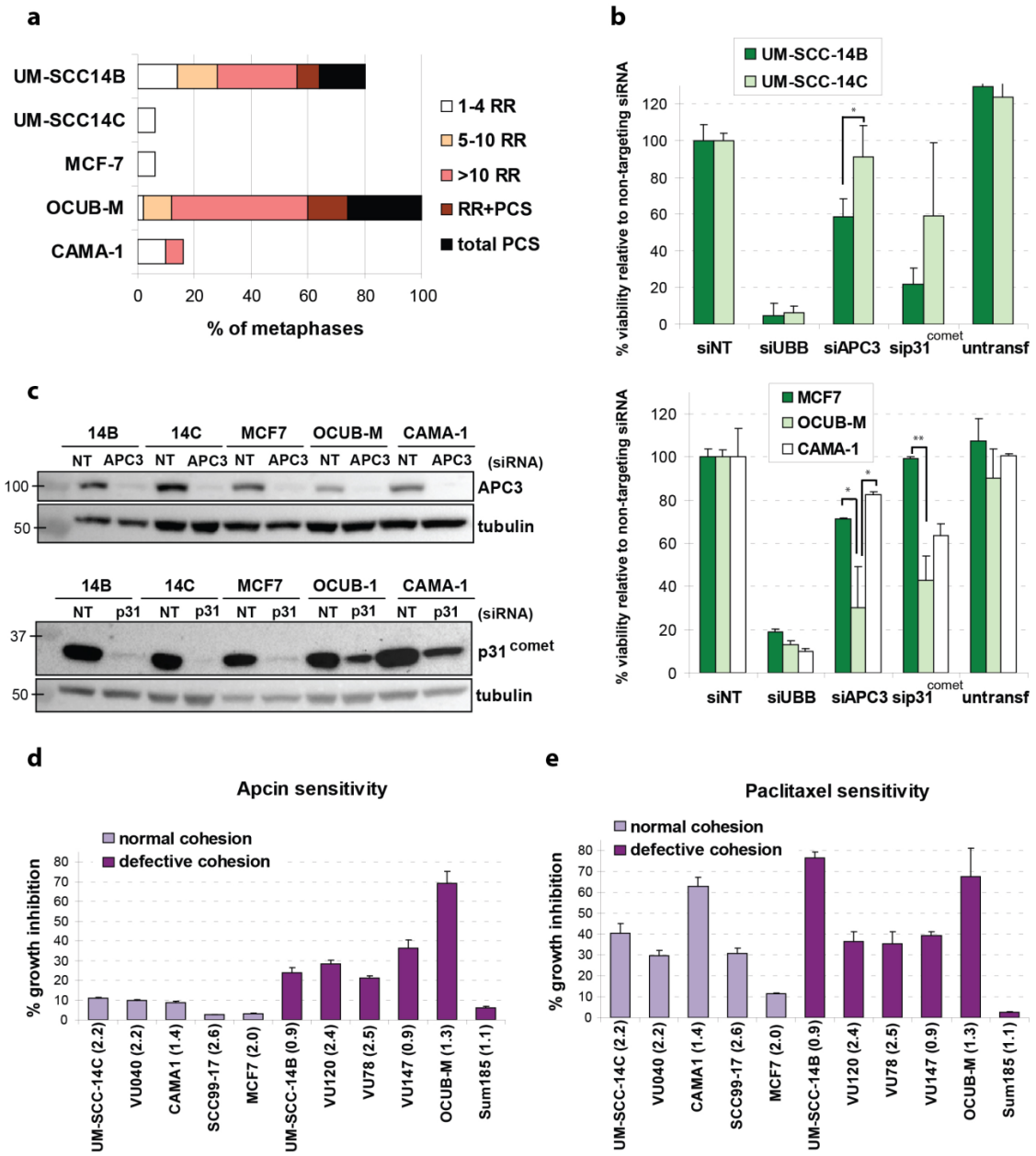

Figure 2: Defective sister chromatid cohesion sensitizes to APC/C inhibition. *(**a**) Cohesion defect analysis of five tumor cell lines (**b,c**) Cells were transfected with the indicated siRNAs. Protein levels were analyzed after three days by western blot and cell viability was measured after five days using a CellTiter-Blue assay. Error bars denote standard deviations of at least three technical replicates. (**d,e**) A panel of tumor cell lines with known cohesion status was seeded at optimized densities in two 96-wells plates. The next day, viability was assayed in one plate (t=0), whereas in the other plate medium was replaced with medium containing DMSO, apcin (150 µM) or paclitaxel (2 nM) and viability was measured three days later. We calculated the percentage growth inhibition of treated versus untreated cells and corrected this for the number of cell divisions (indicated between brackets) in untreated cells during the experiment. Error bars denote standard deviations of at least three technical replicates. Apcin sensitivity was significantly higher (p=0.030) in cohesion defective cells as compared to cells without cohesion defects, whereas paclitaxel sensitivity did not differ (p=0.537) using a Wilcoxon rank-sum test.*

APC/C inhibition aggravates cohesion defects and causes mitotic death

Apparently, cohesion defects make cells particularly vulnerable to a delay in mitosis when APC/C activity is reduced. We used time-lapse microscopy in order to analyze the mitotic events related to this sensitivity in live cells as they progressed through mitosis. Microscopic fields were analyzed for 16h and mitosis durations from nuclear envelope breakdown (NEB) to anaphase or cell death are shown in ***Fig. 3a***. This shows that the duration of mitosis strongly correlates with cell death. Moreover, a larger percentage of APC3 depleted DDX11^{-} cells undergo mitotic death as compared with APC3 depleted DDX11^{+} cells. This difference is probably larger than displayed, as many DDX11^{-} cells were still in mitosis at the end of the movie (***Fig 3a***. bar graph). In line with these observations, consecutive flow cytometry analyses (Supplementary ***Fig. 5a-c***) revealed an increased mitotic fraction in DDX11^{-} cells (day 2) that is followed by a strong induction of a fraction with 4N DNA content that stain negative for phospho-Histone H3 (day 3), probably representing mitoses that do not produce two new cells due to cytokinesis failure. APC/C inhibition using different siRNAs shows comparable results (Supplementary ***Fig. 5d***). Importantly, 24h apcin treatment also specifically blocked DDX11^{-} cells in mitosis (***Fig. 3b***). We then performed a cohesion defect analysis, which revealed a striking enhancement of premature chromatid separation upon APC3 knockdown in DDX11^{-} cells (***Fig.3c***).

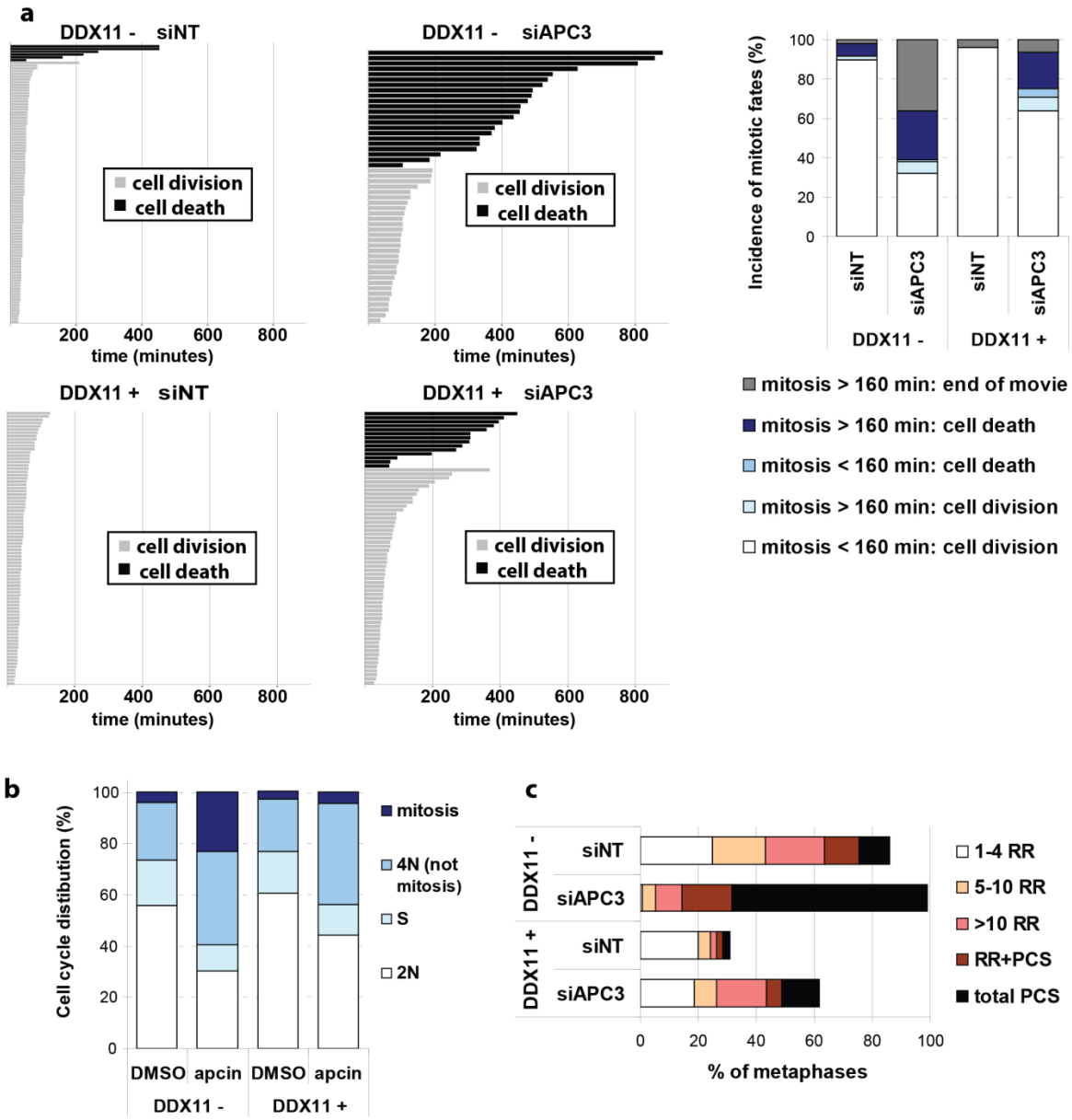

Figure 3: APC/C inhibition leads to a lethal mitotic delay and further loss of cohesion. *(**a**) DDX11⁻ and DDX11⁺ cells were transfected with the indicated siRNAs. Two days after transfection, cells were analyzed for 16h using live cell imaging to measure the duration of mitosis from the time of nuclear envelope breakdown (NEB) until anaphase or (if no anaphase was visible) viable mitotic exit, or cell death. Mitosis duration significantly correlated with mitotic fate; $p=2.21*10^{-8}$ in DDX11⁻ cells and $p=4.67*10^{-5}$ in DDX11⁺ cells, using a students t-test. (**b**) DDX11⁻ and DDX11⁺ cells were treated with 150 µM apcin for 24h and analyzed by flow cytometry. (**c**) DDX11⁻ and DDX11⁺ cells were transfected with APC3 siRNA for three days and metaphases were analyzed for cohesion defects. Means of two independent experiments are shown.*

We reasoned that such severe cohesion defects might explain the observed cell death. If that is indeed the case, directly reinforcing cohesion during metaphase should rescue cohesion, mitotic progression and viability. To test this, we used an siRNA targeting WAPL, a protein required to remove the majority of cohesin complexes from chromosome arms during

prophase[43, 44]. Indeed, WAPL knockdown partially restored sister chromatid cohesion in DDX11⁻ cells and also reverted the accumulation of mitotic cells and lethality upon APC3 knockdown (*Fig. 4a-d*).

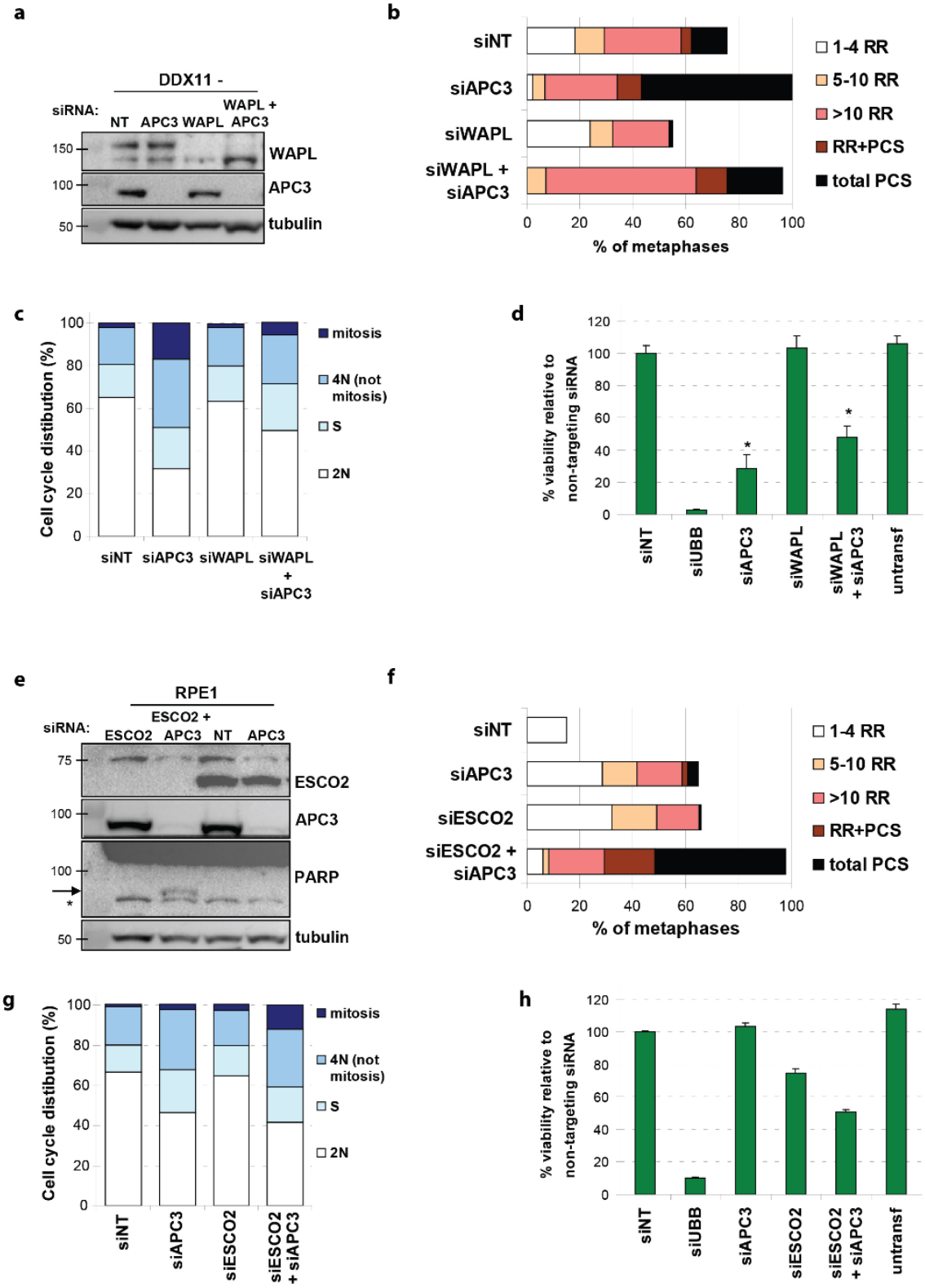

Figure 4: Cohesin levels determine sensitivity to APC/C inhibition. *(a-d) DDX11⁻ cells were first transfected with either non-targeting or WAPL siRNA, to obtain an efficient knockdown. Two*

*days later, cells were again transfected with the indicated siRNAs. At day 3 after the second transfection round, cells were harvested for western blot (**a**), cohesion defect analysis (**b**), and flow cytometry (**c**). At day 4, viability was measured with a CellTiter-Blue assay (**d**). Viability upon siAPC3 only was significantly different from siWAPL+siAPC3 (p=0.002 using a students t-test), indicated by an asterisk. (**e-h**) RPE1 cells were transfected with the indicated siRNAs. Western blot (**e**), cohesion defect analysis (**f**) and flow cytometry (**g**) were performed two days after transfection. Means of two independent experiments are shown. The asterisk indicates non-specific background staining. At day 4, viability was measured with a CellTiter-Blue assay (**h**). A students t-test revealed p=0.057 when comparing viability upon siAPC3 only and siESCO2+siAPC3. Error bars denote standard deviations of three technical replicates.*

We then asked whether the opposite was also true: can artificially weakening sister chromatid cohesion in otherwise normal cells sensitize them to lethal APC/C inhibition? Indeed, co-depletion of ESCO2 and APC3 in RPE1 cells resulted in severe cohesion defects, increased mitotic delay, caspase-dependent PARP cleavage (indicative of apoptosis induction) and reduced cell viability (***Fig. 4e-h***). Co-depletion of Rad21 and APC3, or of DDX11 and APC3, gave the same results (Supplementary ***Fig. 6***).Notably, acute knockdown of DDX11 in RPE1 cells did not alter APC3 levels and by using varying concentrations of siAPC3 we also excluded that small differences in APC3 expression underlie the differential sensitivity of $DDX11^-$ and $DDX11^+$ cells (Supplementary ***Fig. 7***).In conclusion, our findings indicate that weakened sister chromatid cohesion at the start of mitosis, together with a reduction of APC/C activity, induce prolonged mitosis, massive premature chromatid separation and mitotic death.

Weak cohesion plus APC/C inhibition leads to cohesion fatigue

To investigate whether the observed cell death was strictly related to mitosis, we accelerated mitosis by blocking the spindle checkpoint using the Mps1 inhibitor reversine[45] (***Fig. 5a-d***; the experiment including $DDX11^+$ cells is shown in Supplementary ***Fig. 8***). Indeed, reversine reduced caspase-dependent PARP cleavage and partially rescued cell viability in response to APC3 knockdown (***Fig. 5a,b***). Furthermore, the increase of mitotic fraction and cohesion defects (***Fig. 5c,d***) was strongly reduced. These results show that a spindle checkpoint-dependent arrest contributes to lethality by APC/C inhibition in cohesion defective cells. This is in line with previous reports showing that the mitotic arrest induced by APC/C inhibition is dependent on activation of the spindle checkpoint[22, 46]. This mechanism involves a phenomenon known as 'cohesion fatigue'; a gradual loss of sister chromatid cohesion that can be observed during a prolonged mitosis[47, 48]. Importantly, cohesion fatigue is thought to largely depend on microtubule pulling forces. We therefore used nocodazole to block the development of tension across sister kinetochores. Indeed, APC3 knockdown did not further increase the cohesion defects in $DDX11^-$ cells in the absence of a functional mitotic spindle (***Fig. 5e***). We then investigated whether residual activity of Separase, the enzyme that becomes activated upon APC/C-mediated Securin degradation[49], is also responsible for additional cohesion loss. In line with the reported APC/C and Separase independence of cohesion fatigue[47], the effects of APC3

knockdown on cohesion, cell cycle and viability did not change when Separase was co-depleted (*Fig. 5f-i*).

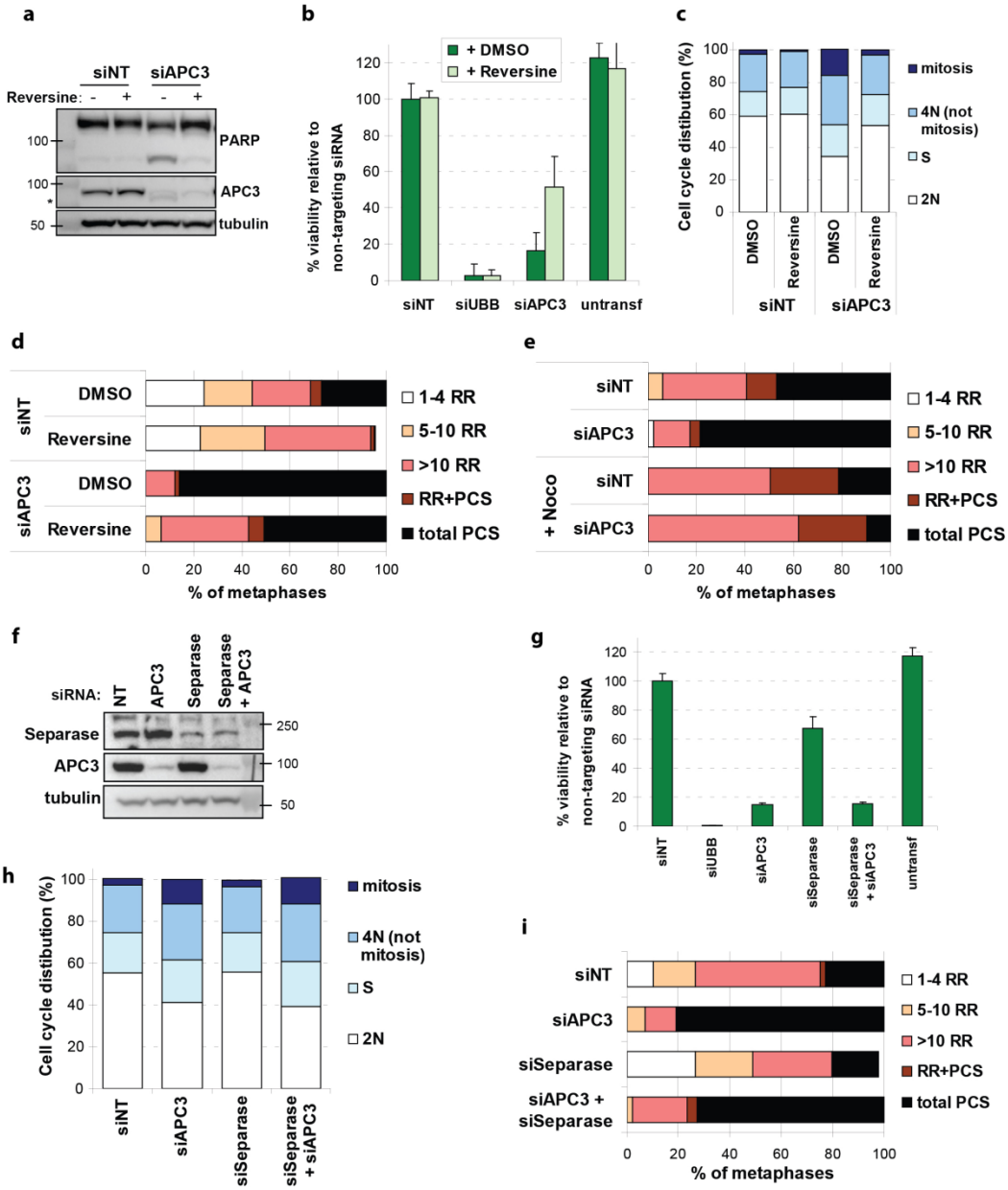

Figure 5: Cohesion fatigue explains the synergy of weak cohesion and APC/C inhibition. *(**a-d**) DDX11⁻ cells were transfected with the indicated siRNAs and after 1 day 100 nM reversine or DMSO was added. Western blot, flow cytometry and cohesion defect analysis were performed two days after transfection and cell viability was measured four days after transfection. The asterisk indicates detection of residual cleaved PARP signal in the APC3 blot. (**e**) DDX11⁻ cells were depleted of APC3 for 30h. After shaking off mitotic cells, cells were incubated with 100 ng/mL nocodazole for an additional 14h and analyzed by cohesion defect analysis. (**f-i**) DDX11⁻ cells were transfected with the indicated siRNAs. Western blot, flow cytometry and cohesion defect analysis were performed two days after transfection and cell viability was measured four*

days after transfection. Representatives of two independent experiments are shown. Error bars denote standard deviations of at least three technical replicates.

To visualize sister chromatid alignment at the metaphase plate, we then used GFP-H2B expressing RPE1 cells and analyzed chromosome congression by time-lapse fluorescence microscopy (***Fig. 6*** and Supplementary Movie 1-6). Combined depletion of ESCO2 and APC3 caused a high percentage of mitoses to lose chromosome alignment on the metaphase plate, a process we termed chromosome scattering. The majority of these cells arrested in mitosis for many hours, and in almost all cases where APC3 RNAi was combined with ESCO2 RNAi, the prolonged mitotic arrest culminated in cell death. Single APC3 knockdown also increased metaphase duration, but this was in most cases followed by a normal anaphase and cell division, although in some cells the chromosomes also left the metaphase plate prior to the start of anaphase. In such cases, APC3 RNAi cells eventually divided perpendicular to the culture dish (Supplementary Movie 3,4), which indicated that the spindle had rotated, an effect sometimes observed after APC/C inhibition[50]. In addition, increased microtubule detachment from kinetochores may lead to a similar phenotype, for example resulting from impaired APC/C-dependent cyclin A degradation[51]. This does not necessarily induce a permanent mitotic arrest, but may still allow gradual cyclin B degradation and eventually mitotic exit, which would also explain cell division following scattering under conditions when only APC3 is depleted. It seems reasonable, however, that the more severe chromosome scattering observed in cohesion defective cells upon depletion of APC3 largely reflects the premature chromatid separation that we observed in our cohesion defect analyses of fixed cells (***Fig. 4f***). In summary, when APC3 is depleted, cells delay in metaphase, which can lead to some scattering of the chromosomes away from the metaphase plate, but this eventually leads to anaphase and cytokinesis (***Fig 6c,d***). However, when APC3 is depleted under conditions of impaired sister chromatid cohesion, a form of scattering is observed that relates to cohesion fatigue and causes cell death.

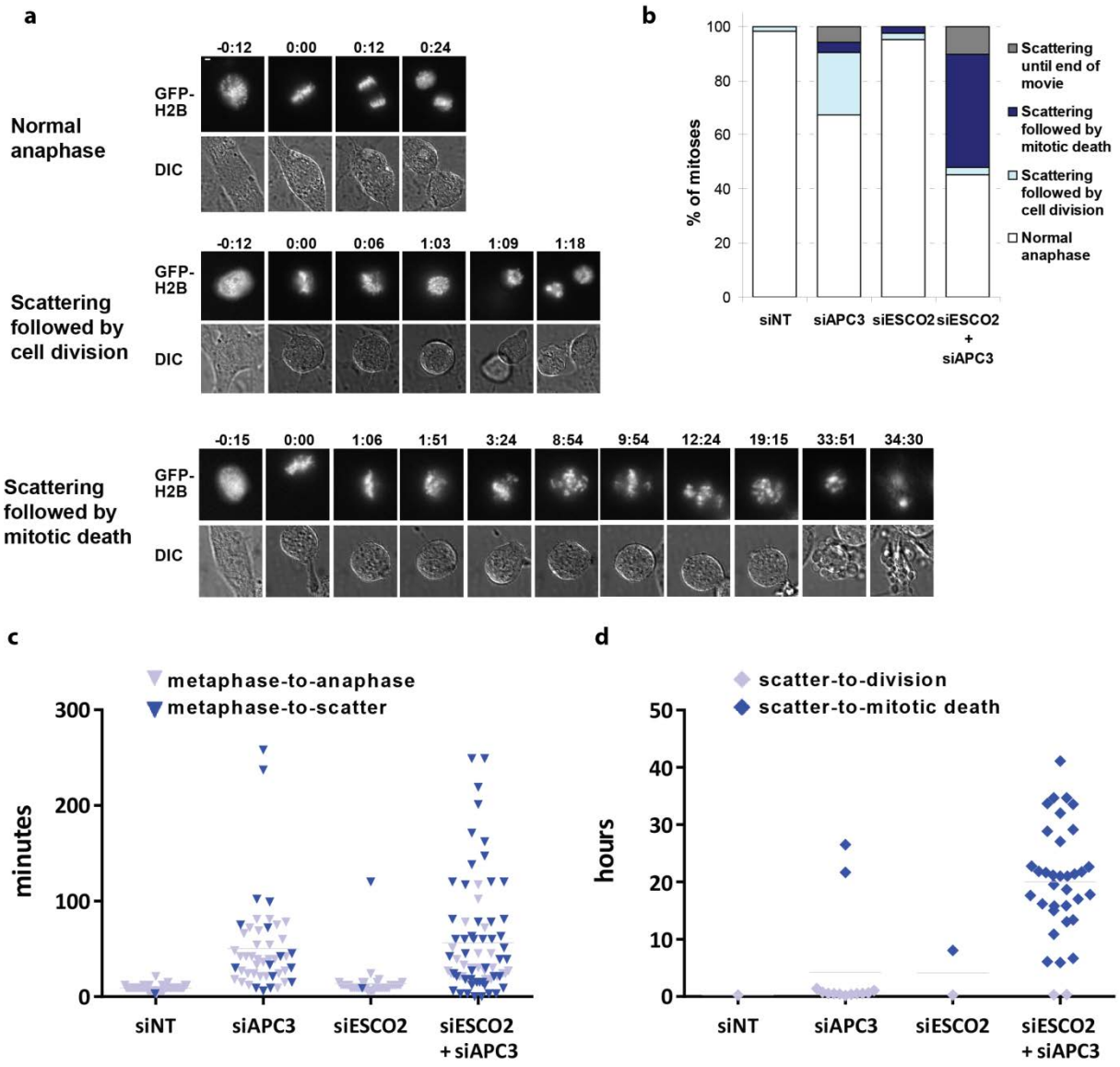

Figure 6: Severely prolonged mitosis with scattered chromosomes results in mitotic death. *RPE1 cells were imaged every 3 minutes for 48h using time-lapse microscopy, starting two days after transfection with the indicated siRNAs. (**a**) Representative examples of the observed phenotypes 'normal anaphase' (siESCO2), 'scattering followed by cell division' (siAPC3) or 'scattering followed by mitotic death' (siESCO2+siAPC3). Bar 5 µM. (**b**) Percentages of mitotic fates observed in the different conditions (siNT N=55, siAPC3 N=52, siESCO2 N=42, siESCO2+siAPC3 N=64). (**c**) Duration (in minutes) from the time of metaphase plate formation until either a normal anaphase or chromosome scattering was observed. (**d**) Duration (in hours) until the cells with scattered chromosomes (the dark blue cells in **c**) show either cell division or mitotic death.*

DISCUSSION

Mitotic cells require sister chromatid cohesion for maintaining a physical connection between replicated DNA molecules, in order to resist pulling forces and allow chromosome bi-orientation. Mutations in this network may facilitate tumorigenesis, possibly because they increase the chance of acquiring further genetic alterations[10]. However, such defects might also be disadvantageous in specific conditions, which would provide an opportunity to target those tumors. Regardless, cohesion defects are normally not observed in healthy cells, but can be detected in many tumors, thereby forming an interesting new target for cancer therapy. Here, we show that impaired sister chromatid cohesion, which is in itself not fatal, could become particularly detrimental when a cell encounters a substantial reduction of APC/C activity. It is important to note that a complete abolishment of APC/C activity is lethal in all cells (reviewed in[52]), but, perhaps depending on cellular context, it has become clear from various studies that cells may well tolerate reduced APC/C activity[53-55]. Our synthetic lethality screen revealed enhanced sensitivity of DDX11 mutant cells for reduced protein expression of different subunits of the APC/C, as well as the Cdc20 activating MAD2L1BP/p31^{comet} that silences the mitotic checkpoint. We did not identify additional APC/C subunits in the RNAi screen, which may be due to incomplete knockdown and effects that fall outside the window of differential tolerance, or from the induction of lethal off-target effects by some siRNAs. Importantly, enhanced sensitivity to APC/C inhibition was further validated in several additional cell lines with weakened sister chromatid cohesion. This indicates that it should be possible to pinpoint a discriminative level of APC/C inhibition that is therapeutically relevant.

We propose a model in which the enhanced sensitivity of cohesion defective cells to APC/C activity involves the previously reported appearance of unscheduled chromatid separation during a metaphase arrest termed 'cohesion fatigue'[47] (*Fig. 7*). Although all cells face a prolonged mitosis when APC/C activity is partially reduced, most normal cells will eventually manage to sufficiently reduce cyclin B1 and Securin levels, allowing normal cell division scheduled in synchrony with anaphase. However, cells with impaired cohesion at the start of mitosis will sooner reach the point at which chromatid connections on one or more paired sister chromatids become insufficient to resist spindle pulling forces. The resulting premature sister chromatid separation and concomitant loss of tension and attachment to the spindle will re-activate the SAC, or prevent its timely inactivation[56]. This in turn feeds forward to block

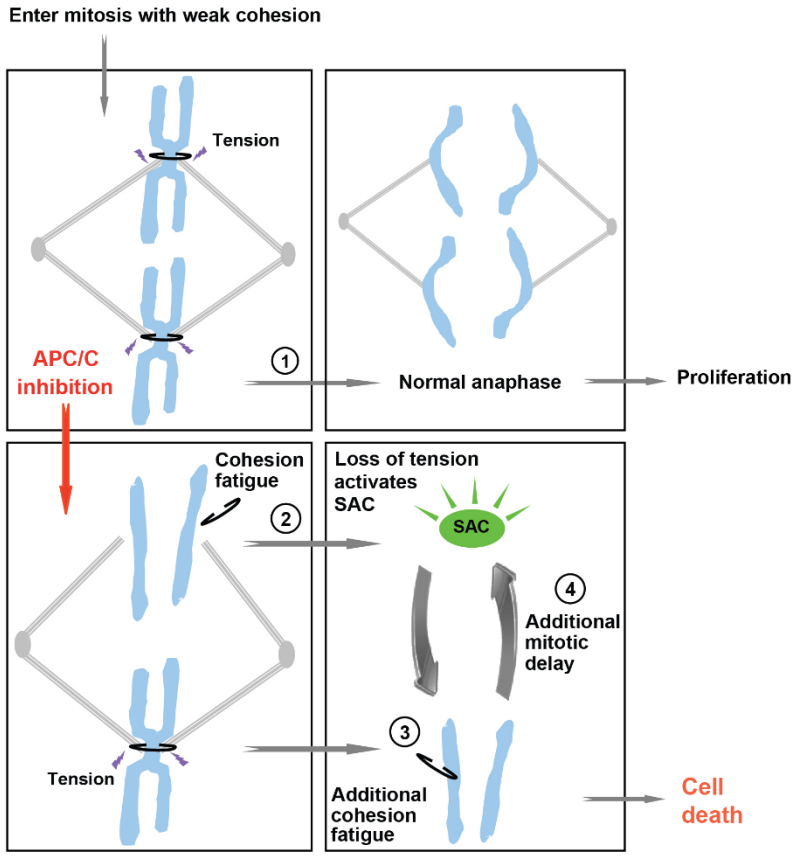

Model. *Cells entering mitosis with weakened cohesion normally manage to resist spindle tension until anaphase (1). Partial APC/C inhibition slows down cyclin B1 degradation and causes a prolonged mitosis with an intact mitotic spindle. During this prolonged mitosis, a gradual loss of sister chromatid cohesion may occur, that is dependent on microtubule pulling forces. This may cause some chromosomes to lose functional cohesion, resulting in 'cohesion fatigue' (2). Loss of tension on the kinetochores of those prematurely separated chromosomes then re-activates the SAC, leading to full inhibition of the APC/C and further blockage of mitotic exit. This can cause additional sister chromatid pairs to undergo cohesion fatigue (3), which in turn keeps the SAC activated (4). Eventually, this will result in death in mitosis or aberrant exit from mitosis as one or more aneuploid cells.*

APC/C-Cdc20 activity more effectively, which prolongs mitosis even more and increases the chance of additional paired sister chromatids losing cohesion. Eventually, many of these cells die in mitosis, or exit mitosis as non-productive daughter cells.

The cellular responses to mitotic delay are widely variable and appear to depend on an intriguing molecular competition between pathways leading to either apoptosis or slippage[23, 57]. Our findings suggest that the outcome of this race is strongly influenced by the level of sister chromatid cohesion at the start of mitosis, and the residual activity of the APC/C in prometaphase. We propose that under conditions of further APC/C inhibition, slippage is prevented and cells eventually die by apoptosis due to a more severe mitotic blockade.

APC/C activity exerts both pro- and anti-proliferative effects, which complicates its use as a target in cancer therapy. The differential oscillation of its co-activators Cdc20 and Cdh1 confers an important level of APC/C regulation[58]. Whereas APC/C^{Cdc20} drives mitosis, APC/C^{Cdh1} is mainly involved in maintaining the G0/G1 state. It has been suggested that inactivation of APC/C^{Cdh1} might contribute to cancer growth, through stabilization of oncogenic substrates that fuel proliferation[54]. Indeed, $Cdh1^{-/+}$ mice are more susceptible to spontaneous tumors[59]. Therefore, it seems desirable to exclusively inhibit APC/C^{Cdc20}. This argues for a strategy of APC/C^{Cdc20} inhibition, such as exemplified by the novel APC/C inhibitor apcin, in favour of one that inhibits both APC/C^{Cdch1} and APC/C^{Cdc20}, for example by proTAME, a drug which generally prevents cofactor binding to the APC/C. Interestingly, combining apcin with proTAME synergistically blocks mitotic exit[42]. This may relate to a similar mechanism as described above: in cells without pre-existing cohesion defects, APC/C inhibition resulting from combined treatment may be sufficiently strong to arrest cells in mitosis long enough to cause cohesion fatigue. Loss of tension then re-activates the SAC, thereby establishing a feed-forward loop (*Fig. 7*). It also indicates that apcin alone can only partially inhibit APC/C activity during mitosis. This could be advantageous in therapy, because basal APC/C function permits cell division of healthy somatic cells.

The increased apcin sensitivity could be translated to most cell lines with cohesion defects. It should be noted, however, that apcin did not inhibit growth of all cohesion-defective cells. Although numerous pharmacological and intracellular factors could influence the drug response, this observation may also indicate that not every condition that we characterize as 'defective cohesion' in metaphase spreads leads to a substantial acceleration of the process 'cohesion fatigue'. The precise nature of defective sister chromatid cohesion, such as those arising from reduced total levels of cohesive rings, their improper distribution along chromosomes or disturbed chromatin organization, may be relevant. Cohesion defects may result from replicative stress, such as those found in pRB-negative cells[60], so they could occur even more frequently than currently anticipated based on common mutations of known cohesin factors[1]. Pharmacological inhibition of the APC/C has long been considered unfeasible in a clinical setting. However, here we identified defective sister chromatid cohesion, an emerging hall mark of many tumours, as a novel foothold for cancer therapy by APC/C inhibitors. Future work will need to be directed at finding biomarkers of cohesion defects, that might predict response to apcin, and testing the effects of apcin or other APC/C inhibitors in animal cancer models.

Acknowledgments

We thank Petra van der Lelij for her contribution to establishing the $DDX11^{+}$ cell line and Hein te Riele for support and critical comments on the manuscript. This work is dedicated to the memory of Johan de Winter, who initiated and supervised this project until he deceased in August 2013. This work was supported by a Human Frontier Science Program (HFSP) project grant (grant number RGP0053/2010 to R.M.F.W.) and a KWF Research Grant VU 2011-4983 to

R.H.B, V.W.v.B, J.d.W. and R.M.F.W.). Work in the lab of R.W.K. is supported by NIH RO1 GM66492.

Author contributions

J.d.L, J.P.d.W., R.H.B., V.W.v.B., and R.M.F.W. conceived the experiments. J.d.L., A.F., A.B.O., I.v.d.M., M.A.R. and D.A.R. carried out the experiments. R.W.K. provided apcin and helped to design the apcin related experiments. R.X.d.M. performed statistical data analysis. The manuscript was prepared by J.d.L. and R.M.F.W. and edited by R.H.B., V.W.v.B., and R.W.K.

The authors declare no competing financial interests.

Supplementary data

Supplementary Figure 1: Statistical analysis of screen data.

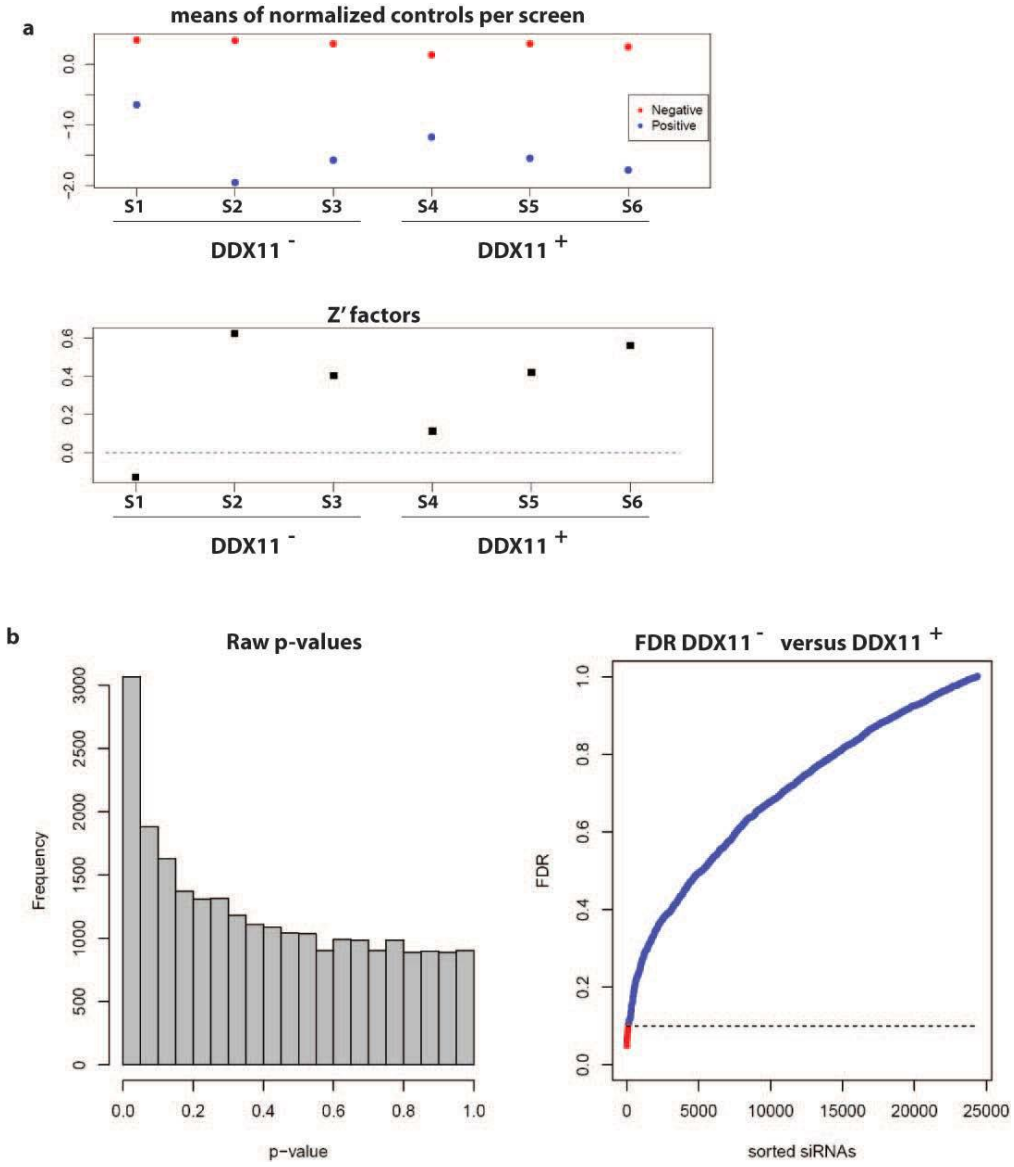

(a) Means of controls (top) and Z' factors (bottom) calculated for the log2-normalized data of all six screens. Per screen and control type (positive, negative) a total of 544 values are used. The negative control means are stable across screens, but the positive control means vary more. Screen 1 produced a relatively high positive control mean and, as a result, a Z' factor below 0. This was caused by poor cell growth in this particular case and therefore, this screen was excluded from further analysis. (b) Left: P-values computed per siRNA, for the difference between DDX11$^-$ and DDX11$^+$ cell lines. The enrichment of p-values near zero suggests a subset of siRNAs produces different results between the two cell lines. Right: FDRs corresponding to the p-values, where the number selected can be easily read for each FDR-control level. At the chosen control level of 0.10, 113 siRNAs are selected, of which 11 may be false positives.

Supplementary Figure 2: Increased sensitivity of DDX11- cells to APC2 knockdown.

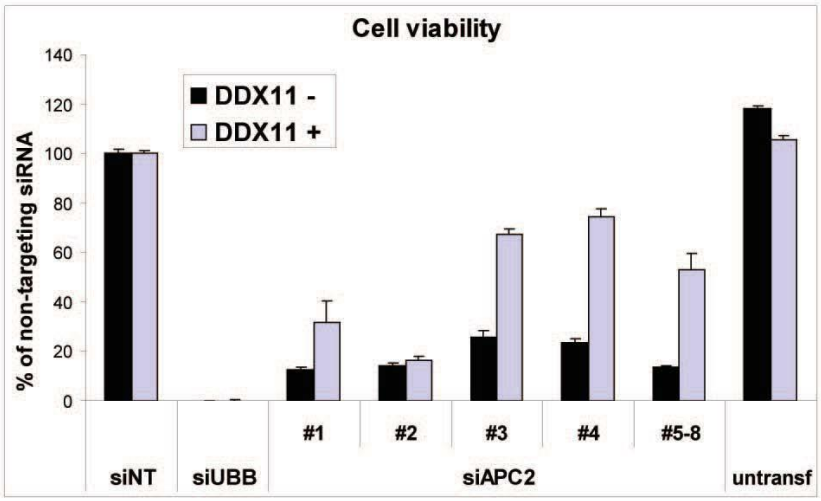

Cells were transfected with a pool of four APC2 siRNAs (#5-8, which do not overlap with the sequences of siAPC2 #1-4 used in Fig. 1c). Viability was measured at day 4 with a CellTiter-Blue assay.

Supplementary Figure 3: ESCO2 mutation sensitizes to siRNA-mediated APC/C inhibition.

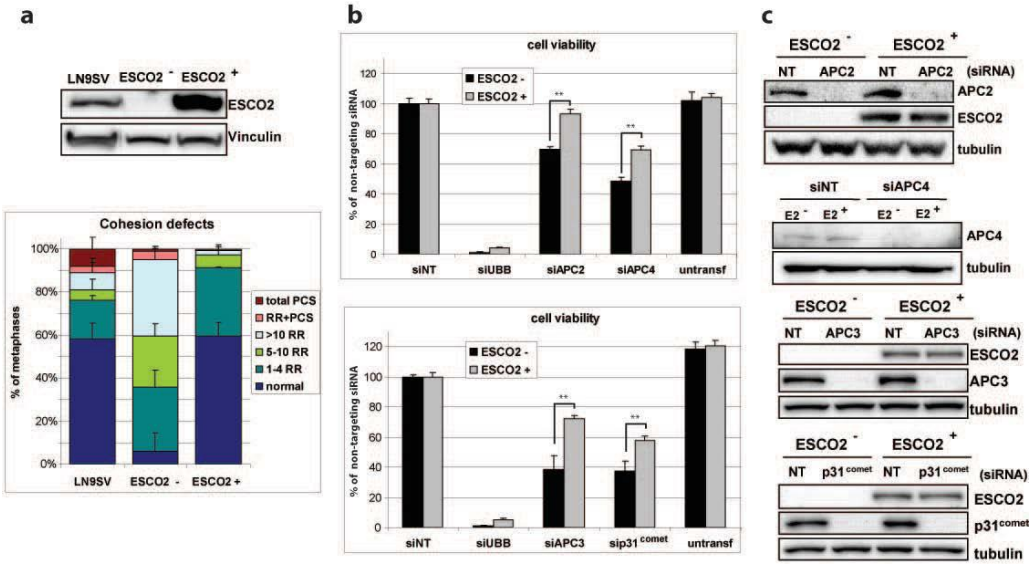

*(**a**) Western blot and cohesion defect analysis of ESCO2⁻ and ESCO2⁺ cells next to SV40-immortalized wild-type LN9SV cells. Error bars denote standard deviations of two independent experiments. Two irrelevant lanes between lane 1 and 2 were spliced out. (**b,c**) Cells were transfected with the indicated siRNAs. Protein levels were analyzed after three days by western blot and cell viability was measured after five days using a CellTiter-Blue assay. Error bars denote standard deviations of at least three technical replicates.*

Supplementary Figure 4: DDX11 mutation sensitizes to pharmacological APC/C inhibition.

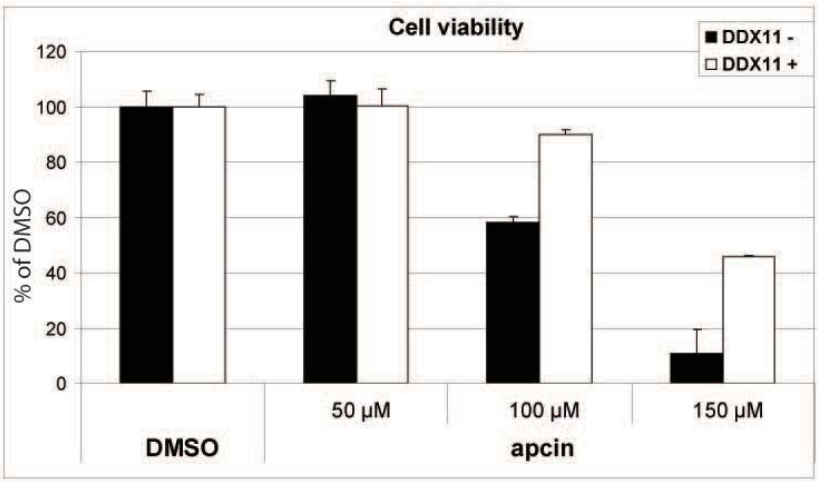

DDX11⁻ and DDX11⁺ cells were treated with different concentrations of apcin for three days and cell viability was measured using a CellTiter-Blue assay. Error bars denote standard deviations of eight technical replicates.

Supplementary Figure 5: Increased 4N DNA content upon knockdown of APC/C components.

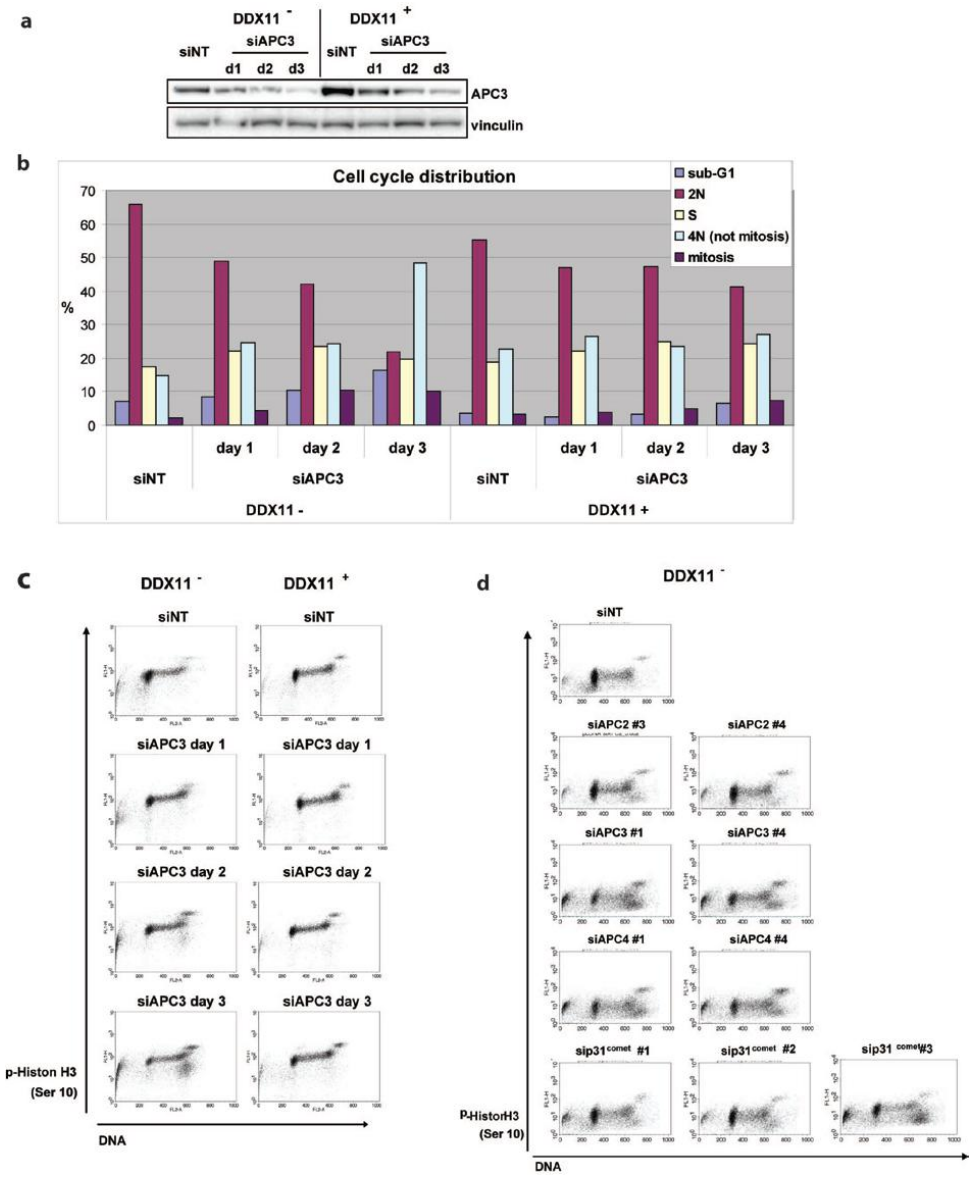

*(**a-c**) Cells were harvested at different time-points after siAPC3 transfection and analyzed by western blot and flow cytometry using co-staining of propidium iodide and phospho-Histone H3. DDX11⁻ cells were transfected with indicated siRNAs, harvested after three days and analyzed by flow cytometry.*

Supplementary Figure 6: Synthetic lethality of Rad21 and APC3, as well as of DDX11 and APC3.

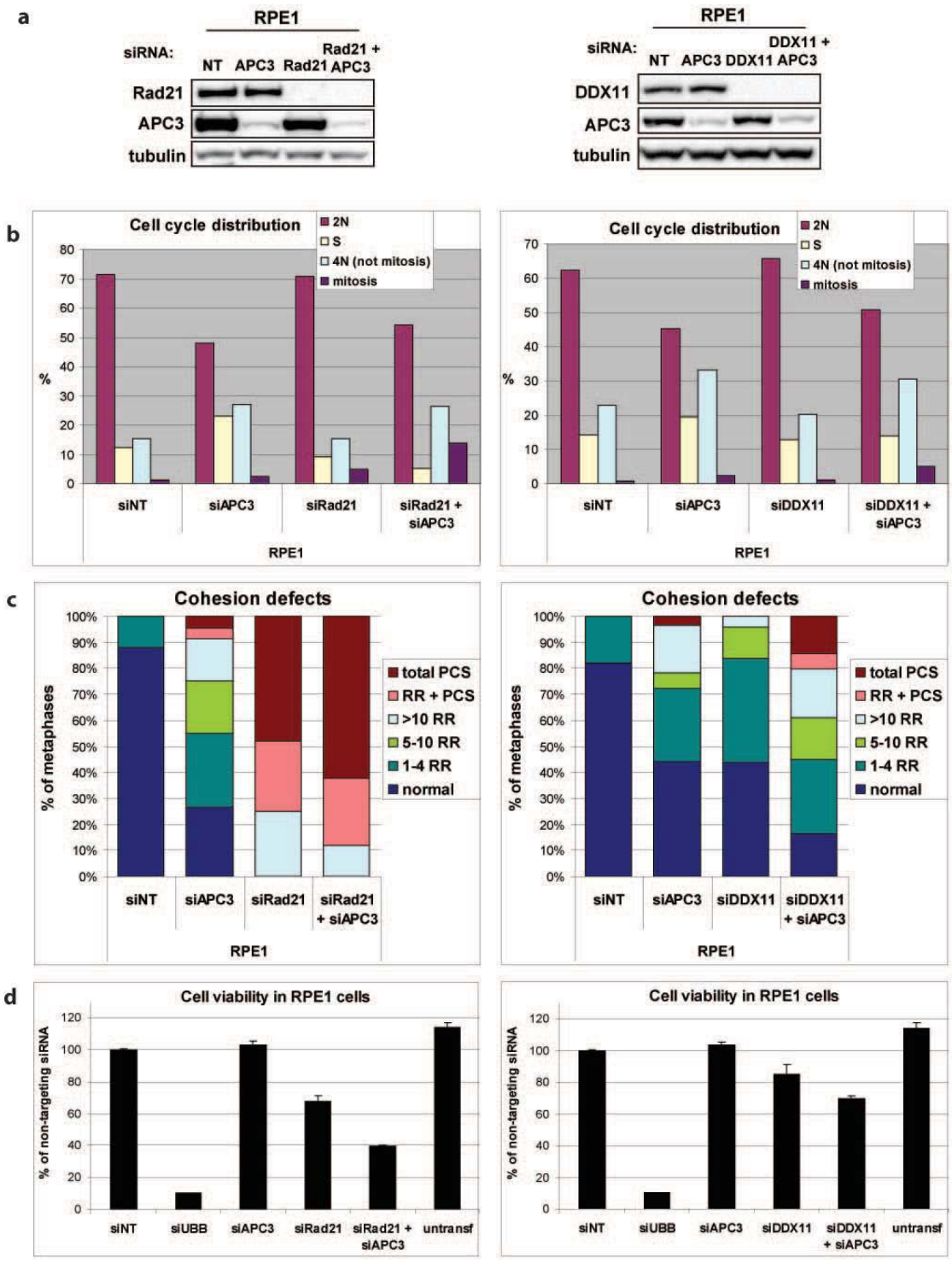

RPE1 cells were transfected with the indicated siRNAs. Western blot (a) flow cytometry (b) and cohesion defect analysis (c) were performed two days after transfection. Viability was measured at day four with a CellTiter-Blue assay (d). Error bars denote standard deviations of three technical replicates.

Supplementary Figure 7: Titrating siRNA concentration confirms differential sensitivity of DDX11$^-$ and DDX11$^+$ cells to APC3 inhibition.

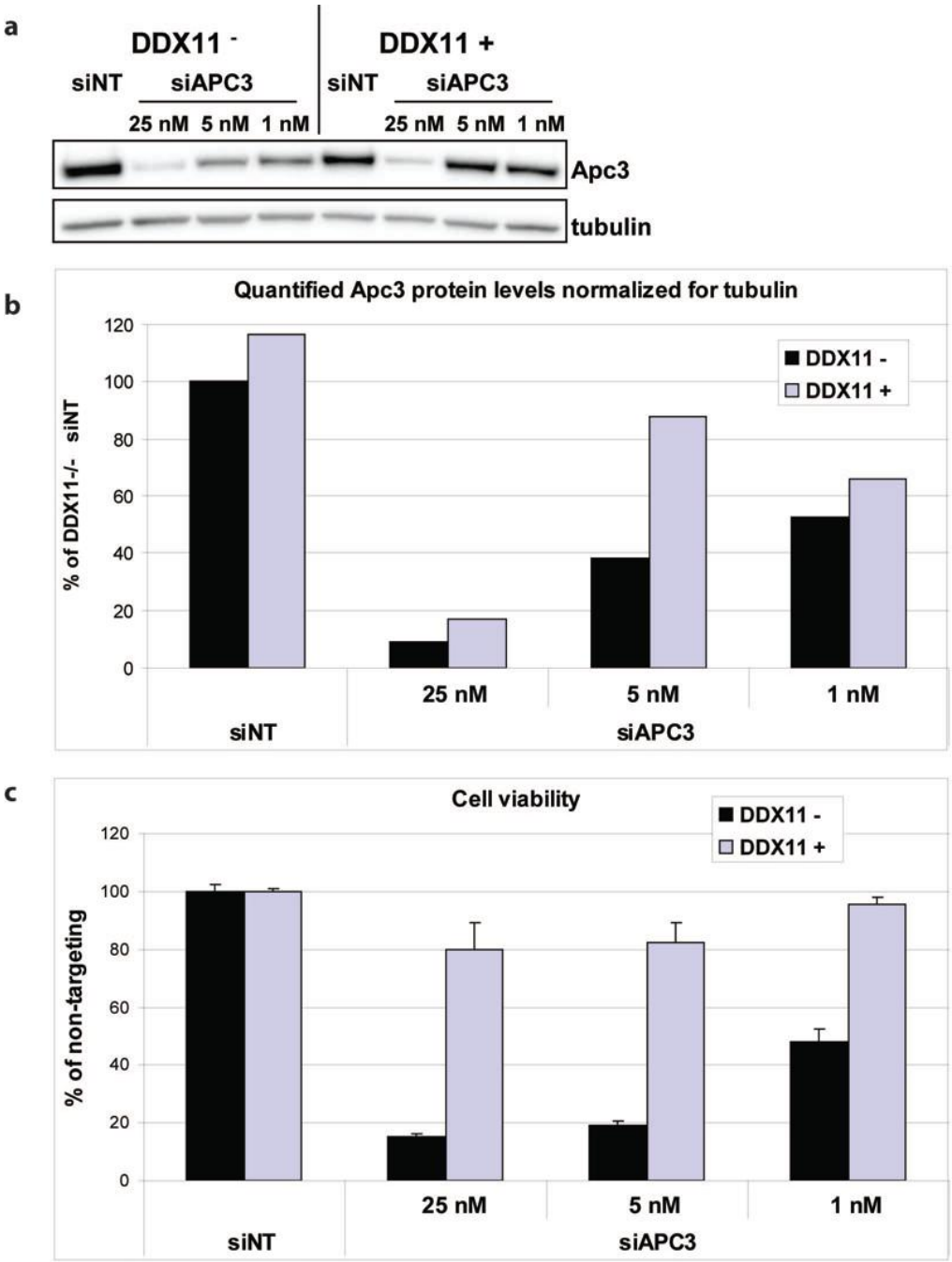

Cells were transfected with different concentrations of APC3 siRNA and protein levels were analyzed by western blot (a). Bands were quantified and normalized to tubulin (b). Cell viability was measured with a CellTiter-Blue assay (c). Note that 1 nM siAPC3 in DDX11$^-$ cells causes a much weaker knockdown than 25 nM in DDX11$^+$ cells, while the effect on viability is still stronger in DDX11$^-$ cells.

Supplementary Figure 8: Responses to APC/C inhibition are dependent on the spindle assembly checkpoint.

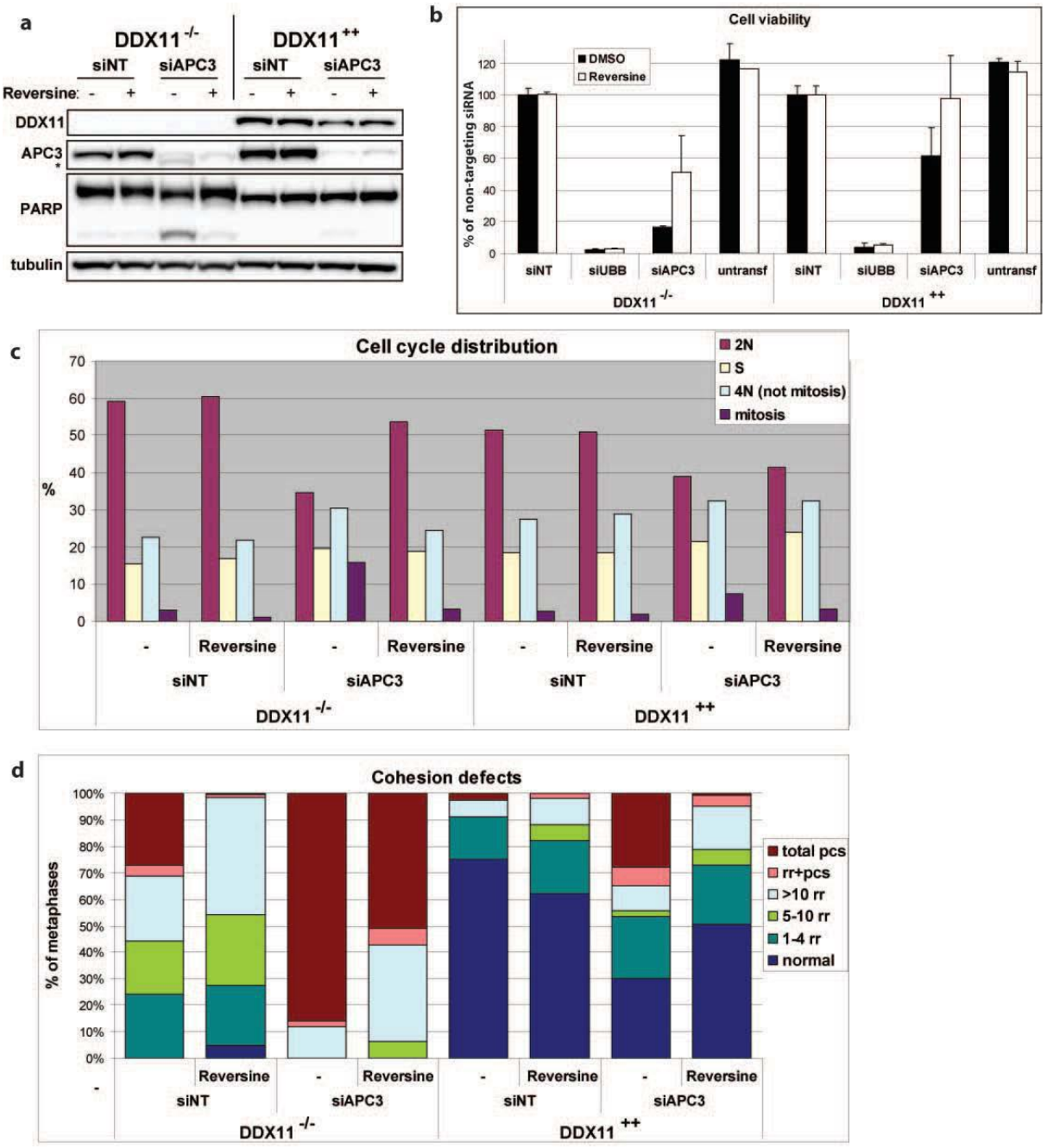

Cells were transfected with the indicated siRNAs and after 1 day 100 nM reversine or DMSO was added. Western blot, flow cytometry and cohesion defect analysis were performed two days after transfection and cell viability was measured four days after transfection. Error bars denote standard deviations of at least three technical replicates. The asterisk indicates detection of residual cleaved PARP signal in the APC3 blot. Note that the data for DDX11- cells are also shown in Fig. 5a-d.

Supplementary Figure 9: Uncropped western blots of main figure experiments

Figure 1a

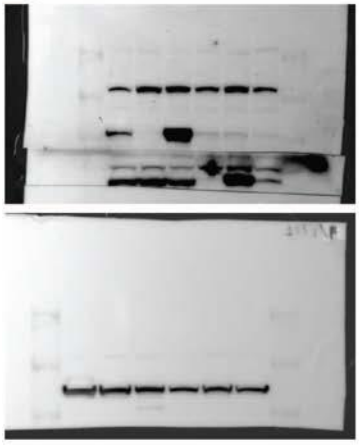

Figure 1d

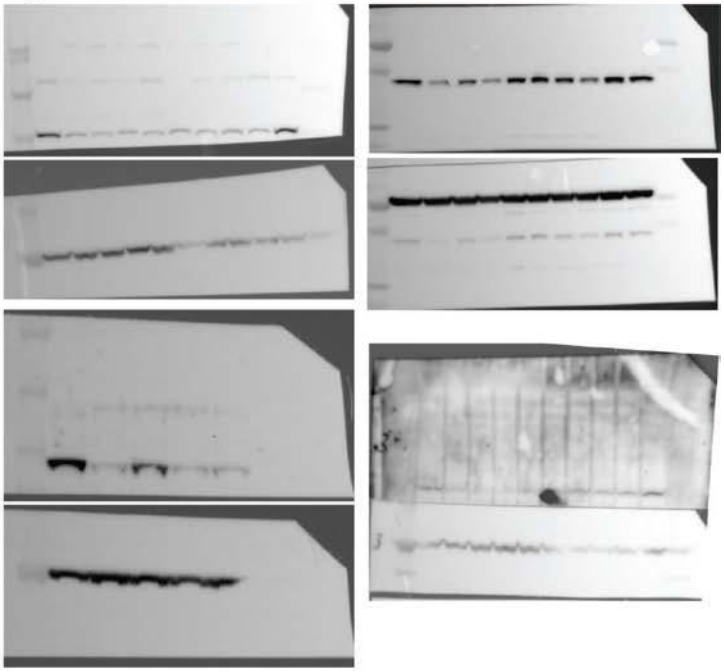

Figure 2c

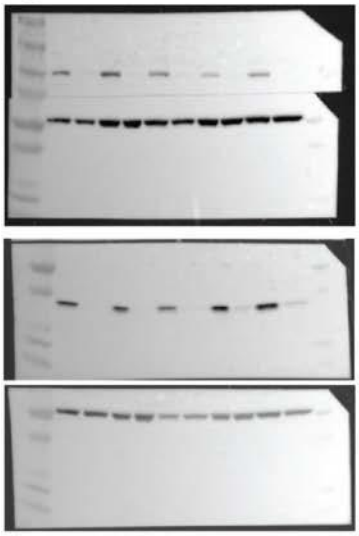

Figure 4a

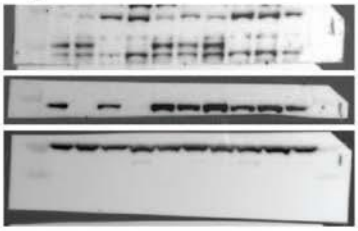

Figure 4e

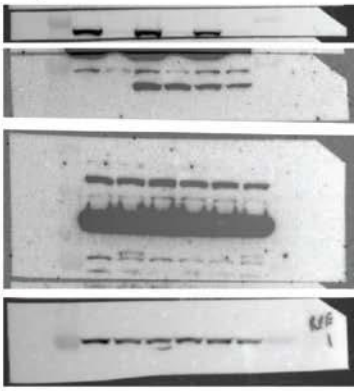

Figure 5a

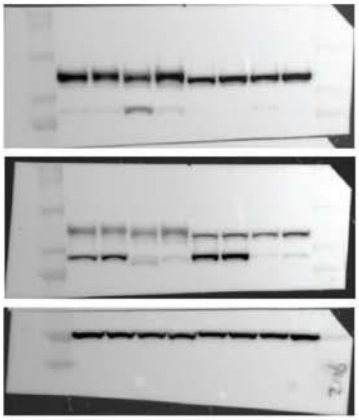

Figure 5f

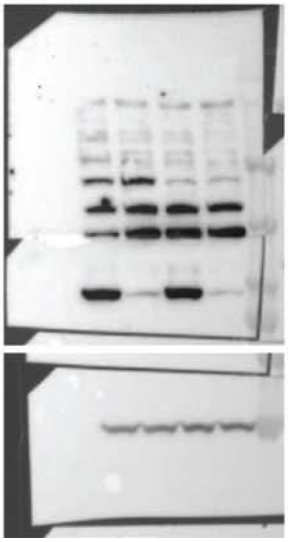

MATERIALS AND METHODS

Cell lines and drug treatments

Human fibroblasts derived from a previously described WABS patient[39] were immortalized with hTERT and SV40 large T antigen, stably transfected with DDX11 cDNA or an empty vector, and single colonies were analyzed for DDX11 protein levels. The official names of the resulting cell lines are VU1149+SV40+DDX11 and VU1149+SV40+pcDNA, however for clarity they were renamed $DDX11^{+}$ and $DDX11^{-}$ in this manuscript. Wild-type fibroblasts LN9SV and RBS fibroblasts VU1199+SV40 ($ESCO2^{-}$) and VU1199+SV40+V5-ESCO2 ($ESCO2^{+}$) have been described before[41]. Head and neck squamous cell carcinoma (HNSCC) cell line VU-SCC-9917 was established from an HPV-negative T2N2B tumor in the oral cavity of a 62-year old woman. HNSCC cell lines VU-SCC-120, VU-SCC-147, VU-SCC-78 and VU-SCC-40 were described previously[61]. Luminal breast cancer cell lines MCF7, CAMA-1, OCUB-M and Sum185PE were kindly provided by J. Martens, Erasmus MC Rotterdam, Netherlands. MCF7 is listed in the database of commonly misidentified cell lines, ICLAC. The authenticity was assessed by comparing the generated Short Tandem Repeat (STR) profile with the source STR profiles present in the American Type Culture Collection and the Deutsche Sammlung von Mikroorganismen und Zellkulturen[62]. Human fibroblasts, human Retinal Pigment Epithelial cells (RPE1) as well as the cancer cell lines used in this study were cultured in Dulbecco's Modified Eagle's Medium (DMEM, GIBCO) with 10% FBS (Hyclone) and 1% L-glutamine (Invitrogen). The Mps1 inhibitor reversine as well as the spindle poisons paclitaxel (taxol) and nocodazole were purchased from Sigma -Aldrich. The APC/C inhibitor apcin has been recently described[42].

The APC/C inhibitor proTAME, which causes cohesion fatigue under certain conditions[22], could not be used in the long term cell viability assays that we describe here, due to variations in the stability of this APC/C inhibitor under cell culture conditions.

Genome-wide siRNA screens

The $DDX11^{-}$ and $DDX11^{+}$ cell lines were subjected to a high-throughput reverse transfection protocol in 384-well tissue culture plates (Cellstar, Greiner Bio-One) using established automated liquid handling procedures. 1.5 pmol siRNA SMARTpools from the siARRAY Whole Human Genome library (Catalog items G-003500 (Sept05), G-003600 (Sept05), G-004600 (Sept05) and G-005000 (Oct05); Dharmacon, Thermo Fisher Scientific) were dispensed into the wells and plates were stored in -20 °C. The non-targeting siControl#2 and the siPlk1 SMARTpool were used as controls. Lipofectamin RNAiMAX transfection reagent (Life Technologies) in OptiMem (GIBCO) was added to the wells using a Multidrop Combi (Thermo Fisher Scientific). After two hours, per well 500 cells in 40 µL growth medium were seeded to a final volume of 60 µL. Plates were incubated for 96 hours at 37°C/5% CO_2. Cell viability was determined by adding 6 µL CellTiter-Blue reagent (Promega). After 4 hours of incubation at 37°C, the reaction was stopped by adding 30 µL 3% SDS and fluorescence (560_{Ex} /590_{Em}) was measured using an Infinite F200 microplate reader (Tecan). The potency of the selected hits was validated in a

deconvolution screen: DDX11$^-$ and DDX11$^+$ cell lines were screened with four distinct siRNAs for each gene using a similar approach as described above.

Analysis of screen data

Data were read into R and configured using the package cellHTS2[63]. Log-transformed intensities were normalized using a linear regression on data for all screens, correcting for experiment-wide plate and screen effects. This helps making plate averages across all screens the same, although individual plate averages may differ, as well as making screen averages the same across the entire experiment. This normalization preserves differences between screens, as it will affect all wells belonging to the same plate in the precise same way and as such it preserves the effect between cell lines under study. We then used an empirical-Bayes linear regression model[64] to find siRNAs that led to differential cell growth in DDX11$^-$ compared to DDX11$^+$ cell lines. FDR-corrected p-values were selected if they were at most 0.10, so it is expected that at most 10% of those selected are false positives[65]. This regression model is particularly suitable to handling data from experiments as this one, where a small number of samples is available per group (only 2 samples in one group and 3 in the other), and a large number of siRNAs is tested simultaneously.

siRNA transfection and viability assay

We used a standard siRNA concentration of 25 nM, except for the co-depletions in RPE1 cells, for which we used 2.5 nM per single siRNA. The RNAiMAX dilution factor was optimized for each cell line separately: 1200x for RPE1, DDX11$^-$, DDX11$^+$, UM-SCC-14B and UM-SCC-14C; 800x for ESCO2$^-$, ESCO2$^+$, OCUB-M, MCF7 and CAMA-1. Unless differently stated, we used siRNA#4 for APC3 and the pool of four siRNAs for ESCO2, WAPL and Separase. In CellTiter-Blue assays, we used either siPlk1 or siUBB (Ubiquitin B) as positive control for transfection efficiency. The sequences of siRNAs that were used in the deconvolution screen are provided in Supplementary Data 2. In addition, the following sequences were used: non-targeting siRNA UAAGGCUAUGAAGAGAUAC; siPLK1 pool CAACCAAAGUCGAAUAUGA, CAAGAAGAAUGAAUACAGU, GAAGAUGUCCAUGGAAAUA, CAACACGCCUCAUCCUCUA;

siUBB pool CCCAGUGACACCAUCGAAA, GACCAUCACUCUGGAGGUG, GUAUGCAGAUCUUCGUGAA, GCCGUACUCUUUCUGACUA; siAPC2 pool #5-8 GAGAUGAUCCAGCGUCUGU, GACAUCAUCACCCUCUAUA, GAUCGUAUCUACAACAUGC, GAGAAGAAGUCCACACUAU; siWAPL pool CAAACAGUGAAUCGAGUAA, CCAAUCAAGGGAUCUGUUA, GAAGGAGACUUUUCAAUAA, GCAAACACAUGGAGGAUUG; siSeparase pool CCGAGGAUCACUUGAAAUA, GGAGAAGGCUCACAGUUAC, GAUCGUUUCCUAUACAGUA, GGAACGAAUUCUCUUUGUC.

The viability assays in follow-up experiments were carried out in 96-wells plates. Cells were counted and seeded in at least triplicates in a total volume of 100 µL medium. Optimized cell densities were: DDX11$^-$ 3000/well, DDX11$^+$ 3000/well, ESCO2$^-$ 4000/well, ESCO2$^+$ 4000/well, SCC-99-17 3000/well, VU120 3000/well, VU147 8000/well, MCF7 4000/well, VU78 2500/well,

CAMA-1 4000/well, OCUB-M 8000/well, VU0040 8000/well, Sum185 8000/well, UM-SCC-14B 3000/well, UM-SCC-14C 3000/well. Cells were incubated with 10 µL CellTiter-Blue reagent (Promega) for 2-4 hours and fluorescence (560_{Ex} /590_{Em}) was measured in a microplate reader (TriStar LB 941, Berthold Technologies).

Immunoblotting

Proteins were isolated in lysis buffer (50 mM Tris-HCl pH 7.4, 150 mM NaCl, 1% Triton X-100) with protease- and phosphataseinhibitors, separated by 3-8% or 8-16% SDS-PAGE (NU-PAGE), blotted onto polyvinylidene fluoride transfer membranes, incubated with the appropriate primary and secondary antibodies, andbands were visualized by chemoluminescence (Amersham). Antibodies used for detection are mouse anti-DDX11 (Abnova #H00001663-B01P, dilution 1:1000), mouse anti-vinculin (H-10, Santa Cruz #sc-25336, dilution 1:1000), rabbit anti-APC2 (kind gift from J. Pines, dilution 1:500), mouse anti-α-tubulin (B-5-1-2, Santa Cruz #sc-23948, dilution 1:5000), mouse anti-APC3 (BD Transduction laboratories, #610454, dilution 1:1000), goat anti-APC4 (C-18, Santa Cruz #SC-21414, dilution 1:500), rabbit anti-$p31^{comet}$ (Abcam #ab150363, dilution 1:1000), guinea pig anti-ESCO2[41] (dilution 1:1000), mouse anti-Rad21 (Oncogene #NA80, dilution 1:1000) and rabbit anti-WAPL (Bethyl #A300-268A, dilution 1:1000). Uncropped images of western blots are provided in Supplementary Figure 9.

Flow cytometry

Cells were harvested, washed in PBS and fixed in ice-cold 70% EtOH. For mitosis detection, cells were incubated with rabbit anti-pS10-Histone H3 (Millipore) for 1h and with Alexa Fluor 488 goat-anti-rabbit (Invitrogen) for 30 min. Cells were washed and resuspended in PBS with 1:10 PI/RNase staining buffer (BD Biosciences) and analyzed by flow cytometry on a BD FACSCalibur (BD Biosciences). Cell-cycle analysis was conducted with BD CellQuest software (BD Biosciences).

Time-lapse microscopy

Cells were seeded in a 35 mm glass-bottom dish (Willcowells). Acquisition of DIC images started 48 h post-transfection on a microscope (Axio Observer Z1; Carl Zeiss) in a heated culture chamber (5% CO2 at 37°C). The microscope was equipped with an LD 0.55 condenser and 40× NA 1.40 Plan Apochromat oil DIC objective. Images were taken using AxioVision Rel. 4.8.1 software (Carl Zeiss) with a charge-coupled device camera (ORCA R2 Black and White CCD [Hamamatsu Photonics] or Roper HQ [Roper Scientific]) at 100-ms exposure times. Images were analyzed using MetaMorph software (Universal Imaging).

Cohesion defect analysis

For cohesion defect analysis, cells were incubated with 200 ng/mL Demecolcin (Sigma-Aldrich) in medium for 20 min, harvested, resuspended in 75 mM KCl for 20 min and fixed in methanol/acetic acid (3:1). Cells were dropped onto glass slides, stained with 5% Giemsa

(Merck) and cohesion defects were microscopically analyzed. Per condition, 25 metaphases per slide were counted on two coded slides as technical replicate. For coding, we covered the text, randomly distributed the slides on the bench and numbered the slides in random order.

Reference List

1. Losada,A. Cohesin in cancer: chromosome segregation and beyond. *Nat. Rev. Cancer*14, 389-393 (2014).

2.Deardorff,M.A. *et al.* Mutations in cohesin complex members SMC3 and SMC1A cause a mild variant of cornelia de Lange syndrome with predominant mental retardation. *Am. J. Hum. Genet.*80, 485-494 (2007).

3.Deardorff,M.A. *et al.* RAD21 Mutations Cause a Human Cohesinopathy. *Am. J. Hum. Genet.*(2012).

4.Deardorff,M.A. *et al.* HDAC8 mutations in Cornelia de Lange syndrome affect the cohesin acetylation cycle. *Nature*(2012).

5. Krantz,I.D. *et al.* Cornelia de Lange syndrome is caused by mutations in NIPBL, the human homolog of Drosophila melanogaster Nipped-B. *Nat. Genet.*36, 631-635 (2004).

6.Schule,B., Oviedo,A., Johnston,K., Pai,S., & Francke,U. Inactivating mutations in ESCO2 cause SC phocomelia and Roberts syndrome: no phenotype-genotype correlation. *Am. J. Hum. Genet.*77, 1117-1128 (2005).

7. Vega,H. *et al.* Roberts syndrome is caused by mutations in ESCO2, a human homolog of yeast ECO1 that is essential for the establishment of sister chromatid cohesion. *Nat. Genet.*37, 468-470 (2005).

8.van der Lelij,P. *et al.* Warsaw breakage syndrome, a cohesinopathy associated with mutations in the XPD helicase family member DDX11/ChlR1. *Am. J. Hum. Genet.*86, 262-266 (2010).

9. Balbas-Martinez,C. *et al.* Recurrent inactivation of STAG2 in bladder cancer is not associated with aneuploidy. *Nat. Genet.*45, 1464-1469 (2013).

10. Barber,T.D. *et al.* Chromatid cohesion defects may underlie chromosome instability in human colorectal cancers. *Proc. Natl. Acad. Sci. U. S. A*105, 3443-3448 (2008).

11. Guo,G. *et al.* Whole-genome and whole-exome sequencing of bladder cancer identifies frequent alterations in genes involved in sister chromatid cohesion and segregation. *Nat. Genet.*(2013).

12.Kon,A. *et al.* Recurrent mutations in multiple components of the cohesin complex in myeloid neoplasms. *Nat. Genet.*(2013).

13. Leiserson,M.D. *et al.* Pan-cancer network analysis identifies combinations of rare somatic mutations across pathways and protein complexes. *Nat. Genet.*47, 106-114 (2015).

14. Solomon,D.A. *et al.* Mutational inactivation of STAG2 causes aneuploidy in human cancer. *Science*333, 1039-1043 (2011).

15. Solomon,D.A. *et al.* Frequent truncating mutations of STAG2 in bladder cancer. *Nat. Genet.*(2013).

16. Haarhuis,J.H., Elbatsh,A.M., & Rowland,B.D. Cohesin and Its Regulation: On the Logic of X-Shaped Chromosomes. *Dev. Cell*31, 7-18 (2014).

17. Hauf,S. *et al.* Dissociation of cohesin from chromosome arms and loss of arm cohesion during early mitosis depends on phosphorylation of SA2. *PLoS. Biol.*3, e69 (2005).

18. Liu,H., Rankin,S., & Yu,H. Phosphorylation-enabled binding of SGO1-PP2A to cohesin protects sororin and centromeric cohesion during mitosis. *Nat. Cell Biol.*15, 40-49 (2013).
19. McGuinness,B.E., Hirota,T., Kudo,N.R., Peters,J.M., & Nasmyth,K. Shugoshin prevents dissociation of cohesin from centromeres during mitosis in vertebrate cells. *PLoS. Biol.*3, e86 (2005).
20.Nishiyama,T., Sykora,M.M., Huis in 't Veld PJ, Mechtler,K., & Peters,J.M. Aurora B and Cdk1 mediate Wapl activation and release of acetylated cohesin from chromosomes by phosphorylating Sororin. *Proc. Natl. Acad. Sci. U. S. A*110, 13404-13409 (2013).
21. Tang,Z. *et al.* PP2A is required for centromeric localization of Sgo1 and proper chromosome segregation. *Dev. Cell*10, 575-585 (2006).
22.Lara-Gonzalez,P. & Taylor,S.S. Cohesion fatigue explains why pharmacological inhibition of the APC/C induces a spindle checkpoint-dependent mitotic arrest. *PLoS. One.*7, e49041 (2012).
23. Gascoigne,K.E. & Taylor,S.S. Cancer cells display profound intra- and interline variation following prolonged exposure to antimitotic drugs. *Cancer Cell*14, 111-122 (2008).
24. Collin,P., Nashchekina,O., Walker,R., & Pines,J. The spindle assembly checkpoint works like a rheostat rather than a toggle switch. *Nat. Cell Biol.*15, 1378-1385 (2013).
25.Dick,A.E. & Gerlich,D.W. Kinetic framework of spindle assembly checkpoint signalling. *Nat. Cell Biol.*15, 1370-1377 (2013).
26. Sudakin,V., Chan,G.K., & Yen,T.J. Checkpoint inhibition of the APC/C in HeLa cells is mediated by a complex of BUBR1, BUB3, CDC20, and MAD2. *J. Cell Biol.*154, 925-936 (2001).
27. Hagting,A. *et al.* Human securin proteolysis is controlled by the spindle checkpoint and reveals when the APC/C switches from activation by Cdc20 to Cdh1. *J. Cell Biol.*157, 1125-1137 (2002).
28. Clute,P. & Pines,J. Temporal and spatial control of cyclin B1 destruction in metaphase. *Nat. Cell Biol.*1, 82-87 (1999).
29. Clijsters,L., Ogink,J., & Wolthuis,R. The spindle checkpoint, APC/C(Cdc20), and APC/C(Cdh1) play distinct roles in connecting mitosis to S phase. *J. Cell Biol.*201, 1013-1026 (2013).
30. Peters,J.M. The anaphase promoting complex/cyclosome: a machine designed to destroy. *Nat. Rev. Mol. Cell Biol.*7, 644-656 (2006).
31.Nicklas,R.B., Campbell,M.S., Ward,S.C., & Gorbsky,G.J. Tension-sensitive kinetochore phosphorylation in vitro. *J. Cell Sci.*111 (Pt 21), 3189-3196 (1998).
32. Vanoosthuyse,V. & Hardwick,K.G. A novel protein phosphatase 1-dependent spindle checkpoint silencing mechanism. *Curr. Biol.*19, 1176-1181 (2009).
33.Howell,B.J. *et al.* Cytoplasmic dynein/dynactin drives kinetochore protein transport to the spindle poles and has a role in mitotic spindle checkpoint inactivation. *J. Cell Biol.*155, 1159-1172 (2001).
34. Hagan,R.S. *et al.* p31(comet) acts to ensure timely spindle checkpoint silencing subsequent to kinetochore attachment. *Mol. Biol. Cell*22, 4236-4246 (2011).
35. Teichner,A. *et al.* p31comet Promotes disassembly of the mitotic checkpoint complex in an ATP-dependent process. *Proc. Natl. Acad. Sci. U. S. A*108, 3187-3192 (2011).

36. Westhorpe,F.G., Tighe,A., Lara-Gonzalez,P., & Taylor,S.S. p31comet-mediated extraction of Mad2 from the MCC promotes efficient mitotic exit. *J. Cell Sci.*124, 3905-3916 (2011).
37. Xia,G. *et al.* Conformation-specific binding of p31(comet) antagonizes the function of Mad2 in the spindle checkpoint. *EMBO J.*23, 3133-3143 (2004).
38. McLornan,D.P., List,A., & Mufti,G.J. Applying synthetic lethality for the selective targeting of cancer. *N. Engl. J. Med.*371, 1725-1735 (2014).
39. van der Lelij P. *et al.*Warsaw breakage syndrome, a cohesinopathy associated with mutations in the XPD helicase family member DDX11/ChlR1. *Am. J. Hum. Genet.*86, 262-266 (2010).
40. Stoepker,C. *et al.* Defects in the fanconi anemia pathway and chromatid cohesion in head-and-neck cancer. *Cancer Res.*(2015).
41. van der Lelij P. *et al.* The cellular phenotype of Roberts syndrome fibroblasts as revealed by ectopic expression of ESCO2. *PLoS. One.*4, e6936 (2009).
42. Sackton,K.L. *et al.* Synergistic blockade of mitotic exit by two chemical inhibitors of the APC/C. *Nature*(2014).
43. Gandhi,R., Gillespie,P.J., & Hirano,T. Human Wapl is a cohesin-binding protein that promotes sister-chromatid resolution in mitotic prophase. *Curr. Biol.*16, 2406-2417 (2006).
44. Kueng,S. *et al.* Wapl controls the dynamic association of cohesin with chromatin. *Cell*127, 955-967 (2006).
45. Santaguida,S., Tighe,A., D'Alise,A.M., Taylor,S.S., & Musacchio,A. Dissecting the role of MPS1 in chromosome biorientation and the spindle checkpoint through the small molecule inhibitor reversine. *J. Cell Biol.*190, 73-87 (2010).
46. Zeng,X. *et al.* Pharmacologic inhibition of the anaphase-promoting complex induces a spindle checkpoint-dependent mitotic arrest in the absence of spindle damage. *Cancer Cell*18, 382-395 (2010).
47. Daum,J.R. *et al.* Cohesion fatigue induces chromatid separation in cells delayed at metaphase. *Curr. Biol.*21, 1018-1024 (2011).
48. Stevens,D., Gassmann,R., Oegema,K., & Desai,A. Uncoordinated loss of chromatid cohesion is a common outcome of extended metaphase arrest. *PLoS. One.*6, e22969 (2011).
49. Hauf,S., Waizenegger,I.C., & Peters,J.M. Cohesin cleavage by separase required for anaphase and cytokinesis in human cells. *Science*293, 1320-1323 (2001).
50. Dawson,I.A., Roth,S., & Artavanis-Tsakonas,S. The Drosophila cell cycle gene fizzy is required for normal degradation of cyclins A and B during mitosis and has homology to the CDC20 gene of Saccharomyces cerevisiae. *J. Cell Biol.*129, 725-737 (1995).
51. Kabeche,L. & Compton,D.A. Cyclin A regulates kinetochore microtubules to promote faithful chromosome segregation. *Nature*502, 110-113 (2013).
52. Zhang,J., Wan,L., Dai,X., Sun,Y., & Wei,W. Functional characterization of Anaphase Promoting Complex/Cyclosome (APC/C) E3 ubiquitin ligases in tumorigenesis. *Biochim. Biophys. Acta*1845, 277-293 (2014).
53. Huang,H.C., Shi,J., Orth,J.D., & Mitchison,T.J. Evidence that mitotic exit is a better cancer therapeutic target than spindle assembly. *Cancer Cell*16, 347-358 (2009).

54. Penas,C., Ramachandran,V., & Ayad,N.G. The APC/C Ubiquitin Ligase: From Cell Biology to Tumorigenesis. *Front Oncol.*1, 60 (2011).
55. Wolthuis,R. *et al.* Cdc20 and Cks direct the spindle checkpoint-independent destruction of cyclin A. *Mol. Cell*30, 290-302 (2008).
56. Rattani,A. *et al.* Dependency of the spindle assembly checkpoint on Cdk1 renders the anaphase transition irreversible. *Curr. Biol.*24, 630-637 (2014).
57. Huang,H.C., Mitchison,T.J., & Shi,J. Stochastic competition between mechanistically independent slippage and death pathways determines cell fate during mitotic arrest. *PLoS. One*.5, e15724 (2010).
58. Visintin,R., Prinz,S., & Amon,A. CDC20 and CDH1: a family of substrate-specific activators of APC-dependent proteolysis. *Science*278, 460-463 (1997).
59. Garcia-Higuera,I. *et al.* Genomic stability and tumour suppression by the APC/C cofactor Cdh1. *Nat. Cell Biol.*10, 802-811 (2008).
60. Manning,A.L. *et al.* Suppression of genome instability in pRB-deficient cells by enhancement of chromosome cohesion. *Mol. Cell*53, 993-1004 (2014).
61. Hermsen,M.A. *et al.* Centromeric breakage as a major cause of cytogenetic abnormalities in oral squamous cell carcinoma. *Genes Chromosomes. Cancer*15, 1-9 (1996).
62. Riaz,M. *et al.* miRNA expression profiling of 51 human breast cancer cell lines reveals subtype and driver mutation-specific miRNAs. *Breast Cancer Res.*15, R33 (2013).
63. Boutros,M., Bras,L.P., & Huber,W. Analysis of cell-based RNAi screens. *Genome Biol.*7, R66 (2006).
64.Smyth, G. K. Limma: linear models for microarray data. eds. Gentleman, R., Carey, V., Dudoit, S., Irizarry, R., & Huber, W. In*:* 'Bioinformatics and Computational Biology Solutions using R and Bioconductor'. 397-420. 2005. New York, Springer.
65. Benjamini,Y. & Hochberg,Y. Controlling the false discovery rate: a practical and powerful approach to multiple testing. *J Roy Statist Soc Ser B (Methodological)*57, 289-300 (1995).

Chapter 5

Non-Redundant Roles in Sister Chromatid Cohesion of the DNA Helicase DDX11 and the SMC3 Acetyl Transferases ESCO1 and ESCO2

Atiq Faramarz, Jesper A. Balk, Janne J.M. van Schie, Anneke B. Oostra, Cherien A. Ghandour, Martin A. Rooimans, Rob M.F. Wolthuis and Job de Lange

Published in PLoS ONE (slightly modified form) 15 (2020): e0220348

Abstract

In a process linked to DNA replication, duplicated chromosomes are entrapped in large, circular cohesin complexes and functional sister chromatid cohesion (SCC) is established by acetylation of the SMC3 cohesin subunit. Roberts Syndrome (RBS) and Warsaw Breakage Syndrome (WABS) are rare human developmental syndromes that are characterized by defective SCC. RBS is caused by mutations in the SMC3 acetyl transferase ESCO2, whereas mutations in the DNA helicase DDX11 lead to WABS. We found that WABS-derived cells predominantly rely on ESCO2, not ESCO1, for residual SCC, growth and survival. Reciprocally, RBS-derived cells depend on DDX11 to maintain low levels of SCC. Synthetic lethality between DDX11 and ESCO2 correlated with a prolonged delay in mitosis, and was rescued by knockdown of the cohesin remover WAPL. Rescue experiments using mouse or human cDNAs revealed that DDX11, ESCO1 and ESCO2 act on different but related aspects of SCC establishment. Furthermore, a helicase-dead DDX11 mutant failed to correct SCC in WABS cells. We propose that DDX11, ESCO1 and ESCO2 control different fractions of cohesin that are spatially and mechanistically separated.

Introduction

Sister chromatid cohesion (SCC) is mediated by cohesin, a presumed DNA-entrapping ring formed by structural maintenance of chromosome 1 and 3 (SMC1 and SMC3), RAD21 and SA1/2. The loader complex MAU2-NIPBL loads DNA into cohesin rings [1-3], whereas it can be released by the cohesin remover WAPL [4]. During DNA replication, stable cohesion is established in a process involving SMC3 acetylation by ESCO1 and ESCO2, which leads to the recruitment of Sororin and subsequent inhibition of WAPL activity [5-7]. The resulting SCC facilitates proper chromosome bi-orientation and equal distribution of genetic material during mitosis. Prior to chromatid separation in anaphase, cohesin needs to be removed, which happens in two rounds and via two distinct pathways [8, 9]. First, the prophase pathway promotes removal of cohesins from chromosome arms by WAPL, in a process involving multiple phosphorylations that restore WAPL activity [10]. Centromere cohesins are protected from the prophase pathway by SGOL1, which recruits the PP2A phosphatase to the centromeres [9, 11, 12]. In a separate step that occurs at the metaphase-to-anaphase transition, the remaining centromeric cohesins are removed by the protease Separase, which is activated by the Anaphase-Promoting Complex/Cyclosome (APC/C) and cleaves the RAD21 subunit [13]. In addition to its role in sister chromatid cohesion, the capacity of cohesin to entrap DNA also allows it to regulate gene transcription [14-16] and promote ribosome biogenesis [17-19].

Mutations in cohesin components or regulators result in a cluster of syndromes called cohesinopathies, characterized by diverse clinical abnormalities including growth retardation, intellectual disability, microcephaly and congenital abnormalities. Four cohesinopathies have been described thus far. Cornelia de Lange syndrome (CdLS) results from autosomal dominant or X-linked mutations in NIPBL, SMC1A, SMC3, RAD21 or HDAC8 [20-26]. Roberts Syndrome (RBS, also called SC phocomelia syndrome) is caused by bi-allelic mutations in ESCO2 [27]. Warsaw Breakage Syndrome (WABS) results from bi-allelic mutations in the DNA helicase DDX11 [28]. Chronic Atrial and Intestinal Dysrhythmia (CAID) syndrome was described in a patient with homozygous missense mutations in SGOL1 [29]. CdLS cells exhibit no obvious defects in SCC [30], and the clinical symptoms are thought to originate from deregulated gene expression (reviewed in [31-33]). By contrast, metaphases derived from RBS, WABS and CAID patient cells show severe cohesion loss [27-29]. The clinical symptoms of these syndromes are likely to originate from a combination of transcriptional defects and reduced progenitor cell proliferation.

ESCO1 and ESCO2, the vertebrate orthologues of yeast Eco1, share a conserved C-terminus that contains a zinc finger motif and an acetyltransferase domain, whereas no similarity is found in the N-terminus [34]. ESCO2 deficiency is embryonic lethal in mice, indicating that ESCO2 functions non-redundantly with ESCO1 [35]. RBS patient derived cells show defective centromere cohesion [36], in line with the observation that ESCO2 localizes to pericentric heterochromatin [35]. ESCO2 expression peaks during S-phase and is subsequently reduced by proteasomal degradation [35, 36] indicating that its prime function is to mediate SCC in the context of DNA replication. In budding yeast, Eco1 is reported to be recruited to the replication fork by replication factor PCNA [37] and in human cells, ESCO2 was found to interact with MCM

components [38, 39], supporting a role for ESCO2 in replication-coupled cohesion. Decreased SMC3 acetylation in human cells reduces replication fork speed [40]. The authors proposed that the primary role of SMC3 acetylation would be to switch cohesin from a conformation that obstructs replication forks to a more open structure that allows fork progression [40]. Unlike ESCO2, ESCO1 is expressed during the whole cell cycle and has been reported to acetylate SMC3 independent of replication, suggesting that ESCO1 also regulates non-canonical roles of cohesin [41]. Nevertheless, ESCO1 knockdown was also found to cause cohesion loss in Hela cells [34, 41] and DT40 chicken cells [42]. A different study reported no effect of ESCO1 knockdown or CRISPR mediated knockout on cohesion in Hela cells, and the authors proposed a model in which ESCO1 facilitates structural cohesion rather than replicative cohesion, thereby indirectly reinforcing cohesion that was established by ESCO2 [43].

DDX11 belongs to a group of ATP-dependent, super-family 2 (SF2) DNA helicases with an iron-sulfur cluster (Fe-S) domain [44]. It is specialized in unwinding certain DNA structures that contain a 5'-single stranded region, including forked duplexes, 5'-flap duplexes and anti-parallel G-quadruplexes (reviewed in [45]). This may be particularly relevant in the context of a DNA replication fork, where potentially long stretches of single stranded DNA can form secondary structures. Indeed, DDX11 and its yeast orthologue Chl1 have been shown to interact with multiple replication factors, such as the sliding clamp PCNA, its loader Replication Factor C complex (RFC), the 5'-flap endonuclease FEN1, the fork protection complex (FPC) component Timeless and with CTF4, which couples the MCM helicase to DNA polymerases [46-50]. How DDX11 deficiency results in cohesion loss is not entirely understood. The helicase-dependent resolution of complex secondary DNA structures that are formed particularly in the lagging strand may be required for successful sister chromatid entrapment, but helicase-independent roles in cohesin loading have also been proposed [50-52]. Interestingly, Eco1 and Chl1 genetically interact [53-55] and synthetic lethality between DDX11 and ESCO2 was also reported in chicken DT40 cells [56].

Here we report synthetic lethality between ESCO2 and DDX11 in different human cell lines. Lethality is accompanied by aggravated cohesion loss in metaphase spreads. Reinforcing arm cohesion by WAPL knockdown rescues synthetic lethality, indicating that lethality results from detrimental loss of SCC. ESCO1 and ESCO2 appear to have both overlapping and non-overlapping roles in SCC, which are conserved between mice and men. Importantly, we show that DDX11 helicase activity can promote SCC establishment. We propose that DDX11 and ESCO2 have functions in SCC that are both spatially and mechanistically distinct.

Results

Synthetic lethality of DDX11 and ESCO2 is conserved in different human cell lines.

We previously generated a unique isogenic cell line pair by functionally correcting fibroblasts derived from a WABS patient [57] and used these in a genome-wide siRNA screen to search for genes that are synthetically lethal with mutant DDX11 [58]. ESCO2 was one of the strongest hits as validated by deconvoluting the siRNA pool (***Figure S1***). This confirms that the synthetic lethality between DDX11 and ESCO2, observed between yeast Chl1 and Eco1 [53-55] and chicken DDX11 and ESCO2 [56], is conserved in patient-derived cells. We used the same WABS cell line and its complemented counterpart to further validate these findings and also to examine the role of ESCO1 in this context. As expected, siRNA mediated ESCO2 knockdown strongly reduced the viability of WABS cells, but not of WABS+DDX11 cells (***Figure 1A***). This lethality correlated with increased levels of caspase-dependent PARP cleavage, reflecting apoptosis induction (***Figure 1B***). By contrast, knockdown of ESCO1 did not significantly affect cell growth in these cells, despite a substantial reduction of acetylated SMC3 which is the main target of ESCO1/ESCO2 acetyltransferases (***Figure 1B***). This suggests that ESCO1 mediated SMC3 acetylation contributes to non-cohesive or non-mitotic roles of the cohesion complex.
In agreement with the effects of co-depleting DDX11 and ESCO1/2 on viability, we observed severely aggravated cohesion defects in WABS cells upon knockdown of ESCO2, whereas ESCO1 knockdown had a moderate effect (***Figure 1C***). Reversely, DDX11 knockdown exhibited a stronger effect on cohesion in RBS cells than in RBS cells corrected with ESCO2 cDNA (***Figure 1D, E***), although the effect was modest. For additional validation, we used CRISPR-Cas9 to create RPE1-TP53KO cells, and subsequently generated DDX11KOs and ESCO2KOs in this genetic background. Knockdown of ESCO2 specifically inhibited growth of RPE1-TP53KO-DDX11KO cells (***Figure 2A***) and caused increased levels of PCS (***Figure 2B***), showing that synthetic lethality cannot be rescued by TP53 loss. Similarly, cohesion defects were severely aggravated upon DDX11 knockdown in RPE1-TP53KO-ESCO2KO cells (***Figure 2C***).

Figure 1

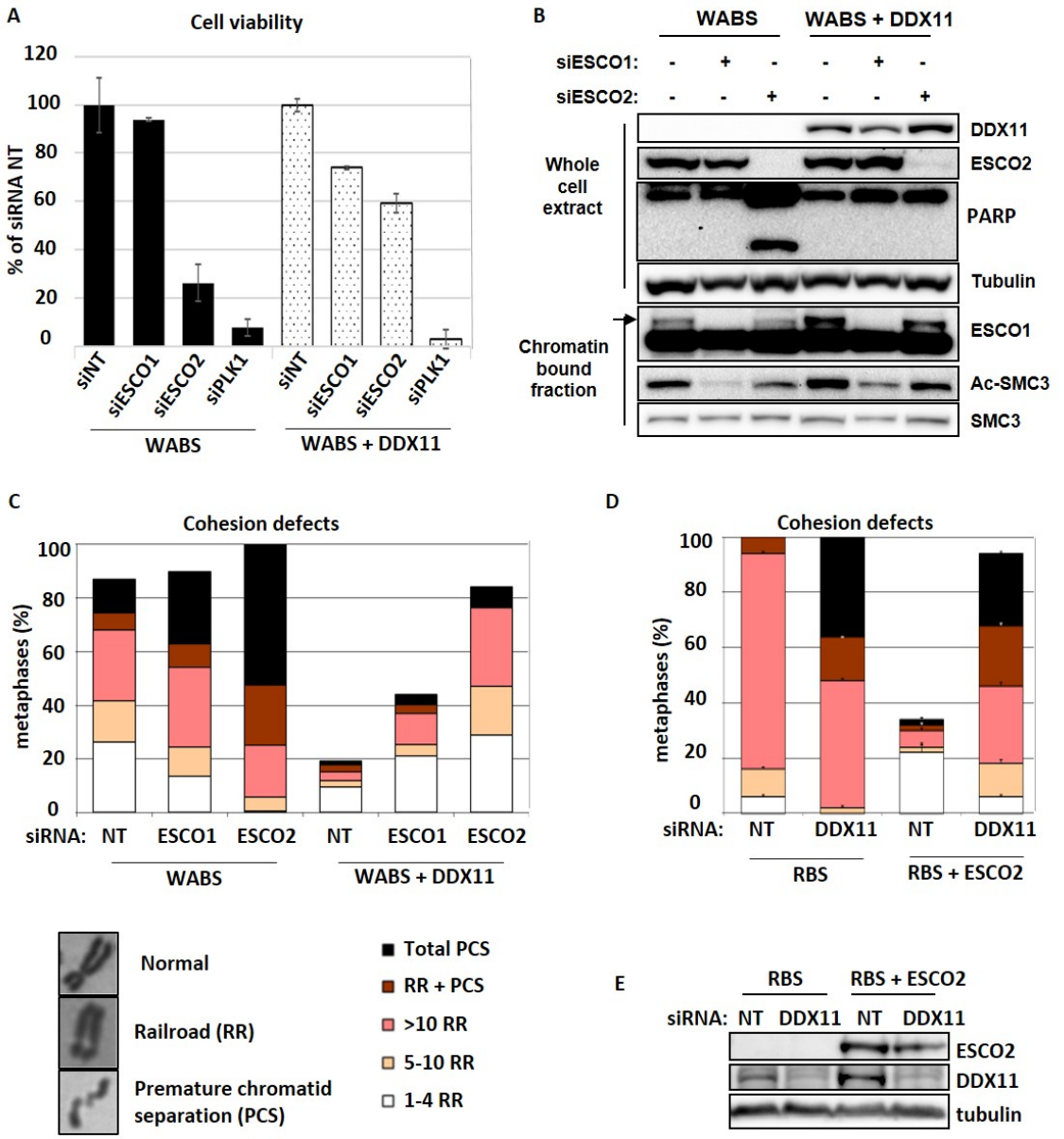

Figure 1: Synthetic lethality of DDX11 and ESCO2 is conserved in fibroblasts of WABS and RBS patients. *(A) WABS fibroblasts and corrected cells were transfected with the indicated siRNAs and cell viability was analyzed after four days, using a cell-titer blue assay. (B) Cells were transfected with indicated siRNAs and analyzed by western blot after three days. WCE, whole cell extract. (C) Cohesion defects were quantified in metaphases spreads of cells transfected as in B. Examples of metaphase chromosomes with normal and railroad (RR) appearance, as well as premature chromatid separation (PCS), are shown. (D, E) RBS fibroblasts and corrected cells were transfected with the indicated siRNAs and assessed after three days by cohesion defect analysis and western blot.*

Figure 2

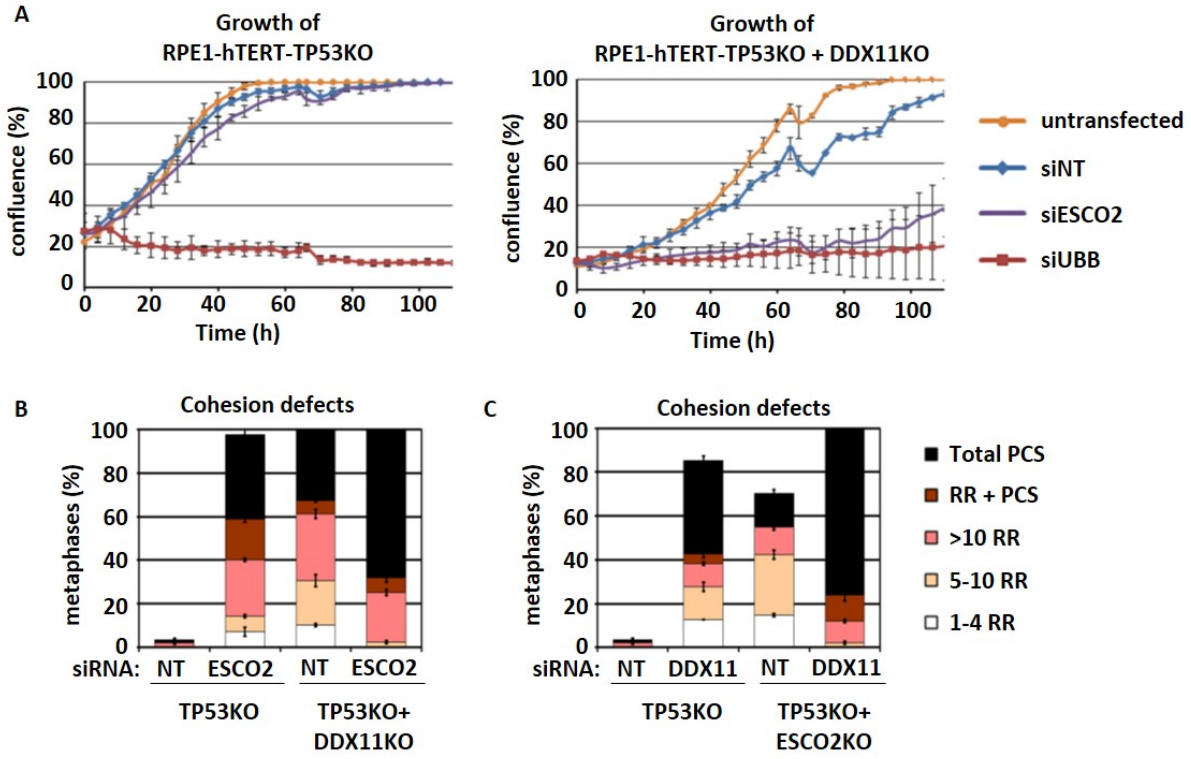

Figure 2: Synthetic lethality of DDX11 and ESCO2 in RPE1 cells. *(A) CRISPR-Cas9 was used to knockout TP53 and DDX11 in RPE1-hTERT cells. The resulting isogenic cell lines were transfected with indicated siRNAs and proliferation was assessed using the IncuCyte. (B) Cells were transfected as in A and analyzed for cohesion defects. (C) CRISPR-Cas9 was used to disrupt the ESCO2 gene in RPE1-hTERT-TP53KO cells. Cells were transfected with indicated siRNAs and analyzed for cohesion defects.*

We further analyzed the effect of ESCO2 knockdown in WABS fibroblasts using flow cytometry, and found a clear induction of cells with a 4N DNA content (*Figure 3A-C*). This includes both p-Histone H3 positive (mitotic cells) and p-Histone H3 negative cells (G2 cells, 4N G1 cells). This could in part reflect a G2 arrest, resulting from replicative stress or reduced DNA repair capacity. In addition, a small fraction of polyploid (>4N) cells appear at day 3. These findings probably reflect an extended metaphase duration via reactivation of the spindle assembly checkpoint that follows from reduced SCC and premature chromatid separation, as previously reported by us and others [58-60]. Eventually these arrested cells die in mitosis (as monitored by an increase in sub-G1 fraction), or may slip out of mitosis without cytokinesis. Cells that slip out of mitosis may subsequently continue to replicate, possibly contributing to the increased 4N fraction and leading to polyploidy.

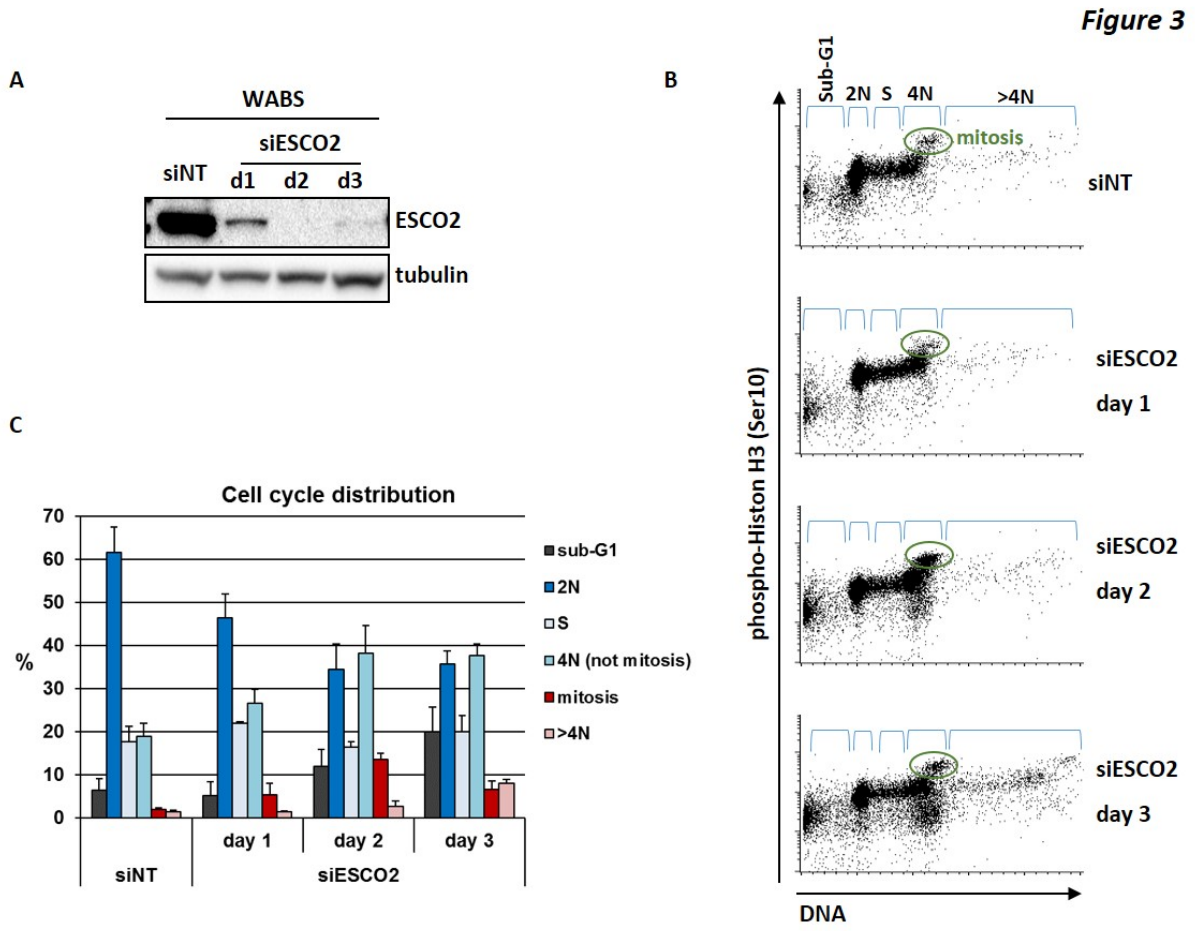

Figure 3: Induction of 4N fractions upon ESCO2 knockdown in WABS fibroblasts. *WABS cells were transfected with the siESCO2, harvested at the indicated time points and analyzed by western blot (A) and flow cytometry (B). (C) Quantification of two independent experiments.*

Synthetic lethality of DDX11 and ESCO2 is rescued by WAPL knockdown.

Next, we tested whether the SCC defects caused by single or double depletion of DDX11 and ESCO2 can be rescued by WAPL knockdown. WAPL plays a key role in removing cohesin rings from chromosome arms during the prophase pathway, so WAPL knockdown specifically causes hyper-cohesion on chromosome arms during metaphase. The cohesion defects in RBS cells could not be rescued by WAPL knockdown (***Figure 4A,B***). Since the WAPL-dependent prophase pathway only affects arm cohesion, this indicates that the effect of ESCO2 is predominantly manifested on centromere cohesion. In WABS cells, however, WAPL knockdown did prevent PCS and rescued both synthetic lethality and PCS by ESCO2 knockdown (***Figure 4C-E***). The remarkable increase in railroad chromosomes in this triple knockdown condition can be explained by a further reduction of centromere cohesion in the absence of both DDX11 and ESCO2, as compared to single DDX11 depletion, combined with reinforcement of arm cohesion by WAPL knockdown.

Figure 4

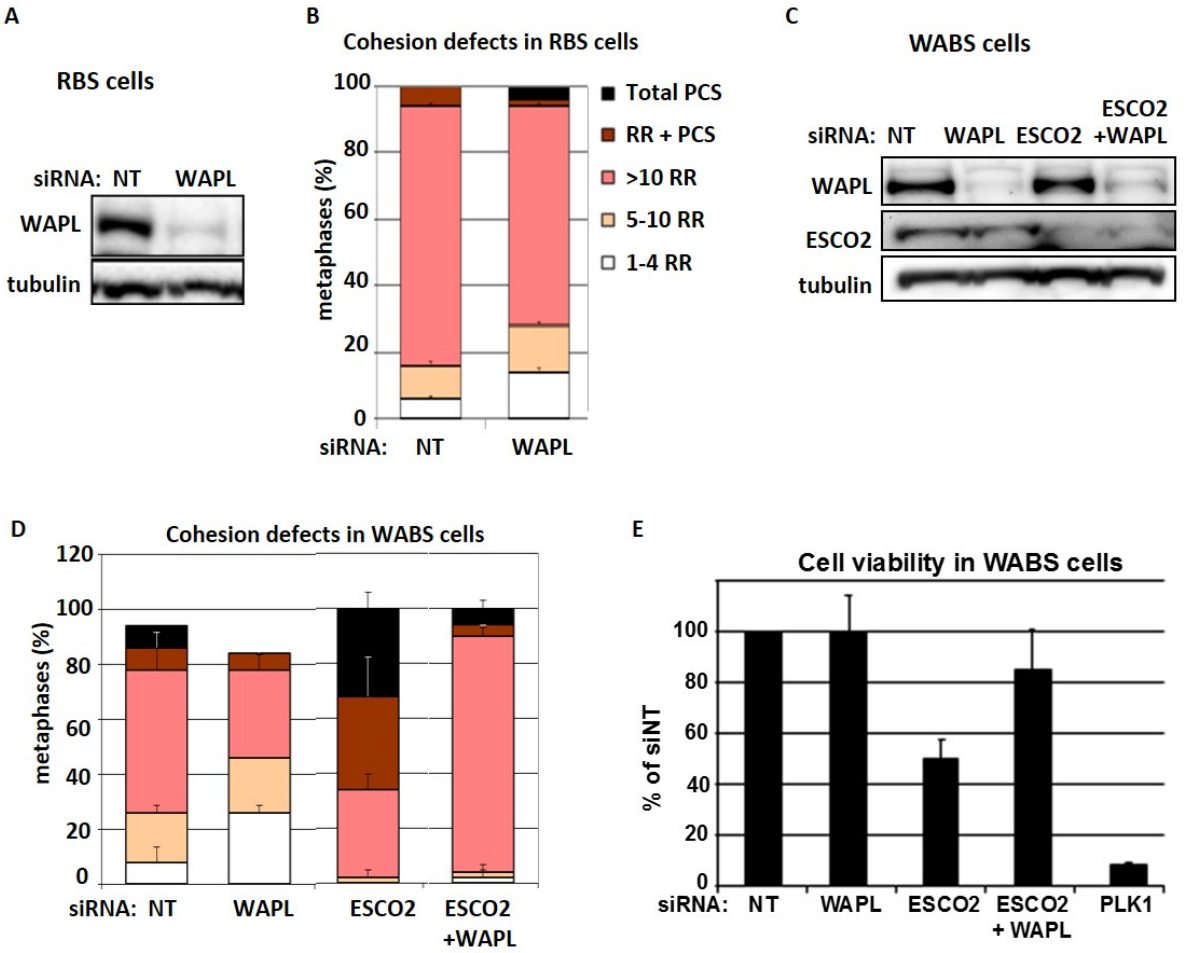

Figure 4: Restoring arm cohesion by WAPL knockdown rescues PCS and lethality.*(A,B) RBS cells were transfected with siWAPL and harvested after three days for western blot and analysis of cohesion defects. (C-E) WABS cells were transfected with the indicated siRNAs and harvested after three days for western blot and analysis of SCC. Viability was assessed after four days with a cell-titer blue assay.*

In summary, co-depletion of DDX11 and ESCO2 results in severe cohesion loss and lethality, which are both rescued by reinforcing cohesion via WAPL knockdown. This indicates that ESCO2 and DDX11 critically facilitate SCC in partially separated contexts.ESCO1 and ESCO2 have separate functions in sister chromatid cohesion. Since ESCO1 and ESCO2 both contribute to SMC3 acetylation, we set out to investigate the extent of their redundancy in SCC by manipulating their expression levels in RBS cells. Depletion of ESCO1 severely aggravated the cohesion defects in RBS cells and we also detected a small effect of ESCO1 depletion in RBS+ESCO2 cells (***Figure 5A,B***), suggesting that ESCO1 has a role in SCC that cannot be entirely compensated for by ESCO2.

Figure 5

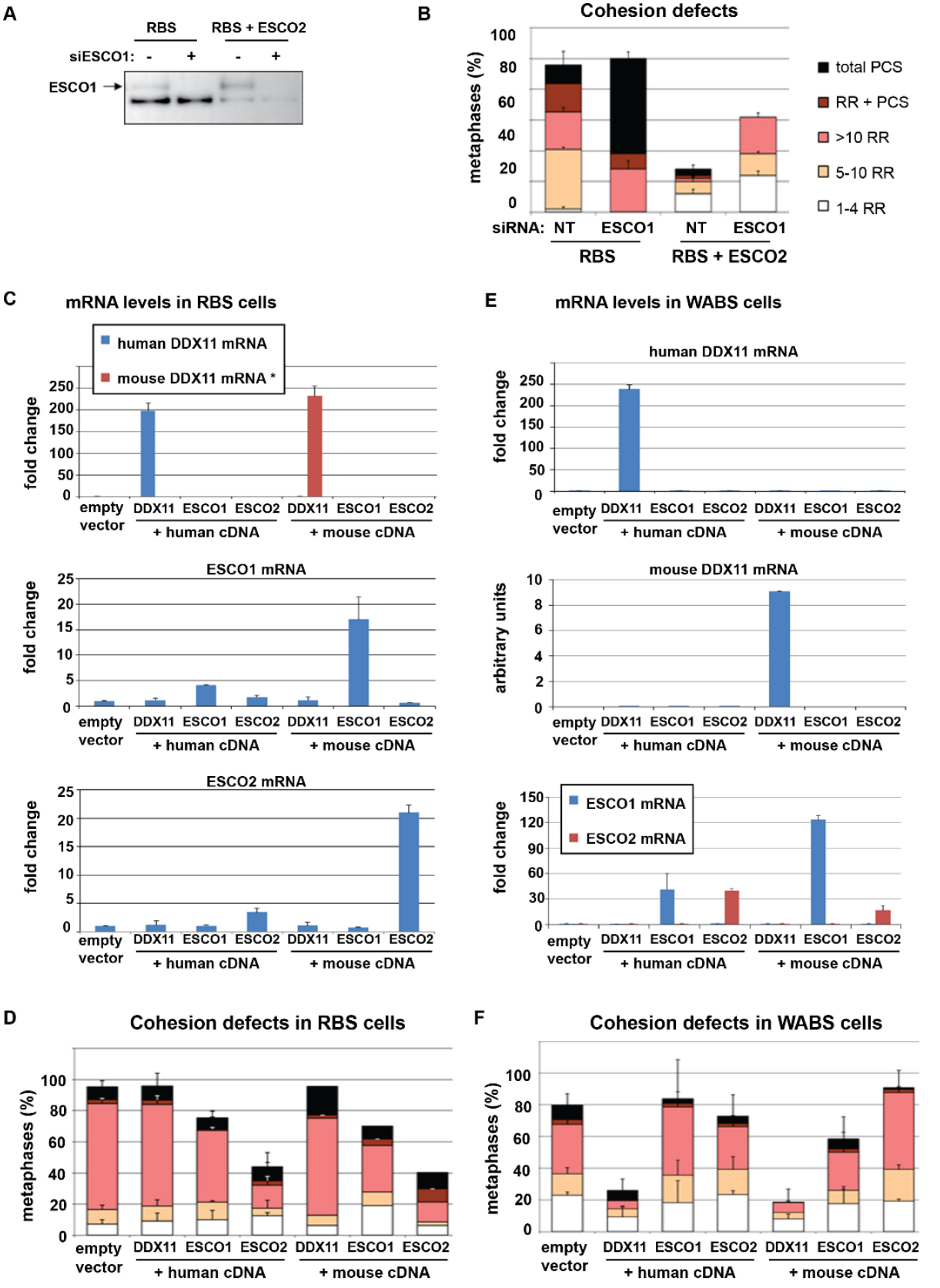

Figure 5: ESCO1, ESCO2 and DDX11 have separable functions in SCC.*(A,B) RBS fibroblasts and corrected cells were transfected with siRNA targeting ESCO1 and harvested after three days for*

Western blot and SCC analysis. Mean and standard deviations of two technical replicates are shown. (C,D) RBS cells were transduced with lentiviral vectors expressing the indicated proteins and selected with puromycin. Overexpression was confirmed with qRT-PCR and cells were analyzed for cohesion defects. Mean and standard deviations of two independent experiments are shown. Fold changes were calculated relative to parental cells. Note that mouse DDX11 mRNA is not detected in human cells, so these values represent arbitrary units (*). DDX11 (E,F) WABS cells were transduced with lentiviral vectors expressing the indicated proteins and selected with puromycin. Overexpression was confirmed with qRT-PCR and cells were analyzed for cohesion defects. Mean and standard deviations of two independent experiments are shown. Fold changes were calculated relative to parental cells.

Next, we investigated whether overexpression of ESCO1 or ESCO2 could rescue the cohesion defects in RBS cells. To assess possible species-specific effects, considering a lethal effect of ESCO1/2 or DDX11 deletion in mice [35, 61, 62], we also performed overexpression experiments using expression constructs of their mouse orthologues. Whereas cohesion in RBS cells could be restored similarly by either human or mouse ESCO2, the effect of ESCO1 was small, indicating that ESCO2 has a unique role in SCC that cannot be replaced by ESCO1 (***Figure 5C,D***). In line with the above described separate roles of ESCO2 and DDX11 in SCC, significant DDX11 overexpression completely failed to rescue the cohesion defects in RBS cells. Next, we overexpressed ESCO1, ESCO2 and DDX11 in WABS cells. Cohesion defects in WABS were similarly restored by cDNAs encoding either human or mouse orthologues of DDX11 (***Figure 5E,F***). Importantly, high levels of either ESCO1 or ESCO2 failed to compensate for DDX11 inactivation, indicating that cohesion loss resulting from impaired DDX11 function cannot be rescued by increased expression of SMC3 acetyltransferases. In conclusion, we find that DDX11, ESCO1, and ESCO2 have separable roles in SCC, which are conserved between human and mouse.

DDX11 helicase activity promotes sister chromatid cohesion

Recent studies in different organisms reported conflicting results regarding whether or not the helicase function of DDX11/Chl1 is required for sister chromatid cohesion [50, 52, 56]. Therefore, we overexpressed the helicase-deficient DDX11-K50R mutant [52, 63, 64] and the DNA-binding mutant DDX11-Q23A [65] in WABS cells and confirmed high nuclear DDX11 expression in the vast majority of cells (***Figure 6A,B***). We then assessed their ability to restore sister chromatid cohesion and find that whereas wtDDX11 rescues the cohesion loss in WABS fibroblasts, both K50R and Q23A show no effect, indicating that DDX11 helicase activity is required to promote or safeguard sister chromatid cohesion in human cells.

Figure 6

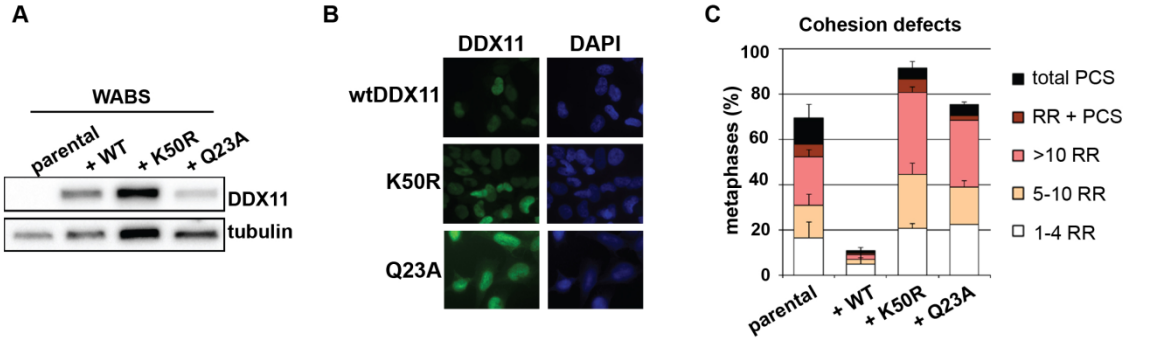

Figure 6: DDX11 helicase activity promotes sister chromatid cohesion. *(A) WABS fibroblasts were stably transfected with WT-DDX11, the helicase mutant K50R or the DNA binding mutant Q23A, and assessed for protein levels using western blot. (B) The expression of ectopic DDX11 was assessed by immunofluorescence. (C) Cells were analyzed for cohesion defects. Mean and standard deviations of two independent experiments are shown.*

DDX11 deficiency causes reduction of SMC3 acetylation and replication fork speed

The interaction of DDX11 with multiple replication fork components [46-50] suggests that it plays a role in cohesin loading in synchrony with DNA replication fork passage. To investigate whether DDX11 also promotes DNA replication itself, we performed DNA fibre assays. Indeed, we found DDX11 knockdown reduces replication fork speed in RPE1-TERT cells, to levels comparable to those observed after ESCO2 depletion (***Figure 7A and 7B***). Based on our observations, we speculate that an important function of DDX11 is to resolve specific secondary DNA structures at the replication fork, thereby promoting replication fork progression and subsequent cohesin loading.

Impaired cohesin loading at replication forks in the absence of DDX11 helicase activity would be predicted to result in reduced cohesive effects of cohesin on DNA. Although we don't observe an effect of DDX11 on SMC3 acetylation in WABS cells (***Figure 7C, 7D and S2***), it is possible that fluctuations are masked by SMC3 acetylation that occurs in the context of non-canonical or non-cell-cycle related cohesin activities (*e.g.* gene transcription). Indeed, when the ESCO1-dependent effects were eliminated by siRNA, DDX11 overexpression seemed to slightly increase SMC3 acetylation, but the effect was not significant (***Figure 7D***). To further examine this, we arrested RPE1-TP53KO-DDX11KO cells in G1 and G2 and compared the levels of SMC3 acetylation (***Figure 7E,F***).

Figure 7

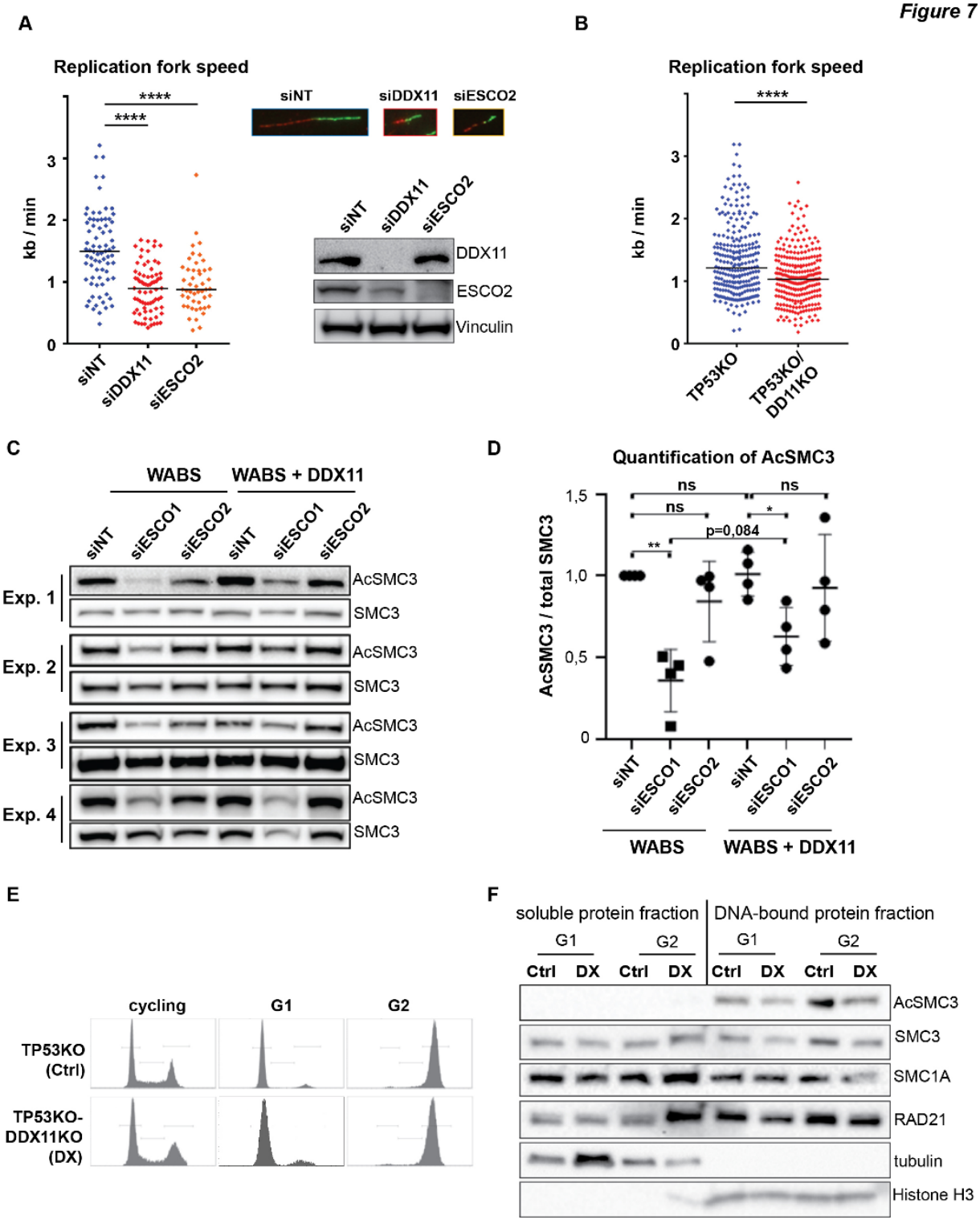

Figure7: DDX11 deficiency slows replication fork speed and reduces SMC3 acetylation. *(A) RPE1-hTERT cells were transfected with indicated siRNAs for two days and analyzed by western blot. Replication fork speed was assessed with a DNA fiber assay using a double labeling protocol. Black lines indicate the median. P-values were calculated by a non-parametric one-way ANOVA test. **** p<0,0001. Representative images of DNA fiber tracts are shown. (B) RPE1-TP53KO and RPE1-TP53KO-DDX1KO cells were analyzed with a DNA fiber assay. (C) WABS fibroblasts and corrected cells were transfected with the indicated siRNAs and analyzed by western blot*

*after three days. Additional antibody incubations are provided in **Figure S2**. (D) Quantification of AcSMC3 levels normalized to total SMC3, using image-lab software and. Mean and standard deviations are shown. P-values were calculated using a two-tailed t-test. * p<0,05; **<0,01; ns not significant. (E) RPE1-TP53KO and RPE1-TP53KO-DDX11KO cells were arrested in G1 using the Cdk4/6 inhibitor Palbociclib (20h, 10 µM) and in G2 using the Cdk1 inhibitor RO3306 (20h, 10 µM) and assessed by flow cytometry. (F) cells from (E) were lysed, and soluble and DNA-bound protein fractions were separated and analyzed by western blot. Ctrl, TP53KO cells; DX, TP53KO-DDX11KO cells.*

This revealed an increase in Ac-SMC3 in TP53KO cells in G2 as compared to G1 cells, whereas this increase was less pronounced in RPE1-TP53KO-DDX11KO cells. However, the effect was subtle and combined loss of DDX11 and ESCO2 had no synergistic impact on SMC3 acetylation (***Figure 7D***), despite severely aggravated cohesion loss. So, apart from a small, partially collaborative function between DDX11 and ESCO2 in promoting SMC3 acetylation, there clearly is also an Ac-SMC3-independent role of DDX11 in sister chromatid cohesion. This might relate to DNA replication fork stability or a role for DDX11 in second strand capture to promote cohesion, such as proposed by [66]. We propose that the DDX11 helicase promotes proper cohesin loading at replication forks, indirectly contributing to subsequent acetylation and stable sister chromatid cohesion.

Discussion

In this study we provide evidence of synthetic lethality between ESCO2 and DDX11 in different human cell lines. Lethality correlated with prolonged mitosis and strongly aggravated loss of SCC, suggesting that mitotic arrest is triggered by premature chromatid separation and subsequent mitotic checkpoint activation, as we described before [58]. In line, we also observed signs of apoptosis induction and polyploidy. The synthetic lethality of DDX11 and ESCO2, as well as the failure of overexpression of one to compensate for loss of the other, indicates that ESCO2 and DDX11 act in different pathways leading to SCC establishment. Importantly, both lethality and cohesion loss were rescued by WAPL knockdown. This suggests that loss of only one of these proteins leads to a level of cohesion loss that can still be tolerated in most cells, but their combined loss causes near to complete cohesion loss, which is detrimental for cell viability.

The observed effects of WAPL knockdown suggest that the SCC resulting from the activity of these pathways is in part spatially separated at the chromosomes. An attractive explanation for the synthetic lethality between ESCO2 and DDX11 is that they largely function in spatially separated contexts. A previous study showed that ESCO2 loss particularly affects cohesion in pericentromeric regions [35], which is also illustrated by the large number of railroad chromosomes observed in metaphase spreads of RBS cells. It has to be noted that RPE1-ESCO2KO cells also exhibit considerable levels of PCS, indicating that the role of ESCO2 clearly is not restricted to establishing SCC at centromeres alone. Indeed, ESCO2 has been reported to bind PCNA and MCM complexes [37-39], and ESCO2 loss delays fork progression [40]. However, WAPL knockdown hardly rescues the cohesion loss in RBS cells, probably because inhibition of WAPL mainly reinforces arm cohesion by blocking the prophase pathway [4, 6, 67]. By contrast, WAPL knockdown partially rescues cohesion defects in DDX11 deficient cells, suggesting that DDX11 facilitates SCC on both chromosome arms and centromeres. This functional separation model receives particular support from our observation that in siESCO2 treated WABS cells, WAPL depletion only prevents PCS, but at the same time increases the amount of railroad chromosomes (*Figure 3E*).

The evolutionary divergence of yeast Eco1 into two vertebrate orthologues, ESCO1 and ESCO2, is accompanied by functional specialization and differential regulation of their protein levels. For example, ESCO1 is expressed during the whole cell cycle, whereas ESCO2 protein expression peaks in S-phase [35, 36]. This suggests that ESCO2 mainly fulfills the role of establishing SCC prior to regulated chromatid separation in mitosis, whereas ESCO1 directs cohesin's non-canonical activities such as those related to gene transcription. Indeed, ESCO1 was reported to acetylate SMC3 in a replication-independent manner, via a unique interaction with PDS5 [41]. This might also explain why we observe a larger effect on SMC3 acetylation of ESCO1 knockdown as compared to ESCO2 knockdown. In line with earlier reports [34, 41, 42], we show here that ESCO1 also contributes to canonical SCC, albeit only to a small extent. Whereas we observed some compensating effects of overexpressing ESCO1 in RBS cells, both knockdown

and overexpression studies indicated that ESCO1 and ESCO2 have largely non-overlapping roles in SCC. This might relate to location-specific effects on SCC of ESCO1 and ESCO2; ESCO2-dependent acetylation has a preference for centromeric cohesins, whereas ESCO1 might preferentially acetylate cohesin at chromosome arms. It will be interesting to further quantify the levels of cohesive cohesin on chromosome arms and centromeres in ESCO1 and ESCO2 deficient human cells. Importantly, we could not distinguish the activities of human or mouse versions of DDX11 or ESCO1/2. Therefore, the paradox that ESCO2 loss is embryonically lethal in mice [35], whereas most human RBS patients contain loss of function mutations in ESCO2 [68], can probably not be explained by differences in the mouse and human ESCO1 and ESCO2 coding sequences. Possibly, the typical acrocentric architecture of murine chromosomes makes them more vulnerable to SCC deprivation and/or ESCO2 deficiency.

We show that the helicase activity of DDX11 critically promotes SCC in human cells. DDX11 is thought to resolve certain complex secondary DNA structures including GC-rich regions and/or anti-parallel G-quadruplexes [69, 70]. The duplex or quadruplex resolving capacities of DDX11 helicases may contribute to SCC by facilitating loading of the second strand into cohesin rings, which was reported to require single stranded DNA [66]. Alternatively, secondary DNA structures that are normally substrates of DDX11 may be prone to breakage when DDX11 is absent, requiring repair and WAPL/PDS5-dependent cohesin removal to provide access of repair factors to the break site [71].

Both DDX11 [46-50] and ESCO2 [37-39] interact with multiple replication fork components, indicating that they promote cohesin loading and cohesion establishment in synchrony with DNA replication fork passage. Possibly, DDX11 acts upstream of ESCO1/2 to facilitate cohesin loading and subsequent SMC3 acetylation. However, this is difficult to reconcile with the severe synthetic lethality of DDX11 and ESCO2: loss of one factor would disrupt the pathway, whereas loss of the second factor would have a small additional effect. As an alternative for spatially separated activities, DDX11 and ESCO2 may participate in mechanistically distinct cohesion establishment pathways. An important notion could be that there seems to be no synergistic effect of DDX11 and ESCO2 co-depletion on SMC3 acetylation. Moreover, we find that increasing SMC3 acetylation by overexpressing ESCO1 or ESCO2 cannot rescue the cohesion defects in DDX11 deficient cells. This may suggest that DDX11 has an Ac-SMC3-independent role in cohesion establishment. Indeed, several reports proposed that there are two parallel pathways to facilitate SCC [53, 72, 73]. Genetic dissection in yeast suggested that loss of Chl1 specifically disrupts one such pathway, but leaves the other intact. In conclusion, we propose that DDX11, ESCO1 and ESCO2 control different fractions of cohesin that are spatially and mechanistically separated.

Acknowledgements

We thank Pascal Walther and Mariah Kes for validating DDX11KO and ESCO2KO RPEs, and Hein te Riele for critical reading of the manuscript. This work was supported by the Netherlands Organisation for Scientific research (TOP-GO grant 854.10.013), the Cancer Center Amsterdam (grant CCA2015-5-25) and by the Dutch Cancer Society (Young Investigator grant 10701/2016-2, to JdL). We dedicate this work to the memory of Johan de Winter, who initiated this study.

Figure S1

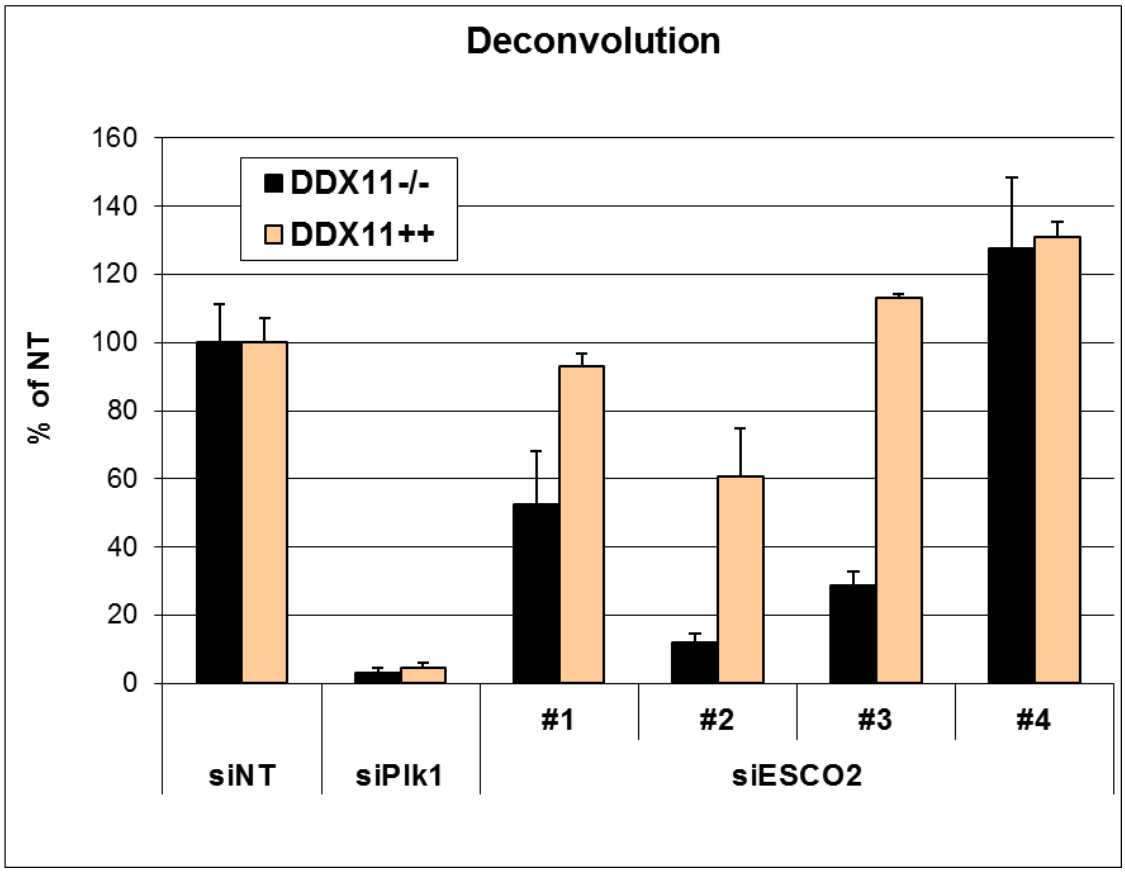

Figure S1: Deconvolution of siRNAs targeting ESCO2.*WABS fibroblasts and corrected cells were transfected with the indicated siRNAs and cell viability was analyzed after four days, using a cell-titer blue assay.*

Figure S2

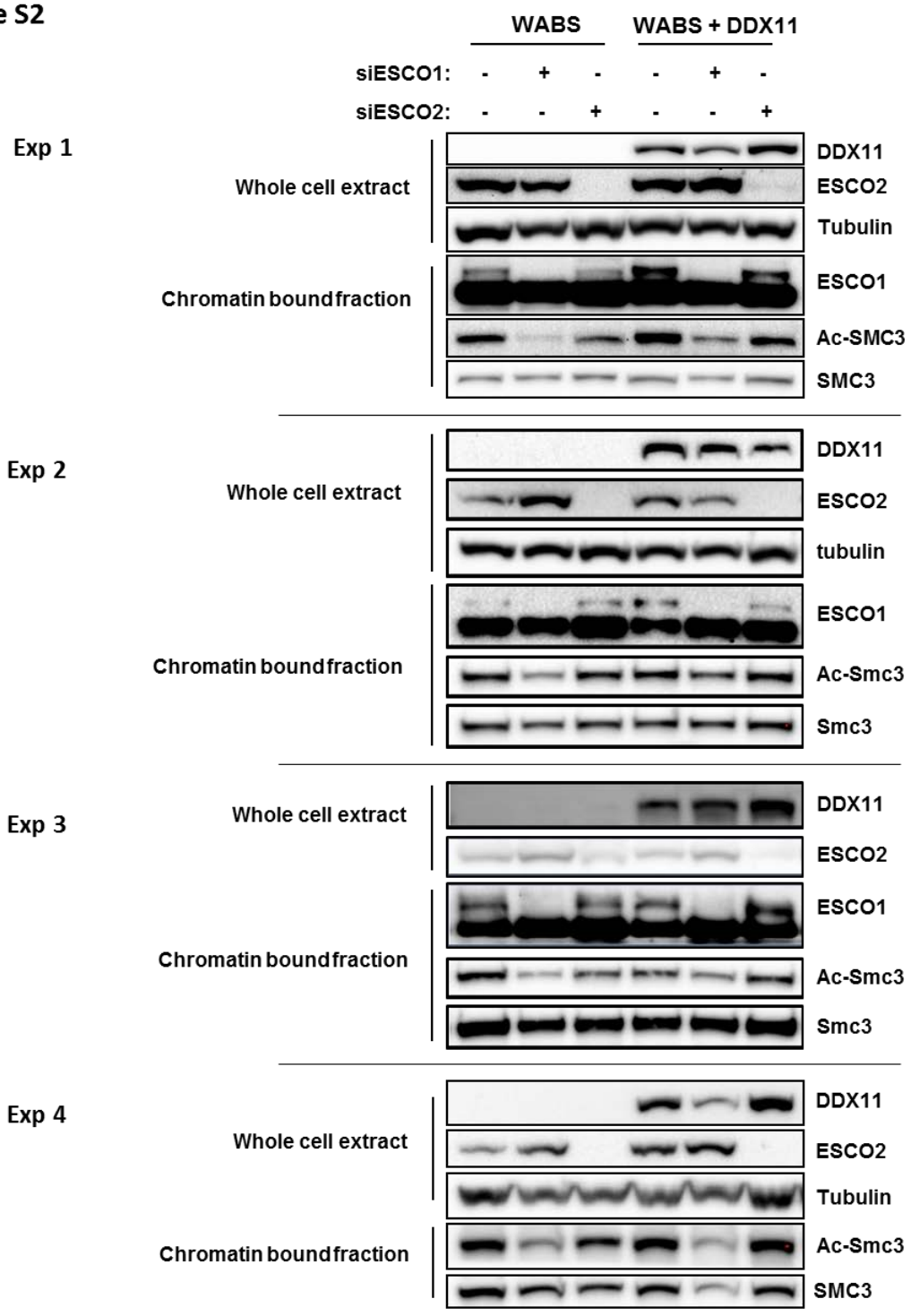

Figure S2: Effect of DDX11, ESCO1 and ESCO2 on SMC3 acetylation.*Cells were transfected with indicated siRNAs and analyzed by Western blot.*

Materials and methods

Cell culture and construction of cell lines. RPE1-hTERT cells (American tissue collection) and SV40 transformed fibroblasts, including WABS [28], RBS [36] and LN9SV control [74], were cultured in Dulbecco's Modified EaglesMedium (DMEM, Gibco), supplemented with 10% FCS, 1 mM sodium pyruvate and antibiotics.

CRISPR-Cas9 was used to construct DDX11 and ESCO2 knockouts in RPE1 cells. The generation of RPE1-hTERT_TetOn-Cas9_TP53KO cells is also described in a currently submitted manuscript [71]. Briefly, Cas9 cDNA was cloned into the pLVX-Tre3G plasmid (Clontech) and lentiviral Tre3G-Cas9 and Tet3G particles were produced in HEK293T cells using the Lenti-X HT packaging system (Clontech). Transduced cells were selected with 10 µg/mL puromycin and 400 µg/mL G418. Cells were treated with 100 ng/mL doxycycline (Sigma-Aldrich) to induce Cas9 expression and transfected with 10 nM synthetic crRNA and tracrRNA (Dharmacon or IDT) using RNAiMAX (Invitrogen). The following crRNA sequences were used: TP53 (CCATTGTTCAATATCGTCCG), DDX11-specific (GGCTGGTCTCCCTTGGCTCC), ESCO2 (TAAGTGGTACCTCAATCCAC). Single clones were assessed by Sanger sequencing using the following primers: TP53-Fw (GAGACCTGTGGGAAGCGAAA, TP53-Rv GCTGCCCTGGTAGGTTTTCT), DDX11-Fw (AACAACCCACCCTCCCCAAG), DDX11-Rv (TGCCTCACTCTCTCCAGACC), ESCO2-Fw (ATCAAAAAGGTAGAAGATGTCCAAGAAC) , ESCO2-Rv (GCCTGTTTGATGGGTTCTGC).

Proliferation assays. Adherent cells, the IncuCyte Zoom instrument (Essen Bioscience) was used. RPE1 cells (1500 / well) and fibroblasts (3000 / well) were seeded in 96-wells plates and imaged every 4 hours with a 10x objective. IncuCyte software was used to quantify confluence from four non-overlapping bright field images per well, for at least three replicate wells. Doubling time was calculated for the period required to grow from approximately 30% to 70% confluence, using the formula doubling time (h) = required time (h) * log(2) / (log(confluence endpoint(%)) – log(confluence starting point(%))).

siRNA transfections. For knockdown experiments, 25 nM siRNA (Dharmacon) was transfected using RNAiMAX (Invitrogen). Sequences: non-targeting siRNA UAAGGCUAUGAAGAGAUAC, siDDX11 GCAGAGCUGUACCGGGUUU, CGGCAGAACCUUUGUGUAA, GAGGAAGAACACAUAACUA, UGUUCAAGGUGCAGCGAUA, siESCO1 GGACAAAGCUACAUGAUAG, siESCO2 CAAAAUCGAGUGAUCUAUA GAGAGUAGUUGGGUGUUUA, AAUCAAGGCUCACCAUUUA, GAAGAAAGAACGUGUAGUA, siUBB CCCAGUGACACCAUCGAAA, GACCAUCACUCUGGAGGUG, GUAUGCAGAUCUUCGUGAA, GCCGUACUCUUUCUGACUA.

Proliferation assays

Proliferation assays were performed in 96-wells plates. Cells were counted and seeded in at least triplicates in a total volume of 100µl medium. Optimized cell densities were: WABS cells 3,000/well, RBS cells 4,000/well, RPE1 cells 1500/well. For WABS and RBS cells, cells were

incubated with 10µl CellTiter-Blue reagent (Promega) for 2–4h and fluorescence (560Ex/590Em) was measured in a microplate reader (TriStar LB 941, Berthold Technologies). To monitor cell growth of RPE1 cells, the IncuCyte Zoom instrument (Essen Bioscience) was used. Cells were imaged every 4h with default software settings and a 10x objective. The IncuCyte software was used to quantify confluence from four non-overlapping bright field images.

qRT-PCR. Total RNA was extracted with the High Pure Isolation Kit (Roche) and cDNA was prepared with the iScript cDNA Synthesis Kit (Biorad). Quantitative reverse transcription polymerase chain reaction (qRT-PCR) was performed using SYBR Green (Roche) on a LightCycler 480 (Roche). Levels were normalized to the geometric mean of at least two housekeeping genes. Primer sequences:

hDDX11-Fw AACCTGTTCAAGGTGCAGCGATAC, hDDX11-Rv GAGAAGCTGGTCGCAGGGT

mDDX11-Fw TTGTGGCTGTTTTGGGAGGTAATG, mDDX11-Rv CACCTGGCTCTGAAAGAGAAAGTC

h/mESCO1-Fw CCTGGTGCTGCTCAACATT, h/mESCO1-Rv CAGGAGTGGGATCTGAGAAAGC

m/hESCO2-Fw ATCAAAAAGGTAGAAGATGTCCAAGAAC, m/hESCO2-Rs GCCTGTTTGATGGGTTCTGC

HPRT1-Fw TGACACTGGGAAAACAATGCA, HPRT-Rv GGTCCTTTTCACCAGCAAGCT

TBP-Fw TGCACAGGAGCCAAGAGTGAA, TBP-Rv CACATCACAGCTCCCCACCA

B2M-Fw ATGAGTATGCCTGCCGTGTGA, B2M-Rv GGCATCTTCAAACCTCCATG

Immunoblotting. Cells were lysed in lysis buffer (50 mM Tris-HCl pH 7.4, 150 mM NaCl, 1% Triton X-100) with protease- and phosphatase inhibitors (Roche). For DNA-bound protein fractions, cells were lysed in lysis buffer for 10 min and centrifuged at 1300 g for 10 min. The pellet was subsequently lysed in lysis buffer containing 5 units/µL benzonase nuclease (Sigma) for 1 h and centrifuged at maximum speed for 5 min. Proteins were separated by 3-8% or 8-16% SDS-PAGE (NU-PAGE or BioRad) and transferred to immobilon-P membranes (Millipore). Membranes were blocked in 5% dry milk in TBST-T (10 mM Tris-HCl pH 7.4, 150 mM NaCl, 0.04% Tween-20), incubated with primary and peroxidase-conjugated secondary antibodies (DAKO Glostrup, Denmark) and bands were visualized by chemoluminescence (Amersham). Antibodies used for detection are mouse anti-DDX11 (B01P, Abnova), mouse anti-α-tubulin (B-5-1-2, Santa Cruz #sc-23948), mouse anti-vinculin (H-10, Santa Cruz sc-25336), guinea pig anti-ESCO2 [36], mouse anti-ESCO1 (gift from JM Peters), rabbit anti-PARP (9542, Cell signaling), AcSM3 (gift from K Shirahige), rabbit anti-SMC3 (A300-060A, Bethyl), rabbit anti-WAPL (A300-268, Bethyl), mouse anti-vinculin (H-10, sc-25336, Santa Cruz).

Flow cytometry. Cells were harvested and washed in PBS and fixed in ice-cold 70% EtOH. For mitosis detection, cells were incubated with rabbit anti-pS10-Histone H3 (Millipore) for 1 h and with Alexa Fluor 488 goat-anti-rabbit (Invitrogen) for 30 min. Cells were washed and resuspended in PBS with 1:10 PI/RNase staining buffer (BD Biosciences) and analyzed by flow cytometry on a BD FACSCalibur (BD Biosciences). Cell cycle analysis was conducted with BD CellQuest software (BD Biosciences).

Analysis of cohesion defects. Cells were incubated with 200 ng/mL demecolcin (Sigma-Aldrich) for 20 minutes. Cells were harvested, resuspended in 0.075 M KCl for 20 minutes and fixed in methanol/acetic acid (3:1). Cells were washed in fixative three times, dropped onto glass slides and stained with 5% Giemsa (Merck). Cohesion defects were counted in 25 metaphases per slide on two coded slides per condition.

References:

1.Ciosk R, Shirayama M, Shevchenko A, Tanaka T, Toth A, Shevchenko A, et al. Cohesin's binding to chromosomes depends on a separate complex consisting of Scc2 and Scc4 proteins. Mol Cell. 2000;5(2):243-54. PubMed PMID: 10882066.
2.Fernius J, Nerusheva OO, Galander S, Alves Fde L, Rappsilber J, Marston AL. Cohesin-dependent association of scc2/4 with the centromere initiates pericentromeric cohesion establishment. Curr Biol. 2013;23(7):599-606. doi: 10.1016/j.cub.2013.02.022. PubMed PMID: 23499533; PubMed Central PMCID: PMCPMC3627958.
3.Watrin E, Schleiffer A, Tanaka K, Eisenhaber F, Nasmyth K, Peters JM. Human Scc4 is required for cohesin binding to chromatin, sister-chromatid cohesion, and mitotic progression. Curr Biol. 2006;16(9):863-74. doi: S0960-9822(06)01346-7 [pii];10.1016/j.cub.2006.03.049 [doi].
4.Kueng S, Hegemann B, Peters BH, Lipp JJ, Schleiffer A, Mechtler K, et al. Wapl controls the dynamic association of cohesin with chromatin. Cell. 2006;127(5):955-67.
5.Heidinger-Pauli JM, Unal E, Koshland D. Distinct targets of the Eco1 acetyltransferase modulate cohesion in S phase and in response to DNA damage. Mol Cell. 2009;34(3):311-21.
6.Rowland BD, Roig MB, Nishino T, Kurze A, Uluocak P, Mishra A, et al. Building sister chromatid cohesion: smc3 acetylation counteracts an antiestablishment activity. Mol Cell. 2009;33(6):763-74.
7.Nishiyama T, Ladurner R, Schmitz J, Kreidl E, Schleiffer A, Bhaskara V, et al. Sororin mediates sister chromatid cohesion by antagonizing Wapl. Cell. 2010;143(5):737-49.
8.Hauf S, Roitinger E, Koch B, Dittrich CM, Mechtler K, Peters JM. Dissociation of cohesin from chromosome arms and loss of arm cohesion during early mitosis depends on phosphorylation of SA2. PLoS Biol. 2005;3(3):e69. doi: 10.1371/journal.pbio.0030069. PubMed PMID: 15737063; PubMed Central PMCID: PMCPMC1054881.
9.Waizenegger IC, Hauf S, Meinke A, Peters JM. Two distinct pathways remove mammalian cohesin from chromosome arms in prophase and from centromeres in anaphase. Cell. 2000;103(3):399-410. PubMed PMID: 11081627.
10.Zhang N, Panigrahi AK, Mao Q, Pati D. Interaction of Sororin protein with polo-like kinase 1 mediates resolution of chromosomal arm cohesion. J Biol Chem. 2011;286(48):41826-37. doi: 10.1074/jbc.M111.305888. PubMed PMID: 21987589; PubMed Central PMCID: PMC3310079.
11.McGuinness BE, Hirota T, Kudo NR, Peters JM, Nasmyth K. Shugoshin prevents dissociation of cohesin from centromeres during mitosis in vertebrate cells. PLoS Biol. 2005;3(3):e86. doi: 04-PLBI-RA-0678R1 [pii];10.1371/journal.pbio.0030086 [doi].
12.Liu H, Rankin S, Yu H. Phosphorylation-enabled binding of SGO1-PP2A to cohesin protects sororin and centromeric cohesion during mitosis. Nat Cell Biol. 2013;15(1):40-9. doi: ncb2637 [pii];10.1038/ncb2637 [doi].
13.Peters JM. The anaphase promoting complex/cyclosome: a machine designed to destroy. Nat Rev Mol Cell Biol. 2006;7(9):644-56.

14.Skibbens RV, Marzillier J, Eastman L. Cohesins coordinate gene transcriptions of related function within Saccharomyces cerevisiae. Cell Cycle. 2010;9(8):1601-6. doi: 10.4161/cc.9.8.11307. PubMed PMID: 20404480; PubMed Central PMCID: PMCPMC3096706.
15.Parelho V, Hadjur S, Spivakov M, Leleu M, Sauer S, Gregson HC, et al. Cohesins functionally associate with CTCF on mammalian chromosome arms. Cell. 2008;132(3):422-33. doi: 10.1016/j.cell.2008.01.011. PubMed PMID: 18237772.
16.Wendt KS, Yoshida K, Itoh T, Bando M, Koch B, Schirghuber E, et al. Cohesin mediates transcriptional insulation by CCCTC-binding factor. Nature. 2008;451(7180):796-801. doi: 10.1038/nature06634. PubMed PMID: 18235444.
17.Xu B, Sowa N, Cardenas ME, Gerton JL. L-leucine partially rescues translational and developmental defects associated with zebrafish models of Cornelia de Lange syndrome. Hum Mol Genet. 2015;24(6):1540-55. doi: 10.1093/hmg/ddu565. PubMed PMID: 25378554; PubMed Central PMCID: PMCPMC4351377.
18.Zakari M, Yuen K, Gerton JL. Etiology and pathogenesis of the cohesinopathies. Wiley Interdiscip Rev Dev Biol. 2015;4(5):489-504. doi: 10.1002/wdev.190. PubMed PMID: 25847322.
19.Bose T, Lee KK, Lu S, Xu B, Harris B, Slaughter B, et al. Cohesin proteins promote ribosomal RNA production and protein translation in yeast and human cells. PLoS Genet. 2012;8(6):e1002749. doi: 10.1371/journal.pgen.1002749 [doi];PGENETICS-D-11-02119 [pii].
20.Krantz ID, McCallum J, DeScipio C, Kaur M, Gillis LA, Yaeger D, et al. Cornelia de Lange syndrome is caused by mutations in NIPBL, the human homolog of Drosophila melanogaster Nipped-B. Nat Genet. 2004;36(6):631-5.
21.Tonkin ET, Wang TJ, Lisgo S, Bamshad MJ, Strachan T. NIPBL, encoding a homolog of fungal Scc2-type sister chromatid cohesion proteins and fly Nipped-B, is mutated in Cornelia de Lange syndrome. Nat Genet. 2004;36(6):636-41.
22.Gillis LA, McCallum J, Kaur M, DeScipio C, Yaeger D, Mariani A, et al. NIPBL mutational analysis in 120 individuals with Cornelia de Lange syndrome and evaluation of genotype-phenotype correlations. Am J Hum Genet. 2004;75(4):610-23. doi: 10.1086/424698. PubMed PMID: 15318302; PubMed Central PMCID: PMCPMC1182048.
23.Musio A, Selicorni A, Focarelli ML, Gervasini C, Milani D, Russo S, et al. X-linked Cornelia de Lange syndrome owing to SMC1L1 mutations. Nat Genet. 2006;38(5):528-30. doi: 10.1038/ng1779. PubMed PMID: 16604071.
24.Deardorff MA, Kaur M, Yaeger D, Rampuria A, Korolev S, Pie J, et al. Mutations in cohesin complex members SMC3 and SMC1A cause a mild variant of cornelia de Lange syndrome with predominant mental retardation. Am J Hum Genet. 2007;80(3):485-94. doi: 10.1086/511888. PubMed PMID: 17273969; PubMed Central PMCID: PMC1821101.
25.Deardorff MA, Wilde JJ, Albrecht M, Dickinson E, Tennstedt S, Braunholz D, et al. RAD21 Mutations Cause a Human Cohesinopathy. Am J Hum Genet. 2012.
26.Deardorff MA, Bando M, Nakato R, Watrin E, Itoh T, Minamino M, et al. HDAC8 mutations in Cornelia de Lange syndrome affect the cohesin acetylation cycle. Nature. 2012.

27.Vega H, Waisfisz Q, Gordillo M, Sakai N, Yanagihara I, Yamada M, et al. Roberts syndrome is caused by mutations in ESCO2, a human homolog of yeast ECO1 that is essential for the establishment of sister chromatid cohesion. Nat Genet. 2005;37(5):468-70.
28.van der Lelij P, Chrzanowska KH, Godthelp BC, Rooimans MA, Oostra AB, Stumm M, et al. Warsaw breakage syndrome, a cohesinopathy associated with mutations in the XPD helicase family member DDX11/ChlR1. Am J Hum Genet. 2010;86(2):262-6.
29.Chetaille P, Preuss C, Burkhard S, Cote JM, Houde C, Castilloux J, et al. Mutations in SGOL1 cause a novel cohesinopathy affecting heart and gut rhythm. Nat Genet. 2014;46(11):1245-9. doi: 10.1038/ng.3113. PubMed PMID: 25282101.
30.Castronovo P, Gervasini C, Cereda A, Masciadri M, Milani D, Russo S, et al. Premature chromatid separation is not a useful diagnostic marker for Cornelia de Lange syndrome. Chromosome Res. 2009;17(6):763-71. doi: 10.1007/s10577-009-9066-6. PubMed PMID: 19690971.
31.Banerji R, Eble DM, Iovine MK, Skibbens RV. Esco2 regulates cx43 expression during skeletal regeneration in the zebrafish fin. Dev Dyn. 2016;245(1):7-21. doi: 10.1002/dvdy.24354. PubMed PMID: 26434741.
32.Remeseiro S, Cuadrado A, Losada A. Cohesin in development and disease. Development. 2013;140(18):3715-8. doi: 10.1242/dev.090605. PubMed PMID: 23981654.
33.Skibbens RV, Colquhoun JM, Green MJ, Molnar CA, Sin DN, Sullivan BJ, et al. Cohesinopathies of a feather flock together. PLoS Genet. 2013;9(12):e1004036. doi: 10.1371/journal.pgen.1004036. PubMed PMID: 24367282; PubMed Central PMCID: PMCPMC3868590.
34.Hou F, Zou H. Two human orthologues of Eco1/Ctf7 acetyltransferases are both required for proper sister-chromatid cohesion. Mol Biol Cell. 2005;16(8):3908-18.
35.Whelan G, Kreidl E, Wutz G, Egner A, Peters JM, Eichele G. Cohesin acetyltransferase Esco2 is a cell viability factor and is required for cohesion in pericentric heterochromatin. EMBO J. 2011.
36.van der Lelij P, Godthelp BC, W. vZ, D. vG, Oostra AB, Steltenpool J, et al. The cellular phenotype of Roberts syndrome fibroblasts as revealed by ectopic expression of ESCO2. PLoS One. 2009;4(9):e6936.
37.Moldovan GL, Pfander B, Jentsch S. PCNA controls establishment of sister chromatid cohesion during S phase. Mol Cell. 2006;23(5):723-32.
38.Ivanov MP, Ladurner R, Poser I, Beveridge R, Rampler E, Hudecz O, et al. The replicative helicase MCM recruits cohesin acetyltransferase ESCO2 to mediate centromeric sister chromatid cohesion. EMBO J. 2018;37(15). Epub 2018/06/23. doi: 10.15252/embj.201797150. PubMed PMID: 29930102; PubMed Central PMCID: PMCPMC6068434.
39.Minamino M, Tei S, Negishi L, Kanemaki MT, Yoshimura A, Sutani T, et al. Temporal Regulation of ESCO2 Degradation by the MCM Complex, the CUL4-DDB1-VPRBP Complex, and the Anaphase-Promoting Complex. Curr Biol. 2018;28(16):2665-72 e5. Epub 2018/08/14. doi: 10.1016/j.cub.2018.06.037. PubMed PMID: 30100344.

40.Terret ME, Sherwood R, Rahman S, Qin J, Jallepalli PV. Cohesin acetylation speeds the replication fork. Nature. 2009;462(7270):231-4.
41.Minamino M, Ishibashi M, Nakato R, Akiyama K, Tanaka H, Kato Y, et al. Esco1 Acetylates Cohesin via a Mechanism Different from That of Esco2. Curr Biol. 2015;25(13):1694-706. doi: 10.1016/j.cub.2015.05.017. PubMed PMID: 26051894.
42.Kawasumi R, Abe T, Arakawa H, Garre M, Hirota K, Branzei D. ESCO1/2's roles in chromosome structure and interphase chromatin organization. Genes Dev. 2017;31(21):2136-50. doi: 10.1101/gad.306084.117. PubMed PMID: 29196537; PubMed Central PMCID: PMCPMC5749162.
43.Alomer RM, da Silva EML, Chen J, Piekarz KM, McDonald K, Sansam CG, et al. Esco1 and Esco2 regulate distinct cohesin functions during cell cycle progression. Proc Natl Acad Sci U S A. 2017;114(37):9906-11. doi: 10.1073/pnas.1708291114. PubMed PMID: 28847955; PubMed Central PMCID: PMCPMC5604028.
44.Wu Y, Brosh RM, Jr. DNA helicase and helicase-nuclease enzymes with a conserved iron-sulfur cluster. Nucleic Acids Res. 2012;40(10):4247-60. doi: 10.1093/nar/gks039. PubMed PMID: 22287629; PubMed Central PMCID: PMCPMC3378879.
45.Pisani FM, Napolitano E, Napolitano LMR, Onesti S. Molecular and Cellular Functions of the Warsaw Breakage Syndrome DNA Helicase DDX11. Genes (Basel). 2018;9(11). doi: 10.3390/genes9110564. PubMed PMID: 30469382; PubMed Central PMCID: PMCPMC6266566.
46.Rudra S, Skibbens RV. Sister chromatid cohesion establishment occurs in concert with lagging strand synthesis. Cell Cycle. 2012;11(11):2114-21.
47.Petronczki M, Chwalla B, Siomos MF, Yokobayashi S, Helmhart W, Deutschbauer AM, et al. Sister-chromatid cohesion mediated by the alternative RF-CCtf18/Dcc1/Ctf8, the helicase Chl1 and the polymerase-alpha-associated protein Ctf4 is essential for chromatid disjunction during meiosis II. J Cell Sci. 2004;117(Pt 16):3547-59.
48.Mayer ML, Pot I, Chang M, Xu H, Aneliunas V, Kwok T, et al. Identification of protein complexes required for efficient sister chromatid cohesion. Mol Biol Cell. 2004;15(4):1736-45. doi: 10.1091/mbc.E03-08-0619. PubMed PMID: 14742714; PubMed Central PMCID: PMC379271.
49.Cali F, Bharti SK, Di Perna R, Brosh RM, Jr., Pisani FM. Tim/Timeless, a member of the replication fork protection complex, operates with the Warsaw breakage syndrome DNA helicase DDX11 in the same fork recovery pathway. Nucleic Acids Res. 2016;44(2):705-17. doi: 10.1093/nar/gkv1112. PubMed PMID: 26503245; PubMed Central PMCID: PMCPMC4737141.
50.Cortone G, Zheng G, Pensieri P, Chiappetta V, Tate R, Malacaria E, et al. Interaction of the Warsaw breakage syndrome DNA helicase DDX11 with the replication fork-protection factor Timeless promotes sister chromatid cohesion. PLoS Genet. 2018;14(10):e1007622. doi: 10.1371/journal.pgen.1007622. PubMed PMID: 30303954; PubMed Central PMCID: PMCPMC6179184.

51.Rudra S, Skibbens RV. Chl1 DNA Helicase Regulates Scc2 Deposition Specifically during DNA-Replication in Saccharomyces cerevisiae. PLoS One. 2013;8(9):e75435. doi: 10.1371/journal.pone.0075435 [doi];PONE-D-13-27117 [pii].
52.Samora CP, Saksouk J, Goswami P, Wade BO, Singleton MR, Bates PA, et al. Ctf4 Links DNA Replication with Sister Chromatid Cohesion Establishment by Recruiting the Chl1 Helicase to the Replisome. Mol Cell. 2016;63(3):371-84. doi: 10.1016/j.molcel.2016.05.036. PubMed PMID: 27397686; PubMed Central PMCID: PMCPMC4980427.
53.Borges V, Smith DJ, Whitehouse I, Uhlmann F. An Eco1-independent sister chromatid cohesion establishment pathway in S. cerevisiae. Chromosoma. 2013.
54.Chen Z, McCrosky S, Guo W, Li H, Gerton JL. A Genetic Screen to Discover Pathways Affecting Cohesin Function in Schizosaccharomyces pombe Identifies Chromatin Effectors. G3 (Bethesda). 2012;2(10):1161-8.
55.Skibbens RV. Chl1p, a DNA helicase-like protein in budding yeast, functions in sister-chromatid cohesion. Genetics. 2004;166(1):33-42.
56.Abe T, Kawasumi R, Arakawa H, Hori T, Shirahige K, Losada A, et al. Chromatin determinants of the inner-centromere rely on replication factors with functions that impart cohesion. Oncotarget. 2016;7(42):67934-47. doi: 10.18632/oncotarget.11982. PubMed PMID: 27636994; PubMed Central PMCID: PMCPMC5356530.
57.van der Lelij P, Oostra AB, Rooimans MA, Joenje H, de Winter JP. Diagnostic Overlap between Fanconi Anemia and the Cohesinopathies: Roberts Syndrome and Warsaw Breakage Syndrome. Anemia. 2010;2010:565268.
58.de Lange J, Faramarz A, Oostra AB, de Menezes RX, van der Meulen IH, Rooimans MA, et al. Defective sister chromatid cohesion is synthetically lethal with impaired APC/C function. Nat Commun. 2015;6:8399. doi: ncomms9399 [pii];10.1038/ncomms9399 [doi].
59.Daum JR, Potapova TA, Sivakumar S, Daniel JJ, Flynn JN, Rankin S, et al. Cohesion fatigue induces chromatid separation in cells delayed at metaphase. Curr Biol. 2011;21(12):1018-24. doi: S0960-9822(11)00588-4 [pii];10.1016/j.cub.2011.05.032 [doi].
60.Stevens D, Gassmann R, Oegema K, Desai A. Uncoordinated loss of chromatid cohesion is a common outcome of extended metaphase arrest. PLoS One. 2011;6(8):e22969. doi: 10.1371/journal.pone.0022969 [doi];PONE-D-11-09005 [pii].
61.Cota CD, Garcia-Garcia MJ. The ENU-induced cetus mutation reveals an essential role of the DNA helicase DDX11 for mesoderm development during early mouse embryogenesis. Dev Dyn. 2012;241(8):1249-59. Epub 2012/06/09. doi: 10.1002/dvdy.23810. PubMed PMID: 22678773.
62.Inoue A, Li T, Roby SK, Valentine MB, Inoue M, Boyd K, et al. Loss of ChlR1 helicase in mouse causes lethality due to the accumulation of aneuploid cells generated by cohesion defects and placental malformation. Cell Cycle. 2007;6(13):1646-54. doi: 4411 [pii].
63.Farina A, Shin JH, Kim DH, Bermudez VP, Kelman Z, Seo YS, et al. Studies with the human cohesin establishment factor, ChlR1. Association of ChlR1 with Ctf18-RFC and Fen1. J Biol Chem. 2008;283(30):20925-36.
64.Hirota Y, Lahti JM. Characterization of the enzymatic activity of hChlR1, a novel human DNA helicase. Nucleic Acids Res. 2000;28(4):917-24. doi: gkd190 [pii].

65.Ding H, Guo M, Vidhyasagar V, Talwar T, Wu Y. The Q Motif Is Involved in DNA Binding but Not ATP Binding in ChlR1 Helicase. PLoS One. 2015;10(10):e0140755. doi: 10.1371/journal.pone.0140755. PubMed PMID: 26474416; PubMed Central PMCID: PMCPMC4608764.
66.Murayama Y, Samora CP, Kurokawa Y, Iwasaki H, Uhlmann F. Establishment of DNA-DNA Interactions by the Cohesin Ring. Cell. 2018;172(3):465-77 e15. doi: 10.1016/j.cell.2017.12.021. PubMed PMID: 29358048; PubMed Central PMCID: PMCPMC5786502.
67.Gandhi R, Gillespie PJ, Hirano T. Human Wapl is a cohesin-binding protein that promotes sister-chromatid resolution in mitotic prophase. Curr Biol. 2006;16(24):2406-17.
68.Vega H, Trainer AH, Gordillo M, Crosier M, Kayserili H, Skovby F, et al. Phenotypic variability in 49 cases of ESCO2 mutations, including novel missense and codon deletion in the acetyltransferase domain, correlates with ESCO2 expression and establishes the clinical criteria for Roberts syndrome. J Med Genet. 2010;47(1):30-7.
69.Bharti SK, Khan I, Banerjee T, Sommers JA, Wu Y, Brosh RM, Jr. Molecular functions and cellular roles of the ChlR1 (DDX11) helicase defective in the rare cohesinopathy Warsaw breakage syndrome. Cell Mol Life Sci. 2014;71(14):2625-39. doi: 10.1007/s00018-014-1569-4 [doi].
70.Wu Y, Sommers J, Khan I, J. dW, Brosh R. Biochemical characterization of Warsaw Breakage Syndrome helicase. J Biol Chem. 2011.
71.Benedict B, van Schie J, Oostra A, Balk J, Wolthuis R, te Riele H, et al. WAPL-dependent repair of damaged replication forks underlies oncogene-induced loss of sister chromatid cohesion. submitted manuscript. 2019.
72.Srinivasan M, Petela NJ, Scheinost JC, Collier J, Voulgaris M, M BR, et al. Scc2 counteracts a Wapl-independent mechanism that releases cohesin from chromosomes during G1. Elife. 2019;8. Epub 2019/06/22. doi: 10.7554/eLife.44736. PubMed PMID: 31225797; PubMed Central PMCID: PMCPMC6588348.
73.Xu H, Boone C, Brown GW. Genetic dissection of parallel sister-chromatid cohesion pathways. Genetics. 2007;176(3):1417-29.
74.Hermsen MA, Joenje H, Arwert F, Welters MJ, Braakhuis BJ, Bagnay M, et al. Centromeric breakage as a major cause of cytogenetic abnormalities in oral squamous cell carcinoma. Genes Chromosomes Cancer. 1996;15(1):1-9.

Chapter 6

DDX11 Helicase Activity Protects Against G-Quadruplex Induced Chromosomal Breakage at Replication Forks and Concomitant Loss of Sister Chromatid Cohesion

Atiq Faramarz, Janne van Schie, Jesper Balk, Anneke Oostra, Martin Rooimans, Joanna Parish, Grant Stewart, Cynthia De Almeida Estéves, Katja Dumic, Ingeborg Barisic, Karin Diderich, Francesca Pisani, Najim Ameziane, Rob Wolthuis and Job de Lange

Submitted to Nature Communications for publication, in slightly modified form

Abstract

Warsaw Breakage Syndrome (WABS) is a rare DNA damage syndrome as well as a cohesinopathy caused by bi-allelic mutations in the DNA helicase DDX11. Here, we report multiple compound heterozygous WABS cases showing reduced DDX11 protein levels, high sensitivity to topoisomerase and PARP inhibitors, spontaneous loss of sister chromatid cohesion and reduced DNA replication fork speed. We identify weak alleles encoding unstable DDX11 protein and show that DDX11 knockdown further enhances cohesion loss in several patient-derived cell lines. Knocking out DDX11 in RPE1-TERT cells causes p53-dependent growth inhibition, chromosome breaks and cohesion defects, while the nearly identical, expressed pseudogene DDX12p has no redundant role in proliferation and cohesion. Importantly, stabilization of G-quadruplex (G4) structures, a presumed substrate of DDX11 helicase, induces chromosomal breaks, cohesion loss, and growth inhibition in a manner strongly dependent on DDX11 but less on FANCJ. Finally, the DNA helicase activity of DDX11 is essential for G4 stabilizer resistance and maintenance of sister chromatid cohesion. We propose that DDX11 protects against G4-induced double stranded breaks during DNA replication and facilitates efficient cohesin loading by resolving secondary structures at the replication fork.

Introduction

Warsaw Breakage Syndrome (WABS) was discovered in 2010 in a patient displaying clinical overlap with Fanconi Anemia (FA), including growth retardation, microcephaly and abnormal skin pigmentation, although bone marrow failure was not observed [1]. At the cellular level, WABS cells showed Mitomycin C (MMC)-induced breaks but in contrast to FA cells also exhibited spontaneous loss of sister chromatid cohesion, which was significantly exacerbated by treatment with MMC or the topoisomerase I inhibitor Camptothecin. Bi-allelic inactivation of the DEAD/H Box helicase DDX11 was identified as the underlying genetic defect in WABS patients. So far, sixteen WABS individuals from twelve different families have been reported [1-7].

DDX11 (also known as ChlR1) is one of two human orthologues of yeast Chl1, which was identified in a screen for mutants affecting chromosome segregation [8,9]. The other orthologue is DDX12p (also known as ChlR2) [10,11], a presumed pseudogene which is linked to a late-evolutionary duplication of a chromosomal region containing DDX11. Parish and colleagues showed that DDX11 protein is localized in the nucleus and supports sister chromatid cohesion [12], which fits with later findings in WABS cells. DDX11 loss in mice is embryonically lethal [13,14], apparently conflicting the observed viability of yeast Chl1 mutants [8,9,15] and the relatively moderate symptoms of human WABS patients.

Sequence similarities classify DDX11 in a subgroup of ATP-dependent, super-family 2 (SF2) DNA helicases that contain an iron-sulfur cluster (Fe-S) between the Walker A and B boxes [16]. Other members include FANCJ, RTEL1 and XPD/ERCC2, all linked to genetic disorders characterized by defects in DNA repair mechanisms. A number of *in vitro* studies [17-20] revealed that DDX11 is able to unwind duplex DNA with 5'-3' directionality and generally prefers a 5' single stranded region. As reviewed in [21], *in vitro* substrates include forked duplexes, 5′ flap structures (relevant in the processing of Okazaki fragments), three-stranded D-loops (an early HR repair intermediate) and anti-parallel G-quadruplexes (G4). Interestingly, combined mutation of *chl-1* and *dog-1* (the C*. elegans* homologs of DDX11 and FANCJ*)* caused an increased number of poly-guanine tract deletions as compared to single dog-1 mutants, suggesting a potential role for DDX11 in resolving G4 or related poly-guanine duplex structures in vivo [22].

Yeast Chl1 mutant strains show increased sensitivity to DNA damaging agents including MMS and UV [15,23]. In addition, Chl1 supports the establishment of sister chromatid cohesion [24,25], a process that is coupled to DNA replication [26,27]. DNA replication is coordinated by large protein complexes forming the "replisome". Unwinding of the template strand is performed by the Cdc45-MCM (mini-chromosome-maintenance)-GINS (go-ichi-ni-san) (CMG) complex. Specialized DNA polymerases synthesize DNA in conjunction with a homo-trimeric proliferating cell nuclear antigen (PCNA) sliding clamp loaded onto DNA by the replication factor C (RFC) complex. Polymerase ε acts on the leading strand, whereas the lagging strand is replicated by polymerases α and δ. Other replisome components include Tof1/Timeless, Csm3/Tipin, Mrc1/Claspin and CTF4/AND-1, which all play important roles in maintaining replication fork

stability by coordinating DNA template unwinding with DNA synthesis and the association with checkpoint proteins (reviewed in [28]).

Chl1 interacts genetically with multiple components of the alternative RFC^{CTF18} complex, including CTF18, CTF8 and DCC1, which are implicated in cohesion establishment, too [25,29-32]. Physical interactions were also reported between Chl1 and PCNA [33], CTF4 [34], and the 5'-flap endonuclease FEN1 [35]. Human DDX11 was reported to bind RFC^{CHTF18}, which stimulated DDX11 helicase activity *in vitro*; to Fen1, promoting Fen1 activity; and to PCNA [18]. Furthermore, a role for DDX11 was proposed in stabilization of the replication fork through an interaction with Timeless, which stimulated DDX11 helicase activity *in vitro* and promoted sister chromatid cohesion [36-38]. How DDX11 deficiency results in cohesion loss is not clear. Possibly, DDX11 facilitates sister chromatid entrapment by resolving secondary DNA structures formed at replication sites, particularly in the lagging strand. Indeed, abolishing the ATPase activity in yeast Chl1 resulted in loss of Chl1 function [39]. However, dominant helicase-independent roles in cohesin loading have also been proposed [34,38,40].

Here, we identify seven new WABS patients from five different families. WABS derived cells display loss of sister chromatid cohesion, increased sensitivity to Camptothecin and PARP inhibitors and reduced replication fork speed. The investigated WABS cells possess residual DDX11 activity, originating from an unstable protein, which however is capable of rescuing sister chromatid cohesion when overexpressed. Loss of DDX11 causes p53-dependent growth restriction. While we show that DDX12p is expressed as mRNA, we observed no complementary role for DDX12p in WABS cells. DDX11 helicase activity is required for sister chromatid cohesion and to prevent DNA breaks induced by G4 stabilizing drugs. We propose that DDX11 unwinds G4 structures that arise when replication forks travel through G-rich regions, to prevent breaks and to promote efficient DNA entrapment by cohesin rings and genomic stability.

Results

Clinical characterization of seven new WABS cases

The first WABS patient was reported by our lab in 2010 [1], which we now call WABS01. Here, we investigated seven new patients (WABS02 – WABS08) from different origins, who were diagnosed with Warsaw Breakage Syndrome (Figure 1A). WABS02 (male) is the second child of non-consanguineous Dutch parents, initially diagnosed as Nijmegen Breakage Syndrome, although no NBS1 mutations were found [41]. He showed growth retardation, microcephaly, deafness and abnormal skin pigmentations. WABS03 (male) is the second child of non-consanguineous parents from Uruguay. He received pediatric intensive care for several months due to respiratory problems, and showed severe developmental delay, microcephaly, sensorineural deafness and multiple broncho-obstructive episodes. Also congenital hypothyroidism, low sets of ears and a nose-retrognathia were observed. WABS04 (female) is the first child of non-consanguineous Dutch parents, initially diagnosed as FA with unknown genetic cause [42]. She was born at the 7th month of pregnancy and weighted 750 g and had epileptic episode at 3 years. At the age of 45, the following clinical features were recorded: growth and mental retardation, deafness, microcephaly, skin pigmentation (café-au-lait spots), facial dysmorphy, bulbous nose, clinodactyly of the 5th fingers, insulin-dependent diabetes mellitus and frequent respiratory and middle-ear infections. She died at the age of 64, but no autopsy report is available. WABS04 had three unaffected siblings and a brother with clinical features that may have been overlapping, but he died before a diagnosis was reached (see [42]). WABS05 (male) is the fourth child of non-consanguineous parents from Croatia. He showed pre-natal growth retardation; his birth weight, after 36 weeks, was 1660 g. He suffered epileptic seizure at the age of seven, and further displayed brachy-microcephaly, moderate to severe intellectual disability, bronchial asthma clinodactyly of the 5th fingers, flexion contractures of thumbs and sandal gap of toes and he is deaf-mute. Cytogenetic investigation showed a 47XXY karyotype and cohesion defects. WABS06 (female) is the older sister of WABS05. Her birth weight, after 37 weeks, was 2100g. She shows brachy-microcephaly, abnormal skin pigmentation (café au lait spots), clinodactyly of the 5th fingers, sandal gap of toe and is deaf-mute. At early age, her intellectual development was estimated to be normal but later declined. WABS07 (male) is a child of Dutch parents. The pregnancy was prematurely abrogated due to severe growth restrictions and placental abnormalities. Furthermore, the fetus showed mild dysmorphic characteristics, lung hypoplasia, increased liver-brain ration, unilateral kidney dysplasia and skin abnormalities. WABS08 is a younger child of the same parents, whose pregnancy was also prematurely abrogated due to severe growth retardation. In addition, multiple miscarriages with unknown genotype were reported, possibly relevant in light of the placental malformations that were observed in DDX11 knockout mice [13]. Table 1 summarizes the clinical phenotypes of all known WABS cases, including the seven patients of this study. Notably, while microcephaly coinciding with deafness appear to be dominant diagnostic features, anemia is not reported, ruling out FA. Furthermore, not all characteristics are shared

between all patients indicating that WABS is a heterogeneous disease, similar to other cohesinopathies [43-45].

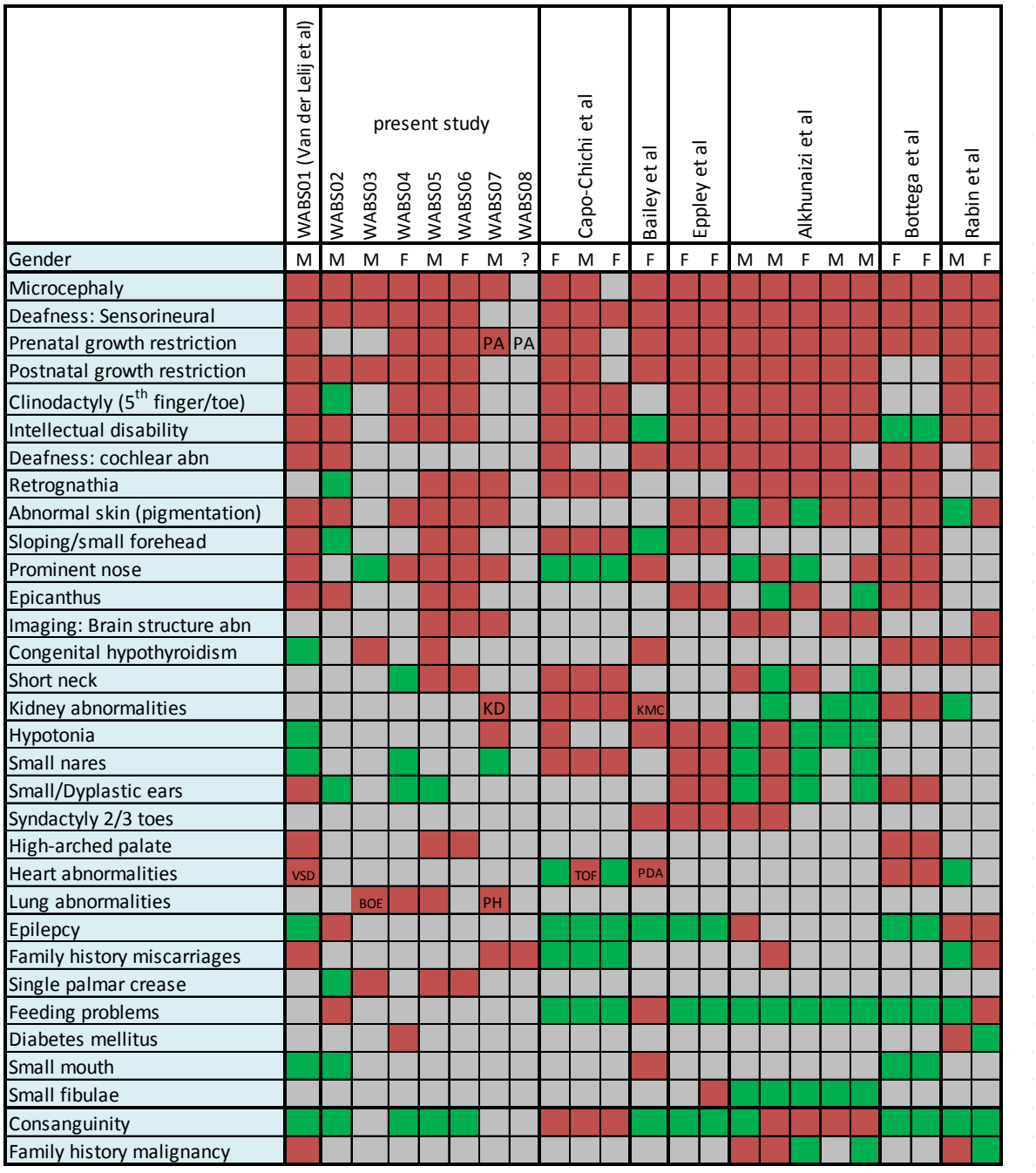

Table 1: Clinical features of known WABS patients. *A red color indicates that this condition was described for the particular patient; green indicates that the condition was not found; grey indicates unknown. PA: placenta abnormality. VSD: ventricular septal defect. TF: Tetraology of Fallot. PDA: patent ductus arteriosus. MK: Multicystic Kidney. KD: Kidney Dysplasia. BE: Broncho-obstructive episodes. PH: Pulmonary hypoplasia.*

Molecular characterization of newly identified WABS cases

Bi-allelic mutations in DDX11 were detected in these patients using whole exome sequencing and/or RNA sequencing, which we validated using Sanger sequencing of genomic DNA and cDNA (Figure 1A and Figure S1). For patient WABS03, only one correctly segregating missense mutation (p.R140Q) could be identified next to the indicated c.1403 duplication. However, we could not convincingly establish whether this is a pathogenic mutation (see below).

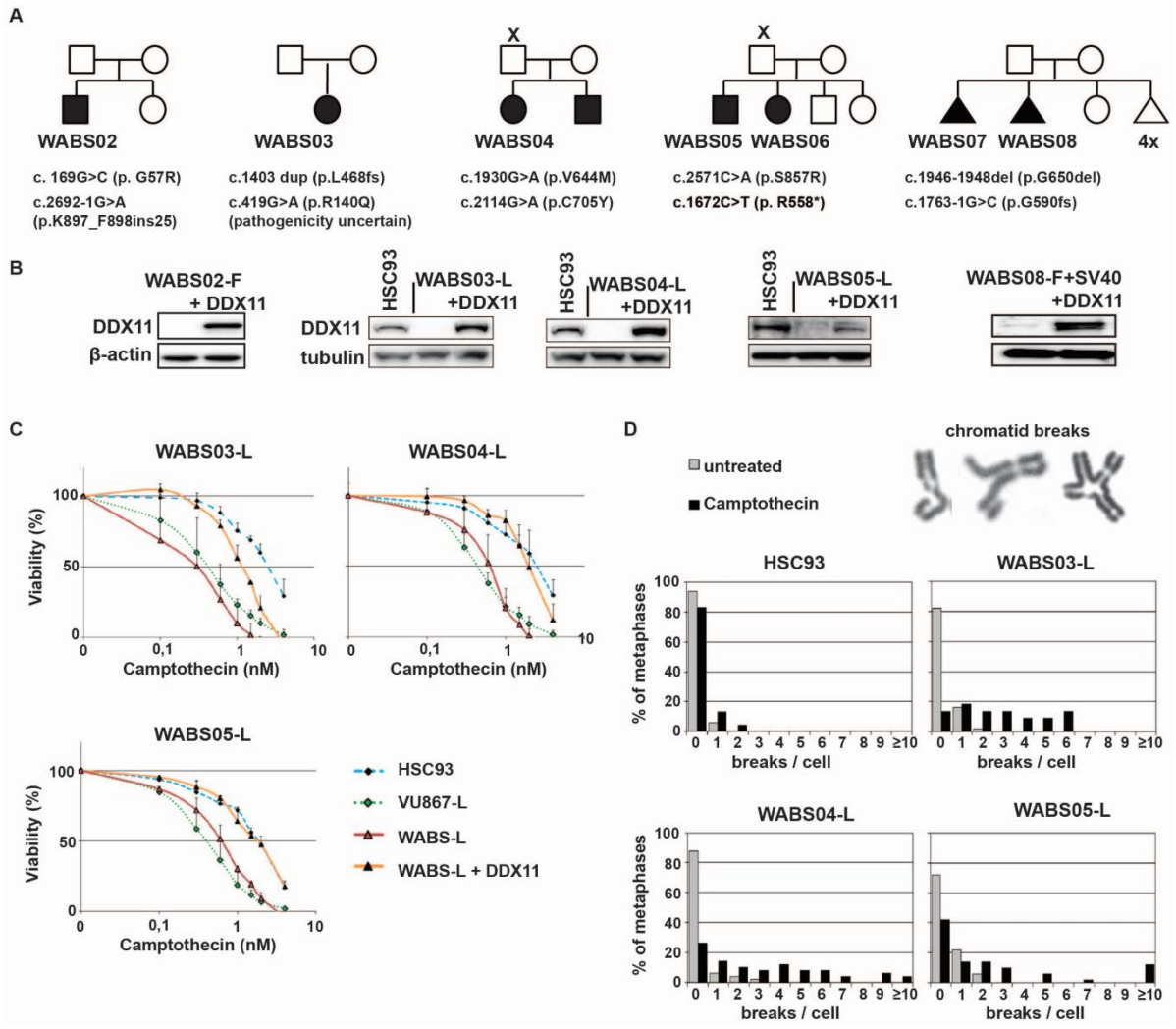

Figure 1: Identification of multiple new cases confirm that WABS is a DNA damage syndrome, causally linked to reduced DDX11 protein expression. *A, Pedigrees of seven new WABS patients. X indicates absence of paternal DNA; ? indicates uncertain whether patient has WABS; diamond indicates unknown sex; triangle indicates fetus. B, Western blots of patient-derived lymphoblasts (L) and fibroblasts (F). DDX11 protein levels were restored by stable transfection of DDX11 cDNA. C, Wildtype lymphoblasts HSC93, FANCM-deficient lymphoblasts VU867-L [165], three WABS-derived lymphoblasts and their complemented counterparts were continuously exposed to increasing Camptothecin concentrations. After three population doublings of untreated cells, cells were counted and plotted as percentage of untreated cells. Mean and standard deviations of three independent experiments are shown. D, metaphase spreads of cells treated as in C were assessed for chromosome breaks. Depicted examples of counted*

aberrations include a chromatid gap, a dislocated broken piece and a chromatid interchange figure ('triradial').

DDX11 sequencing is sometimes hampered by the pseudogene DDX12p, which shares 98% sequence similarity to DDX11, as well as by multiple sub-telomeric DDX11L sequences that are highly similar to the DDX11 C-terminus [46]. Since DDX12p is also transcribed into mRNA, in several occasions we had to clone and sequence multiple PCR fragments to confirm the mutations are really present in DDX11 (Figure S1A-E). Cells derived from five patients displayed reduced DDX11 protein levels (Figure 1B), as reported previously for other WABS patients. Moreover, patient cells showed increased Camptothecin (CPT) sensitivity in WABS lymphoblasts (Figure 1C), which correlated with the induction of chromosomal breaks (Figure 1D).

In addition to this characteristic breakage phenotype, we also observed spontaneous cohesion loss as previously described [1], which was aggravated by CPT treatment and corrected by stably expressing DDX11 cDNA (Figure 2A). Confirming an earlier report from our lab [47], WABS cell lines exhibited high sensitivity to PARP inhibition, comparable to FA cell lines and considerably more than Roberts Syndrome and Cornelia de Lange Syndrome cells (Figure 2B). In line, WABS01 fibroblasts exhibited increased cohesion loss, G2/M induction and cell death ('sub-G1') upon treatment with Talazoparib (Figure S2). DDX11 has a role in averting DNA damage in unperturbed cells as well, reflected by increased γH2AX foci in WABS cells as compared to corrected cells (Figure 2C). Since DDX11 is known to interact with a number of replication fork components, its primal activity seems to reside at the DNA replication fork. To assess whether DDX11 also affects replication fork speed directly, we performed a DNA fiber assay on WABS lymphoblasts. We found that DDX11 deficient cells show a consistently reduced fork speed as compared to DDX11 proficient cells (Figure 2D), in line with our previous observations in RPE1 cells (Chapter 5 of this thesis). In conclusion, WABS patient cells display CPT-induced chromosomal breaks, as well as spontaneous DNA damage signaling, DNA replication stress and cohesion loss.

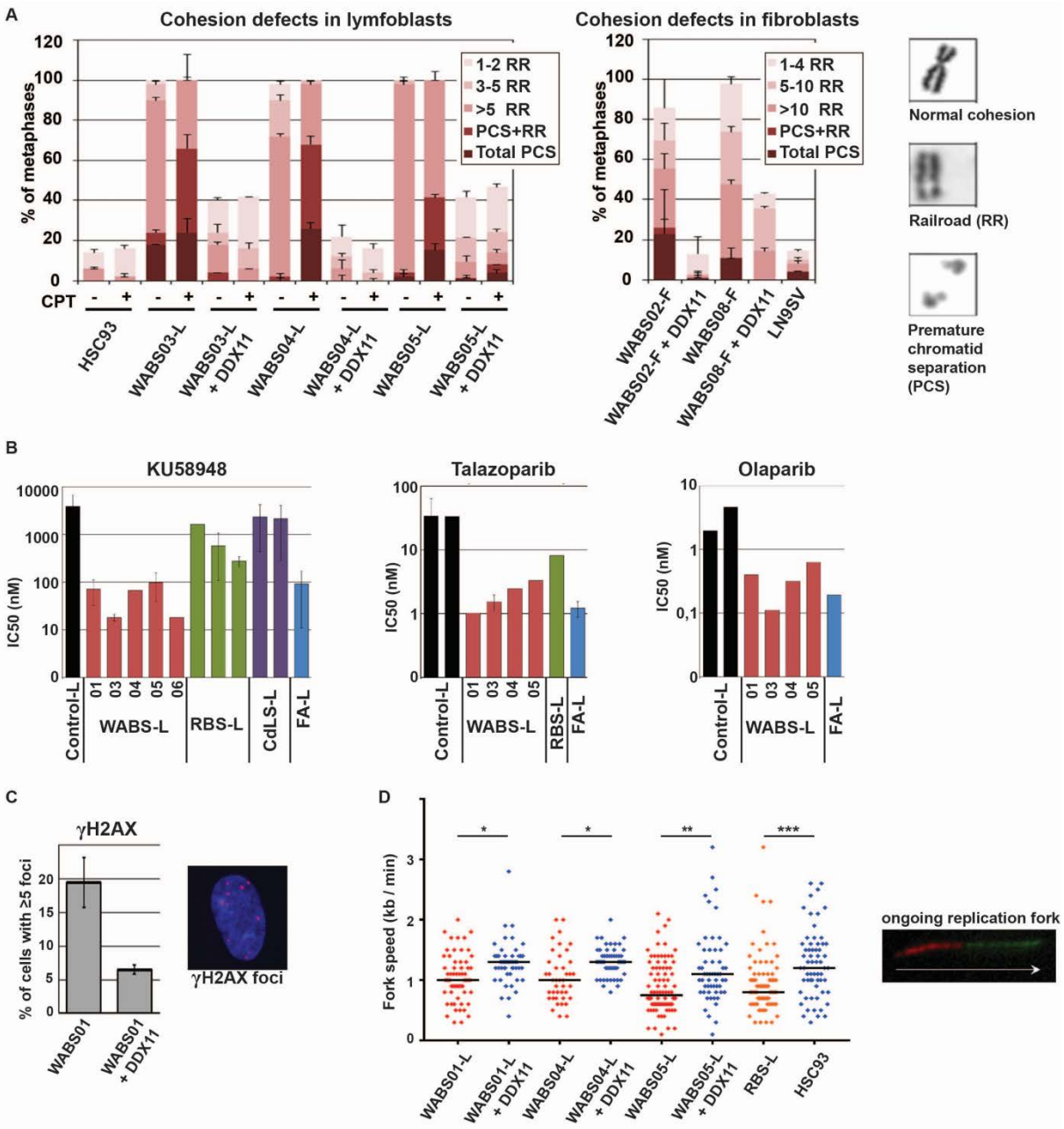

Figure 2: WABS cells display cohesion loss, PARP inhibitor sensitivity, DNA damage signaling and DNA replication stress. *A, Metaphase spreads of WABS cells were assessed for cohesion defects. Mean and standard deviations of three (lymphoblasts) or two (fibroblasts) independent experiments are shown. CPT = 2.5 nM Camptothecin treatment for 48h. Examples of a normal chromosome, a railroad chromosome (RR) and premature chromatid separation (PCS) are shown. B, Lymphoblasts from different patients were continuously exposed to increasing concentrations of PARP inhibitors KU58948, Talazoparib and Olaparib. After three population doublings of untreated cells, cells were counted and the amounts were determined as percentage of untreated cells. IC50 values from each dose-response curve were determined using curve fitting. Standard deviations were derived from multiple independent experiments. C, Immunofluorescence detection of γH2AX foci. Mean and standard deviation of three independent experiments are shown. D, Replication fork speed of WABS lymphoblasts was*

*assessed with a DNA fiber assay using a double labeling protocol. The example track represents an ongoing fork. Blue dots, DDX11 proficient; red dots, DDX11 deficient; orange dots, ESCO2 deficient RBS lymphoblasts (positive control). Black lines indicate the median. P-values were calculated by a non-parametric one-way ANOVA test. * p<0,05; ** p<0,01; *** p<0,001.*

DDX11 missense alleles reduce protein stability

Remarkably, all patients contain at least one DDX11 allele that potentially is only mildly defective (missense mutation or in frame insertion/deletion) and might yield a partially active protein. Indeed, we detected faint but specific DDX11 protein bands on Western blot (Figure 3A). Whereas DDX11 mRNA levels of the different WABS cells were all largely comparable to controls (Figure 3B), treatment with the proteasome inhibitor Marizomib partially restored DDX11 protein levels (Figure 3C), indicating that DDX11 protein stability is reduced in WABS cells.

To test whether this directly results from the identified missense mutations, we overexpressed cDNAs representing the newly identified weak DDX11 alleles in WABS01 fibroblasts (Figure 3D). In line with the observed unaffected mRNA levels in WABS cells, the mutant DDX11 cDNAs exhibited relatively normal mRNA stability, determined by quantifying the reduction of DDX11 mRNA upon Actinomycin-mediated transcription blockage (Figure S3A). We then treated these cells with Cycloheximide, which stabilizes mRNA and at the same time blocks translation, to assess protein stability. DDX11 mutants showed accelerated protein reduction, although the effect of R140Q was small (Figure 3E and Figure S3B). The R140Q variant, found in WABS03, has an allele frequency of 0,002 and is predicted to be damaging by some mutation significance prediction algorithms (*e.g.* Mutation Taster and PolyPhen-2) but not consistently. Blocking protein degradation by Marizomib or by the lysosome inhibitor Chloroquine revealed that the DDX11 mutants are more rapidly stabilized than wt-DDX11, while R140Q shows a small increase (Figure 3F and Figure S3C, D).

We used the same cells to evaluate DDX11 localization using immunofluorescence (Figure 3G). Whereas wt-DDX11 shows nuclear localization, several mutants (G57R, S857R and C705Y) also show substantial cytoplasmic localization. The R140Q mutant localized to the nucleus. While no other putative clinically relevant variants were identified in the cDNA sequence of this DDX11 allele, we conclude that the evidence for this variant to be disease causing is still incomplete.

Nevertheless, taken together these results suggest that WABS cells from different origins may contain residual DDX11 activity. To further test this, we measured the alterations in cohesion loss upon transfection of WABS cells with DDX11 siRNA (Figure 3H and Figure S4A). Although the extent of DDX11 knockdown was modest in some cases, the level of cohesion loss was consistently enhanced. In summary, multiple patient-derived DDX11 mutations cause destabilization and / or mislocalization of the DDX11 protein. DDX11 is still partially active in

the investigated WABS patients, possibly suggesting that complete loss of DDX11 is incompatible with survival, as found in mice [13,14].

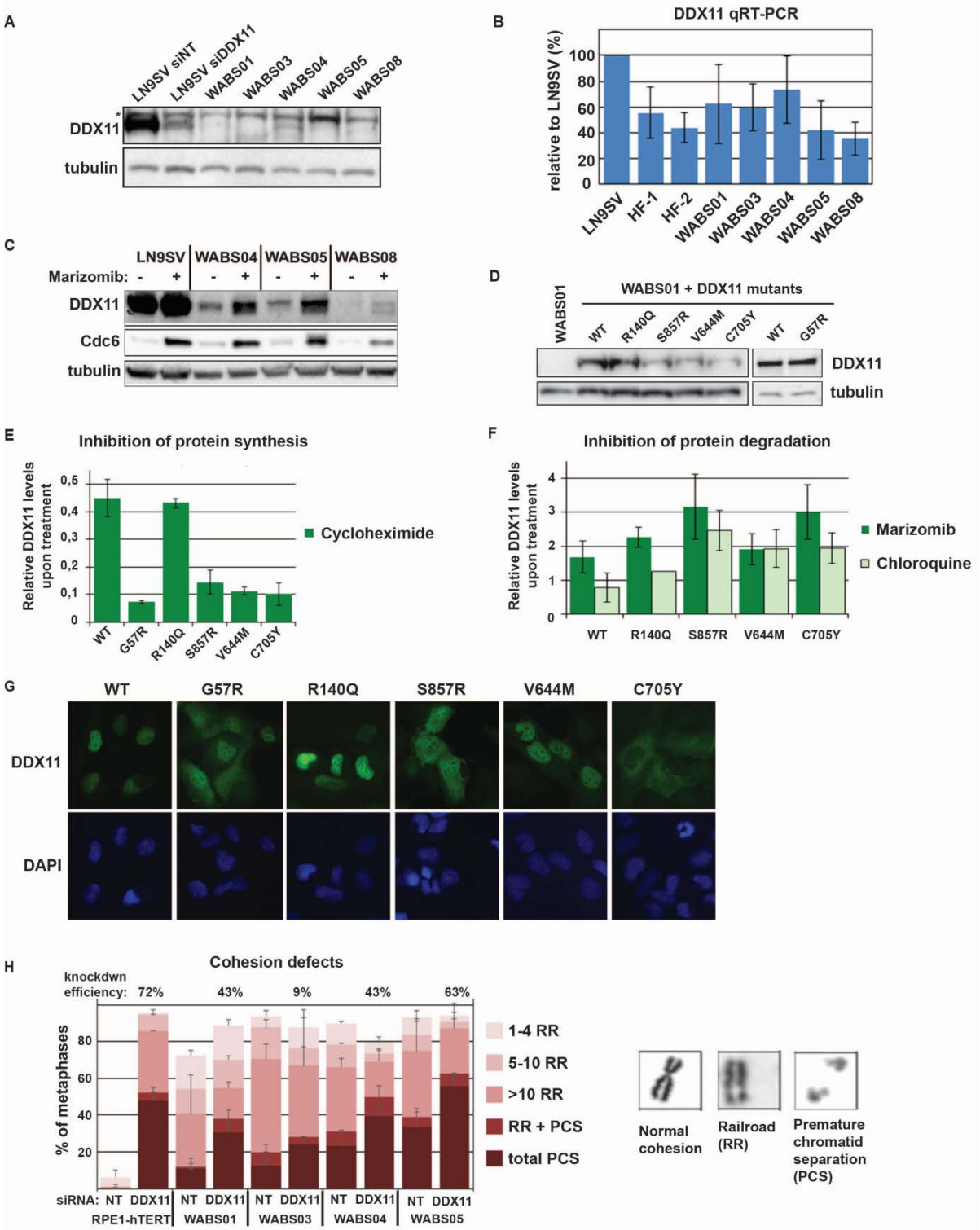

Figure 3: DDX11 missense alleles reduce protein stability. *A, WABS fibroblasts were analyzed for DDX11 protein levels by western blot. As control, LN9SV fibroblasts were transfected with non-targeting or DDX11 siRNA for two days. The asterisk indicates a non-specific band. B, RNA from WABS fibroblasts and three control fibroblasts were analyzed for DDX11 expression by qRT-PCR. Mean and standard deviations of five independent experiments are shown. C, WABS cells were*

treated with 500 nM Marizomib for 5h to inhibit proteasomal degradation and analyzed by Western blot. Cdc6 was included as a positive control. D, WABS01 cells were stably transfected with cDNAs encoding either WT-DDX11 or several patient-derived DDX11 mutants and DDX11 protein levels were analyzed by Western blot. E, Cells from D were treated with 62,5 µg/mL Cycloheximide for 3h to inhibit protein synthesis and analyzed by western blot. Bands were quantified using Image Lab software, normalized to tubulin and the decrease of DDX11 protein levels during the Cycloheximide treatment was determined for each mutant. F, Similarly, protein degradation was inhibited by treatment with Marizomib (500 nM, 5h) or with the lysosome inhibitor Chloroquine (25 µM, 24h). Increase of DDX11 protein levels during the treatment was determined for each mutant. Mean and standard deviations of at least three independent experiments are shown. Examples of western blots that were quantified in E and F are provided in Figure S3B-D. G, DDX11 expression and localization in WABS01 cells expressing different DDX11 versions were assessed by immunofluorescence. H, RPE1-hTERT cells and four WABS fibroblasts were transfected with indicated siRNAs (day 1 and day 4) and analyzed for cohesion defects seven days after the first transfection. Accompanying qRT-PCR (Supplemental Figure 3) was performed to determine knockdown efficiency, which is indicated as percentage in the figure. Mean and standard deviations of three independent experiments are shown. NT, non-targeting.

DDX11 knockout impairs proliferation and DNA damage response in a p53-dependent fashion

We then used CRISPR-Cas9 to construct DDX11 knockout RPE1 cells, using previously generated RPE1-TetOn-Cas9 and RPE1-TetOn-Cas9-TP53KO cells [48]. Analysis of multiple clones revealed only one clone (of eleven) with bi-allelic DDX11 inactivation in TP53-wt cells, whereas four out of eight clones in the TP53KO background contained a frameshift inducing indel in both alleles (Figure 4A). This difference could relate to p53-dependent effects on CRISPR efficiency [49,50], but since DDX11KO in wt TP53 cells caused elevated p53 protein levels (Figure 4B) and reduced growth rate (Figure 4C), it appears more likely that loss of DDX11 activates p53. In line with this hypothesis, we observed increased expression of the p53 target gene p21 both in siDDX11 or DDX11KO cells (Figure 4D), and, importantly, transfection with p53 siRNA accelerated the proliferation of DDX11KO cells (Figure 4C). In conclusion, DDX11 inactivation triggers a p53-dependent growth delay.

Similar to WABS cells, RPE1-DDX11KO cells showed increased sensitivity to Camptothecin, as well as to the DNA polymerase inhibitor Aphidicolin and the PARP inhibitor Talazoparib (Figure 4E). Moreover, analysis of 53BP1 foci and γH2AX foci revealed increased DNA damage signaling (Figure 4F). Finally, DDX11 deficient cells exhibited increased sensitivity to the Rad51 inhibitor BO-2 (Figure 4G), suggesting that DDX11 deficient cells are hyper-dependent on continuous DNA damage repair via a Rad51-dependent pathway.

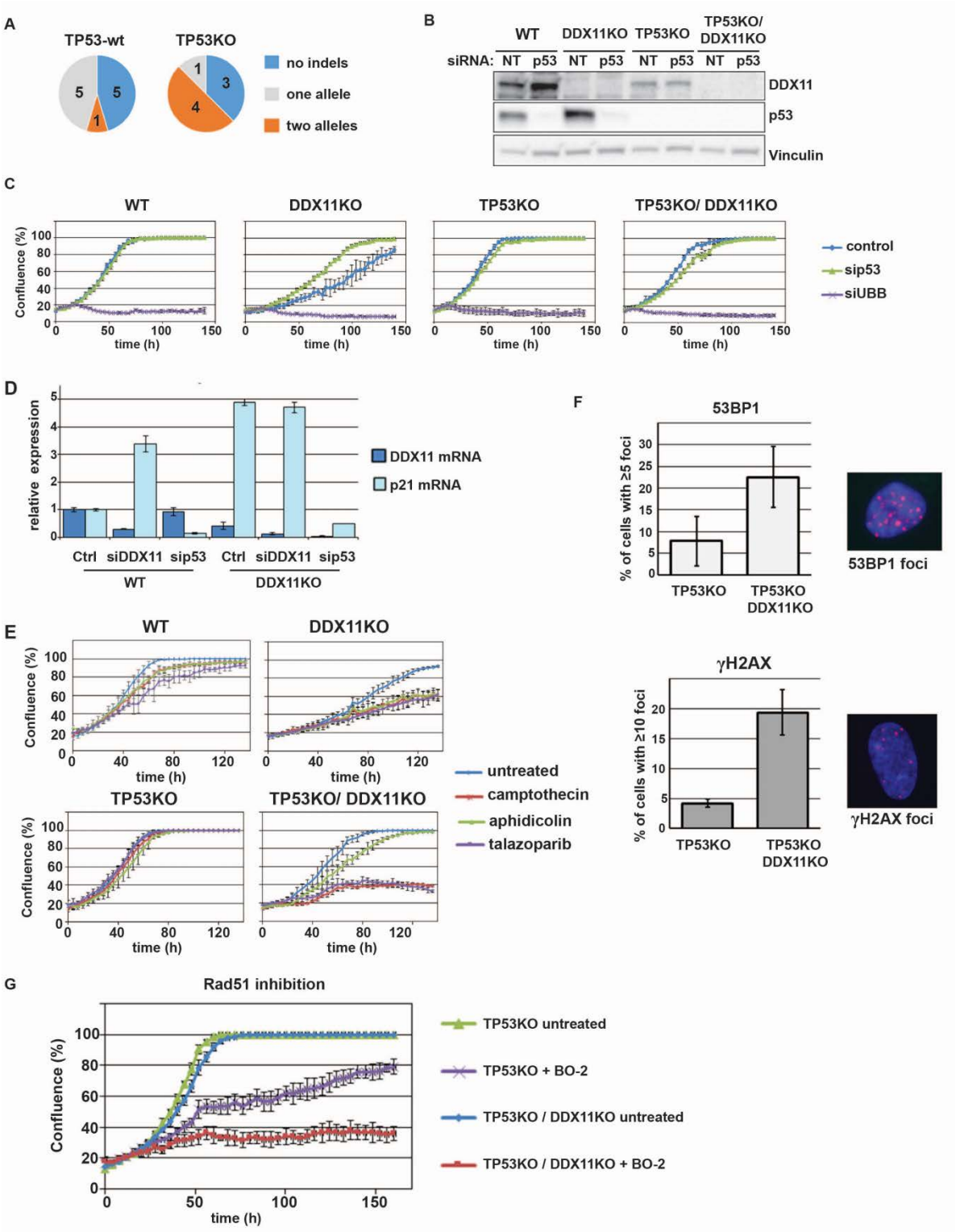

Figure 4: DDX11 knockout impairs proliferation and DNA damage response in a p53-dependent fashion. *A, RPE1-hTERT cells and RPE1-hTERT-TP53KO cells, both containing a doxycycline inducible Cas9 construct, were transfected with DDX11 guide RNA and indels were analyzed using Sanger sequencing. More detailed information on guide RNA design and validation of clones is provided in Figure S5. B, Cells were transfected with indicated siRNA's, lysed after two days and analyzed by western blot. Note that DDX11KO cells have elevated p53 levels. C, In parallel with B, cells were transfected with siRNA and proliferation was monitored using*

IncuCyte software. UBB siRNA was used to control transfection efficiency. A representative of two independent experiments is shown, with mean and standard deviations of three replicates. Note that sip53 specifically accelerates growth of wtTP53-DDX11KO cells. D, RPE1-hTERT and RPE1-hTERT-DDX11KO cells were transfected with indicated siRNAs. After two days, mRNA levels were assessed with qRT-PCR. Mean and standard deviations of three technical replicates are shown. E, Cells were treated with 10 nM Camptothecin, 200 nM Aphidicolin or 200 nM Talazoparib and growth was monitored using IncuCyte software. Mean and standard deviations of three technical replicates are shown. F, Immunofluorescence detection of 53BP1 foci (left) and γH2AX foci right). Mean and standard deviation of three independent experiments are shown. G, RPE1-hTERT cells were cultured in a 96-wells plate in the presence or absence of the Rad51 inhibitor BO-2 (10μM). Growth was monitored using IncuCyte software. Mean and standard deviations of three technical replicates are shown.

No evidence for a redundant role of the pseudogene DDX12p in sister chromatid cohesion and proliferation

Considering high sequence similarities, we aimed to investigate whether the pseudogene DDX12p, which is absent in mice, could partially compensate for loss of DDX11. We designed qRT-PCR primers that specifically amplify DDX11 or DDX12p, utilizing a small difference in the sequences of exon 17 of DDX11 and DDX12p, respectively (Figure S4B). This revealed that the DDX11 siRNA we have used also depletes DDX12p mRNA (Figure 5A). Remarkably, WABS cells express DDX12p mRNA at comparable levels as control cells (Figure 5B). We decided to construct specific DDX11 or DDX12p knockout cells, using guide RNA (gRNA) target sites close to a large intronic region that is present in DDX11, but not in DDX12p (Figure 5C). This enables specific amplification of both DDX11 and DDX12p genomic DNA by using specific forward primers, either inside (DDX11, blue arrow) or spanning this region (DDX12p, red arrow). The sequence targeted by gRNA 1 (also used to construct the cell lines in Figure 4) is present in both DDX11 and DDX12p, whereas gRNA 2 is specific for DDX11. Since RPE1 cells do not contain a PAM site adjacent to the gRNA 2 sequence in DDX12p, we had to choose a different location to specifically target DDX12p (gRNA 3), which targets both DDX12p alleles and one DDX11 allele in RPE1 cells (harbouring a SNP in the second DDX11 allele). We generated a panel of six cell lines (two clones for each gRNA) that is described in detail in Figure S5. Importantly, we found that loss of DDX11, but not DDX12p, increases the cellular doubling time (Figure 5D) and induces cohesion loss (Figure 5E) in RPE1 cells. To determine the full DDX12p mRNA sequence, we cloned and sequenced multiple PCR fragments (Figure S6A) and also performed a 3'RACE PCR (Figure S6B). This revealed that an intact start codon, all exons and a poly-A tail can be found in DDX12p transcripts, although some exon-skipping isoforms were also detected. This suggests that an intact DDX12p ORF might exist. However, we also found a 5 bp deletion in exon 8 that would lead to a truncated protein of only 300 amino acids (Figure S6A). In conclusion, we found no evidence that DDX12p encodes a protein that could functionally compensate for DDX11 loss.

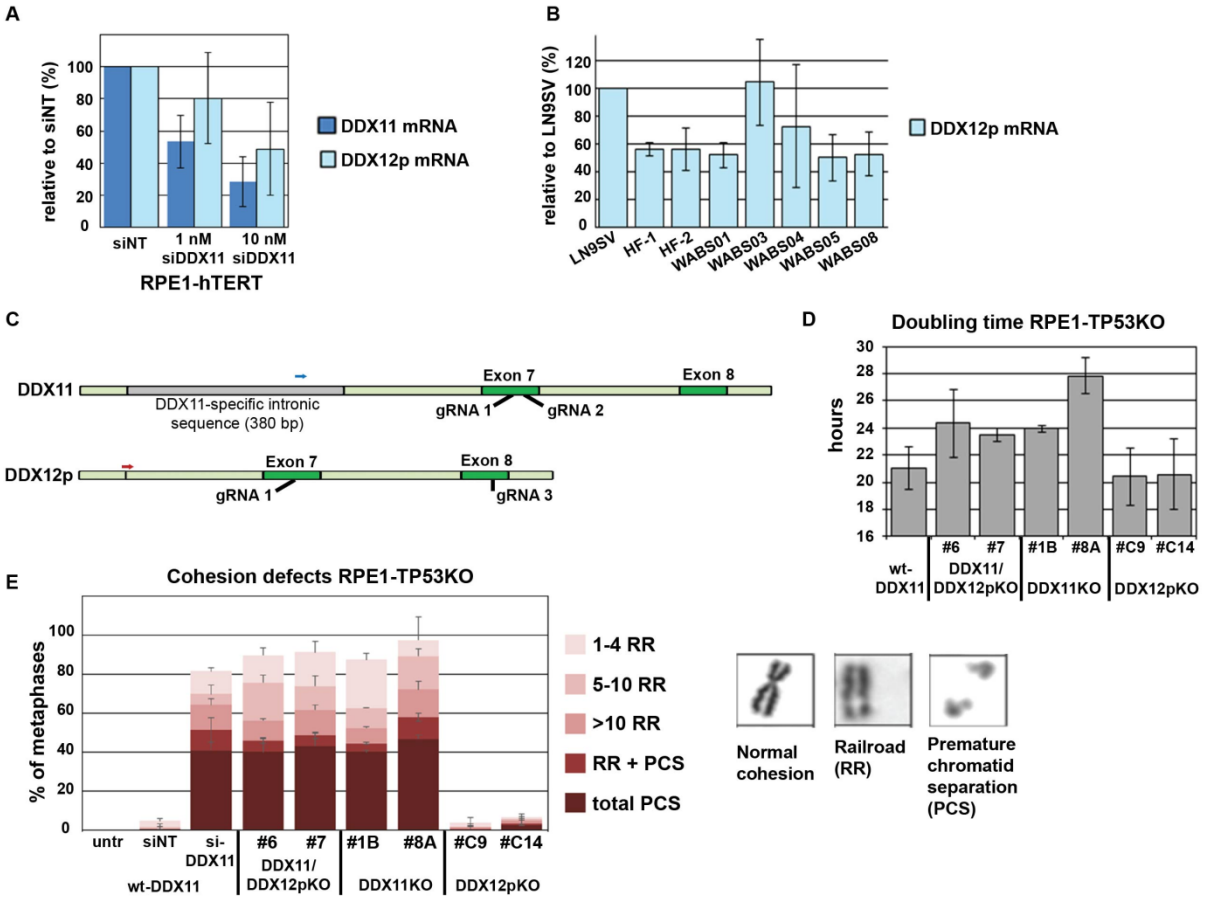

Figure 5: No evidence for a redundant role of the pseudogene DDX12p in sister chromatid cohesion and proliferation. *A, RPE1-hTERT cells were transfected with siRNA to DDX11 (1 nM or 10 nM) and analyzed for DDX11 and DDX12p mRNA levels using specific qRT-PCR. The specificity of qRT-PCR primers was validated in Figure S5. B, DDX12p mRNA levels were assessed in three SV40 transformed control fibroblasts and five WABS fibroblasts. C, CRISPR design for constructing DDX11 and DDX12p knockouts in RPE1-hTERT-TP53KO cells. For more detailed information and validation of clones, see Figure S5. D, A panel of RPE1-hTERT-TP53KO cells containing specific DDX11 and/or DDX12p knockout was seeded in 96-wells plates and growth rate was analyzed using IncuCyte software. The resulting growth curves were used to calculate doubling times. Mean and standard deviations of two independent experiments are shown. E, The same panel was analyzed for cohesion defects. As control, RPE1-hTERT-TP53KO cells were transfected with siDDX11 for two days. Mean and standard deviations of two independent experiments are shown.*

G-quadruplex stabilization is not tolerated by DDX11 deficient cells

Anti-parallel G-quadruplex (G4) structures, four-stranded structures formed by guanine-rich nucleic acids, were previously reported to be a particular DDX11 substrate *in vitro* [20]. Therefore, we tested two G4-stabilizing compounds, Quarfloxin and CX5461 [51], for their effect on RPE1-DDX11KO cells. G4 stabilization caused particular growth inhibition in RPE1-DDX11KO cells

(Figure 6A), accumulation of chromosomal breaks (Figure 6B) and increased DNA damage signaling, as indicated by 53BP1 foci (Figure 6C). Moreover, we detected considerable cohesion loss in RPE1 cells upon G4 stabilization (Figure 6D). These findings indicate that the excess of unresolved DDX11 substrates in itself forms a source of cohesion loss and DNA damage.

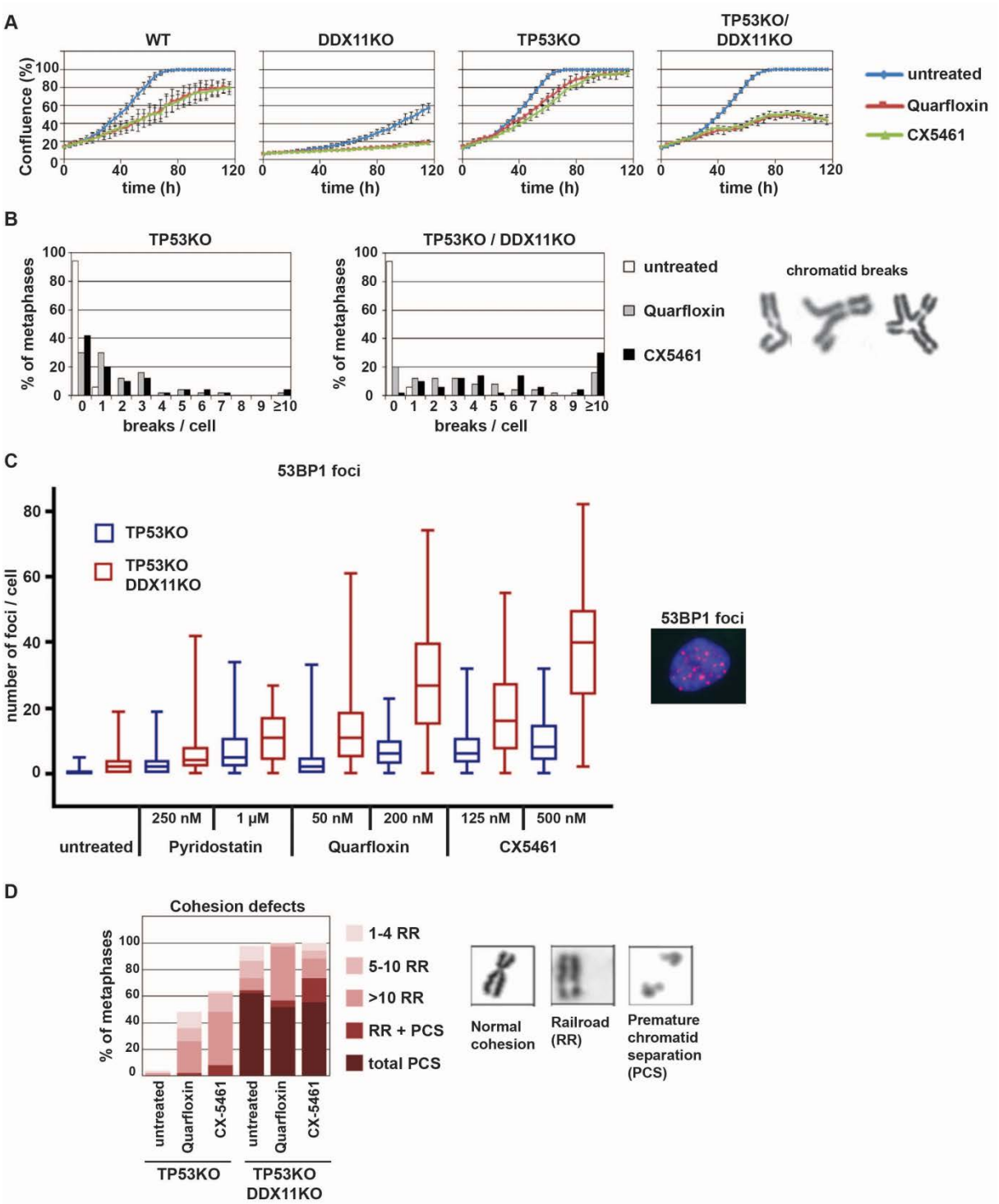

Figure 6: G-quadruplex stabilization is not tolerated by DDX11 deficient RPE1 cells.*A, Cells were cultured in 96-wells plates and treated with 200 nM Quarfloxin or 500 nM CX5461. Growth was monitored using IncuCyte software. Mean and standard deviations of three technical replicates are shown. B, Cells were treated with 200 nM Quarfloxin or 500 nM CX5461 for 24h and*

chromosomal breaks were scored in metaphase spreads. C, Cells were treated as indicated and 53BP1 staining was analyzed by immunofluorescence. The number of foci was counted in 50 cells per condition. D, Cells were treated with 200 nM Quarfloxin or 500 nM CX5461 for 24h and cohesion defects were analyzed.

In line with the observations in RPE1 cells, G4 stabilization showed particular toxicity in WABS lymphoblasts (Figure 7A) and fibroblasts (Figure S7A). In addition, treatment with G4 stabilizers resulted in the accumulation of chromosomal breaks (Figure 7B) and aggravated cohesion loss (Figure 7C). In contrast to RPE1 cells with wt-DDX11, WABS01+wtDDX11 cells did not show cohesion loss upon G4 stabilization, suggesting that overexpression of DDX11 increases cellular resistance to these compounds. Since both Quarfloxin and CX5461 were shown to inhibit ribosomal DNA (rDNA) transcription [52,53], we then asked whether this contributes to the observed toxicity to WABS cells. To this end, we assessed the effect of the rDNA binding agent Bmh21, which causes blockage of RNA polymerase I and degradation of its catalytic subunit [54,55]. At concentrations that block rDNA transcription (Figure S7B), WABS01 cells were not sensitive to Bmh21 (Figure S7C), so we conclude that the sensitivity of DDX11 deficient cells to Quarfloxin and CX5461 primarily relates to G4 stabilization. Interestingly, when we compared fibroblasts from WABS patients to fibroblasts from Fanconi Anemia patients defective for the related DNA helicase FANCJ, we found that WABS cells are most sensitive to Quarfloxin, whereas FANCJ cells show the highest sensitivity to MMC (Figure 7D). This suggests that DDX11 is the dominant DNA helicase to resolve Quarfloxin-stabilized structures. FANCJ helicase also possesses some activity towards these substrates, as indicated by a partial resistance induced by FANCJ overexpression.

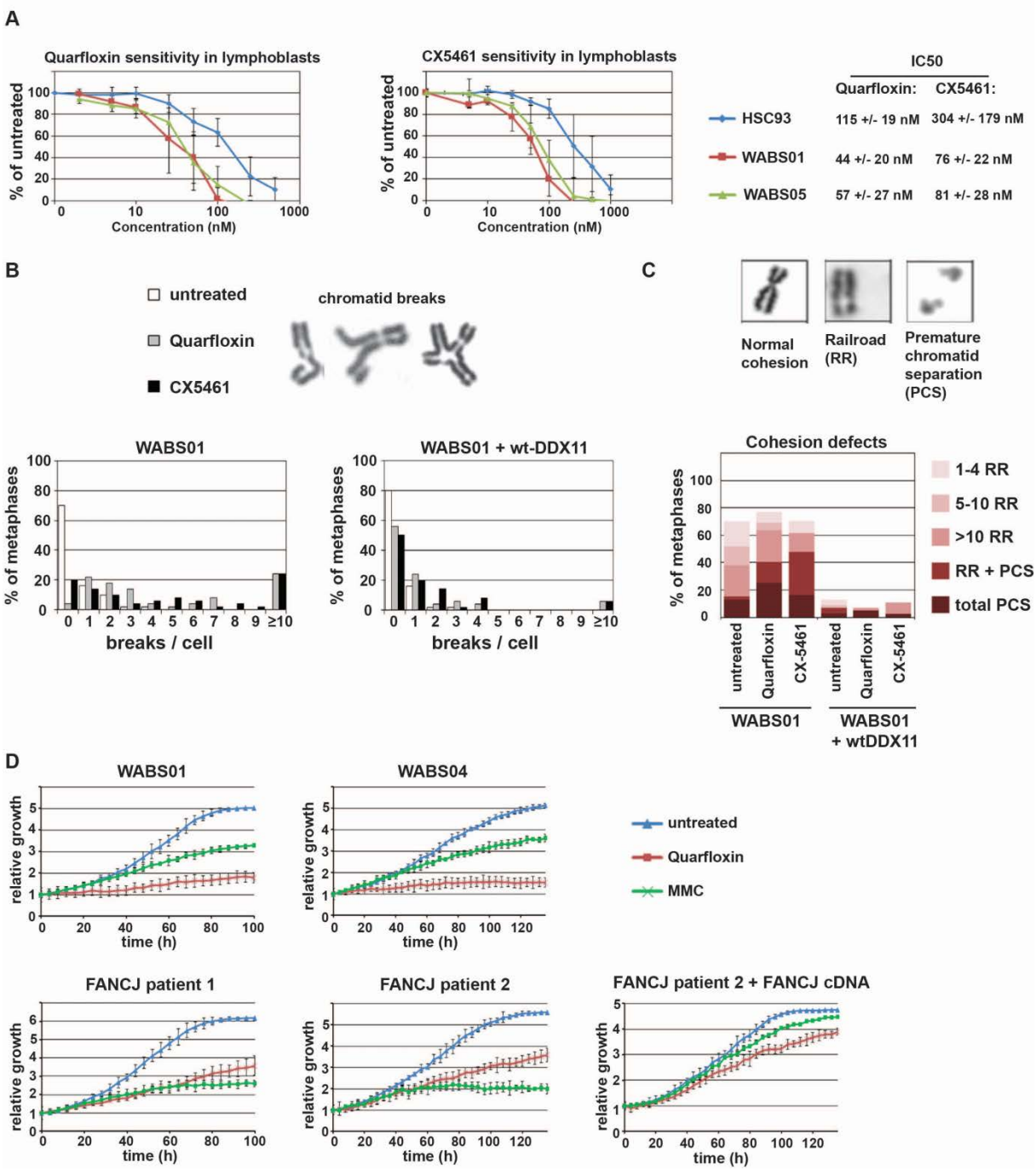

Figure 7: G-quadruplex stabilization is not tolerated by WABS cells.*A, WABS01, WABS05 and HSC93 control lymphoblasts were continuously exposed to increasing concentrations Quarfloxin or CX5461. After three population doublings of untreated cells, cells were counted and plotted as percentage of untreated cells. Mean and standard deviations of at least three independent experiments are shown. IC50 values from each dose-response curve were determined using curve fitting and shown as averages +/- standard deviations at the right. B, WABS fibroblasts were treated with 200 nM Quarfloxin or 500 nM CX5461 for 24h and chromosomal breaks were scored in metaphase spreads. C, WABS fibroblasts were treated with 200 nM Quarfloxin or 500 nM CX5461 for 24h and cohesion defects were analyzed. D, Fibroblasts derived from WABS patients and FANCJ patients were cultured in 96-wells plates and treated with 10 nM MMC or*

100 nM Quarfloxin nM CX5461. Growth was monitored using IncuCyte software. Mean and standard deviations of four technical replicates are shown.

DDX11 helicase activity is required for sister chromatid cohesion

To further investigate the role of DDX11 helicase activity in sister chromatid cohesion, we introduced DDX11-K50R, a previously described helicase-dead mutant [56], into TP53KO-DDX11KO RPE1 cells (Figure 8A). Whereas wt-DDX11 overexpression rescued the cohesion loss in DDX11KO cells, the K50R mutant had no effect (Figure 8B). Furthermore, DDX11-K50R could not restore DNA replication fork speed (Figure 8C). These findings are in line with our previous findings using K50R correction in WABS01 fibroblasts (Chapter 5 of this thesis). The observation that WABS cells possess some residual DDX11 activity predicts that the patient-derived DDX11 missense mutants are still functional when overexpressed. Indeed, we found that three patient-derived missense mutants could (at least partially) correct the cohesion loss in WABS01 cells: R140Q, V644M and S857R (Figure 8D). Two others, G57R and C705Y, showed no activity. The C705Y mutant originates from WABS04, so it appears that the residual DDX11 activity in this patient results from the V644M allele. The second allele in patient WABS02, in which the G57R allele was also found, contains a splice-site mutation that results in retention of intron 26 and an in-frame insertion of 25 amino acids at DDX11 C-terminus, which may yield a functional DDX11 protein. We noticed that G57R is located close to the Walker A helicase motif I, whereas C705Y is located in helicase motif V (Figure S8A). Both regions are highly conserved between different DDX11 orthologues and, to a lesser extent, between other FeS-domain containing SF2 helicases. This suggests that DNA helicase activity is also impaired in these mutants. Indeed, purified DDX11-C705Y protein showed impaired *in vitro* helicase activity (Figure S8B). Moreover, the Quarfloxin sensitivity of WABS01 fibroblasts could be rescued by most patient-derived missense mutants, but not by helicase-dead mutants (Figure 8E). We conclude that DDX11 depends on its helicase function to facilitate normal DNA replication and prevent DNA damage and cohesion loss, presumably by resolving G4 structures that arise when replication forks travel through G-rich regions.

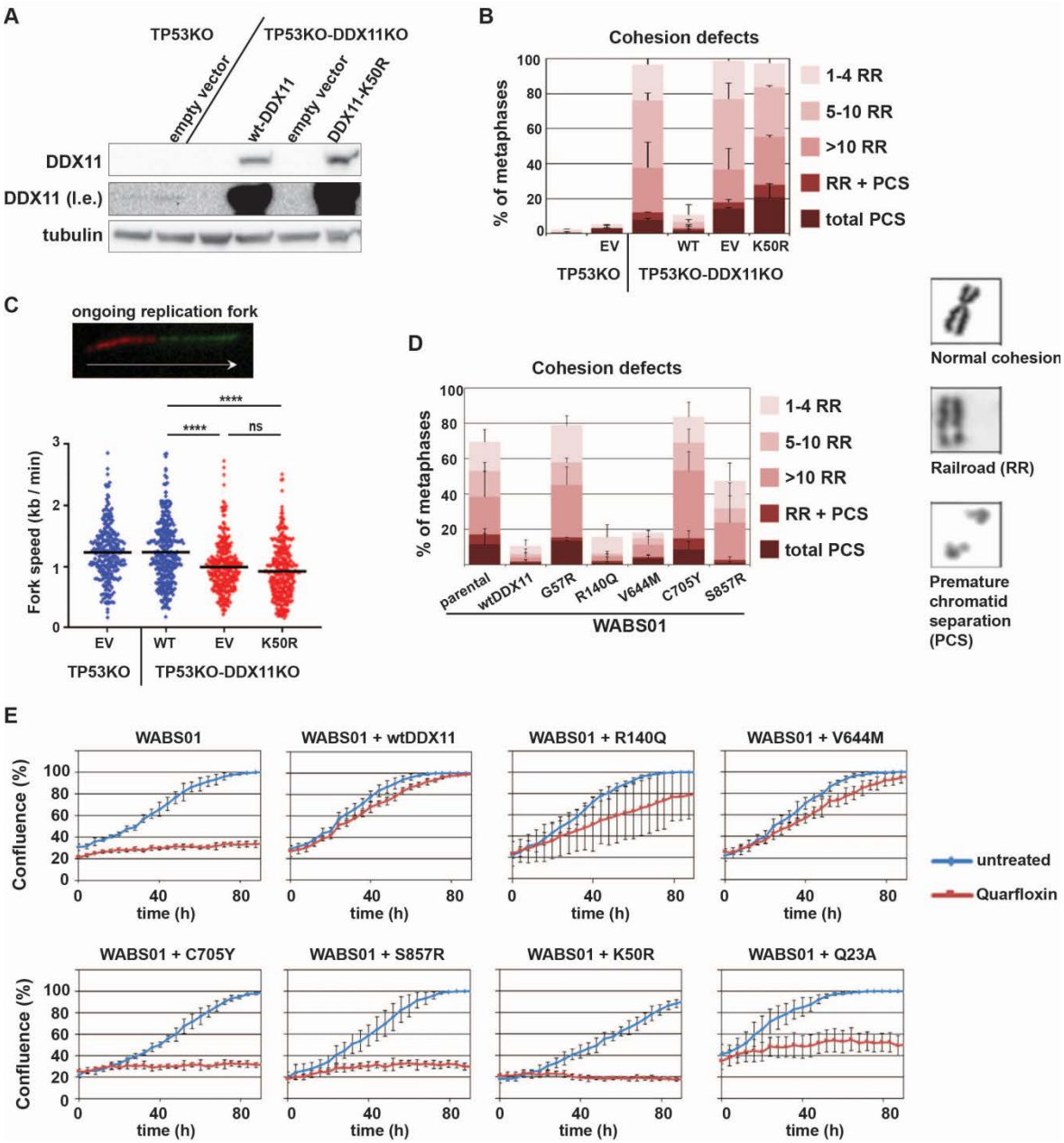

Figure 8: DDX11 helicase activity is required for G4 stabilizer resistance and sister chromatid cohesion in WABS. *A, WABS01 cells were stably transduced with empty vector (EV), wtDDX11 or DDX11-K50R and analyzed by western blot. l.e. long exposure. B, Cells were analyzed for cohesion defects. Mean and standard deviations of two independent experiments are shown. C, Replication fork speed was assessed with a DNA fiber assay using a double labeling protocol. The example track represents an ongoing fork. Blue dots, DDX11 proficient; red dots, DDX11 deficient. Black lines indicate the mean. P-values were calculated by a non-parametric one-way ANOVA test. **** p<0,0001. D, WABS01 cells, stably transfected with different DDX11 mutants, were analyzed for cohesion defects. Mean and standard deviations of at least three independent experiments are shown.*

Discussion

We show here that WABS cells possess residual DDX11 activity and find that several patient-derived DDX11 mutants encode a functional but unstable protein. Although most published DDX11 mutants were not functionally studied, all published WABS patients appear to harbor at least one pathogenic mutation that could potentially yield a protein product with partial activity. Indeed, DDX11-R378P has reduced protein stability [2], whereas DDX11-R263Q, although located in the FeS cluster and displaying reduced helicase activity, could still unwind a forked duplex structure at higher concentrations [4]. These observations, combined with the embryonic lethality of DDX11 knockout mice [13,14], the lack of functional redundancy of the pseudogene DDX12p and the fact that DDX11 knockout causes severe, p53-dependent growth inhibition in human RPE1 cells, indicate that DDX11 is essential for human development. Notably, caution is needed when pinpointing disease-causing DDX11 mutations, particularly when prenatal testing for WABS is intended. Mutations with a mild effect on protein function are common in WABS patients, but it may be difficult to distinguish these from rare, non-pathogenic DDX11 variants. For example, DDX11-R140Q could rescue sister chromatid cohesion in WABS01 cells. It showed reduced protein stability in some experiments, but this effect was mild . Thus, while patient WABS03 is undoubtedly a WABS patient and we found no other mutation in the relevant DDX11 allele that correctly segregated, we have insufficient evidence to prove that R140Q is pathogenic.

With the seven cases of this study, a total of 23 WABS cases have now been described. Whereas WABS clinically resembles Fanconi Anemia, the anemia phenotype is lacking. The clinical spectrum is heterogeneous and shows considerable overlap with the cohesinopathies Roberts Syndrome (RBS) and Cornelia de Lange Syndrome (CdLS), with the most notable exceptions being limb reductions, which are not found in WABS, and abnormal skin pigmentation, which is not found in RBS and CdLS [1-7]. WABS is classified as a cohesinopathy, because of the spontaneous railroad chromosomes and PCS that are observed in metaphase spreads. This characteristic is also found in RBS, but not in CdLS, which may be explained by the milder impact of CdLS mutations on cohesin functions. In yeast, the different processes that are regulated by cohesin were shown to be differentially affected by modulating cohesin levels [57]. It has been proposed that the clinical overlap between RBS and CdLS can be attributed to overlapping effects on gene transcription, whereas the observed differences might relate to additional effects on sister chromatid cohesion and DNA repair in RBS [58]. Although most cohesinopathy cells display some level of increased genotoxic sensitivity, the MMC-induced breakage phenotype is particularly pronounced in WABS cells, which is found in most (except one [2]) published cases, as well as in the three WABS cases in which chromosomal breakage was investigated in this study. Moreover, drug toxicity patterns, in particular the sensitivity to PARP inhibitors, indicate either impaired homologous recombination in WABS cells, or pinpoint to increased sensitivity to DNA replication stress [59]. We find that also in the absence of drugs, DDX11 deficiency leads to DNA damage. In line with this observation, the clinical phenotype of

WABS overlaps with chromosomal instability syndromes such as FA[60] and NBS [61]. Thus, WABS can be classified as both a cohesinopathy and a breakage syndrome.

Stabilization of G4 structures by Quarfloxin and CX5461 strongly induces DNA damage signaling and chromosomal breakage in DDX11 deficient cells. The sensitivity of WABS cells to Quarfloxin even exceeds that of FANCJ deficient cells. This observation was somewhat unexpected, considering reports that the G4 stabilizer Telomestatin (TMS) strongly affects FANCJ deficient cells [62], whereas DNA damage inflicted by TMS is hardly affected by DDX11 [63]. However, different G4 interacting compounds appear to selectively bind different types of G-quadruplexes, as discussed in [64]. For example, TMS stabilizes the formation of a telomeric G4 structure, thereby inhibiting telomerase [65], whereas Quarfloxin selectively targets a G4 structure that is commonly found in ribosomal DNA and in promoter sequences [53]. Quarfloxin accumulates in the nucleolus and disrupts the binding of G4 structures and Nucleolin, thereby inhibiting ribosome biogenesis. A nucleolar localization has also been reported for DDX11 [66], suggesting that DDX11 has specialized in unwinding different substrates than FANCJ.

Besides their role in promoting sister chromatid cohesion in unperturbed conditions, yeast Chl1 and human DDX11 are also involved in the response to damage related to DNA replication stress [12,15,23,67,68]. A separation of these two functions was suggested for yeast Chl1, based on the observation that the DNA helicase activity of Chl1 was only required for replication fork progression and the response to fork stalling, whereas its role in sister chromatid cohesion was suggested to be helicase-independent and rather relies on interaction with CTF4 [34]. It remains to be tested whether human DDX11 also interacts with the human CTF4 orthologue AND-1, and if yes, what would be the functional consequence of this. Importantly, we find that the helicase function of human DDX11 is not only required for the response to G4 stabilizing drugs, but also for sister chromatid cohesion, in line with our previous findings (Chapter 5 of this thesis) and observations in chicken DT40 cells [69]. Besides the previously characterized helicase-deficient mutant K50R [56], also two patient-derived mutations in or near conserved helicase motifs (G57R and C705Y) impaired the rescue of cohesion defects in DDX11 deficient cells. Of note, a G57R mutant mouse was embryonic lethal (unpublished data by the group of Hein te Riele, Division of Tumor Biology and Immunology, NKI-AVL, Amsterdam), further indicating that this is a *null* allele and DDX11 helicase function is crucial for development. The requirement for the DDX11 helicase function for sister chromatid cohesion may suggest that its roles in different processes cannot be separated.

How, then, would DDX11 promote sister chromatid cohesion? Based on its interaction with Fen1, it was suggested that Chl1 allows efficient maturation of Okazaki fragments and the subsequent loading of cohesin [70-72]. An alternative model proposes that Chl1 might help cohesin rings that already bind double-stranded DNA to capture a second ssDNA molecule [73]. This process depends on the Scc2-Scc4 cohesin loader, and the role of Chl1 may relate to its role in Scc2 deposition during S-phase [74]. Based on the helicase dependency in our experiments, we infer that DDX11 primarily functions to resolve complex secondary structures in the lagging strand, which favors formation of ssDNA that facilitates second strand capture by cohesin.

Possibly, the binding of DDX11 to several replisome components facilitates the correct positioning of DDX11 to unwind its substrates. Since experiments in yeast revealed that RPA binding hindered entry of the second strand into cohesin rings [73], a possible hypothesis could be that the formation of G4 structures in the lagging strand prevents both premature DNA synthesis and RPA coating of ssDNA. Upon resolution of G-quadruplexes by DDX11, these sites would provide an ideal 'landing platform' for cohesin loading. In the absence of DDX11, unresolved G4 structures are prone to breakage, leading to reduced fork speed and inefficient cohesin loading. However, experiments in human cells reported that RPA promotes cohesin loading and cohesion establishment [75]. Considering the well-known role of RPA in DNA damage checkpoint signaling, it will be interesting to study the interplay between DDX11 and RPA in normal and replication stress conditions.

Acknowledgements

We thank Henri van de Vrugt for the RPE1-hTERT_TetOn-Cas9 cells and for many helpful comments on the manuscript, Mark Grannetia and Pascal Walther for constructing and validating DDX11 knockout cells, Govind Pai for his help with DNA fiber assays, Laura McFarlene-Majeed for the Western blot of WABS02 cells, Stefanie Henriet for follow-up counseling of patient WABS02, Hein te Riele, Haico van Attikum and Quinten Waisfisz for insightful discussions, and all our colleagues for valuable feedback and support. This work was supported by the Cancer Center Amsterdam (grant CCA2015-5-25), the Dutch Cancer Society (KWF grant 10701/2016-2, a young investigator grant to JdL) and by the Netherlands Organisation for Scientific research (NWO TOP-GO grant 854.10.013). We dedicate this work to the memory of Johan de Winter, who initiated the studies of Warsaw Breakage Syndrome in our lab.

Author contributions

A.F., J.v.S., J.B., A.O., M.R., M.G., P.W., N.A., F.P. and J.d.L carried out the experiments, which were supervised by R.W. and J.d.L. J.P., G.S., C.D.A.E, K.D, I.B and K.D. providedpatient samples and clinical data. The manuscript was prepared by A.F. and J.d.L. and edited by J.v.S. and R.W.

The authors declare no competing financial interests.

Supplemental information

Figure S1

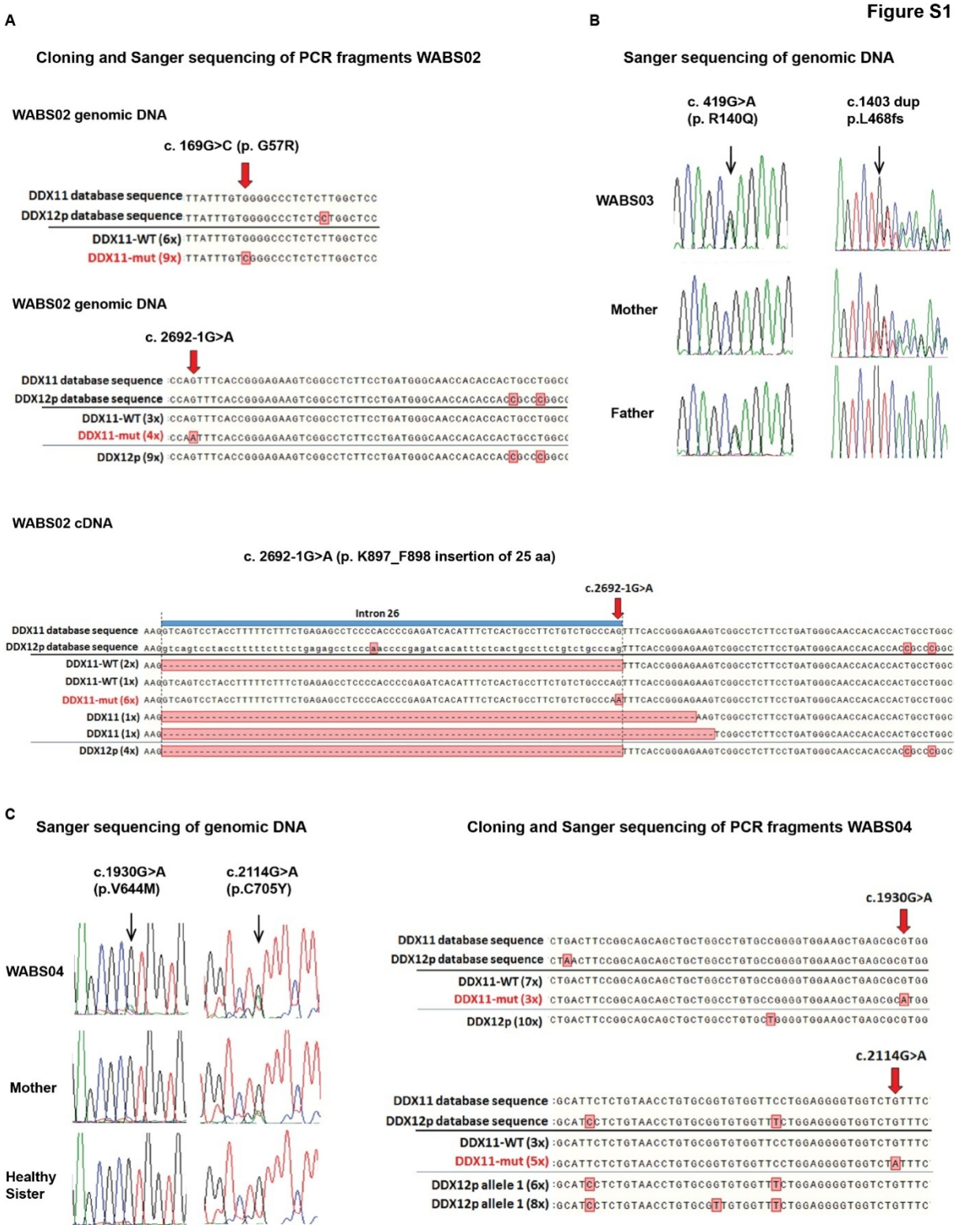

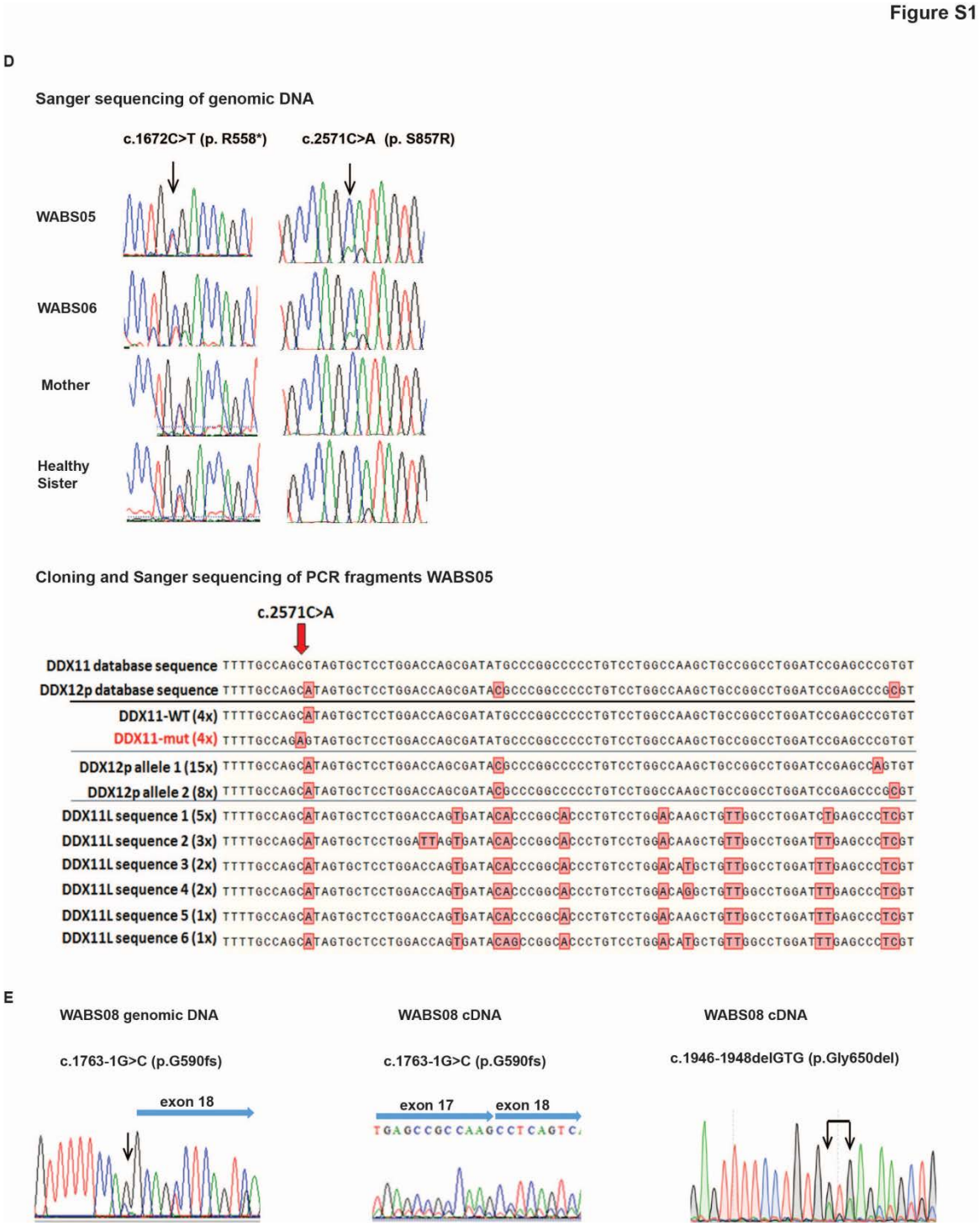

Figure S1: Confirmation of pathogenic DDX11 mutations in WABS patients. *A, Confirmation ofDDX11 mutations in WABS02. PCR fragments, amplified from genomic DNA, were ligated into a zero-blunt plasmid, transformed into competent bacteria and DNA from single colonies was sequenced. Sequences were aligned to database DDX11 and DDX12p. One allele contains a c.169G>C missense mutation that leads to a p.G57R substitution, while the other allele contains a point mutation affecting the last base of intron 26 (c.2692-1G>A), resulting in retention of intron 26 and an in-frame insertion of 25 amino acids at the C-terminus of DDX11.This was*

confirmed by sequencing WABS02 cDNA: of seven intron 26 containing reads, six harbored the mutation.B,Sanger sequencing of genomic DNA of patient WABS03 and both parents. The paternal allele contains a c.419G>A missense mutation that leads to a p.R140Q substitution. The maternal allele contains a c.1403 duplication, leading to a frameshift (p.L468fs). C, Sanger sequencing of genomic DNA of patient WABS04, the mother and a healthy sister. The maternal allele contains a c.2114G>A missense mutation that leads to a p.C705Y substitution. The second allele, which is not found in the mother and in the healthy sister, contains a c.1930G>A missense mutation that leads to a p.V644M substitution. To confirm that the mutations are located in DDX11, PCR fragments were ligated into a zero-blunt plasmid, transformed into competent bacteria and DNA from single colonies was sequenced. Sequences were aligned to database DDX11 and DDX12p. D, Sanger sequencing of genomic DNA of patients WABS05 and WABS06, the mother and a healthy sister. The maternal allele contains a c.1672C>T nonsense mutation, leading to a premature stop (p.R558). The second allele contains a c.2571C>A missense mutation, leading to p.S857R substitution. To confirm that mutation c.2571C>A is located in DDX11, PCR fragments were ligated into a zero-blunt plasmid, transformed into competent bacteria and DNA from single colonies was sequenced. Sequences were aligned to database DDX11 and DDX12p. E, Sanger sequencing of genomic DNA and cDNA of patient WABS08. One allele contains an intronic mutation (c.1763-1G>C) which leads to alternative splicing of four basepairs and a frameshift (p.G590fs). The second allele contains a splice site mutation that leads to a deletion of three basepairs in the mRNA (c.1946-1948delGTG) and loss of one amino acid (p.G650del).*

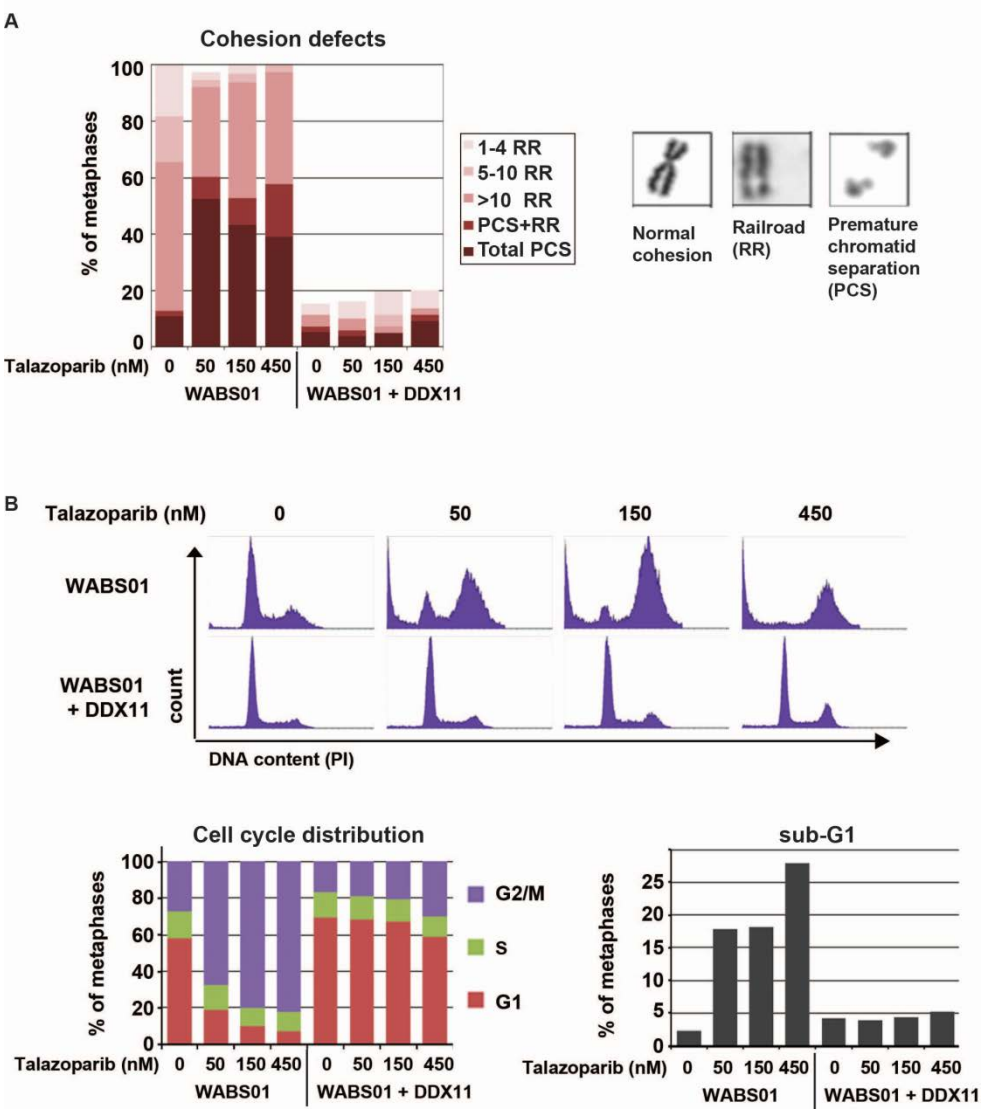

Figure S2: Enhanced cohesion loss, G2/M arrest and cell death upon PARP inhibition in WABS fibroblasts.*A, cells were treated with indicated doses of Talazoparib for 48h and assessed for cohsion defects. B, cells were treated with indicated doses of Talazoparib for 48h, stained with propidium iodide and analyzed by flow cytometry. Quantifications are shown in the lower graphs.*

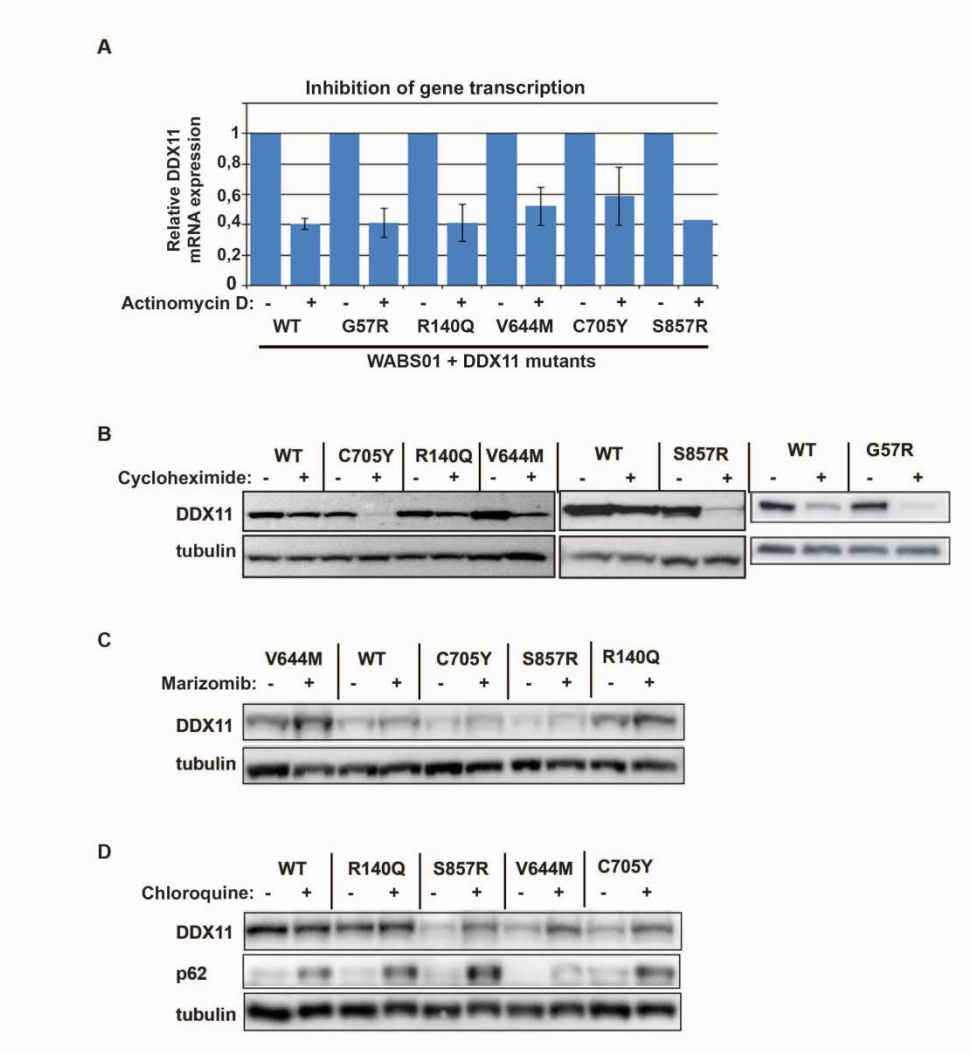

Figure S3: DDX11 missense alleles reduce protein stability. *A, WABS01 cells, stably transfected with cDNAs encoding either WT-DDX11 or several patient-derived DDX11 mutants, were treated with the transcription inhibitor Actinomycin D (5 µg/mL, 4h) and DDX11 mRNA levels were analyzed by qRT-PCR. B-D, Cells were treated with Cycloheximide (62,5 µg/mL, 3h), Marizomib (500 nM, 5h) or Chloroquine (25 µM, 24h). Quantifications are provided in Figure 3E and 3F.*

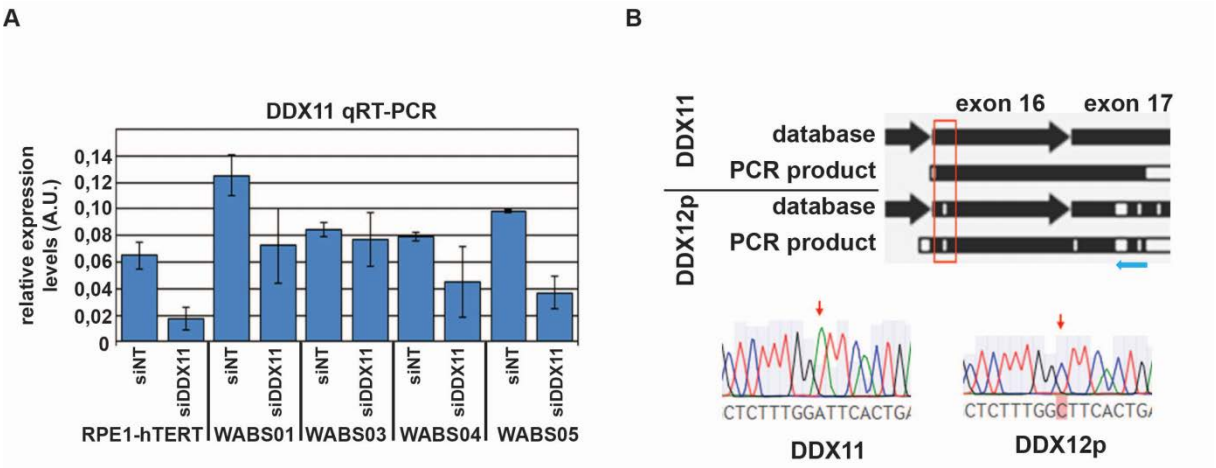

Figure S4: Validation of qRT-PCR primers for DDX11 and DDX12p. *A, RPE1-hTERT cells and four WABS fibroblasts were transfected with indicated siRNAs (day 1 and day 4) and analyzed for mRNA levels seven days after the first transfection using qRT-PCR. Accompanying cohesion analysis is shown in Figure 3H. B, Specific qRT-PCR primers were designed to distinguish between DDX11 and DDX12p cDNA. This is based on a stretch containing multiple differences in exon 17 (blue arrow). Sanger sequencing of the resulting amplicons confirms specificity of the primers (red arrows).*

A

	DDX11		DDX12p	
clone	allele 1	allele 2	allele 1	allele 2
wt-TP53_DDX11/12pKO #13	-13	-13	-8	-9
TP53KO_DDX11/12pKO #6	-11	-13	-10	-11
TP53KO_DDX11/12pKO #7	-2	+1	-8	+5
TP53KO_DDX11KO #1B	+226	?	WT	WT
TP53KO_DDX11KO #8A	-258	?	WT	WT
TP53KO_DDX12pKO #C9	WT	+1	+1	+1
TP53KO_DDX12pKO #C14	WT	+1	+1	+1

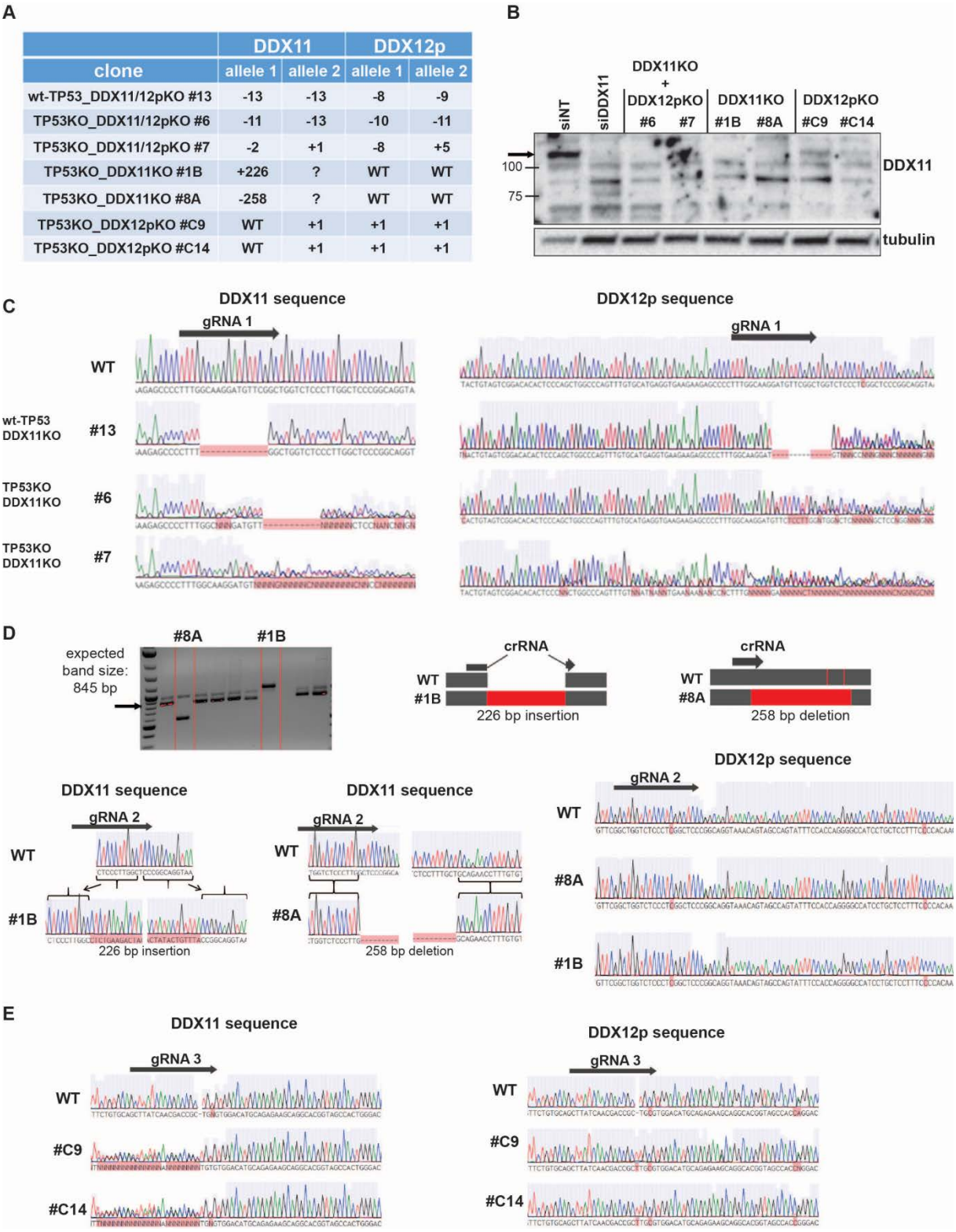

Figure S5: Characterization of CRISPR-induced indels in DDX11 and DDX12p. A, Summary of indels present in DDX11 and DDX12p knockout clones. RPE1-hTERT_TetOn-Cas9 cells were treated with 100 ng/mL doxycycline to induce Cas9 expression, transfected with synthetic crRNA and tracrRNA and seeded in limiting dilution. DNA from single clones was PCR amplified using DDX11 and DDX12p specific primers (shown in A),), sequenced and analyzed by TIDE [75] for bi-allelic frameshift mutations. Clone #13 (TP53wt, DDX11KO) and clone #6 (TP53KO, DDX11KO)

are also used in Figures 4, 6 and 8. B, A panel of RPE1-TP53KO cells with indicated knockout of DDX11 and/or DDX12p was analyzed for DDX11 and tubulin protein levels by western blot. C, Sanger sequencing of indels in DDX11 and DDX12p, created with gRNA 1, confirms frameshifts in the selected clones. D, Analysis of the indels that were created with gRNA2. As we had previously observed that gRNA 2 preferentially causes in-frame indels, we co-transfected a PCR-amplified Zeocin resistance expression cassette, to facilitate gene disruption by Zeocin selection. PCR products from the resulting clones were first analyzed on an agarose gel, indicating loss of the wild-type band in clones #1B and #8A. Sanger sequencing and alignment with control sequence revealed a large insertion and deletion, respectively. We are uncertain what happened to the other allele in both clones, but considering the absence of wildtype product, DDX11 knockout was confirmed. DDX12p sequences are still intact. E, Sanger sequencing of indels in DDX11 and DDX12p, created with gRNA 3. Note that gRNA 3 not only targets both DDX12p alleles, but also one DDX11 allele in RPE1 cells.

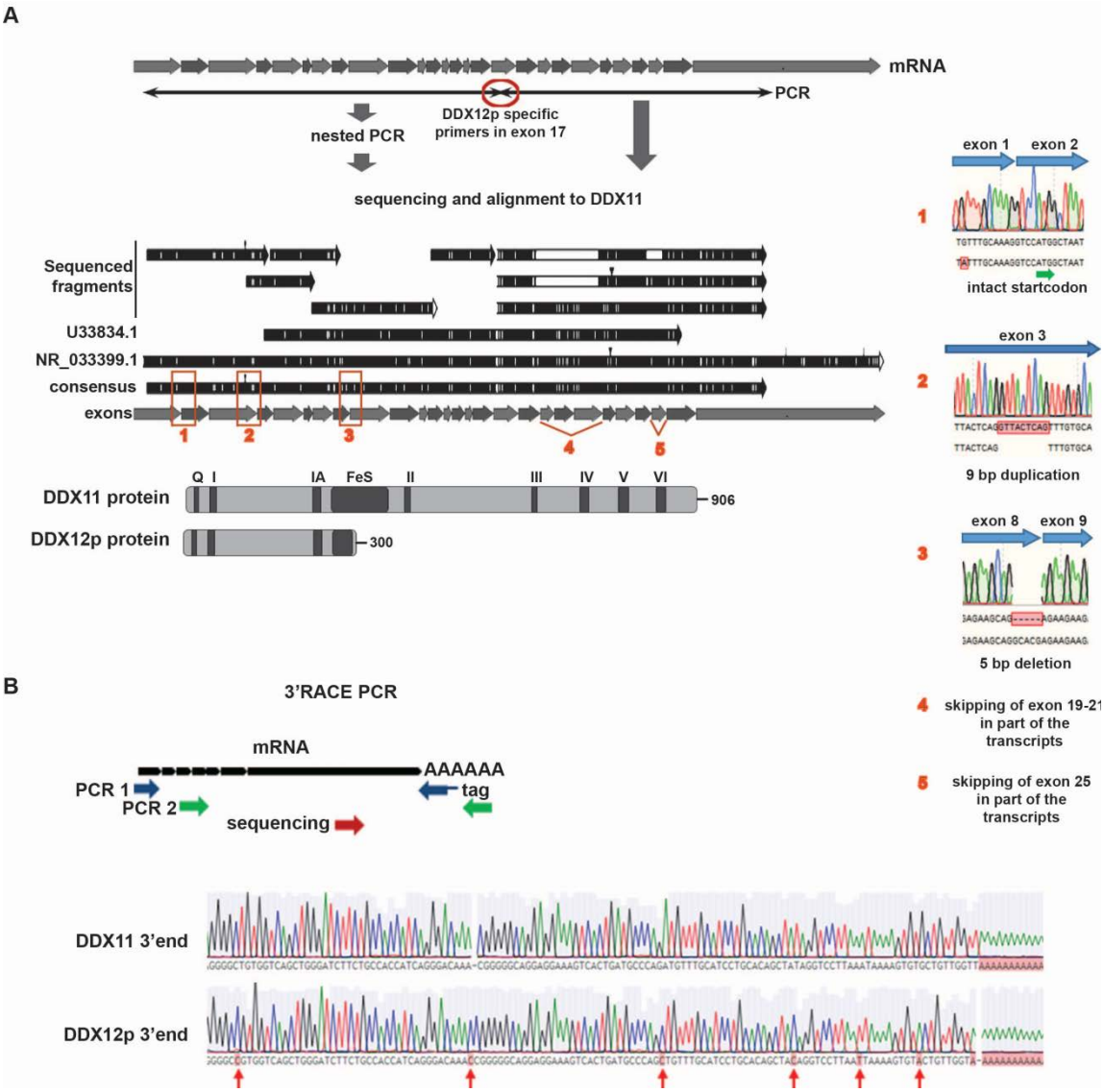

Figure S6: Identification of the DDX12p mRNA sequences in RPE1 cells. A, DDX12p cDNA was amplified using the DDX12p-specific reverse primers in exon 17 (Figure S4). The exon 1-17 amplicon served as template for several subsequent PCR reactions, using primers that do not discriminate between DDX11 and DDX12p. Both the initial exon 17-27 PCR reaction and the nested PCR fragments were ligated into a zero-blunt plasmid, transformed into competent bacteria and DNA of single colonies was sequenced. Sequences were aligned to DDX11 mRNA as well as to the available database mRNA sequence for DDX12p (NR_033399.1 and U3384.1). We find an intact start codon (1) and a 9bp duplication in exon 3 (2). Importantly, the splicing from exon 8 to exon 9 results in a 5bp deletion in the RPE1 DDX12p transcript as compared with database DDX11 and DDX12p sequences (3), resulting in a frameshift and a truncated protein of 300 amino acids. At the 3'end, we find different isoforms that skip exon 19-21 (4) and/or exon 25 (5), but also one that includes all exons. Consensus DDX12p sequence is provided as separate text file. B, 3'RACE PCR confirms a poly-A tail in DDX12p transcripts. RPE1 RNA was reverse transcribed into cDNA using a DDX11/12p forward primer in exon 27 and an oligo-dT reverse primer. A tag on the reverse prime allows a specific 2nd PCR step, and the resulting PCR fragments were ligated into a zero-blunt plasmid, transformed into bacteria and

DNA of single colonies was sequenced. Sequences containing multiple base pairs specifically annotated to DDX12p (database sequence, indicated with red arrows) also contain a poly-A tail.

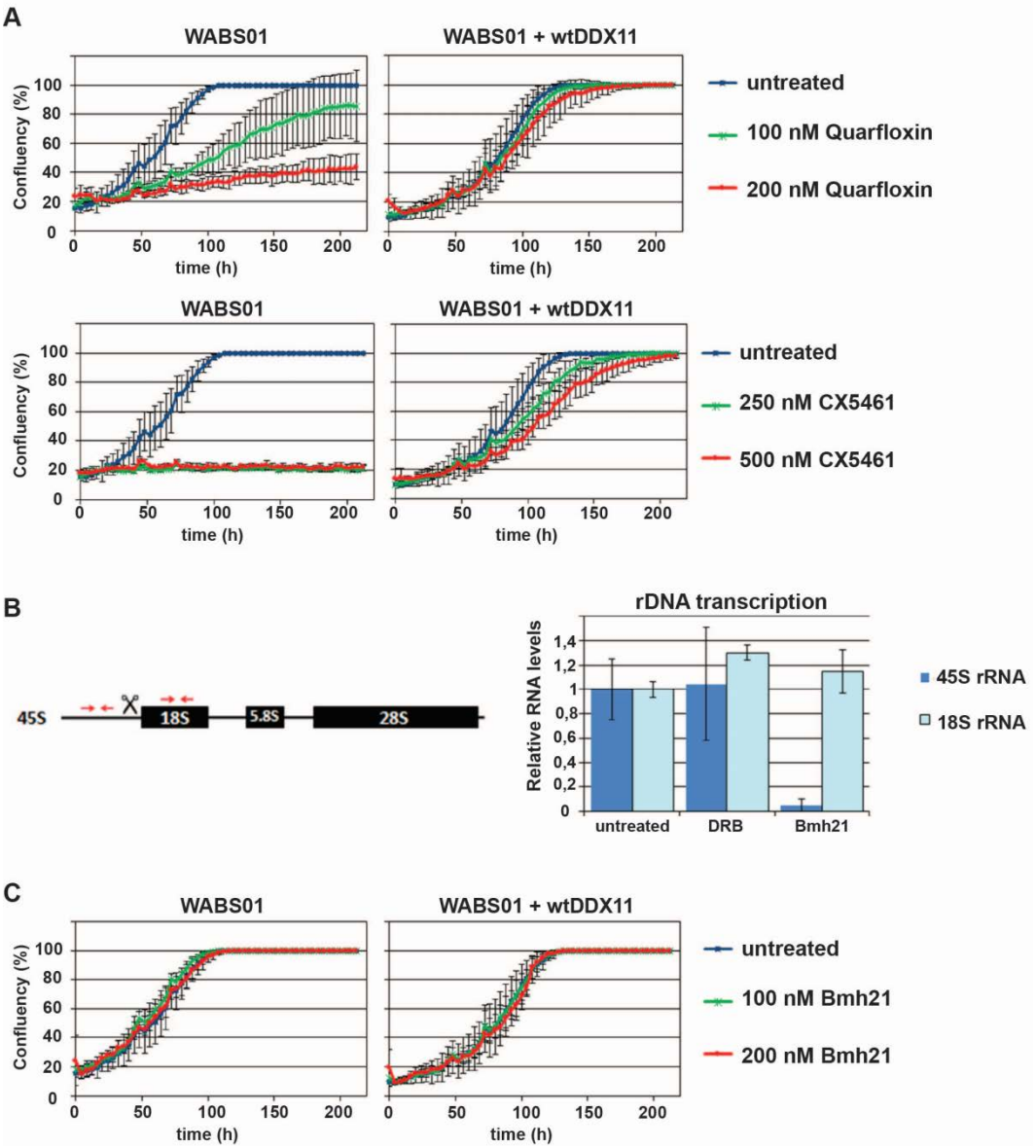

Figure S7: DDX11 deficiency sensitizes to G4 stabilization but not to inhibition of rDNA synthesis. A, WABS01 and WABS01 + wtDDX11 fibroblasts were cultured in 96-wells plates and treated with Quarfloxin or CX5461. Growth was monitored using IncuCyte software. Mean and standard deviations of four technical replicates are shown.B, RPE1-hTERT-TP53KO cells were treated with the RNA polymerase II inhibitor DRB or the RNA polymerase I inhibitor Bmh21 (1 µM, 7h) and analyzed by qRT-PCR for ribosomal RNA expression. Red arrows indicate primer locations: the 45S rRNA primer pair amplifies a region that is rapidly cleaved off the large precursor transcript, thereby measuring active rDNA transcription rate. The 18S rRNA primer pair amplifies a highly stable region that is present in mature rRNA, thereby serving as control. C, WABS01 and WABS01 + wtDDX11 fibroblasts were cultured in 96-wells plates and treated with Bmh21. Growth was monitored using IncuCyte software. Mean and standard deviations of four technical replicates are shown.

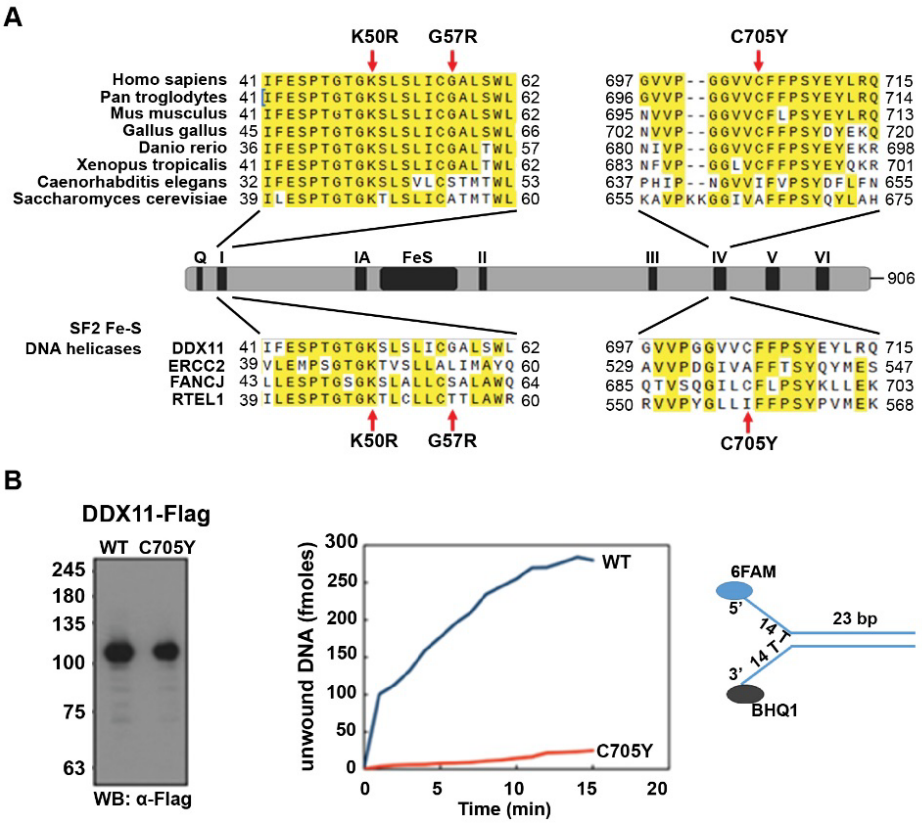

Figure S8: Impaired DDX11 helicase activity in WABS-derived DDX11 mutants.

Biochemical analysis of the DDX11 C705Y mutant protein. A, Schematic representation of the polypeptide chain of Homo sapiens (Hsa) DDX11 and Thermoplasma acidophilum (Tac) XPD, both belonging to the group of SF2 DNA helicases with a Fe-S cluster. Conserved helicase motifs (from I to VI) are indicated in red. Other sequence motifs are indicated with different colours. Abbreviations used are: Q, for Q motif; Fe-S, for Fe-S cluster; Arch, for Arch domain. A multiple sequence alignment of motif IV from human Fe-S cluster DNA helicases is reported. Invariant residues are highlighted in red. Position of the mutated residue (C705Y) of human DDX11 is indicated. B, left panel: Western blot analysis of purified recombinant Flag-tagged DDX11 WT and C705Y mutant was carried out using an anti-Flag M2 monoclonal antibody. Position of protein markers is indicated on the left. Middle panel: plot shows kinetics of DNA unwinding by DDX11 wild type (WT) and the C705Y mutant (C705Y). The reaction was started by adding each protein (600 ng) into the assay mixture (final volume: 30 microL) containing a fluorescein-labelled DNA substrate (20 nM, right panel). Fluorescence emission due to substrate melting was monitored during a 15-min time course. Fluorescence values were converted to unwound DNA as described in the experimental procedure section. Assays were carried out in triplicate and representative graphs are shown.

Material and methods

Compounds

The following drugs were used: Camptothecin, Actinomycin D, Cycloheximide, Marizomib, Chloroquine, Bmh21, BO-2, (all Sigma-Aldrich), Aphidicolin (Santa Cruz), Talazoparib (Axon Medchem), Quarfloxin (CX-3543, Adooq Bioscience) and CX-5461 (Selleckchem).

Sequencing

Appropriate informed consent was obtained from patients or from relatives when applicable. Genomic DNA was isolated using the QIAmp blood kit (Qiagen). Direct Sanger sequencing of DDX11 coding exons was performed for WABS03. WABS05 was analyzed with a custom Haloplex (Agilent) kit targeting the coding regions of all known cohesinopathy genes using 200 ng of genomic DNA to obtain sequencing libraries. Samples tagged with a unique barcode and pooled before 150bp pair-ended sequencing on the Illumina Miseq platform. SureCall software (version 2.0, Agilent) was used to detect variants. Sample WABS04 was enriched for the whole exome using Nimblegen Exome V.3 oligo library kit, barcode-tagged and pooled with a total of six samples, and sequenced on one HiSeq 2000 illumina lane using the 100 paired-end protocol. Exome data analysis was performed using genome analysis tool kit (GATK) (DePristo et al., 2011). Validation of the identified DDX11 mutation was performed by Sanger sequencing. Of note, bi-allelic variants of unknown significance (VUS) in the Duchenne gene DMD, most likely not pathogenic, were found in WABS07 and WABS08.

3'RACE PCR

The second generation 5'/3' RACE Kit (Roche) was used to amplify the 3'UTR of DDX11 and DDX12p from RPE1 cDNA, by using a non-specific forward primer (CCAGACAACATCCTGCCCCT) and a mix of three tagged oligo dT primers (TGCCCAGTTCCCAGTTCCGATTTTTTTTTTTTTTTTG, TGCCCAGTTCCCAGTTCCGATTTTTTTTTTTTTTTC,
TGCCCAGTTCCCAGTTCCGATTTTTTTTTTTTTTTA). The resulting PCR product was used as a template for a second PCR reaction, using a forward primer specific for DDX11 (ATTCCAGGTGCATCCAGGCC) or DDX12p (TATTCCAGGTGCGGGCGTCA) and a reverse primer that anneals to the tag (TGCCCAGTTCCCAGTTCCGA). The resulting PCR fragments were cloned into zero-blunt plasmids and sequenced using specific primers for DDX11 (GGCCCTGCTCCCTATCCTGT) or DDX12p (GGCCCTGCTCTCTATCCTGC).

Cell culture and construction of cell lines

RPE1-hTERT cells (American tissue culture collection) and SV40 transformed fibroblasts, including WABS01 [1], WABS02, WABS03, WABS04, WABS05, WABS08, FANCJ patients 1 and 2 (VU1414F and VU030F [78]) and LN9SV control [79], were cultured in Dulbecco's Modified Eagles

Medium (DMEM, Gibco), supplemented with 10% FCS, 1 mM sodium pyruvate and antibiotics. Epstein-Barr virus (EBV) transformed lymphoblasts, including WABS01-L, WABS03-L, WABS04-L, WABS05-L, RBS-L (ESCO2 deficient), VU867-L (deficient in both FANC-A and FANC-M)[76] and HSC93 control [80], were cultured in Roswell Park Memorial Institute (RPMI, Hyclone) supplemented with 10% FCS, 1 mM sodium pyruvate and antibiotics.

WABS03-L, WABS04-L and WABS05-L were functionally complemented by transfection of pMEP4 plasmid (Invitrogen) expressing wild type DDX11 (transcript variant 1, NM_030653.4) and selected with 70 µg/ml hygromycin-B. WABS02 and WABS08 fibroblasts were stably transfected with pIRES-Neo plasmids containing wtDDX11 or (in the case of WABS01) different DDX11 mutants, that were constructed using overlap extension PCR, and selected with 700 µg/mL G418.

CRISPR-Cas9 was used to construct DDX11 and DDX12p knockouts in RPE1 cells. The generation of RPE1-hTERT_TetOn-Cas9_TP53KO cells is also described in a currently submitted manuscript [48]. Briefly, Cas9 cDNA was cloned into the pLVX-Tre3G plasmid (Clontech) and lentiviral Tre3G-Cas9 and Tet3G particles were produced in HEK293T cells using the Lenti-X HT packaging system (Clontech). Transduced cells were selected with 10 µg/mL puromycin and 400 µg/mL G418. Cells were treated with 100 ng/mL doxycycline (Sigma-Aldrich) to induce Cas9 expression and transfected with 10 nM synthetic crRNA and tracrRNA (Dharmacon or IDT) using RNAiMAX (Invitrogen). The following crRNA sequences were used: TP53 CCATTGTTCAATATCGTCCG, DDX11/12p CTTTGGCAAGGATGTTCGGC,DDX11 specific GGCTGGTCTCCCTTGGCTCC, DDX12p specific GCTTATCAACGACCGCTGCG. Single clones were assessed by Sanger sequencing using the following primers: TP53-Fw GAGACCTGTGGGAAGCGAAA, TP53-Rv GCTGCCCTGGTAGGTTTTCT; DDX11-Fw AACAACCCACCCTCCCCAAG, DDX11-Rv TGCCTCACTCTCTCCAGACC; DDX12p-Fw GCTGGGTGGT GCTGGATATG, DDX12p-Rv CTGCCTACTGTGGTCTCATCGG.

Proliferation assays

Lymphoblasts were seeded in T25 flasks with increasing drug concentrations, and counted again when untreated cells reached approximately three population doublings. IC50 values were determined using curve fitting (www.ic50.tk). For adherent cells, the IncuCyte Zoom instrument (Essen Bioscience) was used. RPE1 cells (1500 / well) and fibroblasts (3000 / well) were seeded in 96-wells plates and imaged every 4 hours with a 10x objective. IncuCyte software was used to quantify confluence from four non-overlapping bright field images per well, for at least three replicate wells. Doubling time was calculated for the period required to grow from approximately 30% to 70% confluence, using the formula doubling time (h) = required time (h) * log(2) / (log(confluence endpoint(%)) – log(confluence starting point(%))).

siRNA experiments

For knockdown experiments, 25 nM siRNA (Dharmacon) was transfected using RNAiMAX (Invitrogen). Sequences: non-targeting siRNA UAAGGCUAUGAAGAGAUAC; siDDX11 GCAGAGCUGUACCGGGUUU, CGGCAGAACCUUUGUGUAA, GAGGAAGAACACAUAACUA,

UGUUCAAGGUGCAGCGAUA; sip53 GAAAUUUGCGUGUGGAGUA, GUGCAGCUGUGGGUUGAUU, GCAGUCAGAUCCUAGCGUC, GGAGAAUAUUUCACCCUUC; siUBB CCCAGUGACACCAUCGAAA, GACCAUCACUCUGGAGGUG, GUAUGCAGAUCUUCGUGAA, GCCGUACUCUUUCUGACUA

qRT-PCR

Total RNA was extracted with the High Pure Isolation Kit (Roche) and cDNA was prepared with the iScript cDNA Synthesis Kit (Biorad). Quantitative reverse transcription polymerase chain reaction (qRT-PCR) was performed using SYBR Green (Roche) on a LightCycler 480 (Roche). Levels were normalized to the geometric mean of at least two housekeeping genes. Primer sequences:

DDX11 Fw AACCTGTTCAAGGTGCAGCGATAC, DDX11 Rv GAGAAGCTGGTCGCAGGGT;
DDX12p Fw AACCTGTTCAAGGTGCAGCGATAC, DDX12p Rv GGGAAGCTGGTTGCGGGAC;
p21 Fw AGCAGAGGAAGACCATGTGGA, p21 Rv AATCTGTCATGCTGGTCTGCC;
45S pre-rRNA Fw GCCTTCTCTAGCGATCTGAGAG, 45S pre-rRNA Rv CCATAACGGAGGCAGAGACA;
18S pre-rRNA AAACGGCTACCACATCCA, 18S pre-rRNA CCTCCAATGGATCCTCGT;
HPRT1 Fw TGACACTGGGAAAACAATGCA, HPRT Rv GGTCCTTTTCACCAGCAAGCT;
TBP Fw TGCACAGGAGCCAAGAGTGAA, TBP Rv CACATCACAGCTCCCCACCA;
B2M Fw ATGAGTATGCCTGCCGTGTGA, B2M Rv GGCATCTTCAAACCTCCATG

Immunoblotting

Cells were lysed in lysis buffer (50 mM Tris-HCl pH 7.4, 150 mM NaCl, 1% Triton X-100) with protease- and phosphataseinhibitors (Roche), except for the Marizomib treated WABS fibroblasts (Figure 2C), which were directly scraped in sample buffer. Proteins were separated by 3-8% or 8-16% SDS-PAGE (NU-PAGE or BioRad) and transferred to immobilon-P membranes (Millipore). Membranes were blocked in 5% dry milk in TBST-T (10 mM Tris-HCl pH 7.4, 150 mM NaCl, 0.04% Tween-20), incubated with primary and peroxidase-conjugated secondary antibodies (DAKO Glostrup, Denmark) and bands were visualized by chemoluminescence (Amersham). Antibodies used for detection are mouse anti-DDX11 (B01P, Abnova), goat anti-β-actin (I-19, Santa Cruz), mouse anti-α-tubulin (B-5-1-2, Santa Cruz #sc-23948), mouse anti-CDC6 (Santa Cruz #sc-9964), mouse anti-p62 (D5L7G, cell signaling), mouse anti-Flag (F3165, Sigma), mouse anti-p53 (DO-1, Santa Cruz #sc-126), mouse anti-vinculin (H-10, Santa Cruz #sc-25336), guinea pig anti-ESCO2 [81].

Analysis of cohesion defect and chromosomal breakage

Cells were incubated with 200 ng/mL Demecolcin (Sigma-Aldrich) for 20 minutes (cohesion defect analysis) or 30 minutes (chromosomal breakage analysis). Cells were harvested,

resuspended in 0.075 M KCl for 20 minutes and fixed in methanol/acetic acid (3:1). Cells were washed in fixative three times, dropped onto glass slides and stained with 5% Giemsa (Merck). Cohesion defects or chromosomal breaks were counted in 50 metaphases per condition on two coded slides. Analysis of breaks was described before [80].

DNA Fiber analysis

Cells were pulse-labeled with 25 µM Chlorodeoxyuridine (CldU) for 20 minutes, followed by 20 minutes 250 µM Iododeoxyuridine (IdU). Approximately 3000 cells were lysed in 7 µL spreading buffer (200 mM Tris-HCl PH 7.4, 50 mM EDTA and 0.5% SDS). Fibers were spread on Superfrost microscope slides, which were tilted ~15^{o}, air-dried for several minutes and fixed in methanol:acetic acid (3:1). DNA was denatured with 2.5 M HCl for 75 minutes, blocked in PBS + 1% BSA + 0.1% Tween20 and incubated for 1 hour with rat-anti BrdU (1:500, Clone BU1/75, Novus Biologicals) and mouse-anti-BrdU (1:750, Clone B44, Becton Dickinson). Slides were fixed with 4% paraformaldehyde for 10 minutes, incubated for 1.5 h with goat-anti-mouse Alexa 488 and goat-anti-rat Alexa 594(both 1:500, Life technologies) and mounted with Vectashield medium. Images of DNA fibers were taken with a Zeiss AxioObserver Z1 inverted microscope using a 63x objective equipped with a Hamamatsu ORCA AG Black and White CCD camera. Fiber tract lengths were assessed with ImageJ and µm values were converted into kilobases using the conversion factor 1 µm = 2.59 kb [83,84].

Immunofluorescence

Cells were grown on cover slips, fixed in 2% paraformaldehyde for 15 min at RT and subsequently in 70% ice cold EtOH for 1h. Cells were permeabilized in 0,3% Triton X-100 for 5 min, blocked in 3% BSA and 0,3% Triton X-100 for 45 min, incubated with primary antibody for 1,5h and secondary antibody for 1h at RT. Cells were mounted using ProLong™ Gold Antifade Mountant with DAPI (Invitrogen) and cells were examined using fluorescence microscopy (Leica). Antibodies used: rabbit anti-DDX11 (ab204788, Abcam), mouse anti-yH2AX (Ser139, JBW301, Millipore), rabbit anti-53BP1 (Novus).

Flow cytometry

Cells were harvested, washed in PBS and fixed in ice-cold 70% EtOH. Cells were washed and resuspended in PBS with 1:10 PI/RNase staining buffer (BD Biosciences) and analyzed by flow cytometry on a BD FACSCalibur (BD Biosciences). Cell-cycle analysis was conducted with BD CellQuest software (BD Biosciences).

In vitro DNA helicase assay

For biochemical analysis of the DDX11 C705Y mutant protein, Flag-tagged DDX11 WT and C705Y mutant were purified. Kinetics of DNA unwinding by DDX11 wild type (WT) and the C705Y mutant (C705Y) were measured in 30 microliter reactions by adding each protein (600 ng) into the assay mixture containing a fluorescein-labelled DNA substrate (20 nM). Fluorescence emission due to substrate melting was monitored. Fluorescence values were converted to unwound DNA (also see reference 37).

References:

1. van der Lelij, P. *et al.*Warsaw breakage syndrome, a cohesinopathy associated with mutations in the XPD helicase family member DDX11/ChlR1. *Am. J. Hum. Genet***86**, 262-266 (2010).
2. Alkhunaizi, E. *et al.* Warsaw breakage syndrome: Further clinical and genetic delineation. *Am J Med Genet A***176**, 2404-2418 (2018).
3. Bailey, C., Fryer, A.E. & Greenslade, M. Warsaw Breakage Syndrome--A further report, emphasising cutaneous findings. *Eur J Med Genet***58**, 235-7 (2015).
4. Capo-Chichi, J.M. *et al.* Identification and biochemical characterization of a novel mutation in DDX11 causing Warsaw breakage syndrome. *Hum. Mutat***34**, 103-107 (2013).
5. Eppley, S., Hopkin, R.J., Mendelsohn, B. & Slavotinek, A.M. Clinical Report: Warsaw Breakage Syndrome with small radii and fibulae. *Am J Med Genet A***173**, 3075-3081 (2017).
6. Bottega, R. *et al.* Two further patients with Warsaw breakage syndrome. Is a mild phenotype possible? *Mol Genet Genomic Med***7**, e639 (2019).
7. Rabin, R. *et al.* Study of carrier frequency of Warsaw breakage syndrome in the Ashkenazi Jewish population and presentation of two cases. *Am J Med Genet A***179**, 2144-2151 (2019).
8. Gerring, S.L., Spencer, F. & Hieter, P. The CHL 1 (CTF 1) gene product of Saccharomyces cerevisiae is important for chromosome transmission and normal cell cycle progression in G2/M. *EMBO J***9**, 4347-58 (1990).
9. Spencer, F., Gerring, S.L., Connelly, C. & Hieter, P. Mitotic chromosome transmission fidelity mutants in Saccharomyces cerevisiae. *Genetics***124**, 237-49 (1990).
10. Amann, J., Kidd, V.J. & Lahti, J.M. Characterization of putative human homologues of the yeast chromosome transmission fidelity gene, CHL1. *J Biol Chem***272**, 3823-32 (1997).
11. Amann, J., Valentine, M., Kidd, V.J. & Lahti, J.M. Localization of chi1-related helicase genes to human chromosome regions 12p11 and 12p13: similarity between parts of these genes and conserved human telomeric-associated DNA. *Genomics***32**, 260-5 (1996).
12. Parish, J.L. *et al.* The DNA helicase ChlR1 is required for sister chromatid cohesion in mammalian cells. *J. Cell Sci***119**, 4857-4865 (2006).
13. Inoue, A. *et al.* Loss of ChlR1 helicase in mouse causes lethality due to the accumulation of aneuploid cells generated by cohesion defects and placental malformation. *Cell Cycle***6**, 1646-1654 (2007).
14. Cota, C.D. & Garcia-Garcia, M.J. The ENU-induced cetus mutation reveals an essential role of the DNA helicase DDX11 for mesoderm development during early mouse embryogenesis. *Dev Dyn***241**, 1249-59 (2012).
15. Ogiwara, H., Ui, A., Lai, M.S., Enomoto, T. & Seki, M. Chl1 and Ctf4 are required for damage-induced recombinations. *Biochem. Biophys. Res. Commun***354**, 222-226 (2007).
16. Wu, Y. & Brosh, R.M., Jr. DNA helicase and helicase-nuclease enzymes with a conserved iron-sulfur cluster. *Nucleic Acids Res***40**, 4247-60 (2012).
17. Bharti, S.K. *et al.* Molecular functions and cellular roles of the ChlR1 (DDX11) helicase defective in the rare cohesinopathy Warsaw breakage syndrome. *Cell Mol. Life Sci***71**, 2625-2639 (2014).
18. Farina, A. *et al.* Studies with the human cohesin establishment factor, ChlR1. Association of ChlR1 with Ctf18-RFC and Fen1. *J. Biol. Chem***283**, 20925-20936 (2008).
19. Hirota, Y. & Lahti, J.M. Characterization of the enzymatic activity of hChlR1, a novel human DNA helicase. *Nucleic Acids Res***28**, 917-924 (2000).
20. Wu, Y., Sommers, J., Khan, I., J., d.W. & Brosh, R. Biochemical characterization of Warsaw Breakage Syndrome helicase. *J. Biol. Chem* (2011).
21. Pisani, F.M., Napolitano, E., Napolitano, L.M.R. & Onesti, S. Molecular and Cellular Functions of the Warsaw Breakage Syndrome DNA Helicase DDX11. *Genes (Basel)***9**(2018).

22. Chung, G., O'Neil, N.J. & Rose, A.M. CHL-1 provides an essential function affecting cell proliferation and chromosome stability in Caenorhabditis elegans. *DNA Repair (Amst)***10**, 1174-82 (2011).
23. Laha, S., Das, S.P., Hajra, S., Sau, S. & Sinha, P. The budding yeast protein Chl1p is required to preserve genome integrity upon DNA damage in S-phase. *Nucleic Acids Res***34**, 5880-5891 (2006).
24. Petronczki, M. *et al.* Sister-chromatid cohesion mediated by the alternative RF-CCtf18/Dcc1/Ctf8, the helicase Chl1 and the polymerase-alpha-associated protein Ctf4 is essential for chromatid disjunction during meiosis II. *J. Cell Sci***117**, 3547-3559 (2004).
25. Skibbens, R.V. Chl1p, a DNA helicase-like protein in budding yeast, functions in sister-chromatid cohesion. *Genetics***166**, 33-42 (2004).
26. Sherwood, R., Takahashi, T.S. & Jallepalli, P.V. Sister acts: coordinating DNA replication and cohesion establishment. *Genes Dev***24**, 2723-2731 (2010).
27. Rhodes, J.D.P. *et al.* Cohesin Can Remain Associated with Chromosomes during DNA Replication. *Cell Rep***20**, 2749-2755 (2017).
28. Kang, S., Kang, M.S., Ryu, E. & Myung, K. Eukaryotic DNA replication: Orchestrated action of multi-subunit protein complexes. *Mutat Res***809**, 58-69 (2018).
29. Ansbach, A.B. *et al.* RFCCtf18 and the Swi1-Swi3 complex function in separate and redundant pathways required for the stabilization of replication forks to facilitate sister chromatid cohesion in Schizosaccharomyces pombe. *Mol Biol Cell***19**, 595-607 (2008).
30. Mayer, M.L. *et al.* Identification of protein complexes required for efficient sister chromatid cohesion. *Mol Biol Cell***15**, 1736-45 (2004).
31. Xu, H., Boone, C. & Brown, G.W. Genetic dissection of parallel sister-chromatid cohesion pathways. *Genetics***176**, 1417-1429 (2007).
32. Tong, A.H. *et al.* Global mapping of the yeast genetic interaction network. *Science***303**, 808-813 (2004).
33. Moldovan, G.L., Pfander, B. & Jentsch, S. PCNA controls establishment of sister chromatid cohesion during S phase. *Mol. Cell***23**, 723-732 (2006).
34. Samora, C.P. *et al.* Ctf4 Links DNA Replication with Sister Chromatid Cohesion Establishment by Recruiting the Chl1 Helicase to the Replisome. *Mol Cell***63**, 371-84 (2016).
35. Rudra, S. & Skibbens, R.V. Sister chromatid cohesion establishment occurs in concert with lagging strand synthesis. *Cell Cycle***11**, 2114-2121 (2012).
36. Leman, A.R., Noguchi, C., Lee, C.Y. & Noguchi, E. Human Timeless and Tipin stabilize replication forks and facilitate sister-chromatid cohesion. *J. Cell Sci***123**, 660-670 (2010).
37. Cali, F., Bharti, S.K., Di Perna, R., Brosh, R.M., Jr. & Pisani, F.M. Tim/Timeless, a member of the replication fork protection complex, operates with the Warsaw breakage syndrome DNA helicase DDX11 in the same fork recovery pathway. *Nucleic Acids Res***44**, 705-17 (2016).
38. Cortone, G. *et al.* Interaction of the Warsaw breakage syndrome DNA helicase DDX11 with the replication fork-protection factor Timeless promotes sister chromatid cohesion. *PLoS Genet***14**, e1007622 (2018).
39. S, L.H. CHL1 is a nuclear protein with an essential ATP binding site that exhibits a size-dependent effect on chromosome segregation. *Nucleic Acids Res***28**, 3056-64 (2000).
40. Rudra, S. & Skibbens, R.V. Chl1 DNA Helicase Regulates Scc2 Deposition Specifically during DNA-Replication in Saccharomyces cerevisiae. *PLoS. One***8**, e75435 (2013).
41. Hiel, J.A. *et al.* Nijmegen breakage syndrome in a Dutch patient not resulting from a defect in NBS1. *J Med Genet***38**, E19 (2001).
42. Kwee, M.L. *et al.* An atypical case of Fanconi anemia in elderly sibs. *Am J Med Genet***68**, 362-6 (1997).
43. Dorsett, D. & Krantz, I.D. On the molecular etiology of Cornelia de Lange syndrome. *Ann N Y Acad Sci***1151**, 22-37 (2009).
44. Kline, A.D. *et al.*Cornelia de Lange syndrome: clinical review, diagnostic and scoring systems, and anticipatory guidance. *Am J Med Genet A***143A**, 1287-96 (2007).

45. Schule, B., Oviedo, A., Johnston, K., Pai, S. & Francke, U. Inactivating mutations in ESCO2 cause SC phocomelia and Roberts syndrome: no phenotype-genotype correlation. *Am. J. Hum. Genet***77**, 1117-1128 (2005).
46. Costa, V. *et al.* DDX11L: a novel transcript family emerging from human subtelomeric regions. *BMC. Genomics***10**, 250 (2009).
47. Stoepker, C. *et al.* DNA helicases FANCM and DDX11 are determinants of PARP inhibitor sensitivity. *DNA Repair (Amst)***26**, 54-64 (2015).
48. Benedict, B. *et al.* WAPL-dependent repair of damaged replication forks underlies oncogene-induced loss of sister chromatid cohesion. *submitted manuscript* (2019).
49. Haapaniemi, E., Botla, S., Persson, J., Schmierer, B. & Taipale, J. CRISPR-Cas9 genome editing induces a p53-mediated DNA damage response. *Nat Med***24**, 927-930 (2018).
50. Ihry, R.J. *et al.* p53 inhibits CRISPR-Cas9 engineering in human pluripotent stem cells. *Nat Med***24**, 939-946 (2018).
51. Xu, H. *et al.* CX-5461 is a DNA G-quadruplex stabilizer with selective lethality in BRCA1/2 deficient tumours. *Nat Commun***8**, 14432 (2017).
52. Drygin, D. *et al.* Targeting RNA polymerase I with an oral small molecule CX-5461 inhibits ribosomal RNA synthesis and solid tumor growth. *Cancer Res***71**, 1418-30 (2011).
53. Drygin, D. *et al.* Anticancer activity of CX-3543: a direct inhibitor of rRNA biogenesis. *Cancer Res***69**, 7653-61 (2009).
54. Peltonen, K. *et al.* Identification of novel p53 pathway activating small-molecule compounds reveals unexpected similarities with known therapeutic agents. *PLoS One***5**, e12996 (2010).
55. Peltonen, K. *et al.* A targeting modality for destruction of RNA polymerase I that possesses anticancer activity. *Cancer Cell***25**, 77-90 (2014).
56. Wu, G. & Li, L. Biochemical characterization of iron-sulfur cluster assembly in the scaffold IscU of Escherichia coli. *Biochemistry (Mosc)***77**, 135-42 (2012).
57. Heidinger-Pauli, J.M., Mert, O., Davenport, C., Guacci, V. & Koshland, D. Systematic reduction of cohesin differentially affects chromosome segregation, condensation, and DNA repair. *Curr. Biol***20**, 957-963 (2010).
58. Banerji, R., Skibbens, R.V. & Iovine, M.K. How many roads lead to cohesinopathies? *Dev Dyn***246**, 881-888 (2017).
59. Maya-Mendoza, A. *et al.* High speed of fork progression induces DNA replication stress and genomic instability. *Nature***559**, 279-284 (2018).
60. Kee, Y. & D'Andrea, A.D. Molecular pathogenesis and clinical management of Fanconi anemia. *J Clin Invest***122**, 3799-806 (2012).
61. Chrzanowska, K.H., Gregorek, H., Dembowska-Baginska, B., Kalina, M.A. & Digweed, M. Nijmegen breakage syndrome (NBS). *Orphanet J Rare Dis***7**, 13 (2012).
62. Wu, Y., Shin-ya, K. & Brosh, R.M., Jr. FANCJ helicase defective in Fanconia anemia and breast cancer unwinds G-quadruplex DNA to defend genomic stability. *Mol Cell Biol***28**, 4116-28 (2008).
63. Bharti, S.K. *et al.* Specialization among iron-sulfur cluster helicases to resolve G-quadruplex DNA structures that threaten genomic stability. *J Biol Chem***288**, 28217-29 (2013).
64. Yang, D. & Okamoto, K. Structural insights into G-quadruplexes: towards new anticancer drugs. *Future Med Chem***2**, 619-46 (2010).
65. Kim, M.Y., Vankayalapati, H., Shin-Ya, K., Wierzba, K. & Hurley, L.H. Telomestatin, a potent telomerase inhibitor that interacts quite specifically with the human telomeric intramolecular g-quadruplex. *J Am Chem Soc***124**, 2098-9 (2002).
66. Sun, X. *et al.* The Warsaw breakage syndrome-related protein DDX11 is required for ribosomal RNA synthesis and embryonic development. *Hum Mol Genet***24**, 4901-15 (2015).
67. Laha, S., Das, S.P., Hajra, S., Sanyal, K. & Sinha, P. Functional characterization of the Saccharomyces cerevisiae protein Chl1 reveals the role of sister chromatid cohesion in the maintenance of spindle length during S-phase arrest. *BMC Genet***12**, 83 (2011).

68. Shah, N. *et al.* Roles of ChlR1 DNA helicase in replication recovery from DNA damage. *Exp. Cell Res***319**, 2244-2253 (2013).
69. Abe, T. *et al.* Chromatin determinants of the inner-centromere rely on replication factors with functions that impart cohesion. *Oncotarget***7**, 67934-67947 (2016).
70. Rudra, S. & Skibbens, R.V. Sister chromatid cohesion establishment occurs in concert with lagging strand synthesis. *Cell Cycle***11**, 2114-21 (2012).
71. Farina, A. *et al.* Studies with the human cohesin establishment factor, ChlR1. Association of ChlR1 with Ctf18-RFC and Fen1. *J Biol Chem***283**, 20925-36 (2008).
72. Bharti, S.K. *et al.*Molecular functions and cellular roles of the ChlR1 (DDX11) helicase defective in the rare cohesinopathy Warsaw breakage syndrome. *Cell Mol Life Sci***71**, 2625-39 (2014).
73. Murayama, Y., Samora, C.P., Kurokawa, Y., Iwasaki, H. & Uhlmann, F. Establishment of DNA-DNA Interactions by the Cohesin Ring. *Cell***172**, 465-477 e15 (2018).
74. Rudra, S. & Skibbens, R.V. Chl1 DNA helicase regulates Scc2 deposition specifically during DNA-replication in Saccharomyces cerevisiae. *PLoS One***8**, e75435 (2013).
75. Zheng, G., Kanchwala, M., Xing, C. & Yu, H. MCM2-7-dependent cohesin loading during S phase promotes sister-chromatid cohesion. *Elife***7**(2018).
76. Meetei, A.R. *et al.* A human ortholog of archaeal DNA repair protein Hef is defective in Fanconi anemia complementation group M. *Nat Genet***37**, 958-63 (2005).
77. Brinkman, E.K., Chen, T., Amendola, M. & van Steensel, B. Easy quantitative assessment of genome editing by sequence trace decomposition. *Nucleic Acids Res***42**, e168 (2014).
78. Levitus, M. *et al.* The DNA helicase BRIP1 is defective in Fanconi anemia complementation group J. *Nat Genet***37**, 934-5 (2005).
79. Hermsen, M.A. *et al.*Centromeric breakage as a major cause of cytogenetic abnormalities in oral squamous cell carcinoma. *Genes Chromosomes. Cancer***15**, 1-9 (1996).
80. Ishida, R. & Buchwald, M. Susceptibility of Fanconi's anemia lymphoblasts to DNA-cross-linking and alkylating agents. *Cancer Res***42**, 4000-6 (1982).
81. van der Lelij, P. *et al.* The cellular phenotype of Roberts syndrome fibroblasts as revealed by ectopic expression of ESCO2. *PLoS. One***4**, e6936 (2009).
82. Oostra, A.B., Nieuwint, A.W., Joenje, H. & de Winter, J.P. Diagnosis of fanconi anemia: chromosomal breakage analysis. *Anemia***2012**, 238731 (2012).
83. Parra, I. & Windle, B. High resolution visual mapping of stretched DNA by fluorescent hybridization. *Nat Genet***5**, 17-21 (1993).
84. Tuduri, S., Tourriere, H. & Pasero, P. Defining replication origin efficiency using DNA fiber assays. *Chromosome Res***18**, 91-102 (2010).

Chapter 7

General Discussion

Atiq Faramarz, Rob Wolthuis and Job de Lange

General discussion

Cohesinopathies

Cohesinopathies originate from defects in either structural components or regulators of the cohesin protein complex. Thus far, four cohesinopathy syndromes are classified: Roberts syndrome (RBS), Cornelia de Lange syndrome (CdLS), Warsaw breakage syndrome (WABS) and Chronic Atrial and Intestinal Dysrhythmia (CAID). Cohesinopathy patients show a heterogeneous spectrum and varying degree of clinical symptoms, including growth retardation, intellectual disability and multiple congenital abnormalities.

WABS was firstly diagnosed in our lab in 2010 and is caused by bi-allelic mutations in the *DDX11/ChlR1* gene [1]. DDX11 belongs to the group of Fe-S containing, ATP-dependent super-family 2 (SF2) DNA helicases. This family also includes FANCJ, XPD and RTEL1, which are related to different genetic syndromes. FANCJ mutations are genetically linked to Fanconi Anemia (FA), characterized by congenital abnormalities, bone marrow failure and cancer predisposition [2]. Mutations in XPD underlie a rare skin disorder, Xeroderma Pigmentosum, which is characterized by extreme UV sensitivity and neurological abnormalities [3]. RTEL1 mutations are associated with Dyskeratosis Congenita, a premature aging syndrome [4].

New WABS cases, prevalence and diagnostic complications

Chapter 6 of this thesis describes the identification of seven individuals with WABS, thereby increasing the total number of reported WABS patients to 23 [1, 5-9,10]. Thus far, there is no clear evidence for a WABS patient to have two complete *null* mutations in DDX11, and several patient-derived DDX11 mutants that we investigated encode a functional, but unstable protein. This suggests that WABS patients have some residual DDX11 activity that is required for survival. Indeed, DDX11 knockout is embryonic lethal in mice and we discovered that complete disruption of the DDX11 gene using CRISPR-Cas9 in human RPE1 cells leads to severe, p53-dependent growth retardation.

It is possible that the prevalence of WABS is underestimated due to diagnostic overlap with FA [11]. Cells from both WABS and FA patients show high sensitivity and chromosomal breakage upon treatment with DNA-crosslinking agents, which is considered the “golden standard” for FA diagnosis. Indeed, we identified a WABS case that was mistakenly reported as uncharacterized FA (WABS04, chapter 6). The presence of defective sister chromatid cohesion in WABS cells, however, specifically distinguishes WABS from FA. Definitive confirmation of WABS further requires mutational analysis of the *DDX11* gene. This can be a challenge due to the presence of the pseudogene *DDX12p*, which has 98% sequence similarity with the *DDX11* gene. *DDX12p* is primate-specific and is proposed to originate from a late-evolution duplication of a chromosomal region containing DDX11. Additionally, multiple sub-telomeric regions were shown to contain sequences that are highly similar to the DDX11 C-terminus [12]. These high sequence similarities can make it difficult to conclude whether a mutation is present in DDX11

or in a related sequence. DDX11 mutational analysis will therefore greatly benefit from the development and implementation of long-read sequencing techniques.

DDX11 and FANCJ helicases have different specificities

DDX11 and FANCJ are structurally related, iron-sulfur containing DNA helicases, whose mutational inactivation is linked to diseases that have also overlapping clinical phenotypes [11]. Both are shown to be involved in resolving secondary DNA structures, such as hairpins and G-quadruplexes (G4), formed in G-rich regions of the genome [13, 14]. Interestingly, *in vitro* studies using different G4-DNA structures demonstrated different G4 substrate specificity of DDX11 and FANCJ. FANCJ but not DDX11 was able to unwind uni-molecular G4 DNA substrates [13], whereas DDX11 efficiently resolved forked duplex DNA, a three-stranded D-loop substrate, and anti-parallel bi-molecular G4 structure [13, 15]. In addition, the helicase activity of DDX11, but not FANCJ, is stimulated by Timeless, a component of the replication fork protection complex (FPC). Timeless physically interacts with DDX11 and enhances its ability to unwind forked DNA and bi-molecular DNA substrates up to 10-fold and 4-fold, respectively [15]. Moreover, in genome-wide siRNA screens, CRISPR screens and siFANCJ transfection experiments, DDX11 deficient cells did not seem to be particularly sensitive to FANCJ loss (data not shown). In conclusion, despite substantial similarities, FANCJ and DDX11 seem to have unique helicase specificities.

DDX11 helicase activity supports both sister chromatid cohesion and replication fork progression

In vitro studies suggest that DDX11 is specialized in unwinding certain DNA structures with a preference for 5' overhangs, including forked duplexes, 5'-flap duplexes and anti-parallel G-quadruplexes (reviewed in Pisani et al (2018) [16]. Which specific structures are the most relevant DDX11 substrates in living cells remains elusive. Interestingly, treating WABS cells with various G4-DNA stabilizers, such as Quarfloxin and CX5461, inhibited their proliferation, suggesting that G4 structures are indeed unwound by DDX11 *in vivo* (chapter 6). Importantly, Quarfloxin treatment also caused cohesion defects, suggesting that resolving these structures is required for efficient cohesion establishment. Furthermore, overexpression of the helicase-dead DDX11-K50R mutant, as well as two patient-derived DDX11 mutants with presumed loss of helicase activity, could not rescue cohesion defects and sensitivity to G4 stabilization in WABS cells (chapter 5 and 6). Together, this indicates that human DDX11 requires its helicase activity to perform its function.

These findings contradict a recent model that proposed that the helicase activity of Chl1 is not important for sister chromatid cohesion, but rather to facilitate restart of stalled replication forks [17]. The cohesion promoting function of Chl1 was attributed to a physical interaction with CTF4 (AND-1 in humans) via a CTF4 Interacting Protein (CIP) motif [17]. This motif is conserved in other components of the replication fork, including DNA polymerase α p180 polypeptide and the GINS subunit Sld5. It will be interesting to identify the exact location of the CIP-box in human DDX11 and study its contribution to DNA replication and sister chromatid cohesion. Yeast Chl1 genetically interacts with numerous replication factors, including PCNA, Ctf18, Ctf4, FEN1,

Eco1, FPC and CTF18. Downregulation of many of these proteins causes both delayed replication fork speed and cohesion defects [17, 18]. In agreement with these observations, also human DDX11 promotes replication fork progression in unperturbed conditions (**chapter 5 and 6**).

Taken together, we propose a model (**figure 1**) in which DDX11 helicase activity is required to resolve secondary DNA structures during replication, including anti-parallel G-quadruplexes present in G-rich regions on both chromosome arms and in pericentromeric regions. Because the loading of the second strand into cohesin rings was reported to require single stranded DNA [19], the DNA resolving function of DDX11 may facilitate sister chromatid cohesion. Alternatively, in the absence of DDX11, secondary structures that are normally substrates of DDX11 may be prone to breakage, repair of which requires WAPL/PDS5-dependent cohesin removal to provide access of repair factors to the break site (Benedict et al, submitted manuscript) [20]. Either way, this would inevitably lead to cohesion loss. The ESCO1/2 dependent acetylation of SMC3 may come into play at a later stage, to counteract WAPL activity and possibly to enable completion of lagging strand duplication by affecting the conformation of cohesin.

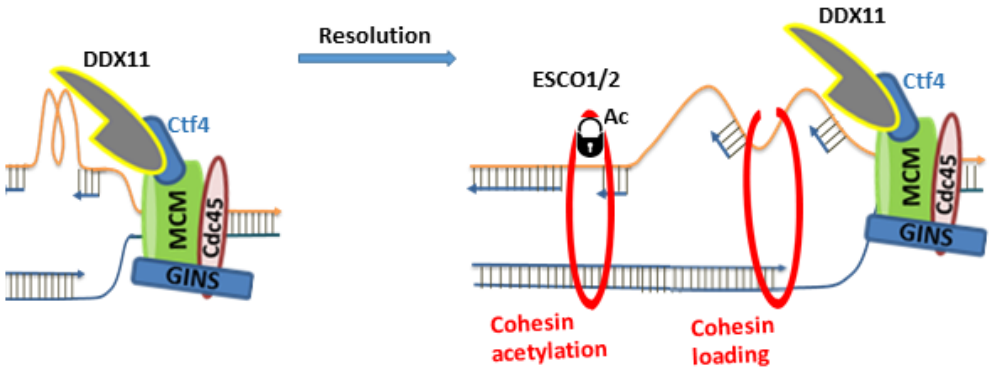

Figure 1: Speculative model of the differential contributions of DDX11 and ESCO1/2 to replication fork progression and sister chromatid cohesion. *DDX11 resolves complex secondary DNA structures in the lagging strand to facilitate DNA synthesis and second strand capture by cohesin. Cohesin acetylation may not only prevent WAPL activity but also induce a more open conformation that enables lagging strand duplication.*

Role of DDX11 in different DNA repair pathways

Besides its role in normal replication fork progression, DDX11 is also involved in the response to different drugs that induce DNA damage. DDX11 deficient cells are sensitive to the inter-strand crosslinker mitomycin C (MMC), the topoisomerase I inhibitor camptothecin and to PARP inhibitors (**chapters 3 and 6**). This role in DNA repair mechanisms appears to be evolutionary conserved. For instance, budding yeast Chl1 was shown to maintain genomic stability upon UV irradiation [21]. Timeless, a DDX11 interacting protein, is shown to physically interact with PARP-1 and is recruited to laser-induced DNA damage sites, facilitating homologous recombination [22]. In collaboration with the lab of Haico van Attikum, we discovered that yeast Chl1 is recruited to laser-induced DNA damage (data not shown). This

may indicate that DDX11 cooperates with Timeless to promote homology directed repair, possibly by resolving secondary structures that may be formed after extensive end resection.

Understanding how DDX11 performs its functions in different DNA damage repair pathways and whether these functions are separated from its role in sister chromatid cohesion is also relevant in the context of cancer. Genetic alterations of cohesin components, most notably STAG2, are reported in different cancers (chapter 1). DDX11 is involved in the survival of advanced melanomas and suggested to protect melanoma cells from chromosome segregation defects and apoptosis [23]. Thus, targeting DDX11 might be an effective tool to kill melanoma cells. Moreover, identification of critical pathways that are synthetically lethal with pathways involving sister chromatid cohesion and/or DDX11, might yield novel approaches to selectively kill cancer cells.

Identification of synthetic lethal networks in cohesion-defective cancers

In chapter 4 of this thesis we discovered synthetic lethality between DDX11 and several subunits of the Anaphase Promoting Complex or Cyclosome (APC/C). Chapter 5 describes how the synthetic lethality of DDX11 and ESCO2 originates from severely enhanced cohesion loss that is incompatible with survival. Both studies indicate that further weakening of sister chromatid cohesion in tumor cells in which cohesion is already impaired, might be a feasible approach to target such cells while sparing normal cells. This strategy requires both a reliable detection of cohesion loss *in vivo* and the development of novel drugs with sufficient potency and specificity. We showed that a newly synthesized APC/C-inhibiting drug, apcin, can kill cohesion-defective cancer cell lines (chapter 4), so the development of apcin-derivatives with *in vivo* applicability might be rewarding. In addition, directly targeting cohesion regulating enzymes such as ESCO2 and DDX11, possibly in combination with certain DNA damaging agents or PARP inhibitors, may have therapeutic potential. It will be important to better understand the interplay between sister chromatid cohesion, DNA replication and DNA damage repair pathways to select the most promising strategies.

How loss of DDX11 causes WABS

How mutations in DDX11 cause developmental defects in WABS is still an open question. A couple of research groups unsuccessfully attempted to generate mouse models for WABS [24, 25]. Initially, Inoue *et al* tried in 2007 to develop a DDX11 knockout mouse. These mice seemed to have growth retardation at embryonic day (E) 7.5 and the embryos could not survive beyond E10.5. Cells isolated from DDX11 knockout embryos showed a prolonged G2/M phase, defective sister chromatid cohesion and aneuploidy. The second attempt was by Cota and Garcia-Garcia in 2012, applying potent mutagen, ethylnitrosourea (ENU), to generate DDX11 mutant mice. In this experiment, a mutation in DDX11 helicase motif V was induced, which seemed to be a *null* allele of *DDX11* and the mutant embryos died at embryonic day 8.5. This in mind, the group of Hein te Riele generated a WABS mouse model with a patient-derived *DDX11* allele (DDX11-G57R), anticipating that this seemingly mild mutation would be only partially

inactive and still compatible with survival. Unfortunately, this mutation also resulted in embryonic lethality at E10 (data not shown). Chapter 6 shows that this mutation is actually a *null* allele that fails to restore sister chromatid cohesion and Quarfloxin resistance in WABS cells. Therefore, a mouse model with only partially reduced DDX11 activity, which would be very helpful to study the role of DDX11 in development, is still lacking.

Besides its role in sister chromatid cohesion and DNA replication, DDX11 is also reported to be involved in heterochromatin formation, suggesting that it may affect expression of developmental genes during embryogenesis [26]. Experiments in both isolated DDX11$^{-/-}$ MEFs and DDX11-depleted HeLa cells showed that DDX11 is targeting heterochromatin protein 1 α (HP1α) to pericentric- and telomeric-regions, which is required for overall organization of heterochromatin and centromere clustering [26]. Moreover, studies in HeLa cells and zebrafish embryos demonstrated that DDX11 localizes at the nucleolus, binding preferentially to hypo-methylated rDNA gene loci and interacting with RNA polymerase I [27]. DDX11 knockdown suppressed ribosomal RNA synthesis and led to an altered epigenetic status of ribosomal gene clusters. These findings suggest that WABS developmental defects might be associated with aberrant nucleolar functions. Investigating gene expression patterns in e.g. WABS cells, DDX11KO RPEs, DDX11KO MEFS and cells isolated from zebrafish embryos, will further clarify the role of DDX11 in gene transcription and development.

BOX 1: Cohesion Defects and Drug Sensitivities

STAG2-deficient cancer cells display increased sensitivity to chemotherapeutic agents: Recently, glioblastoma and Ewing sarcoma cells with STAG2 mutations were reported to be sensitive to a panel of chemotherapeutic agents, ionizing radiation and small molecule inhibitors of DNA double-strand break repair [194]. In addition, STAG2 deficiency in these cells was correlated to retarded cell proliferation after treating with alkylating agents, DNA crosslinking, topoisomerase inhibitors, PARP inhibitors. The sensitivity of STAG2-mutated cancer cells was suggested to be a result of replication fork disruption and accumulation of DNA double strand breaks [194].

Cohesion defective tumor cells are sensitive to APC/C inhibitors: In Chapter of 4 of this thesis, using cohesion-defective head and neck squamous cell carcinoma and luminal-type breast cancer cell lines, we showed that these cells are sensitive to a newly developed drug, *apcin*, a substrate competitive APC/C inhibitor [201]. We uncovered a remarkable correlation between *apcin* sensitivity and level of cohesion defects in these cancer cells.

PARP sensitivity of glioblastoma with STAG2 mutations: Inhibition of poly ADP-ribose polymerase (PARP) has been discovered many years ago to be a promising drug for the treatment of BRCA1- and BRCA2-mutated tumors[205,206]. PARP inhibitors appeared to be able to selectively kill cancer cells via synthetic lethality. In 2014 *Bailey. et al* demonstrated PARP-inhibitors sensitivity in different glioblastoma cell lines with truncating STAG2 mutations. Upon PARP-inhibitor treatment, the cells showed proliferation defects, accompanied by G2 accumulation and genomic instability. In addition we show in Chapter 3 of this thesis that DDX11 mutated WABS cells are sensitive to PARP inhibition as well. Further, the effect of PARP inhibition was enhanced when it was combined with other drugs such as topoisomerase I inhibitor (*camptothecin*) and an alkylating agent (*temozolomide*) in STAG2-mutated glioblastoma.

STAG1 depletion sensitizes STAG2-mutated cancer cells to PARP inhibitors: Two separate studies suggested a robust synthetic lethal interaction between STAG2 and its homologue STAG1 [12,207]. STAG2 inactivation was illustrated to create cancer-specific therapeutic vulnerabilities, where STAG1 inhibition in these cells resulted in severe cohesion defects and prolonged mitosis and apoptosis. Moreover, downregulation of STAG1 in STAG2-mutated Ewing sacroma and bladder urothelial carcinoma cells are both susceptible to DNA damage (especially double stranded breaks) and defective DNA repair. In addition, depletion of SA1 in SA2-mutated cells sensitized them to *olaparib,* accompanied with severe cohesion defects, prolonged mitosis and apoptosis [207].

STAG2 knockdown sensitizes pancreatic adenocarcinoma cells to different platinum-based chemotherapy agents including cisplatin : Pancreatic ductal adenocarcinoma (PDA) is an extremely lethal cancer type, with 4% STAG2 mutations [170]. siRNA knockdown of STAG2 in PDA cells was demonstrated to increase sensitivity to platinum-based drugs such as *cisplatin*,*carboplatin* and *oxaliplatin*.

References

1. van der Lelij, P. *et al.* Warsaw breakage syndrome, a cohesinopathy associated with mutations in the XPD helicase family member DDX11/ChlR1. *Am. J. Hum. Genet* **86**, 262-266 (2010).
2. Levitus, M. *et al.* The DNA helicase BRIP1 is defective in Fanconi anemia complementation group J. *Nat Genet* **37**, 934-935 (2005).
3. Egly, J.M. & Coin, F. A history of TFIIH: two decades of molecular biology on a pivotal transcription/repair factor. *DNA Repair (Amst)* **10**, 714-721 (2011).
4. Ballew, B.J. *et al.* Germline mutations of regulator of telomere elongation helicase 1, RTEL1, in Dyskeratosis congenita. *Hum Genet* **132**, 473-480 (2013).
5. Alkhunaizi, E. *et al.* Warsaw breakage syndrome: Further clinical and genetic delineation. *Am J Med Genet A* **176**, 2404-2418 (2018).
6. Bailey, C., Fryer, A.E. & Greenslade, M. Warsaw Breakage Syndrome--A further report, emphasising cutaneous findings. *Eur J Med Genet* **58**, 235-237 (2015).
7. Bottega, R. *et al.* Two further patients with Warsaw breakage syndrome. Is a mild phenotype possible? *Mol Genet Genomic Med*, e639 (2019).
8. Capo-Chichi, J.M. *et al.* Identification and biochemical characterization of a novel mutation in DDX11 causing Warsaw breakage syndrome. *Hum. Mutat* **34**, 103-107 (2013).
9. Eppley, S., Hopkin, R.J., Mendelsohn, B. & Slavotinek, A.M. Clinical Report: Warsaw Breakage Syndrome with small radii and fibulae. *Am J Med Genet A* **173**, 3075-3081 (2017).
10. Rabin, R. *et al.* Study of carrier frequency of Warsaw breakage syndrome in the Ashkenazi Jewish population and presentation of two cases. *Am J Med Genet A* **179**, 2144-2151 (2019).
11. van der Lelij, P. *et al.* The cellular phenotype of Roberts syndrome fibroblasts as revealed by ectopic expression of ESCO2. *PLoS. One* **4**, e6936 (2009).
12. Costa, V. *et al.* DDX11L: a novel transcript family emerging from human subtelomeric regions. *BMC. Genomics* **10**, 250 (2009).
13. Bharti, S.K. *et al.* Specialization among iron-sulfur cluster helicases to resolve G-quadruplex DNA structures that threaten genomic stability. *J Biol Chem* **288**, 28217-28229 (2013).
14. Guo, M. *et al.* A distinct triplex DNA unwinding activity of ChlR1 helicase. *J. Biol. Chem* **290**, 5174-5189 (2015).
15. Cali, F., Bharti, S.K., Di Perna, R., Brosh, R.M., Jr. & Pisani, F.M. Tim/Timeless, a member of the replication fork protection complex, operates with the Warsaw breakage syndrome DNA helicase DDX11 in the same fork recovery pathway. *Nucleic Acids Res* **44**, 705-717 (2016).
16. Pisani, F.M., Napolitano, E., Napolitano, L.M.R. & Onesti, S. Molecular and Cellular Functions of the Warsaw Breakage Syndrome DNA Helicase DDX11. *Genes (Basel)* **9** (2018).
17. Samora, C.P. *et al.* Ctf4 Links DNA Replication with Sister Chromatid Cohesion Establishment by Recruiting the Chl1 Helicase to the Replisome. *Mol Cell* **63**, 371-384 (2016).
18. Petronczki, M. *et al.* Sister-chromatid cohesion mediated by the alternative RF-CCtf18/Dcc1/Ctf8, the helicase Chl1 and the polymerase-alpha-associated protein Ctf4

is essential for chromatid disjunction during meiosis II. *J. Cell Sci* **117**, 3547-3559 (2004).
19. Murayama, Y., Samora, C.P., Kurokawa, Y., Iwasaki, H. & Uhlmann, F. Establishment of DNA-DNA Interactions by the Cohesin Ring. *Cell* **172**, 465-477 e415 (2018).
20. Benedict, B.v.S., J. Oostera, A. Balk, J. Wolthuis, R. te Riele, H. de Lange, J WAPL-dependent repair of damaged replication forks underlies oncogene-induced loss of sister chromatid cohesion. (2019).
21. Ogiwara, H., Ui, A., Lai, M.S., Enomoto, T. & Seki, M. Chl1 and Ctf4 are required for damage-induced recombinations. *Biochem. Biophys. Res. Commun* **354**, 222-226 (2007).
22. Xie, S. *et al.* Timeless Interacts with PARP-1 to Promote Homologous Recombination Repair. *Mol Cell* **60**, 163-176 (2015).
23. Bhattacharya, C., Wang, X. & Becker, D. The DEAD/DEAH box helicase, DDX11, is essential for the survival of advanced melanomas. *Mol Cancer* **11**, 82 (2012).
24. Inoue, A. *et al.* Loss of ChlR1 helicase in mouse causes lethality due to the accumulation of aneuploid cells generated by cohesion defects and placental malformation. *Cell Cycle* **6**, 1646-1654 (2007).
25. Cota, C.D. & Garcia-Garcia, M.J. The ENU-induced cetus mutation reveals an essential role of the DNA helicase DDX11 for mesoderm development during early mouse embryogenesis. *Dev Dyn* **241**, 1249-1259 (2012).
26. Inoue, A., Hyle, J., Lechner, M.S. & Lahti, J.M. Mammalian ChlR1 has a role in heterochromatin organization. *Exp. Cell Res* **317**, 2522-2535 (2011).
27. Sun, X. *et al.* The Warsaw breakage syndrome-related protein DDX11 is required for ribosomal RNA synthesis and embryonic development. *Hum Mol Genet* **24**, 4901-4915 (2015).

Chapter 8

Summary

Summary:

DNA duplication and distribution during cell division is tightly controlled. During S-phase of the cell cycle, every chromosome is identically synthesized and subsequently, two sister chromatids are created. The sister chromatids are kept together until anaphase, where they are separated and pulled towards opposite poles of the cell. This process, which is very crucial for each daughter cell to have the correct set of chromosomes, called sister chromatid cohesion. A ring form protein complex, called cohesin, is responsible for the cohesion between the two sister chromatids. Cohesin complex is composed of three core subunits: SMC1A, SMC3 and RAD21/Scc1 and two HEAT-repeats containing proteins: STAG1/STAG2 and PDS5A/PDS5B.For proper sister chromatid cohesion, cohesin needs to cooperate with multiple other proteins, such as NIPBL and MAU2 (responsible for cohesion loading), WAPL and PDS5 (associated with cohesin unloading), acetyltransferases ESCO1 and ESCO2 (establish cohesion), DDX11 (involved in cohesion maintenance). Mutations in a number of these components and regulators cause several related syndromes, called cohesinopathies (see chapter 2). For examples, mutations in SMC1A, SMC3, RAD21, STAG2 and NIPBL cause Cornelia de Lange syndrome (CdLS), mutations in ESCO2 and DDX11 are respectively responsible for Roberts Syndrome (RBS) and Warsaw Breakage Syndrome (WABS). Besides, cohesin mutations play an important role in the development of several types of cancer and understanding the mechanisms will be very important for future treatment of tumors with impaired cohesion. In this thesis we broaden our understanding regarding general understanding of sister chromatid cohesion.

In chapter 1, we introduce the general understanding of sister chromatid cohesion and the most recent findings. In chapter 2 we discussed the present understanding of the different cohesinopathy syndromes, including clinical features, genetic causes, underlying biology and their possible links with cancer predisposition. In chapter 3 we showed that lymphoblasts derived from WABS, RBS and Fanconi Anemia (FA), which is clinically related to WABS and RBS, are sensitive to inhibition of PARP pathway. Specially, DNA helicases DDX11 and FANCM were identified as determinants of PARP inhibitor response. Since PARP inhibitors are applied in the treatment of *BRCA*-mutated breast and ovarian cancer, identifying additional determinants of PARP inhibitor sensitivity would extend their utility in cancer therapy. In search to find additional synthetic lethal networks in cohesion defective cancer cells, we discovered in chapter 4 synthetic lethality between DDX11 and several subunits of the Anaphase Promoting Complex or Cyclosome (APC/C). In addition, we identified that a newly synthesized APC/C-inhibiting drug, Apicin can selectively kill cohesion defective cancer cells. These findings are important for developing new cancer therapy, which only targets cohesion defective cancer cells. Additionally in chapter 5, we also showed synthetic lethality between DNA helicase DDX11 and SMC3 acetyl transferases ESCO1/ESCO2. WABS derived cells rely on ESCO2, but not ESCO1 for residual sister chromatid cohesion, cellular growth and survival. Also, we demonstrated that DDX11 required for normal replication fork progression without clearly affecting SMC3 acetylation.

In chapter 6 we demonstrated different new WABS patients, with *DX11* containing a null and a weakened allele that encodes an unstable but functional DDX11 protein. We strengthened our findings by creating DDX11-mutated RPE1 cells, where DDX11 knockout is responsible for reduced cell growth in a p53-dependent manner. Also, we showed that specially DDX11 helicase activities are required for sister chromatid cohesion by possibly dissolving G-quadruplex (G4) structures, created during DNA replication. We exhibited that stabilization of G4 structures induces defective sister chromatid cohesion in normal cells and cellular lethality in DDX11-deficient cells. In conclusion, we proposed a model, where DDX11 helicase activity is important for maintaining genomic integrity through dissolving DNA secondary structures and preventing G4-induced breaks during DNA replication. Thus cohesion defects in WABS might result from either defective cohesin loading or excessive cohesin removal from broken replication forks to facilitate DNA repair.

In chapter 7 we summarized and discussed studies described in the thesis and proposed some future perspectives. Overall, the work presented in this thesis is a step forward toward understanding how sister chromatid cohesion functions and its importance in human development and carcinogenesis. Furthermore, our work provides ground for finding out how cohesion defects in tumors can be exploited to develop new anti-cancer therapies (see box 1 in chapter 7).

Acknowledgements

Ultimately it is done!

This work would not have been possible without the help of many many people who I would like to acknowledge and pay my regards to.

Firstly, I would like to begin with my promotor Hein te Riele, thank you very much Hein for your input and your remarkable sharpness during my promotion.

I would like to express my profound gratitude to my former supervisor, late Professor Johan de Winter, for giving me the opportunity to do this project.

Also my current co-promotor and supervisor Rob Wolthuis, please accept my deepest thanks for all your effort, supervision and kindness. You made it really possible and without your support it would not be possible to finish this project.

I Want to thank my second co-promoter Job de Lange. You are not only my co-promotor but also my "brother"-chromatid in the group of cohesion and a fine colleague. My thesis would never be ready without your hard work.

I wish to express my sincere appreciation to the members of Doctorate Committee, Prof.dr. Ruud Brakenhoff, Prof.dr. Haico van Attikum, Prof. dr. John Martens, dr. Kerstin Wendt and dr. Marc Bierings.

Members of oncogenetics section (current and former). My thanks to Josephine Dorsman for all those wok discussions, tips, as well as, always ready to have a small chat with me. Quinten Waisfisz, thanks for your tips concerning mutation analysis of DDX11 and a lot of instructive work discussions. Najim, also many thanks to you for your help and support in actually all parts of my promotion, you gave me so many tips and motivations, not to give up, also thanks for the endless, but interesting discussions during thee breaks, together with Khash and (The vegetarian) Martin.

Lab technicians, Jesper, thank you for finishing eight-years-DDX11-marathon and it is finally submitted. Anneke Oostra thanks for scoring so many metaphase spreads. Martin thanks for growth inhibition tests, cell culturing and also for the personal "gezelligheid" you made it easy to go through hard times in the lab, you are amazing. Also my thanks to dear Saskia, Yne and Davy. Domminique, you are not a technician but fit perfectly here, my thanks to you for your administrative help, your positive and smiley character helped always.

I would like to thank fellow PhD students (former and current), Chantal thank you for lots of help and I am honored to be a co-author with you. Berber, my neighbor in the cell lab. Anneke Haitjema, the entertainment planner of our lab. Monique my neighbor in Amsterdam Noord. Janine, thank you for solving my problem with ENECO. Khash, the bioinformation, thank you for all those fun and talks (in Persian) in the lab, it would have been boring without you.

Irsan (the Cristiano Ronaldo of oncogenetics) thanks for your help in statistics. Maarten, thank you for explaining repeatedly all those complex patterns, I still don't know it. Also my thanks for current colleagues (post docs and PhD students). Janne, thanks for the experiments you did for our WABS article. Also, Iris, Govind, Amr, Klaas, Lianne, Yvonne.

I want to thank a couple my friends, who always were a big support to me. Shekib jan, thank you very much for all your support and for having always confidence in me also thanks for being my paranymph. Orkun Abi (my other paramymph), thank you so much for your support and interest in my project and always with question, how it is going. I also want to thank my other friend Zohour jan, thanks for listening, asking and sometimes scientific discussions (although you are a computer expert).

My family, thanks from the bottom of my heart to my great parents. Father, it is so sad that you are not here, I want to dedicate this book to you. I never forget the first A.B.C lessons you gave me when I was 3.5 years old. Thank you for all of it and May God Bless You. Mother I salute your greatness, you thought me uncountable things and I use this opportunity to thank you and kiss your hands and feet. Now my sisters (Husnia jan, Shila jan and Mari jan) and brothers (Zahid jan, Fawad jan, Wasim jan and Mashal jan) thank you all for your support, patience.

I also want to thank one great person in my life who is my dear uncle Haji Mirza (mama jan), accept my appreciation for everything you did to me and to us as a family. If there is one extra person I can dedicate this book to, it is you.

I thank also each member of my family-in-law, mother-in-law, brothers- and sisters-in-law (from Jamshid jan to Mobina jan), for your supports.

Also I would like to thank my cousin/brother (Rahmat jan) and his wife/my sister (Rika jan). Thanks for all your support and generosities. You were always there for every problem I faced and please accept my countless thanks.

Last but not least, I would like to thank my lovely wife Mozhgan, the motivator. Thank you for your patience, and unconditional support. Every time I got frustrated you pushed me through and gave me the courage to keep going. Also Hajar, my dear daughter/my love, I want to tell you that your presence made it so easy to deal with and forget the stressful promotion period. I thank God for the greatest gift….. you.

Atiq Faramarz